

Springer Theses

Recognizing Outstanding Ph.D. Research

Daniel Klinger

Light-Sensitive Polymeric Nanoparticles Based on Photo-Cleavable Chromophores



Springer

Springer Theses

Recognizing Outstanding Ph.D. Research

For further volumes:
<http://www.springer.com/series/8790>

Aims and Scope

The series “Springer Theses” brings together a selection of the very best Ph.D. theses from around the world and across the physical sciences. Nominated and endorsed by two recognized specialists, each published volume has been selected for its scientific excellence and the high impact of its contents for the pertinent field of research. For greater accessibility to non-specialists, the published versions include an extended introduction, as well as a foreword by the student’s supervisor explaining the special relevance of the work for the field. As a whole, the series will provide a valuable resource both for newcomers to the research fields described, and for other scientists seeking detailed background information on special questions. Finally, it provides an accredited documentation of the valuable contributions made by today’s younger generation of scientists.

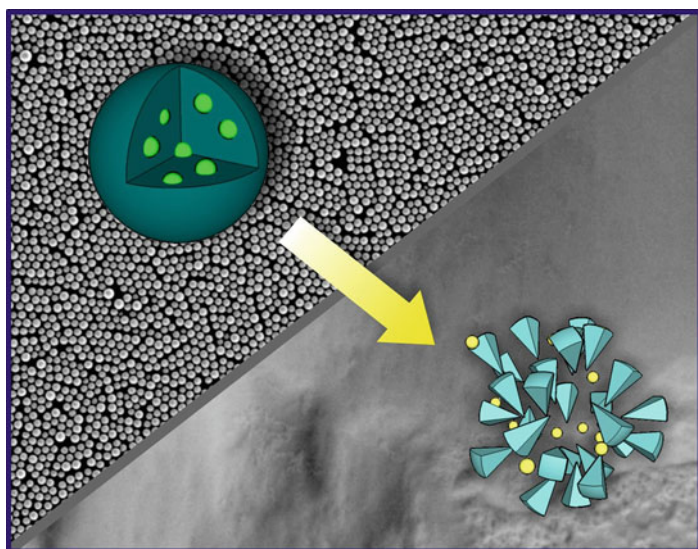
Theses are accepted into the series by invited nomination only and must fulfill all of the following criteria

- They must be written in good English.
- The topic should fall within the confines of Chemistry, Physics, Earth Sciences, Engineering and related interdisciplinary fields such as Materials, Nanoscience, Chemical Engineering, Complex Systems and Biophysics.
- The work reported in the thesis must represent a significant scientific advance.
- If the thesis includes previously published material, permission to reproduce this must be gained from the respective copyright holder.
- They must have been examined and passed during the 12 months prior to nomination.
- Each thesis should include a foreword by the supervisor outlining the significance of its content.
- The theses should have a clearly defined structure including an introduction accessible to scientists not expert in that particular field.

Daniel Klinger

Light-Sensitive Polymeric Nanoparticles Based on Photo-Cleavable Chromophores

Doctoral Thesis accepted by
the University of Mainz, Germany



Author

Daniel Klinger
Materials Research Institute
University of California
Santa Barbara, CA
USA

Supervisor

Prof. Dr. Katharina Landfester
Max Planck Institute for Polymer Research
Mainz
Germany

ISSN 2190-5053

ISBN 978-3-319-00445-7

DOI 10.1007/978-3-319-00446-4

Springer Cham Heidelberg New York Dordrecht London

ISSN 2190-5061 (electronic)

ISBN 978-3-319-00446-4 (eBook)

Library of Congress Control Number: 2013941496

© Springer International Publishing Switzerland 2013

This work is subject to copyright. All rights are reserved by the Publisher, whether the whole or part of the material is concerned, specifically the rights of translation, reprinting, reuse of illustrations, recitation, broadcasting, reproduction on microfilms or in any other physical way, and transmission or information storage and retrieval, electronic adaptation, computer software, or by similar or dissimilar methodology now known or hereafter developed. Exempted from this legal reservation are brief excerpts in connection with reviews or scholarly analysis or material supplied specifically for the purpose of being entered and executed on a computer system, for exclusive use by the purchaser of the work. Duplication of this publication or parts thereof is permitted only under the provisions of the Copyright Law of the Publisher's location, in its current version, and permission for use must always be obtained from Springer. Permissions for use may be obtained through RightsLink at the Copyright Clearance Center. Violations are liable to prosecution under the respective Copyright Law. The use of general descriptive names, registered names, trademarks, service marks, etc. in this publication does not imply, even in the absence of a specific statement, that such names are exempt from the relevant protective laws and regulations and therefore free for general use.

While the advice and information in this book are believed to be true and accurate at the date of publication, neither the authors nor the editors nor the publisher can accept any legal responsibility for any errors or omissions that may be made. The publisher makes no warranty, express or implied, with respect to the material contained herein.

Printed on acid-free paper

Springer is part of Springer Science+Business Media (www.springer.com)

Parts of this Thesis Have Been Published in the Following Journal Articles:

D. Klinger and K. Landfester

Photo-Sensitive PMMA Microgels: Light-Triggered Swelling and Degradation
Soft Matter **2011**, 7 (4), 1426

P. Froimowicz, **D. Klinger**, K. Landfester

Photoreactive Nanoparticles as Nanometric Building Blocks for the Generation of Self-Healing Hydrogel Thin Films
Chem. Eur. J. **2011**, 17, 12465

D. Klinger and K. Landfester

Polymeric Photoresist Nanoparticles: Light-Induced Degradation of Hydrophobic Polymers in Aqueous Dispersion
Macromol. Rapid Comm. **2011**, 32 (24), **1979**

D. Klinger and K. Landfester

Dual Stimuli-Responsive Poly(2-hydroxyethyl methacrylate-*co*-methacrylic acid) Microgels Based on Photo-Cleavable Cross-Linkers: pH-Dependent Swelling and Light-Induced Degradation
Macromolecules **2011**, 44 (24), 9758

D. Klinger, E. M. Aschenbrenner, C. K. Weiss, K. Landfester

Enzymatically Degradable Nanogels by Inverse Miniemulsion Copolymerization of Acrylamide with Dextran Methacrylates as Crosslinkers
Polym. Chem. **2012**, 3, 204

D. Klinger and K. Landfester

Enzymatic- and Light-Degradable Hybrid Nanogels: Crosslinking of Polyacrylamide with Acrylate-Functionalized Dextrans Containing Photocleavable Linkers
J. Polym. Sci.: Part A **2012**, 50 (6), 1062

D. Klinger and K. Landfester

Stimuli-Responsive Microgels for the Loading and Release of Functional Compounds: Fundamental Concepts and Applications
Polymer **2012**, 53, 5209

Supervisor's Foreword

This thesis describes the development of photo-sensitive polymeric nanoparticles and nanogels as potential carriers for the loading and release of functional compounds upon the application of light as an external stimulus. Such triggered release systems represent a rapidly developing and highly versatile concept that is experiencing a growing interest, especially in the biomedical field. Here, combining so-called “smart” stimuli-responsive polymeric nano-structures with pharmaceutically active substances is being increasingly exploited for the targeted delivery of drugs and is believed to be one of the key approaches for future therapeutics. Therefore, developing efficient novel materials in this area represents a highly desirable, but also rather complex task that requires the effective combination of different methodologies and techniques from across a multitude of disciplines. Consequently, a successful design of stimuli-responsive drug delivery systems is characterized by the ability to tune release profiles via the adjustment of the molecular building blocks and the resulting polymeric nano-structure in addition to the capability to predict and optimize its specific interaction with highly intricate biological systems.

In this thesis, all of these challenges are approached in a systematic way. First, light-cleavable crosslinkers and monomers were carefully designed to possess different photolytic properties based on their molecular structure. These new building blocks were then utilized to prepare light-sensitive nanogels and nanoparticles, whereby different response profiles could be realized by the selective copolymerization of these new building blocks with a variety of monomers in mini-emulsion systems. The resulting carrier systems were shown to exhibit the anticipated loading and release characteristics, as determined by their systematically planned chemical structure. At least, these new materials demonstrated good biocompatibility and excellent cell uptake, thus fulfilling crucial prerequisites to biomedical applications.

While the step-wise development of these new systems represents an excellent example for the cross-fertilization between disciplines and has led to several original research publications, this thesis also contains an extended review on

stimuli-responsive microgels highlighting the design principles for the preparation of future materials in this area. Hence, this work will be of great value for a broad audience with interests in organic and polymer chemistry, colloidal and materials sciences, and the biomedical field.

The presented research was conducted at the Max Planck Institute for Polymer Research in Mainz, Germany between 08/2008 and 09/2011 and was honored *summa cum laude* by the University of Mainz.

Mainz, March 2013

Prof. Dr. Katharina Landfester

Acknowledgments

Many people contributed in different ways to this thesis and I express my gratitude to all of them. During my stay at the Max Planck Institute, I always enjoyed the great working environment and the cooperative atmosphere. I especially treasure the opportunity to have met many wonderful colleagues who eventually became very close friends. Here, the great solidarity in our office, the cheerful coffee corner, the soccer matches and the uncountable barbecue parties put the icing on the cake.

First of all, I want to thank Prof. Dr. Katharina Landfester for giving me the opportunity to work in her group. I am grateful for all the fruitful discussions and the support during my work.

I am a fellow of the *International Max Planck Research School* that not only sponsored my participation in several conferences and summer schools, but also gave me the chance to get to know many wonderful colleagues and to broaden my scientific horizon.

I want to thank all of my colleagues which helped me during my work by long discussions, sharing ideas and supporting me. Especially Max, Rüdiger and Pablo have been a great aid if it came to solve synthetic riddles and to work out problems which arose from the difference of doing chemistry in the lab and on a piece of paper. I also want to thank Mela, Daniela and Steffi for all the help with cell experiments, a task I could never have accomplished on my own. Moreover, I want to thank Eugen and Pablo for their contributions to our cooperations. I am grateful for the help of Niki, Steffi, Adrian and Pablo by proof-reading this thesis and I want to thank my office mates Niki, Anke, Max, Vero, Nermeen, Christoph and Adrian for all the fun and the support in 0.304. During my work at the MPI-P I truly worshiped the perfect infrastructure at the institute. Among various people, I especially want to thank the staff from the polymer analytics lab. The help of Beate, Christine and Sandra with HPLC and GPC measurements clearly facilitated my work.

I am exceptionally grateful for all the support from my friends Niki, Steffi and Micha who accompanied me through all the ups and downs of a long journey.

Finally, I want to thank my family, especially my parents who always supported me on my way.

Contents

1	Introduction	1
	References	2
2	Motivation	3
3	Theoretical Part	5
3.1	Polymeric Gels: From Macro to Micro	5
3.2	Synthesis of Microgels	8
3.2.1	Microgel Preparation in Homogeneous Phase	8
3.2.2	Microgel Preparation in Heterogeneous Phase	8
3.3	Stimuli-Responsive Microgels: Features and Applications	13
3.3.1	Microgels for Loading and Release Applications	14
3.3.2	Different Approaches to Stimuli-Responsive Microgels	22
3.4	Photochemistry in Polymeric Nanoscale Materials	42
3.4.1	Light as a Trigger	42
3.4.2	Photoreactions in Polymers	42
	References	48
4	Outline	57
5	Results and Discussion	61
5.1	Photo-Sensitive Microgels Based on Light-Cleavable <i>Monomeric</i> Crosslinkers	61
5.1.1	Photo-Sensitive Polymeric Gel Nanoparticles	61
5.1.2	Photo-Sensitive Hydrogel Nanoparticles	85
5.2	Photo-Sensitive Hydrogel Nanoparticles Based on Light-Cleavable <i>Polymeric</i> Crosslinkers	121
5.2.1	Enzymatically Degradable Nanogels Based on Dextran-Methacrylates as Macromolecular Crosslinkers.	122
5.2.2	Enzymatically- and Light-Degradable Nanogels Based on Functionalized Dextrans as Crosslinkers	138

5.3	Light-Sensitive Microgel-Doxorubicin Conjugates: Labile Drug Attachment via a Photo-Cleavable Linker	152
5.4	Photo-Resist Nanoparticles: Light-Induced Degradation of Hydrophobic Polymers in Aqueous Dispersion	162
5.5	Towards Stimuli-Responsive Core/Shell Nanoparticles Containing a Microgel Core	171
5.5.1	PAAm/PMMA Core/Shell Nanoparticles by Seeded Dispersion Polymerization	173
5.5.2	PAAm/PU Core/Shell Nanoparticles by Free Radical Polymerization of AAm in Preformed Nanocapsules.	178
5.6	Surface Functionalization of Microgels with Photo-Reactive Chromophores	184
5.6.1	Surface Modification of PHEMA and p(HEMA- <i>co</i> -MAA) Microgels with Cinnamoyl Groups	185
5.6.2	Self-Healing Hydrogel Thin Films from Photo-Reactive Microgels	189
	References	190
6	Conclusion and Outlook	195
6.1	Photo-Sensitive Microgels Based on Light-Cleavable Crosslinkers.	195
6.1.1	Photo-Degradable Microgels Based on Photo-Cleavable <i>Monomeric</i> Crosslinkers: Light-Induced Swelling and Degradation in Organic Solvents	196
6.1.2	Photo-Degradable Hydrogel Nanoparticles Based on Photo-Cleavable <i>Monomeric</i> Crosslinkers: Light-Induced Swelling and Degradation in Aqueous Media	196
6.1.3	Photo-Degradable Hydrogel Nanoparticles Based on Photo-Cleavable <i>Polymeric</i> Crosslinkers: Light-Induced Swelling and Degradation in Aqueous Media	197
6.2	Light-Sensitive Microgel-Doxorubicin Conjugates: Labile Drug Attachment via a Photo-Cleavable Linker.	197
6.3	Photo-Resist Nanoparticles	198
6.4	Towards Stimuli-Responsive Core/Shell Nanoparticles Containing a Hydrogel Core	198
6.5	Surface Modification of Microgels with Photo-Reactive Chromophores	199

7 Experimental Part	201
7.1 Materials	201
7.2 Instrumentation	201
7.3 Synthesis of Light-Cleavable Monomeric Crosslinkers	202
7.4 Synthesis of Enzymatically Degradable Macromolecular Cross-Linkers	206
7.5 Synthesis of Enzymatically and Light-Degradable Macromolecular Crosslinkers	207
7.6 Synthesis of Doxorubicin-Methacrylate Containing a Photo-Labile Linker	208
7.7 Synthesis of a Light-Sensitive Monomer for the Preparation of Polymeric Photo-Resist Nanoparticles	212
7.8 Synthesis of a Photo-Degradable Polyurethane by Polycondensation	212
7.9 Photo-Degradation Studies of Light-Cleavable Molecules in Solution	213
7.9.1 Photo-Degradation Studies in Solution via ^1H NMR and Mass Spectroscopy	213
7.9.2 Photo-Degradation Studies by UV-vis Measurements	213
7.9.3 Kinetic HPLC Measurements	213
7.10 Synthesis of Microgels and Polymeric Nanoparticles	214
7.10.1 General Synthetic Protocol for the Formation of Microgels and Non-Crosslinked Polymeric Nanoparticles by Free Radical (Co) Polymerization in (Inverse) Miniemulsion	214
7.10.2 Micro-/Nanogels	214
7.10.3 Photo-Resist Nanoparticles and Polystyrene Reference Nanoparticles	218
7.11 Loading of p(HEMA- <i>co</i> -MAA) Microgels with Myoglobin and Subsequent Release Experiments	219
7.12 Degradation Experiments of Microgels	220
7.12.1 Photo-Degradation	220
7.12.2 Enzymatic Degradation	220
7.13 Degradation Experiments of Photo-Resist Particles	221
7.14 Synthesis of Core/Shell Nanoparticles	221
7.14.1 Seeded Precipitation Polymerization	221
7.14.2 Free Radical Polymerization in Polyurea Nanocapsules	221
7.15 Surface Functionalization of Microgels	222
References	222
Curriculum Vitae and Publications	223

Abbreviations

AA	Acrylic acid
ATRP	Atom transfer radical polymerization
BOC	<i>tert</i> -Butyloxycarbonyl
CDI	Carbonyldiimidazole
CL	Crosslinker
d	Doublet
DBTDL	Dibutyltin dilaurate
DCC	<i>N,N'</i> -dicyclohexylcarbodiimide
DCM	Dichloromethane
dd	Doublet of doublet
DEGDMA	Diethylene glycol dimethacrylate
EGDMA	Ethylene glycol dimethacrylate
Dex	Dextran
Dex-MA	Dextran methacrylate
Dex-PL-MA	Dextran-photo-labile linker-methacrylate
<i>DGS</i>	Degree of swelling
DLS	Dynamic light scattering
DMAP	4-Dimethylaminopyridine
DMF	Dimethylformamide
DMNB-MA	4,5-Dimethoxy-2-nitrobenzyl methacrylate
DMNPA	4,5-Dimethoxy-2-nitrobenzyl alcohol
DMSO	Dimethyl sulfoxide
DNQ	Diazonaphthoquinone
DOX	Doxorubicin
Dox-PL-MA	Doxorubicin-photo-labile linker-methacrylate
<i>DS</i>	Degree of substitution
DVB	Divinylbenzene
EDA	Ethylene diamine
ESI	Electrospray ionization
GPC	Gel permeation chromatography
HEMA	2-Hydroxyethyl methacrylate
HG	Hydrogel
HPLC	High-performance liquid chromatography

<i>I</i>	Intensity
IONP	Iron oxide nanoparticles
<i>J</i>	Coupling constant
KLE	P(E/B)- <i>b</i> -PEG poly(ethylene- <i>co</i> -butylene)- <i>block</i> -poly(ethylene glycol)
K-MAA	Potassium methacrylate
KPS	Potassium persulfate
LCST	Lower critical solution temperature
<i>m</i>	Multiplet
MAA	Methacrylic acid
MA-Cl	Methacryloyl chloride
MBA	<i>N,N'</i> -methylenebisacrylamide
MHz	Megahertz
MMA	Methyl methacrylate
M_n	Number average molecular weight
MS (FD)	Mass spectroscopy (field desorption)
M_w	Weight average molecular weight
NIPAAm	<i>N</i> -isopropylacrylamide
NIR	Near infrared
NMR	Nuclear magnetic resonance
NP	Nanoparticles
N_p	Number of particles
NPDM	2-Nitrophenyldimethanol
O/W	Oil-in-water
PAA	Poly(acrylic acid)
PAAm	Polyacrylamide
PAG	Photoacid generator
PAMAM	Polyamidoamine
PBS	Phosphate buffered saline
PBT	Polybutylene terephthalate
PCCS	Photon cross correlation spectroscopy
PDI	Polydispersity index
PEG	Polyethylene glycol
PEI	Polyethylenimine
PEO	Polyethylene oxide
PHEMA	Poly(2-hydroxyethyl methacrylate)
PMAA	Poly(methacrylic acid)
PMMA	Poly(methyl methacrylate)
PNIPAAm	Poly(<i>N</i> -isopropylacrylamide)
PS	Polystyrene
PU	Polyurethane
PVCL	Polyvinylcaprolactam
PVP	Polyvinylpyrrolidone
<i>q</i>	Quartet
<i>s</i>	Singlet

SEM	Scanning electron microscopy
t	Triplet
TDI	2,4-Toluene diisocyanate
TEM	Transmission electron microscopy
TEMED	Tetramethylethylenediamine
THF	Tetrahydrofuran
UCST	Upper critical solution temperature
UV	Ultraviolet
V-59	2,2'-Azobis(2-methylbutyronitrile)
V-70	2,2'-Azobis(4-methoxy-2,4-dimethylvaleronitrile)
VA-044	2,2'-Azobis(<i>N,N'</i> -dimethyleneisobutyramidine)dihydrochloride
VA-060	2,2'-Azobis{2-[1-(2-hydroxyethyl)-2-imidazolin-2-yl]propane}- dihydrochloride
VCL	<i>N</i> -vinylcaprolactam
vis	Visible part of the optical spectrum
VP	2-Vinylpyridine
VPTT	Volume phase transition temperature
W/O	Water-in-oil
λ	Wavelength
τ	Turbidity

Chapter 1

Introduction

The chemistry of life offers the most sophisticated example of how selectively tailored polymers, polymer assemblies, and interfaces provide a specific chemical function and structure. In natural biopolymers such as proteins, carbohydrates and nucleic acids, the distinct position and nature of functional groups drives a particular three-dimensional structure that influences the function of these materials and also determines their response to external stimuli. Since these features form the basis for constructing and keeping the complicated cell machinery running, understanding the fundamental underlying concepts means learning a lesson from the most influential expert in property control by molecular design: Nature.

Even though there is still a lot to learn and discover, the transfer of several concepts from biology to the world of synthetic polymer chemistry has already been accomplished and is rapidly developing [1]. Especially in the case of stimuli-sensitive macromolecular materials, the gathered knowledge on the response mechanisms of biopolymers has opened up new perspectives to mimic this behavior in synthetic systems. Moreover, it enabled the extension of this approach to the development of novel functional polymers that are sensitive to new signals formerly non-existent in biological systems [1, 2]. Such stimuli-induced changes of specific (polymeric) properties can generally be realized by two orthogonal concepts. The first approach entails changing the materials environment (variations in pH, temperature, or the presence/absence of chemical and biological compounds). Second, applying external fields (light, electrical- or magnetic fields) can stimulate change of polymer properties. Independent of the applied stimulus, the underlying similarities of all these materials are the triggered conformational and chemical changes of the respective polymeric system that translate to the overall response profile of the material. The fact that these small signals are able to induce a comparably huge response at the macroscopic level renders these materials such a fascinating research area. Here, the key point to their successful development is to understand that this behavior is the result of highly cooperative interactions. These depend not only on the type but also on the localization of a vast number of functional groups in a polymeric system.

Having learned this lesson from nature, it is now the task of chemists to transfer these insights in structure- and composition-property relationships to synthetic pathways in order to further develop novel and highly sophisticated artificial materials. In this context, Hawker and Wooley clearly highlighted the importance of the convergence of synthetic organic and polymer chemistries and stated that “*creative approaches using organic chemistry are required to control every facet of macromolecular structure and to enable functional groups to be introduced at defined locations*” [3]. Regarding materials research in general, it becomes obvious that this cross-fertilization between disciplines nowadays is an essential concept to the successful formation of materials exhibiting tailored properties for specific applications. Especially, the increasing number and accuracy of analytical methods, the development of diverse novel processing routes, and the exploitation of self-assembly methods in combination with new tailor-made synthetic polymers have opened up a whole new area of applications in the nanoscale [1, 2].

In this context, the work on photo-sensitive microgels described in this thesis represents an approach to nanoscale materials whose properties are determined by the molecular structure of their components therefore contributing to the development of the “new world” of artificial stimuli-responsive nanomaterials.

References

1. Galaev, I.Y., Mattiasson, B.: ‘Smart’ polymers and what they could do in biotechnology and medicine. *Trends Biotechnol.* **17**, 335–340 (1999)
2. Stuart, M.A.C., Huck, W.T.S., Genzer, J., Muller, M., Ober, C., Stamm, M., Sukhorukov, G.B., Szleifer, I., Tsukruk, V.V., Urban, M., Winnik, F., Zauscher, S., Luzinov, I., Minko, S.: Emerging applications of stimuli-responsive polymer materials. *Nature Materials.* **9** (2), 101–113 (2010)
3. Hawker, C.J., Wooley, K.L.: The convergence of synthetic organic and polymer chemistries. *Science.* **309**, 1200–1205 (2005)

Chapter 2

Motivation

Since the discovery of microgels as a unique class of polymeric nanoscale materials, this research area has gained increasing attention. Especially the incorporation of stimuli-responsive properties into gel nanoparticles allows the preparation of highly functional materials exhibiting bespoke properties for a tremendous variety of applications. In general, the exceptional properties of microgels stem from the combination of their colloidal nature with their internal network structure. Since the latter is characterized by parameters as e.g. the mesh size, the polymer volume fraction or the interaction of embedded functional compounds with the network, the ability to control these factors by the appliance of external triggers represents the underlying concept to stimuli-responsive microgels. The response mechanism of these nanomaterials crucially depends on two important features. First, the overall sensitivity of microgels is defined by the specific type of stimulus to which these materials respond. This is governed by the particular nature of functional groups responsible for the sensitivity of the gel. Second, the location of these moieties in the network structure as well as their specific triggered response mechanism determines the overall stimuli-dependent behavior of the microgels.

Among a broad variety of triggers described in the literature, light-induced responses have attracted much attention since they represent one of the most desirable methods for economical, easy, rapid, and efficient control of the material properties. This can be achieved by tuning light parameters such as wavelength, power, and time of irradiation in a non-contact approach. Therefore, the concept of photo-sensitive nanomaterials such as nanoparticles or microgels is a highly interesting approach not only for applications in nanotechnology and biomedical related fields, but also holds promise for creating ideal model systems for fundamental studies on molecularly controlled structure variations. Moreover, photochemistry in combination with microgels enables the preparation of a multitude of materials with different response mechanisms precisely tailored for a desired application by taking two main design criteria into account:

- (i) The large number of various chromophores and their specific photoreactions allows for tuning the sensitivity of the microgels with respect to the light parameters.
- (ii) The potential to incorporate the respective light-induced changes to a multitude of locations in the polymeric network structure (i.e. polymer backbone, crosslinking points, polymeric side groups) gives rise to a variety of response mechanisms. This facilitates the preparation of different materials based on the same chromophore but exhibiting diverse photolytic variations of their properties.

As these characteristics render photo-sensitive microgels and nanoparticles very versatile materials with respect to their design, preparation and application, the implementation of new materials in this area represents an extremely attractive field of research. In this context, polymeric gel latexes for light-triggered loading and release applications are of special interest. Here, controlling the rates of diffusion of embedded functional substances within the swollen (hydro)gel matrix by light is the underlying concept.

Based on these considerations, the aim of this thesis is the design, synthesis and characterization of novel photo-sensitive microgels and nanoparticles as potential materials for the loading and light-triggered release/accessibility of functional compounds. A crucial prerequisite to resolve the potential of these materials for possible applications is a profound understanding of their stimuli-responsive behavior. Therefore, particular attention is paid on combining the design and characterization of specific response mechanisms on a molecular level with detailed investigations on the influence of these features on the overall sensitivity of the nanoscale polymeric gel particles.

Chapter 3

Theoretical Part

3.1 Polymeric Gels: From Macro to Micro

Gelation of polymers was first investigated in 1931 by Carothers who polymerized multifunctional monomers by polycondensation. He suggested that this phenomenon is a result of linking polymer molecules into a three-dimensional network of infinitely large size [2]. Since the polymer network consists of inter- and intramolecularly connected polymer chains, the entire gel network can indeed be considered as one macroscopic molecule whose size is theoretically only limited by the dimensions of the containing vessel [3].

Starting from these early investigations, the development of new polymerization techniques and the understanding and resulting utilization of specific molecular interactions dramatically expanded the field of polymeric gels over the years. Hence, three dimensional networks are no longer only formed by polycondensation reactions in the presence of multifunctional branching units, but polymeric gels, in general, consist of (organic) polymer components which are crosslinked by either covalent or physical connecting points. Moreover, an additional prerequisite for gels is the ability of such networks to swell upon absorbing specific solvent molecules, thereby distinguishing them from other crosslinked polymeric materials such as resins, elastomers or thermoset polymers.

The unique combination of the structural integrity of a solid with the ability to store fluids and the mobility of functional groups in the swollen networks renders polymeric gels a unique class of materials. The resulting softness, elasticity and the fluid-like transport characteristics for molecules smaller than the gel pores give rise to a broad variety of different applications. Probably the most simple and widespread examples for hydrogels include their utilization as super-absorbers and contact lenses [4]. Furthermore, the combination of more complex and highly

Parts of this chapter are published as: Klinger D., Landfester K.: Stimuli-responsive microgels for the loading and release of functional compounds: fundamental concepts and applications. *Polymer* **53**(23), 5209 (2012). Reprinted with permission from [1]. Copyright 2012 Elsevier.

functionalized polymeric architectures with diverse crosslinking methods has been realized by a tremendous variety of different approaches, resulting in a large number of sophisticated materials with specific functionalities tailored for particular applications. Nowadays, polymeric gels are applied in the fields of e.g. self-healing materials [5], drug-delivery [6, 7], chemical separation [8], sensors [9], shape-memory materials [10, 11] and (self-driven) actuators [12, 13].

The spatial stability of gels in the presence of a variety of solvents is based on their crosslinked network structure. Linkages can be introduced by several processing routes resulting in various materials with specific properties determined by the crosslinking density, the polymer type and the chemical nature of the crosslinks. A detailed overview over a multitude of crosslinking methods can be found in the review of Hennink and van Nostrum [14].

A widely investigated approach to chemically crosslinked gels is the radical polymerization of low molecular weight monovinyl monomers in the presence of multivinyl crosslinking agents. In the case of water swellable materials, Wichterle and Lim were the first to describe the polymerization of 2-hydroxyethyl methacrylate (HEMA) in the presence of ethylene glycol dimethacrylate as crosslinker. Detailed investigations on the reaction conditions yielded such a hydrogel as the first material for soft contact lenses [15]. From here on, the additional introduction of functional groups resulted in stimuli-responsive gels as a new class of materials. A different method to obtain covalently crosslinked networks is based on the linkage of polymeric precursors. Here, the radical polymerization of polymers derivatized with polymerizable groups is a well examined concept. As an example, the formation of hydrogels from polymerizable dextrans was pioneered by Edman et al. by reacting dextran with glycidyl acrylate and polymerizing a solution of the resulting compound [16]. In the group of Hennink, this approach was further developed and the investigated hydrogels from (meth)acrylated dextrans served as enzymatically degradable gels for enzyme immobilization [17]. Moreover, the crosslinking of polymer precursors can also be achieved by the utilization of low-molecular weight crosslinking agents which react with functional groups on the polymeric backbones [18]. Examples include the crosslinking of synthetic polymers such as polyvinylalcohol [19] as well as biopolymers such as gelatin with glutaraldehyde [20].

Physically crosslinked polymeric gels represent another type of gels where the network formation is achieved by non-covalent attractive interactions between the individual polymer chains. In contrast to chemically crosslinked gels, the use of often toxic crosslinking agents is avoided, thus rendering them interesting materials for biological applications. Various interaction mechanisms can be used to create crosslinking points. A very prominent example for physically crosslinked gels is the utilization of hydrophobic interactions or partial crystallization of respective domains in amphiphilic block and graft copolymers. Adapting this concept from the classical ABS rubber has led to an interesting class of materials. As an example, Kim et al. described the utilization of “Biomer” as a segmented polymer consisting of a polyurethane and a polyether. Aggregation of the hard hydrophobic polyurethane segments served not only as crosslinks but also enabled

the loading of a hydrophobic drug into the overall hydrophilic gel [21]. A similar approach was described by Feijen and coworkers who used multiblock copolymers of PEG and polybutylene terephthalate (PBT) to form hydrogels with incorporated lysozyme as hydrophilic model protein [22]. Another concept to physical crosslinks is the utilization of ionic interactions between charged polymers and their respective counterions. As an interesting example, the crosslinking of chitosan as cationic biopolymer with glycerol-phosphate disodium salt was found to depend on the temperature. Liquid mixtures containing biological materials below room temperature were injected subcutaneously in rats and gel formation occurred in situ [23]. Additional approaches to physically crosslinked gels include, among others, the pH-dependent crosslinking by hydrogen bonds in mixtures of poly((meth)acrylic acid) and PEG [24] or the crosslinking by antigen–antibody interactions [25].

Comparing physical and chemical approaches, it can be stated that chemically crosslinked networks are normally characterized by an increased stability compared to the physically crosslinked gels. This feature is based on the covalent linkage of the polymer chains which ensures a good structural integrity. Nevertheless, crosslinking polymerizations also bear some drawbacks influencing the properties of the final material. Among other parameters, the structure of the crosslinking agent as well as the difference in hydrophilicity of monomer and crosslinker can play a crucial role regarding the crosslinking efficiency and homogeneity [26].

Besides the field of macroscopic gels which represent insoluble polymeric materials, it was in 1935 when Staudinger was the first who found a crosslinking polymerization of a dilute solution of divinylbenzene to result in a soluble polymer of low viscosity [27]. The conclusion that *this polymer is a product consisting of strongly branched, 3-dimensional molecules* was the groundbreaking perception which led to the development of colloidal macromolecules of globular shape as a new class of materials [25, 27, 28]. These inter- and intramolecularly crosslinked macromolecules dispersed in either normal or colloidal solutions are termed microgels, (hydro)gel nanoparticles or nanogels. It is noteworthy that no clear correlation between the actual size of the gel particles and the nomenclature has been established and the terms microgels and nanogels are mostly used interchangeable in the literature. Due to the lack of proper characterization techniques, microgels were playing a negligible role in science and technology of polymers until the beginning of the 1970s. Since then, the progress in chemical design and understanding of the physico-chemical properties of microgels increased steadily and significantly, as can be seen from the rising number of publications [28]. Microgels are an intriguing class of materials since they combine the inherent features of macroscopic hydrogels (e.g. structural integrity in combination with fluid-like transport characteristics) with those of colloidal dispersions (e.g. colloidal stability, high surface area, facile synthesis and control over particle size). Especially the combination of the microgel structure with the growing field of stimuli-responsive polymers and materials gives rise to a tremendous variety of new research areas and applications which will be in the focus of this chapter.

3.2 Synthesis of Microgels

As in the case of macroscopic polymeric gels, similar crosslinking methods can be applied for the formation of microgels. Preparation methods can be generally categorized in two main concepts: (a) the formation of microgels in homogeneous phase and (b) the formation of microgels in heterophase.

3.2.1 *Microgel Preparation in Homogeneous Phase*

Among others, this concept can be realized by two main approaches. Based on the first investigations made by Staudinger, the free radical crosslinking copolymerization of mono- and bis-unsaturated monomers in dilute solutions results in the formation of inter- and intramolecularly crosslinked microgels. In this solution polymerization the internal structure of the prepared microgels crucially depends on the ratio of the amount of the inert good solvent to the monomers [28]. Hence, a higher dilution increases the probability of intramolecular crosslinks. Even though the resulting internal structure of microgels prepared by this method is not well defined, investigations conducted on these systems represent an important step to get insight into the mechanism of gel formation in radical crosslinking polymerizations [3, 29–31].

An alternative approach to microgels includes coacervation and desolvation techniques which are both based on the phase separation of readily formed polymers during the preparation step, thus forming nanoparticles which are subsequently crosslinked. This method has been widely investigated for the formation of microgels from biopolymers such as e.g. (modified) gelatin or chitosan which contain a large number of functional groups available for crosslinking. Hence, the preparation of pH-sensitive chitosan nanoparticles by complex coacervation can be achieved e.g. by physical crosslinking due to electrostatic interactions of the cationic polymer with either anionic polyethyleneimine [32] or tripolyphosphate [33]. Gelatin nanoparticles were successfully prepared by a two-step desolvation route including the chemical crosslinking with glutaraldehyde [34]. Nevertheless, since in these synthetic procedures crosslinking occurs after the nanoparticles formation, the resulting microgels are only crosslinked at the surface due to a hindered diffusion of the crosslinking agent into particle interior [35].

3.2.2 *Microgel Preparation in Heterogeneous Phase*

Another class of synthetic routes to microgels is the heterophase copolymerization of monomers with crosslinking agents in aqueous solution. Here, three main concepts can be distinguished: (a) precipitation polymerization, (b) polymerization

and (physical or chemical) crosslinking of preformed polymers in inverse mini- and (c) microemulsions.

3.2.2.1 Microgels by Dispersion/Precipitation Polymerization

Dispersion and precipitation polymerizations in general, start with the initiation of polymerization in a homogenous solution of monomers and crosslinkers [36–38]. While the polymerization proceeds, the monomer and formed oligomers are soluble until the growing chains reach a critical length. As a result of unfavorable polymer–solvent interactions after reaching a critical chain length, they phase-separate from the continuous medium by enthalpic precipitation, thus forming particle nuclei. In the case of crosslinkers present in the mixture, entropic precipitation occurs favorably and crosslinking prevents the polymer and solvent from freely mixing even in good solvents for the polymer [39]. Here, the boundary to the previously described radical crosslinking polymerization in solution is blurred [28]. Nevertheless, in both cases, the resulting nuclei aggregate into larger particles that continue to grow by capturing other particles, newly formed polymer chains or by absorption and polymerization of monomer. In this context, dispersion polymerizations are characterized by the addition of a stabilizer to control the size and to narrow the distribution of the particles [40]. The described mechanism is schematically illustrated in Fig. 3.1.

The method of precipitation polymerization represents a widely investigated and elegant approach for the preparation of water swellable thermo-sensitive microgels. Especially *N*-isopropylacrylamide (NIPAAm) [41] or *N*-vinylcaprolactam (VCL) [42] are the most applied monomers [43]. In these cases, the enthalpic precipitation of growing oligoradicals occurs due to the unfavorable polymer–solvent interaction at high reaction temperatures. Since the monomers are completely water soluble but the resulting PNIPAAm and PVCL polymers exhibit a lower critical solution temperature (LCST) above which they become insoluble in water, initiation of an aqueous monomer/crosslinker solution results in the formation of precursor particles consisting of collapsed polymer chains if the

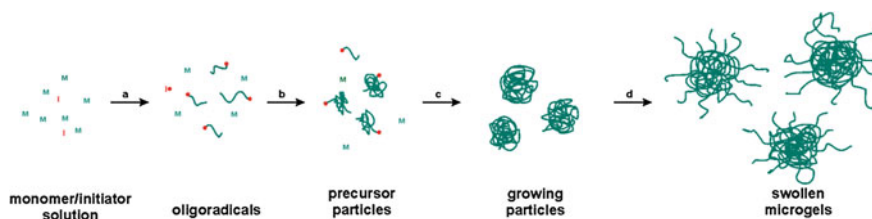


Fig. 3.1 Microgel formation by precipitation polymerization: **a** initiation and chain growth, **b** precipitation and nucleation, **c** particle growth and **d** transfer to good solvent or decrease of temperature below the volume phase transition temperature. Reproduced with permission from [1]. Copyright 2012 Elsevier

reaction temperature is above the LCST. These nuclei further react to the microgels in analogy to the mechanism described above. Stabilization of the collapsed microgels at elevated temperatures can be achieved by e.g. the utilization of potassium peroxydisulfate (KPS) as initiator. The electrostatic stabilization is based on sulfate groups from initiator fragments which are incorporated into polymer chains during the nucleation and growth process [44]. Different ways of stabilization, which in addition offer the possibility of particles size control, are the utilization of either ionic [45] or steric [46] stabilizers or ionic comonomers [47, 48] analogous to surfactant free emulsion polymerizations. After complete polymerization, the microgels dispersion is cooled down to room temperature resulting in a swelling of the networks ($T < \text{LCST}$) and a sterical stabilization of the microgels by dangling chains of the outer swollen particle layer. It is obvious that the use of crosslinking agents is a necessary requirement in order to prevent microgels from dissolution at low temperatures [49]. A tremendous variety of thermo-sensitive microgels has been prepared by this method demonstrating the high impact of this preparation route. Moreover, modifications of the synthetic protocol enabled the formation of more complex microgels structures. As an example, temperature- and pH-sensitive microgels were obtained by copolymerization of NIPAAm with e.g. acrylic acid [50] or aminoethyl methacrylate hydrochloride [51]. In addition, precipitation polymerization of functional monomers in the presence of preformed seed particles was demonstrated to yield such complex structures as e.g. (multi-responsive) [52] core/shell microgels [44, 53] or hollow hydrogel spheres [54].

Even though this preparation method is one of the most widely investigated routes to hydrogel nanoparticles, several limitations have to be taken into account. On one hand, the incorporation of comonomers can only be achieved to a certain extent depending on the hydrophilicity of the respective compound. Hence, for the synthesis of thermo-sensitive hydrogel nanoparticles, the additional introduction of strongly hydrophilic comonomers such as e.g. (meth)acrylic acid is limited as a successful precipitation during the chain growth crucially depends on the overall hydrophobicity of the resulting copolymer [44]. Furthermore, since batch copolymerization of monomers of different reactivity and hydrophilicity was shown to result in core/shell morphologies [42, 55], the preparation of copolymer microgels exhibiting a homogenous distribution of all functionalities is hindered.

3.2.2.2 Microgel Synthesis in Dispersed Droplets

As described in the previous section, precipitation polymerization for the formation of microgels bears some serious drawbacks such as the restriction to network formation by crosslinking polymerization and the limited incorporation of functional comonomers. In order to evade these limitations, microgels synthesis in droplets dispersed in a continuous phase represents a well examined alternative. Here, the restriction of the network-forming reaction to the droplets renders the latter as “nanoreactors”, thus in principle enabling to exploit most of the

crosslinking (physically and chemically) methods described for macroscopic gels for the preparation of microgels.

Microgel Synthesis in Microemulsions

Microemulsions in general can be prepared as direct oil-in-water (O/W) or inverse water-in-oil (W/O) emulsions. For the formation of microgels, especially the W/O emulsion methods are widely investigated to yield water swellable hydrogel nanoparticles [56, 57]. In this approach, the dispersed phase contains the respective compounds for the network formation such as e.g. polymerizable monomer or crosslinkable prepolymers dissolved mostly in water as solvent. The microemulsion is then formed by adding this solution to a continuous organic medium containing large amounts of an oil-soluble surfactant. By stirring this mixture, the thermodynamically stable microemulsion is formed. Microgel formation can then be achieved by e.g. free radical polymerization of mono- and divinyl monomers in the droplets upon initiation from either the droplets interior or the continuous phase [58, 59]. This preparation method allows the preparation of microgels with a high content of ionic groups [60].

Microgel Synthesis in Miniemulsions

In general, miniemulsions are kinetically stable emulsions, thereby distinguishing them from microemulsions [61]. The advantage is the considerably less amount of surfactant needed for successful droplet stabilization as well as the versatility of this approach with respect to the utilization of different monomers [62], the incorporation of functional compounds [63–66] and the precise adjustment of the droplets and particles size [67]. Miniemulsification is generally achieved by applying high shear forces to a pre-emulsion of droplets in a continuous phase. During this procedure, a fission and fusion process of broadly distributed (macro)droplets leads to uniform well defined nanodroplets in the size range between 50 and 500 nm [61, 67, 68]. While the presence of either a sterical or electrostatic surfactant prevents these droplets from coalescence, the kinetic stabilization is accomplished by the suppression of Ostwald ripening by the addition of a costabilizer to the dispersed phase [69, 70]. The negligible solubility of this compound in the continuous phase creates an osmotic pressure in the droplets, thus counteracting the Laplace pressure. As a result the net diffusion between the droplets is inhibited and therefore, stable droplets of the same composition as the dispersed phase prior to emulsification are obtained and can be classified as “nanoreactors” [62]. As a result, the composition of the polymeric particles after polymerization resembles the composition of the monomer phase, thus enabling the equal distribution of all different functionalities in each particle. Similar to microemulsions, also miniemulsions can either be realized as direct (W/O) or inverse (O/W) systems. While the first case is a well established approach to solid

polymeric latexes by free radical polymerization of hydrophobic monomers [61, 68], the inverse method gives rise to the formation of hydrogel nanoparticles by diverse synthetic pathways [35].

One approach is the free radical copolymerization of hydrophilic monomers with crosslinking agents in dispersed droplets of either aqueous solutions of these compounds or their mixture without additional solvent. This pathway results in hydrogel nanoparticles after transferring the polymerized latexes to water as continuous phase. Examples include the formation of polyacrylamide (PAAm) [71, 72] and PHEMA [72, 73] based microgels. Moreover, since the only main requirement for copolymerization of different monomers is their immiscibility with the continuous phase, this approach is highly tolerant to a broad variety of monomers and can be used to prepare e.g. highly charged microgels [74]. Figure 3.2 illustrates the described synthetic pathway schematically.

An alternative to the crosslinking copolymerization of hydrophilic monomers is the gel formation upon crosslinking of preformed polymers in inverse miniemulsion. This concept has been realized by a sophisticated approach which is based on the ultrasonication of a mixture of two inverse miniemulsions A and B containing a solution of a preformed polymer and a solution of the crosslinking agent, respectively. Upon the appliance of high shear forces a fission and fusion process between the individual droplets of both systems results in the mixing of the components which induces the crosslinking reaction. This method was

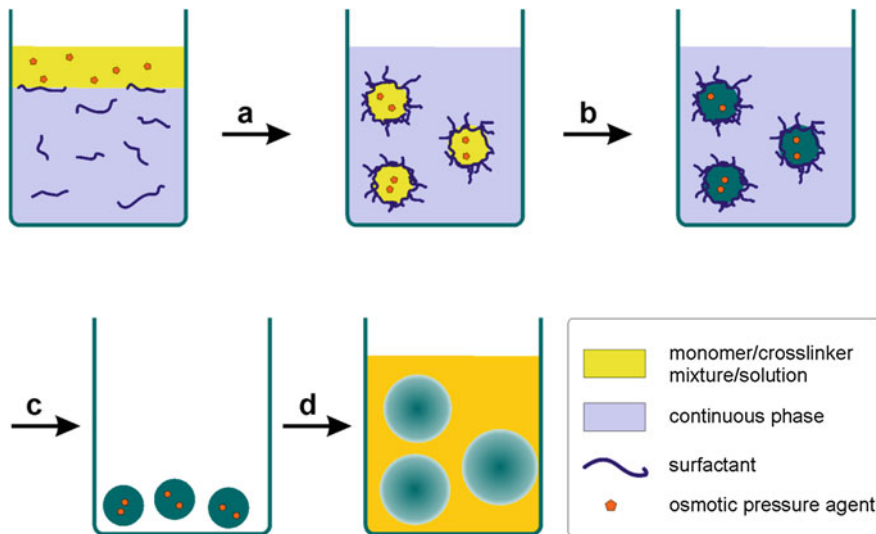


Fig. 3.2 Schematic representation of microgel preparation by radical crosslinking polymerization in (inverse) miniemulsion: **a** emulsification and homogenization, **b** polymerization, **c** removal of excess surfactant by washing/dialysis and subsequent freeze-drying and **d** redispersion of microgels in a good solvent for the network-forming polymer by swelling. Reproduced with permission from [1]. Copyright 2012 Elsevier

successfully applied to the formation of well defined gelatin microgels covalently crosslinked by glutaraldehyde [68, 75]. In addition, more complex gel structures can be obtained as well. As an example the formation of crosslinked starch capsules was achieved by the interfacial crosslinking polycondensation in inverse minemulsion. Here, the dispersed droplets consisted of an aqueous solution of starch which was covalently crosslinked only at the droplets surface by the addition of 2,4-toluenediisocyanate (TDI) to the continuous phase [76].

Microgel Synthesis in Other Compartments

Based on the concept of closed nanoreactors, different supplementary approaches are described in the literature. A highly interesting method was described by Kazakov et al. [77]. By using liposomes as compartments for the photo initiated polymerization of monomers, hydrogel nanoparticles were obtained after solubilization of the lipid double layer. Despite that, the formation method of microgels using micro-fluidics gives rise to well defined spherical particles in the size range of several micrometers [78].

3.3 Stimuli-Responsive Microgels: Features and Applications

Stimuli-responsive or environmentally-sensitive micro- or nanogels are intramolecularly crosslinked polymeric nanoparticles where a specific molecular design of the polymeric network structure allows the incorporation of stimuli-sensitive properties into the gel. In this context, a broad variety of triggers finds application. These can be classified into two main categories: (a) physical stimuli such as e.g. changes in temperature, the appliance of light, electric- or magnetic fields and (b) chemical stimuli including changes in pH, ionic strength or the presence of chemical or biological compounds. Since the latter are often characteristic features of a specific location, microgels changing their properties upon their (re)location in such an environment are often called “smart” materials since they respond to an inherent feature of the location rather than to an externally applied trigger.

The broad selection of triggers and response mechanisms of stimuli-responsive microgels has led to a tremendous variety of applications including, among others, sensors [79], optics [80], colloidal crystals [81, 82], and loading and release applications [83].

3.3.1 *Microgels for Loading and Release Applications*

In the field of biomedical applications, the controlled delivery of pharmaceutically active substances holds promise to be a key concept for future treatment of diseases. Here, hydrogel nanoparticles represent an outstanding approach, since they allow the incorporation of water-soluble drugs, including proteins and nucleic acids, in the gel [84]. The utilization of biocompatible and nonantigenic materials enhances the protection of the payload from hostile enzymes until the delivery to targeted tissues [85]. Due to their chemically crosslinked structure and hydrophilic chains on the surface (preferably non-charged polymers such as e.g. PEG or poly(*N*-vinylpyrrolidone), microgels are characterized by a higher stability for prolonged circulation in the blood stream [86]. This unique feature is often referred to as a “stealth” effect, since opsonisation by macrophages and non-specific binding to cells is dramatically decreased [87]. Moreover, due to their soft architecture, microgels are able to flatten themselves onto vascular surfaces, thus simultaneously anchoring in multiple points. Thereby, their retention in the targeted disease site is enhanced [85]. Additional advantages include the ease of preparation, high stability and the good dispersibility in water [88]. In the special case of stimuli-responsive microgels, the drug loading and release profile can be modulated by external stimuli, thus greatly improving the loading efficiency and enhancing the bioavailability to reduce side effects [44].

Especially the ability to control the loading and release of functional compounds into and from microgels renders stimuli-responsive microgels highly interesting materials not only for the application in biomedical fields but also e.g. in the area of triggered catalysis. Here, the embedding of catalysts in a particulate stimuli-responsive (hydro)gel network allows one to trigger the activity of the catalytically active compound. This can either be achieved by a triggered release of the catalyst from the microgels upon swelling or degradation of the network, or by modulating its accessibility to specific reagents. In the latter case the catalyst remains in the network and the diffusion of substrates to and from the catalyst is triggered e.g. by the swelling of the surrounding gel. Examples realizing these described concepts are based on immobilized enzymes [89, 90] or catalytically active metal nanoparticles embedded in microgels [90–92].

3.3.1.1 Network Characteristics

Polymeric (micro)gels are networks that absorb large quantities of solvent while remaining insoluble due to the crosslinking of the individual polymer chains. As a result of the crosslinking, properties of individual polymers become visible on a macroscopic scale, thus rendering polymeric gels a unique class of materials. A key feature to the determination of the nanoscopic structure of gel networks is the understanding of the solvent-sorption capabilities since the latter is crucially dependent on the molecular interactions between the network-forming polymer

and the solvent as well as e.g. the crosslinking density. Investigations on and mathematical descriptions of the parameters defining the structure of swollen networks were widely studied for the case of macroscopic hydrogels [4, 26, 93]. Even though the developed models can mostly be transferred to their microgels analogues, specific deviations may result from inherent features of these nanoscale materials such as e.g. their high surface area.

In general, for the description of the nanostructure of polymeric gel networks, three parameters are crucial: (1) the polymer volume fraction in the swollen state: $v_{2,s}$, (2) the number average molecular weight between crosslinks: \overline{M}_c and (3) the network mesh size: ξ [7].

For loading and release applications of non-porous (micro)gels, the network mesh size is the most important parameter determining the mobility of embedded functional substances and their rates of diffusion within a swollen (hydro)gel matrix. Especially the comparison of the mesh size of the network relative to the hydrodynamic diameter of the compound to be delivered is of high interest since theoretically, the diffusion of the latter is hindered when mesh sizes approach the size of the payload as shown in Fig. 3.3 [94]. This state can e.g. be beneficial for an efficient loading of functional compounds upon entrapment in the network.

The most important factors that influence the mesh size of a gel are the degree of crosslinking and the interaction of the network-forming polymer with the solvent. Since in stimuli-responsive (micro)gels these properties can be influenced by external triggers (degradation of crosslinks, change in physico-chemical parameters of the polymers), a determination of the mesh size before and after the appliance of the respective stimulus enables to predict the loading and release profile of a specific compound. Therefore it is generally of high importance to be able to derive the mesh size from measurable macroscopic features of the respective (micro)gels. The mesh size (ξ) can be described as follows [95]:

$$\xi = v_{2,s}^{-1/3} (\overline{r}_0^2)^{1/2} = Q^{1/3} (\overline{r}_0^2)^{1/2} \quad (3.1)$$

Here, $v_{2,s}$ is the polymer volume fraction in the respective swollen state and describes the amount of solvent imbedded in the network. It can either be described

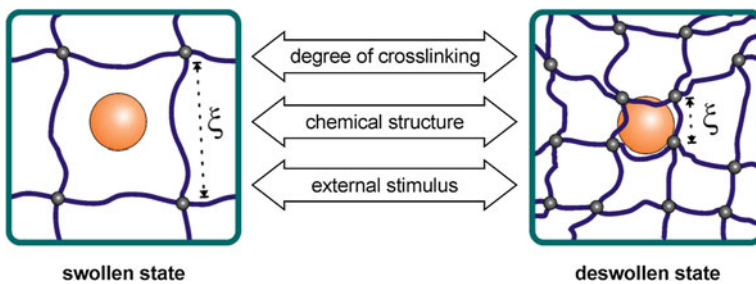


Fig. 3.3 Schematic representation of mesh sizes in swollen and deswollen gel networks. Adapted with permission from [94]. Copyright 1999 Elsevier

as the ratio of the polymer volume (V_p) to the swollen gel volume (V_g) which is the reciprocal of the volumetric swelling ratio (Q). Moreover, Q can be related to the densities of solvent (ρ_1) and polymer (ρ_2) and the mass swollen ratio (Q_m): [93]

$$v_{2,s} = \frac{V_p}{V_g} = Q^{-1} = \frac{1/\rho_2}{Q_m/\rho_1 + 1/\rho_2} \quad (3.2)$$

In the case of microgels, Q can be calculated from the hydrodynamic particle diameters in the swollen and non-swollen state. As these can be determined by e.g. DLS measurements under different conditions (solvents, temperatures, etc.) or combinations of DLS and electron microscopic investigations (SEM, TEM), this parameter is easily accessible. In the case of macroscopic gels, the swelling ratio can be determined by gravimetric analysis as the mass swollen ratio.

The next factor to be determined in order to calculate the gel mesh size based on Eq. (3.1) is the root-mean-squared end-to-end distance of network chains between two adjacent crosslinks in the unperturbed state. As described by Canal and Peppas, it can be calculated as follows [95]:

$$(\bar{r}_0^2)^{1/2} = l(C_n N)^{1/2} = l \left(C_n \frac{2\bar{M}_c}{\bar{M}_r} \right)^{1/2} \quad (3.3)$$

C_n is the Flory characteristic ratio, l is the bond length along the polymer backbone, N is the number of bonds between two adjacent crosslinks, \bar{M}_r is the molecular weight of one repeating unit (monomer) of the respective network-forming polymer and \bar{M}_c is the average molecular weight between two adjacent crosslinks. While for a specific network-forming polymer l , C_n and \bar{M}_r can be obtained from the literature, \bar{M}_c is the last key parameter to be determined in order to calculate the mesh size accordingly to Eq. (3.1). In general, this factor can be obtained from the Flory-Rehner equation [29]:

$$\frac{1}{\bar{M}_c} = \frac{2}{\bar{M}_n} - \frac{\left(\frac{\bar{v}}{V_1}\right) \left[\ln(1 - v_{2,s}) + v_{2,s} + \chi_{12} v_{2,s}^2 \right]}{v_{2,s}^{1/3} - \frac{v_{2,s}}{2}} \quad (3.4)$$

Here, \bar{M}_n is the number average molecular weight and \bar{v} is the specific volume of the polymer prior to crosslinking; χ_{12} is the solvent-polymer interaction parameter. Since this equation was originally derived for neutral divinyl crosslinked networks for which the molecular weight \bar{M}_n of the respective polymer is known, more complex derivations of this equation have been developed by Peppas et al. in order to expand the theory to ionic gels or gels crosslinked during polymerization [4]. As a useful approximation, it has been shown by Mason et al. [96]. that in the case of highly swollen ($Q > 10$) neutral polymeric gels, \bar{M}_c can be derived directly from the swelling ratio as:

$$Q = \left[\frac{\bar{v} \left(\frac{1}{2} - 2\chi_{12} \right) \bar{M}_c}{V_1} \right]^{3/5} = \beta (\bar{M}_c)^{3/5} \quad (3.5)$$

By combining Eqs. (3.5) or (3.4) with (3.3) and subsequently combining (3.3) and (3.1), a simple model is available to determine the mesh sizes of polymeric gels from facile equilibrium swelling experiments. Data obtained from these calculations not only allow one to predict and tailor the loading and release profiles of (micro)gels, but also enable to give information about physical properties of the network such as e.g. mechanical strength and degradability [95–97].

Release From Microgels

In general, the high solvent sorption capabilities of microgels induce completely different release mechanisms compared to non-swollen matrices. The release from (micro)gels is governed by passive diffusion of the payload through the (hydro)gel network and—depending on the rate limiting step of the controlled release—three main categories of release mechanisms can be distinguished:

- (1) Diffusion-controlled
- (2) Swelling-controlled
- (3) Chemically-controlled.

Since an efficient delivery of (pharmaceutically) active compounds from microgels crucially depends on the particular release mechanism, it is of high interest to be able to predict the respective time-dependent release profile. Several simple and sophisticated models have been developed to achieve this goal and are based on the understanding of the underlying mechanism and the identification of the key parameters which govern the release. In the following sections, these considerations are described for the above mentioned different release mechanisms.

Diffusion-Controlled Release Systems

In this case, two main concepts can be distinguished depending on the internal structure of the gel network. Considering porous gels, the pore sizes of the gels are typically much larger than the hydrodynamic diameters of the embedded compounds. As a result, the diffusion coefficient of the specific substance is rather governed by the porosity and tortuosity of the gel than the internal network structure, thus resulting in limited control over the release [98]. In contrast, in homogeneous networks or porous gels with pore sizes comparable to the dimensions of the payload, the polymeric chains in the crosslinked network provide a steric hindrance to the compound to be delivered and therefore influence its diffusion coefficient [98, 99]. Here, the mean free diffusion path length of the embedded compound is decreased as the average free volume per molecule available to the compound is decreased. As a result, the diffusion coefficient is decreased compared to the solute state [97]. This general dependency of the diffusivity on fundamental network characteristics, such as mesh sizes and solvent content, is the underlying concept of several theoretical models which have been

developed for predicting diffusion coefficients of active compounds in gels. In general, the relationship between diffusivity in gels and in solution can be described as follows: [93]

$$\frac{D_g}{D_0} = f(r_s, v_{2,s}, \xi) \quad (3.6)$$

In this equation, D_g and D_0 represent the diffusion coefficients of the respective substance in the gel network and in solution while r_s is the hydrodynamic radius of the substance to be delivered, $v_{2,s}$ is the polymer volume fraction and ξ is the mesh size of the network. While several theories have been developed to describe this relationship, a prominent example for the description of the correlation between diffusivity and network structure is based on a free-volume approach and was developed by Lustig and Peppas as follows [100]:

$$\frac{D_g}{D_0} = \left(1 - \frac{r_s}{\xi}\right) \exp\left(-Y \left(\frac{v_{2,s}}{1 - v_{2,s}}\right)\right) \quad (3.7)$$

Here, Y is the ratio of the critical volume which is required for a translational movement of the embedded compound and the average free volume per molecule of solvent [93].

It becomes obvious that this approach takes into account the assumed crucial influences of the gel mesh sizes and the polymer volume fraction (the degree of solvent sorption) on the diffusivity. Regarding now typical mesh sizes of biomedical hydrogels, values between 5 and 100 nm are reported [86]. Since these size scales are considerably larger than hydrodynamic diameters of most low-molecular weight compounds (e.g. drugs), their diffusion is not significantly retarded. Therefore, a controlled delivery by a simple diffusion controlled pathway is not applicable. In contrast, this mechanism finds application for the delivery of (biologically active) macromolecules such as e.g. peptides, proteins or oligonucleotides since their release can be sustained due to their larger hydrodynamic diameters. Here, it is of special interest to design the internal network structure appropriately to achieve a desired rate of macromolecular diffusion [84]. As a result, a kinetically controlled release system can be obtained [101, 102].

Based on these considerations, the utilization of stimuli-responsive (micro)gels represents a highly advantageous approach to controlled delivery applications since it allows for the adjustment of network properties such as mesh size and polymer volume fraction upon the appliance of an external trigger. According to Eq. (3.7), the diffusion coefficient can thus be triggered externally, thereby significantly enhancing loading efficiencies and control of the release. As an example, a functional macromolecular compound can be embedded in a gel network exhibiting initial mesh sizes smaller than the hydrodynamic diameter of the compound to be delivered, thus ensuring efficient loading by hindered diffusion. By utilization of a stimuli-responsive network-forming polymer, the polymer volume fraction ($v_{2,s}$) as well as the mesh size (ξ) can be controlled by external triggers. If the change results in an increased mesh size and/or a decreased polymer

volume fraction, the diffusion coefficient of the active substance in the gel (D_g) is increased according to Eq. (3.7). This response is widely realized by changes in the physico-chemical parameters of the network-forming polymer which induce an increase in swelling of the network.

Obviously, the mesh size as an important factor governing the diffusion coefficient of the embedded compound is known to crucially depend on the crosslinking density (see Eqs. (3.1) and (3.3)) as well. Hence, by the utilization of cleavable crosslinking points in a network, the mesh size and thereby the diffusivity can be triggered by degradation of crosslinking points. This particular example represents the border to chemically-controlled delivery systems which will be discussed in a following section.

As a last point, it has to be mentioned that diffusion controlled release is, in a lot of cases, much more complex as described in these simplified models. Here, especially interactions between the embedded compound and the polymer network (electrostatic, hydrophobic–hydrophobic, etc.) can cause severe deviations from the predicted release profiles. In order to take these phenomena into account, several theoretical models based on empirically determined diffusion coefficients have been developed to predict the release profile [93].

Swelling-Controlled Release Systems

The mechanism of swelling-controlled release systems is based on the swelling of the gel as the rate limiting step for the release, meaning that the diffusion of the embedded compound is faster than the swelling of the gel matrix. Originally, this concept was widely investigated for macroscopic hydrogels which undergo a swelling-driven phase transition from a glassy/dry state to a rubbery state [103, 104]. The embedded compounds are immobilized in the initial non-swollen network whereas their rapid diffusion is enabled in the swollen gel [93].

Transferring this concept to the nanoscale can be achieved by the utilization of stimuli-responsive microgels. Investigated approaches include the embedding of small-molecule compounds into collapsed gels and their swelling-induced release upon the appliance of an external trigger [105, 106]. A detailed description of different stimuli-responsive microgels is discussed in a following section.

However, in these cases a necessary requirement to distinguish the resulting release mechanism from the chemically-controlled alternative is the fast response to the respective trigger. Only if the change in the chemical nature/physico-chemical properties of the network-forming polymer is faster than the resulting swelling, the release mechanism is still governed by the time-scale of gel swelling and is defined as swelling-controlled.

Chemically-Controlled Release Systems

In chemically-controlled release systems, the release of a functional compound from the gel network is determined by chemical reactions in the matrix. The time-scale of the respective reaction has to be considerably slower than the diffusion of

the compound from the gel and therefore represents the overall rate limiting parameter [93]. Several approaches to chemically controlled delivery systems can be distinguished by the type of chemical reaction inducing the release. Among others, the cleavage of network-forming polymer chains resulting in surface-erosion or bulk-degradation of the (micro)gel and the cleavage of pendant chains between the polymeric network and the compound to be delivered are the most common ones. These mechanisms can be further categorized into (a) purely kinetically-controlled release systems and (b) reaction-diffusion-controlled systems. While in the first case, the (polymeric) bond degradation is the rate limiting step and the diffusion term is comparably negligible, in the second case, polymer/crosslinker degradation and diffusion terms have to be taken into account in order to be able to predict the release profile. In general, all systems based on chemically induced release methods are a class of stimuli-responsive materials.

One example for purely kinetically-controlled systems is the pendant chain approach which is based on the covalent linkage of active compounds to the gel network by cleavable linkers. Especially in the field of drug delivery, these pro-drugs or polymer-drug conjugates are widely investigated to enhance the therapeutic efficacy of drugs [107]. Realization of this approach is mostly achieved by the utilization of either hydrolytically [108, 109] or enzymatically [110] degradable linkers where the release rate is determined by the degradation rate of the respective linker (e.g. simple first-order kinetic relationships for hydrolytic degradation) [93]. If diffusion of the liberated compound is then comparably fast, these systems are purely kinetically-controlled.

Another example of kinetically-controlled release systems is the release of a compound as a result of the surface erosion of a polymeric matrix. Here, the rate of transport of the eroding reagent into the polymer is much slower than the rate of bond hydrolysis. This can be found in the case of hydrophobic (biodegradable) polymeric networks or enzymatically degradable hydrogels. In the latter case the transport rate of the enzyme through the hydrogel layer is significantly retarded in comparison to the enzymatic bond cleavage [111].

In contrast to the kinetically-controlled release systems, reaction-diffusion-controlled systems are characterized by the influence of multiple parameters on the release profile. The theoretical considerations described above mainly consider only one mechanism to dominate the release. For many cases these simplified models either purely based on diffusion, swelling or degradation mechanisms provide a good correlation between experimental data and the predicted release profiles. In reality however, different mechanisms can occur simultaneously. As an example where the deviations from these simplified models become obvious, bulk degrading release systems have to be mentioned [93]. Here, the drug release is governed by both network/crosslink degradation and molecule diffusion, thus defining them as reaction-diffusion-controlled systems. Bulk degradation can either be achieved by the cleavage of the backbones of the network forming polymers or the crosslinking points. In the latter case, the cleavage of crosslinking points correlates with a decreasing crosslinking density and an increasing mesh size. Therefore, the diffusivity of an embedded compound is no longer constant but

increases with propagating crosslinker degradation (i.e. time-dependent mesh size). As a result the respective diffusivity correlation as described in Eq. (3.7) can be simplified during the initial stages of degradation to [96]:

$$1 - \frac{D_g}{D_0} = \frac{r_s}{\xi} \sim e^{-7/5jk_E' t} \quad (3.8)$$

Here, jk_E' is the pseudo-first-order reaction constant for the cleavage of a degradable crosslinking bond. It can be concluded that, upon degradation, the diffusion coefficient D_g increases and that the diffusivity depends on the bond cleavage kinetics [112].

Loading of Microgels

In general, the incorporation of active compounds into (micro)gel matrices can be realized by either one of the two following concepts:

- (1) *post-formation* loading
- (2) *in situ* loading.

In the first case, functional compounds are embedded in preformed (micro)gel networks. For that, the respective materials are mostly soaked in a concentrated solution of the respective substance and loading is achieved by absorption. Regarding the second approach, the embedding of substances to be released is achieved during the network formation [93].

As described in the previous section, the release from microgels is mainly governed by the diffusion of the embedded compound from the network. Several release mechanisms, based on controlling the diffusivity, have been examined. In order to ensure an efficient loading of microgels, an underlying requirement is the prevention of diffusion (i.e. leakage) until the targeted site or time point for release is reached. In dependency on the desired release mechanism, this can be achieved by several different strategies.

Loading pathways for diffusion-controlled release systems. If the diffusivity of embedded compounds is only controlled by adjusting the network parameters to fixed values and thus decreasing the diffusion coefficient of the substance to be released in the gel, a solely kinetically-controlled release mechanism is realized. An efficient loading is hereby dependent on the level of retardation of diffusivity, meaning that only for very slow release kinetics a prevention of leakage can be realized. As a result the diffusion into the gel is very slow as well. Therefore, an *in situ* loading pathway is the concept of choice here. In contrast, the loading efficiency can dramatically be increased by the utilization of stimuli-responsive materials. Especially the utilization of polyelectrolytes as network-forming polymers gives rise to an enhanced loading efficiency by the exploitation of electrostatic interactions between the functional compound and the gel network. A release can be achieved by triggering these interactions by e.g. additional ions competing

with the compound to be delivered thus weakening their attraction to the network. Loading can be either achieved in situ or in a *post-formation* step by adjusting the ionic strength and pH of the dispersion accordingly. If more complex binding ligands are used to ensure attachment of a compound to the network, models for release description have to take both compound-polymer interaction and diffusion into account. Another highly prominent example for a loading concept based on preventing diffusion of compounds by dynamically changing network properties is the entrapment of functional macromolecules. In this case, the mesh size of a collapsed network is smaller than the hydrodynamic diameter of the compound to be delivered, thereby hindering its diffusion. This can either be achieved by an in situ loading approach or by a *post-formation* method whereby the stimuli-sensitive properties of the gel allow the entrapment of a compound by a triggered contraction of the network (i.e. a reduction of mesh sizes). Using either the same reverse stimulus or an orthogonal second one, the substance can be released by increasing the mesh sizes as a result of (micro)gel swelling.

Loading pathways for swelling-controlled release systems. An efficient loading of functional compounds is here realized by their embedding in non-swollen glassy, dry or collapsed gel networks, thus hindering an unwanted diffusion. This can be achieved either in situ by the formation of microgels dispersed in a non-solvent for the polymer chains or by the *post-formation* approach which is based on a (stimulus)induced network collapse or drying of the loaded (micro)gels. While the respective release mechanism is different from diffusion controlled systems, loading can obviously be achieved in a similar way.

Loading pathways for chemically-controlled release systems. Depending on the respective release mechanism, this concept can be realized by different pathways. In the case of bulk-degrading release systems, the entrapment of functional compounds is mainly realized either by (radical) crosslinking copolymerization of monomers and crosslinking agents or covalent or physical crosslinking of pre-formed polymers in the presence of the substance to be released. An efficient loading is ensured by a hindered diffusion due to mesh sizes in the size range of the hydrodynamic diameter of the active molecules. For pendant chain degrading systems, a functional compound is attached to the polymeric network by a degradable linker therefore preventing leakage. This can either be realized by the functionalization of the compound with a polymerizable unit linked to the active molecule via a cleavable linker and the in situ copolymerization with the network forming monomers and crosslinking agents, or by the *post-formation* attachment of the substance to be delivered to the preformed gel network.

3.3.2 Different Approaches to Stimuli-Responsive Microgels

As mentioned before, stimuli-responsive microgels are a unique class of materials since they combine specific interesting features: (a) The characteristics of gel networks such as e.g. the structural integrity and a high solvent content in their

swollen state gives rise to loading and release applications of functional compounds. (b) Transferring these inherent gel features to the nanometer scale bears the advantages of a high surface area and a high diffusibility and mobility of the gel nanoparticles, thus allowing their facile distribution in specific environments. (c) In the case of stimuli-responsive microgels, a big advantage compared to their macroscopic analogues is their comparably much faster response to a stimulus. It was found that relaxation time of the volume change of a gel is proportional to the square of its radius [113].

In this chapter, different approaches to stimuli-responsive microgels are introduced and their potential for loading and release applications is reviewed. Figure 3.4 schematically depicts possible mechanisms for changes of stimuli-responsive microgels characteristics. The respective response of microgels to a specific external trigger is often characterized by a change in the physico-chemical properties of the polymeric network, thus resulting in a controlled swelling and deswelling of the particles. This effect is generally accompanied by changes of numerous important features of the microgels such as, e.g., the solvent content, the mesh size, the refractive index and the interior network permeability (see Fig. 3.4a). Even though this (reversible) volume phase transition is often described as the defining characteristic for stimuli-responsive microgels in the literature, several additional response mechanisms of microgels to an external trigger can be found. Alternatively, the utilization of cleavable crosslinking points in a gel represents a method for triggering the complete (reversible) decomposition of the network architecture by using external stimuli (Fig. 3.4b). Moreover, the introduction of stimuli-sensitive groups onto microgels surfaces can be used to trigger the interaction either between the gel nanoparticles and external compounds or among each other (Fig. 3.4c). As a last example, the utilization of

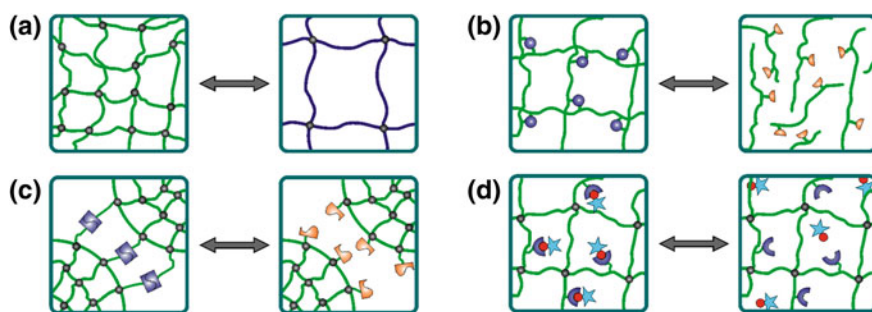


Fig. 3.4 Schematic representation of different mechanisms of stimuli-responsive microgels: **a** gel swelling/deswelling due to stimuli-induced changes in physico-chemical parameters of the network-forming polymer; **b** gel dissolution/formation upon triggered degradation/formation of crosslinking points; **c** externally triggered degradation/formation of intramicrogel aggregates and triggered attachment/release of functional compounds onto/from the interior microgels network. **d** triggered attachment/release of functional compounds onto/from the interior microgels network. Reproduced with permission from [1]. Copyright 2012 Elsevier

linkers—degradable upon the appliance of an external trigger—between functional compounds and the microgel network is worth mentioning (Fig. 3.4d).

Since a discussion of all stimuli-responsive mechanisms would extent the scope of these remarks, the following section deals with the description of stimuli-responsive microgels for loading and release applications by either exploiting triggered changes in the physico-chemical parameters of the network-forming polymer or labile crosslinking points.

3.3.2.1 Stimuli-Responsive Microgels Based on Triggered Changes in the Physico-Chemical Parameters of the Network-Forming Polymer

The fundamental concept of stimuli-responsive microgels based on triggered changes of the physico-chemical parameters of their network-forming polymers is a (reversible) volume phase transition of the gel nanoparticles as response to an external trigger. This behavior is induced by a changed solvation of the polymer chains as a result of reversibly triggered variations in the interplay between solvent–solvent, solvent–polymer and polymer–polymer interactions.

Temperature-Sensitive Microgels

Probably the most prominent approach to thermo-sensitive microgels is based on the utilization of poly(*N*-isopropylacrylamide) (PNIPAAm) as network-forming polymer [44]. This polymer exhibits a lower critical solution temperature (LCST) in water. The underlying mechanism is an endothermic, entropically driven phase transition from a random coil to a collapsed globule at temperatures above ~ 32 °C [114]. Two main effects influence this behavior: on one hand, the hydrogen bonding between amide groups and water molecules and on the other hand, the entropically driven polymer–polymer interactions due to the hydrophobic isopropyl groups. At low temperatures the polymer–water interactions are favored, thus resulting in a random-coil configuration of the polymer. If now the temperature is increased, the hydrophobic polymer–polymer interactions become more dominant, water is expelled due to the weakened hydrogen bonds and the polymer chain reorganizes to a collapsed globule [115]. In the case of microgels formed from crosslinked PNIPAAm polymers, the inherent thermo-sensitive characteristic of the network-forming polymer is transferred to the entire network. Here, at temperatures below the LCST of the polymer, the gel nanoparticles are swollen and shrink upon increasing the temperature. This phase transition occurs at the so called volume phase transition temperature (VPTT) which is close to the LCST of the PNIPAAm chains [116]. Nevertheless, compared to free PNIPAAm chains, the phase transition of microgels consisting of the same crosslinked polymer is not as sharp and shifted to higher temperatures. This deviation was shown to result from the heterogeneous crosslinking apparent in the network. Since in the case of PNIPAAm microgels

longer polymer segments between two crosslinking points collapse at lower temperatures as shorter ones, the observed broad volume phase transition can be considered as a superposition of all phase transition temperatures of the different polymer segments [44, 117].

PNIPAAm based microgels are mostly prepared by precipitation polymerization exploiting the LCST of the polymer for nanoparticles formation. Since the first synthesis of such structures reported by Pelton and Chibante in 1986 [118], the well defined response of these materials to temperature as external trigger has led to a broad variety of sophisticated applications over the years. In this context, the VPTT of PNIPAAm close to the physiological temperature renders these systems highly interesting for biomedical fields such as e.g. drug delivery. However, even though the VPTT of PNIPAAm microgels around 33 °C is already higher than the LCST of the free polymer, the value is still lower than the body temperature. Therefore, various attempts have been performed to increase the VPTT by the incorporation of either anionic [48] or cationic [119] hydrophilic comonomers. Although these attempts were successful to increase the VPTT of the resulting microgels, the volume transition was broadened as well. This effect can be influenced by the exploitation of different crosslinking techniques such as the self-crosslinking of PNIPAAm [120] or the utilization of inorganic clay as crosslinker [121] but results in microgels of a reduced VPTT again. It can be seen that the specific adjustment of the VPTT and the transition broadness to values suitable for applications in biomedical fields is rather complex and still an important research area.

In the context of temperature-controlled drug delivery systems based on PNIPAAm microgels, several loading and release concepts have been investigated. In general, it can be distinguished between release mechanisms based on a gel collapse upon increases in temperature and mechanisms based on gel swelling upon lowering the temperature.

As examples for the release of entrapped drugs in response to increases in temperature, either passively exploiting the higher temperature of some pathological tissues or cells [122] or actively triggering the release by hyperthermia [123] are two concepts worth mentioning. Here, the release is based on a squeeze-out mechanism: as the microgels collapse due to an increased temperature, water is expelled from the network and the drug is released. This concept of drug release upon microgel deswelling was described by Nolan et al. for the delivery of insulin from PNIPAAm microgels [124]. The same volume transition of PNIPAAm microgels can be used for cancer therapy by exploiting the inherent volume change of the microgels even without the need for additionally incorporated pharmaceutically active compounds. As recently described by Lyon and coworkers, the aggregation of collapsed folate functionalized PNIPAAm microgels in the cytosol at elevated temperatures resulted in temperature-dependent cytotoxicity [125].

In contrast to the previously mentioned squeeze-out mechanism induced by heating, the release of entrapped molecules upon cooling-induced particle swelling is based on an increased diffusivity of the embedded compounds in a gel network of increased mesh sizes. A sophisticated approach described by Nayak et al. is

based on thermo-sensitive hollow PNIPAAm microspheres prepared by the removal of a sacrificial core from core/shell microgels [54]. In a similar template-assisted synthetic pathway, Gao et al. prepared thermo-sensitive PNIPAAm nanocapsules loaded with FITC as model protein. While the fluorescent macromolecule was efficiently entrapped in the cavity at temperatures above the LCST of the shell-forming polymer, decreasing the temperature enabled its release [126]. Exploitation of the externally triggered temperature-dependent swelling of microgels for drug delivery applications was recently described by Park et al. using a brief cold-shock treatment to induce the swelling of crosslinked Pluronic (PEO-*b*-PPO-*b*-PEO) based microgels [127].

Although lowering the local temperature is an interesting novel concept to temperature-triggered cancer therapy based on thermo-sensitive materials, the utilization of elevated temperatures as stimulus is comparably more facile to realize by established methods such as e.g. hyperthermia. As mentioned above, the utilization of the “squeeze out” mechanism of negatively temperature-sensitive microgels based on polymers exhibiting a LCST (e.g. PNIPAAm, PVCL [128], etc.) is a widely investigated approach to realize this concept but bears some serious drawbacks. Here, the formation of a skin layer on the deswelling microgels can significantly hinder the desired drug release upon heating [85]. As a consequence, the utilization of materials exhibiting a positive volume phase transition—i.e. an increase in swelling upon increasing temperature—is assumed to dramatically enhance the efficiency of thermo-sensitive microgels for drug delivery applications.

Polymeric materials fulfilling this criterion are polymers exhibiting an upper critical solution temperature (UCST). A widely investigated example is based on copolymers of acrylamide and acrylic acid. In these polymers, the volume change is driven by hydrogen bonds between the macromolecules. At temperatures below the UCST the polymer–polymer interaction is favored, thus resulting in a collapsed coil structure of the macromolecule. Upon increasing the temperature, these interactions are weakened due to the breakage of hydrogen bonds and the polymer–solvent interaction becomes dominant. As a result, the polymer exhibits a random-coil morphology [129, 130]. While the preparation of macroscopic hydrogels from these materials was achieved by hydrophobic association cross-linking by Yang et al. [131], the transfer of this concept to the nanoscale was recently demonstrated by Echeverria et al. by radical crosslinking copolymerization of acrylamide with acrylic acid in the presence of *N,N'*-methylenebis(acrylamide) in inverse emulsion [132]. Microgels prepared by this synthetic pathway represent an interesting alternative to the widely examined systems exhibiting a negative volume phase transition.

Moreover, thermo-sensitive microgels containing functional compounds not only find application in release applications. The temperature-dependent volume phase transition and the corresponding change in mesh sizes of the gel network can also be used to trigger the accessibility of embedded active compounds to substances in the microgel environment. As example, Park et al. described the embedding of β -galactosidase in PNIPAAm-*co*-PAAm microgels and

demonstrated the possibility to trigger the enzymatic hydrolysis of *o*-nitrophenol-*p*-D-galactopyranoside (ONPG) by changing the temperature in either a batch mode or a packed bed reactor [89]. In addition, Ballauff and coworkers investigated the immobilization of catalytically active metal nanoparticles in PS/PNI-PAAm core/shell nanoparticles and demonstrated the temperature triggered catalytic activity [91].

Microgels Sensitive to pH and Ionic Strength

Microgels prepared by crosslinking of weak polyelectrolytes exhibit a pH-dependent volume phase transition. Depending on the composition of the polyelectrolyte, it can be distinguished between acid containing cationic, base containing anionic or acid and base containing amphoteric microgels. The underlying mechanism of the swelling/deswelling of these materials as response to changes of the pH of the surrounding medium is the protonation/deprotonation of the weakly acidic or basic groups along the chain of the network-forming (co)polymers. The key parameter determining the swelling behavior of pH-responsive microgels is the respective critical pH value (pH_c) at which the phase transition occurs. Although this parameter is governed by the chemical nature of the polyelectrolyte, the respective pH value is defined as the point where the degree of ionization of the network-forming polymer changes. As a result of either an increased or decreased osmotic pressure within the microgels, swelling or deswelling occurs. Even though the pH_c is correlated to the respective pK_a or pK_b values of the acidic or basic groups on the polymer backbone, it has been demonstrated that the apparent pH_c value of microgels can deviate from the values of their low molecular weight analogues [85]. Especially the introduction of more hydrophobic (alkyl) moieties to the polyelectrolyte backbone can shift the pH_c values [133].

Anionic microgels. In the case of anionic microgels composed of weak acidic polymers such as e.g. poly(meth)acrylic acid, the gel network is collapsed at pH values below the pK_a of the polyelectrolyte due to the absence of charges and the resulting comparably hydrophobic character of the network. Increasing the pH above the pK_a of the polymer, the acidic groups are deprotonated, thus increasing the hydrophilicity of the polymer. Moreover, due to the presence of generated anionic groups in the network, their electrostatic repulsion and the generated osmotic pressure, the swelling is significantly enhanced. In general, the swelling profile of anionic microgels depends on various parameters of the network-forming polymer such as the amount of acidic groups, their respective pK_a values and the crosslinking density.

The influence of the pK_a value of different acidic moieties attached to a polymeric backbone in the microgel network on the swelling profile was examined by Needham and coworkers [134]. It was shown that in microgels containing a fixed amount of methacrylic acid groups together with similar amounts of different acidic moieties, the pH range of the swelling response shifted by an amount proportional to the solution pK_a 's of the different functional groups.

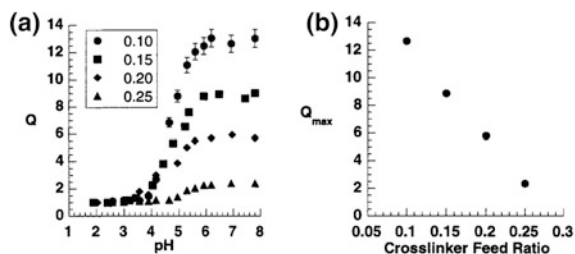


Fig. 3.5 **a** Plot of the equilibrium swelling ratio (Q) for the different cross-link density microgels versus the pH of the external solution. **b** Plot of the maximum swelling (Q_{max}) for the different cross-link density microgels versus the feed ratio for the pHs greater than 5.3. Reproduced with permission from [135]. Copyright 1999 American Chemical Society

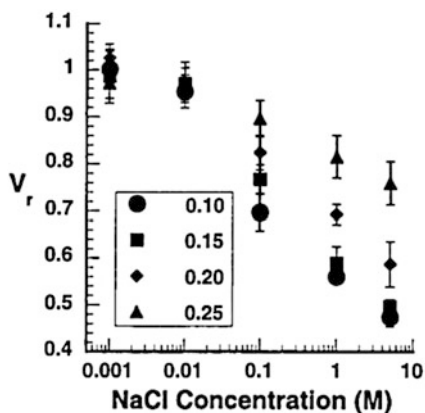
In order to examine the influence of the crosslinking density, detailed investigations on the pH-dependent swelling behavior of poly(methacrylic acid-*co*-acrylic acid) microgels have been performed by Eichenbaum et al. [135]. Microgels were prepared by crosslinking precipitation copolymerization of methacrylic acid and 4-nitrophenyl acrylate in the presence of various amounts of MBA as crosslinking agent. The subsequent hydrolysis of the nitrophenyl groups represents a sophisticated synthetic pathway to highly charged microgels which is challenging by precipitation polymerization of the respective acid monomers. It was demonstrated that the microgels exhibit a volume phase transition from the deswollen to the swollen state upon increasing the pH above pH 5.3. Furthermore, it was observed that the maximum degree of swelling (Q_{max}) at pH values > 5.3 decreased linearly with an increasing degree of crosslinking (i.e. the feed ration of MBA). Figure 3.5 shows the respective plots adapted from the publication [135].

Another highly important factor to be considered in the field of microgels based on polyelectrolytes is the dependency of the swelling profile on the ionic strength of the surrounding medium. Here, the addition of NaCl to highly swollen microgels at pH values above the pH_c was found to result in a decrease of the swelling ratio. This effect can be explained by a shielded electrostatic repulsion of the anionic groups due to the presence of the positively charged sodium counterions. The respective plot derived from the publication is shown in Fig. 3.6 [135].

Since the observed swelling profiles in dependency on the crosslinking density (see Fig. 3.5) were found to be in good agreement with a model derived from the Flory–Huggins thermodynamic theory for the swelling of ionic networks [135], these findings represent an important step to be able to optimize microgels for their specific utilization in loading and release applications.

Loading of anionic microgels can e.g. be achieved via a post-formation pathway by exploiting the electrostatic interactions between anionic groups in the swollen gel network and positively charged macromolecules [136] or low molecular weight drugs [137]. An important factor to be considered is the careful adjustment of the pH of the microgel dispersion to guarantee an efficient loading. In this context, three parameters defining the optimum pH value for loading have

Fig. 3.6 Plot of V_r for the different cross-link density microgels versus NaCl concentration in the high pH regime ($\text{pH} > 5.3$). Reproduced with permission from [135]. Copyright 1999 American Chemical Society



to be taken into account: (1) the microgels should be in their swollen state to ensure the diffusion of the compound into the network, (2) the acidic groups of the network should be deprotonated to enable the loading due to electrostatic interactions with the functional compound and (3) for the same reason, the functional compound should exhibit a positive net charge. While the loading of functional macromolecules such as e.g. proteins into the microgels is further determined by permeability of the gel network and respective size exclusion experiments can even be used to estimate the mesh size of the network [135], the loading of small molecules is dependent on their partition coefficients and resulting binding affinities, molecular packing and the condensation of the network upon loading [135].

Ionic microgels loaded with functional compounds can be used for drug delivery applications by responding to pH changes at the targeted delivery site. Here, it is exploited that the extracellular pH of tumor tissues is more acidic than the pH of the surrounding healthy tissues [138]. Moreover, the pH of intracellular lysosomes or endosomes is shifted to more acidic values than the cytosolic pH [139]. Based on these considerations, Das et al. demonstrated the utilization of PNIPAAm-*co*-PAA microgels for the delivery of doxorubicin [140]. The microgels surface was functionalized with transferrin to enable an enhanced uptake in cancer cells. The drug was released in the slightly acidic cytosol of HeLa cells due to the protonation of the carboxylic acid groups and the corresponding deswelling of the microgels and the weakened electrostatic interaction between drug and polymer network.

In contrast to this release mechanism upon lowering the pH, a pH-induced swelling of particles can also be used to enable drug diffusion out of the network. As example, poly(methacrylic acid-*co*-ethylacrylate) microgels were described by Tan et al. for the swelling induced release of incorporated procaine hydrochloride [141].

Cationic microgels. Regarding cationic microgels based on polymers containing weak basic groups such as e.g. amino moieties, the critical parameter determining their swelling behavior is the $\text{p}K_b$ value of the respective basic groups.

These cationic microgels exhibit a pH-dependent volume phase transition orthogonal to the anionic analogues. While at pH values above the pK_b value the network is collapsed due to the absence of charges, decreasing the pH below the pK_b of the incorporated basic groups induces the protonation of the latter and the positively charged groups cause the swelling of the network.

Microgels exhibiting an increase in their degree of swelling as response to a decrease of the pH represent interesting candidates for drug delivery applications based on a “smart” response to such inherent features as the acidic environment of tumor tissues and intracellular compartments. The respective release mechanism is based on enhanced drug diffusion from the network as a result of increased mesh sizes. Hence, these systems are an orthogonal approach to the previously mentioned squeeze out mechanism of anionic microgels.

The positive charges responsible for microgel swelling can be introduced to the network by various different approaches and by the utilization of several functional groups. In the field of drug and gene delivery, these cationic groups bear several advantages. On one hand, the cellular uptake of cationic compounds by adsorptive endocytosis is assumed to be enhanced by their electrostatic interaction with the negatively charged cell membrane [142]. On the other hand, cationic polyelectrolytes represent a well examined system for the complexation of DNA and oligonucleotides. In this context, polyethyleneimine (PEI) represents the “golden standard” for polyelectrolyte gene delivery systems [143].

Cationic microgels based on PEI as pH-sensitive polyelectrolyte were prepared by crosslinking of bis-activated polyethylenoxide (PEO) (both ends activated with 1,1'-carbonyldiimidazol) with PEI in an emulsification-evaporation method [144]. The cationic PEO-*cl*-PEI microgels exhibited a pH-dependent swelling profile and were used for the loading and release of either anionic amphiphilic molecules or oligonucleotides.

Another approach for the loading and release of oligonucleotides was recently described by Deka et al. [145]. Radical crosslinking copolymerization of various compositions of 2-vinylpyridine (VP) and divinylbenzene (DVB) in an emulsion polymerization yielded cationic microgels in the size range of 90–220 nm. The microgels exhibited a sharp increase in diameter upon decreasing the pH of the surrounding medium below pH 4.3. The correlating increase in network permeability was used for the simultaneous post-formation loading of the microgels with iron oxide nanoparticles and oligonucleotides. An efficient loading was hereby achieved by the entrapment of the comparably large compounds by increasing the pH. The simultaneous release was demonstrated to occur as a response to a decrease in pH.

Despite their potential for the loading and release of functional compounds of large hydrodynamic diameters, cationic microgels have also been described for the delivery of small molecule drugs. Kumacheva and coworkers reported on the synthesis of cationic microgels based on chitosan ionically crosslinked by sodium tripolyphosphate [146]. The gel nanoparticles were conjugated with apo-transferrin, and loaded with methotrexate disodium as cytotoxic drug for cancer treatment. Loading was achieved by electrostatic interactions between the

negatively charged drug and the positively charged polymer network. The loaded microgels were found to enter HeLa cells via receptor mediated endocytosis and release the drug as a response to the intracellular low-pH environment by swelling, thus killing the immortalized cancer cells.

Light-Sensitive Microgels

As described in the previous sections, a (reversible) volume phase transition in hydrogel nanoparticles as a result of a triggered change in the physico-chemical parameters of the network-forming polymer is often induced by the alteration of the hydrophilicity of polymer bound functional groups. In the case of light as external stimulus, several chromophores are known to change their polarity upon irradiation, thus being potential candidates for such approaches. Here, especially light-triggered isomerization reactions are worth mentioning. As an example, azobenzenes undergo a *trans-cis* isomerization upon the irradiation with UV light whereby the *cis* state of the molecule is characterized by an enhanced dipole moment resulting in an increased hydrophilicity. Since this reaction is reversible either via temperature or visible light induced relaxation, attaching these chromophores to a polymeric backbone represents an interesting approach for the light-triggered alteration of the overall hydrophilicity of the respective polymer. This concept was successfully applied for the formation of light-sensitive hydrogels changing their degree of swelling upon irradiation with UV light. These were synthesized by the crosslinking copolymerization of acrylamide with *trans*-4-methacroyloxyazobenzene in the presence of MBA as crosslinking agent [147]. Moreover, double stimuli responsive materials exploit the influence of the light-triggered isomerization of azobenzenes on the response range of the respective orthogonal trigger. Examples include the irradiation-induced shift of the LCST of copolymers from NIPAAm and an azobenzene group containing monomer [148] as well as the shrinking of initially swollen p(acrylic acid-*co*-acrylamido azobenzene) hydrogels (at pH values above the pK_a of the AA) by the *cis-trans* isomerization of the azobenzene moieties [149]. Even though these examples represent promising approaches to light-triggered materials (based on direct changes of the physico-chemical parameters of the polymer), their utilization in the nanoscale is up to now mainly applied to light-sensitive block copolymer micelles [150] or polymerosomes [151, 152].

Nevertheless, light-sensitive microgels can be realized by an indirect approach based on hybrid materials. These systems are composed of a photo-sensitive moiety embedded in a temperature-sensitive polymeric network. The underlying concept is the photothermal effect, meaning that upon irradiation at the resonance wavelength of the respective light-responsive compound, the light energy is translated to heat by non-irradiative relaxation. As a result to the locally increased temperature of the surrounding thermo-sensitive network, the latter exhibits a volume phase transition. Although this concept can be achieved by the utilization of a broad variety of photo-sensitive compounds and temperature-sensitive

polymers, the embedding of dyes [153, 154] or metal nanoparticles (NP) [155] into PNIPAAm gels are the most widely examined approaches.

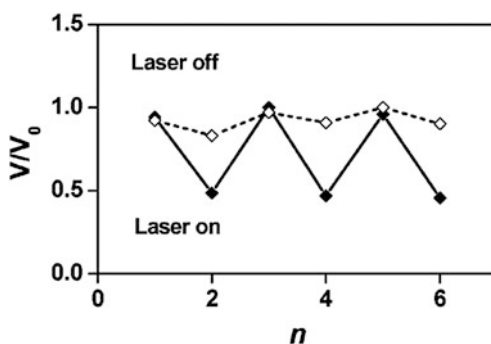
Especially the incorporation of Au or Ag nanoparticles or -rods into thermo-sensitive microgels is a highly interesting concept and the preparation of such materials can be achieved by different pathways including the in situ reduction or precipitation of NP in the network [156], the network formation around NP seeds by precipitation polymerization [157], the adsorbance of NPs onto microgels surfaces [79] or their absorbance into the network [158]. Despite their different origin, the final materials exhibit the similar light-induced volume phase transition of the network. Figure 3.7 depicts the irradiation-induced variation of the relative volume of hybrid Au nanorods containing p(NIPAAm-co-AA) microgels in comparison to pure polymeric microgels as described by Kumacheva and coworkers [159].

Regarding the potential of these materials for biomedical applications it is highly beneficial that the absorption spectra of noble metal NPs can be tuned over a wide spectral range to absorb light in the NIR window (650–900 nm) while exhibiting a large optical cross-section and no self-quenching effects [160]. The inherent advantage of this particular resonance wavelength is its minimal absorbance by skin and tissue, therefore enabling a penetration depth of several hundreds of micrometers up to centimeters [151]. Another big advantage of thermo-sensitive hybrid microgels in the field of cancer treatment is the combination of their inherent ability to influence cell viability due to the photo-induced hyperthermia [161] with the potential of the externally triggered release of specific chemotherapeutics [162], thereby dramatically enhancing the therapeutic efficacy [85].

Multi-Responsive Microgels, Complex Stimuli-Responsive Microgel Architectures and Stimulus-Induced Transformation of Hydrophobic Polymeric Nanoparticles to Microgels

Multi-responsive microgels in general are materials responding to more than one external trigger. The previously described Au@PNIPAAm hybrid microgels are an

Fig. 3.7 Variation in volume of pure (\diamond) and hybrid (\blacklozenge) p(NIPAAm-co-AA) microgels plotted as a function of the number of *laser on* and *laser off* events n . Both microgel systems were irradiated at $\lambda = 810$ nm. Reprinted with permission from [159]. Copyright 2004 American Chemical Society



example for a special class of these materials, since the response to one trigger A (light) results in the creation of a second stimulus B (heat) which finally induces a response of the polymeric material. Therefore, the pure microgels are only sensitive to one trigger (B, heat). In contrast, actually double-stimuli responsive materials can be divided into gels responding orthogonally to either one of the single stimuli (type “A or B”) and in networks which exhibit a response only if all stimuli are applied simultaneously (type “A and B”) [85]. Since the latter are characterized by an enhanced selectivity of their response to the respective specific combination of triggers, the type “A or B” microgels are potential materials for new loading and release techniques based on the subsequent appliance of different stimuli. For the preparation of such compounds it has to be taken into account that the co-existence of various stimuli-responsive components within one microgel can result in an interference of the respective sensitivities. This effect can be desired and was already described earlier in the context of the influence of pH-sensitive groups on the VPTT of thermo-sensitive microgels (see Sect. ‘Temperature-Sensitive Microgels’) [163]. However, a differentiation between the individual responses to different stimuli can be achieved by the spatial separation of the specific functional groups responsible for the respective sensitivities. A sophisticated approach to realize this concept is the preparation of core/shell microgels consisting of different stimuli-responsive network-forming polymers in the core and the shell. Jones and Lyon described the preparation of PNIPAAm(core)/PNIPAAm-co-PAA(shell) microgels and demonstrated the appearance of a temperature-dependent multistep volume phase transition for high pH values where the PAA component is highly charged [52]. In a similar approach, core/shell microgels consisting of two different thermo-sensitive polymers were prepared by Berndt and Richtering [164]. Since the core was formed from PNIPAAm and the shell from poly(*N*-isopropylmethacrylamid) (PNIPMAAm) exhibiting a comparably higher LCST of 45 °C, the temperature-dependent swelling profile revealed two phase transitions corresponding to the two LCSTs of the respective polymers. These materials are potential systems for the independent release of different compounds from separated compartments within one carrier.

As mentioned above, multi-responsive microgels of complex architectures give rise to new loading and release mechanisms. An interesting example in this research area was described by Needham et al. [165]. They prepared pH-sensitive PMAA microgels and exploited the anionic character of the gel for the loading of positively charged doxorubicin upon electrostatic interactions with the network. The drug was efficiently entrapped in the carrier system by lowering the pH and by subsequently coating the collapsed microgels with a lipid double layer. The latter served as a diffusion barrier for the loaded drug and prevented the core/shell particles from swelling upon immersing these in aqueous medium of a pH > p*K*_a of PMAA. A successful release was achieved by selectively disrupting the shell upon the appliance of short electric pulses as second trigger orthogonal to the pH-sensitivity used for loading.

If it comes to release applications of microgels in the biomedical field, most investigated systems are limited to the incorporation of hydrophilic active

compounds into hydrophilic networks. In order to extend this concept to the delivery of hydrophobic compounds, hydrophobic nanoparticles consisting of poly(lactic-glycolic acid) represent an approach based on the biodegradability of the polymer backbone. Nevertheless, these materials cannot be assigned to the field of microgels. An alternative mechanism for the delivery of hydrophobic compounds from hydrophilic microgels was recently demonstrated by Griset et al. [106]. The described concept is based on the generation of swollen hydrogel nanoparticles from hydrophobic polymer latexes as a result of a stimulus-induced transition of the hydrophilicity of the network-forming polymer from hydrophobic to hydrophilic. To this extend, crosslinked particles consisting of a hydrophobic polymer containing acetal protected diol groups in the backbone were prepared by inverse miniemulsion polymerization. As a response to a pH change to slightly acidic conditions (pH 5), these nanoparticles expanded several hundred-fold in volume due to the acid catalyzed deprotection of the diol groups, thus generating the swollen hydrogel. Figure 3.8 depicts the underlying mechanism. If loaded with paclitaxel as poorly water soluble anti cancer drug, this drug delivery system was shown to prevent establishment of lung cancer in vivo.

3.3.2.2 Stimuli-Responsive Microgels Based on Cleavable Crosslinking Points

The fundamental concept of stimuli-responsive microgels based on either complete or partial cleavage of crosslinking points is the resulting increase in swelling or total dissolution of the microgels. As a result of the decreasing crosslinking density during this process, the mesh sizes in the network are increased, thus

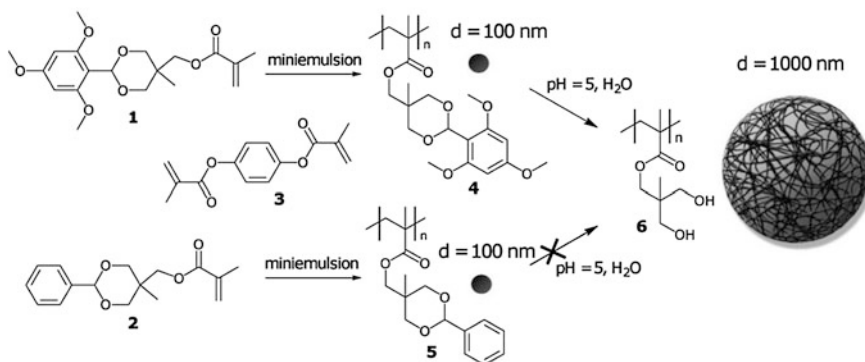


Fig. 3.8 Synthesis of nanoparticles with differing pH responsiveness obtained from crosslinking polymerization of either 1 or 2 in the presence of 3. The protecting group of nanoparticle 4 but not 5 is cleaved at a pH of ~ 5 . This transformation reveals the hydrophilic hydroxyl groups and formation of nanoparticle 6 with resulting expansion of the hydrogel nanoparticle in water. Reproduced with permission from [106]. Copyright 2009 American Chemical Society

giving rise to enhanced diffusivity of embedded compounds which can be used for release applications. Several different triggers have been examined to induce the crosslinker's degradation and will briefly be discussed in this section.

Microgels Containing Hydrolytically Cleavable Crosslinkers

A widely investigated concept to degradable microgels is based on the utilization of crosslinking agents containing hydrolytically cleavable groups [166]. In this area, a facile approach is based on ester moieties, since their hydrolysis can be triggered by several changes of the chemical environment such as the presence of hydroxide ions, protons or enzymes. While this inherent feature has been exploited for the preparation of biodegradable nanoparticles from e.g. poly(lactic-co-glycolic acid) [167], Kim and Graham successfully transferred this concept to hydrogel nanoparticles. The microgels prepared from crosslinked poly(caprolactone diol) were shown to be degradable upon incubation in acidic, alkaline or enzymatic solution of esterase at physiological temperature [168]. Even though these materials represent interesting candidates for release applications, their degradation is rather unspecific with respect to the types of external triggers and, as a result, the degradation rate is comparably low. However, for many applications a fast and precise response to a specific stimulus is desired in order to increase the respective efficacy. Thus, increasing the hydrolytic lability of crosslinking points represents an active research area and can be achieved by the precise adjustment of the molecular structure of crosslinkers (i.e. the incorporation of highly sensitive labile groups). Jhaveri and Carter exploited the well known acid-sensitivity of tertiary esters and prepared degradable PMMA microgels with 2,5-dimethyl-2,5-hexanediol dimethacrylate (DHDMA) as crosslinking agent [169]. These polymeric microgels were found to be degradable upon the addition of *p*-toluenesulfonic acid even in the absence of water, thereby representing an example for the specific degradability in dependency on one particular trigger (i.e. the presence of protons).

Transferring this conception to drug delivery applications, it is of special interest to design carrier systems responding to an inherent feature of the site targeted for the release. As mentioned before, this can be achieved by taking advantage of the slightly acidic pH values in cancer tissues and intracellular compartments. In comparison to tertiary esters, requiring elevated temperatures and a highly acidic pH for their fast degradation, acetals as protection groups are well known to be hydrolysable under mild conditions, thus rendering them beneficial for their utilization as labile moieties in biomedical applications. Fréchet and coworkers prepared acid-degradable poly(acrylamide) microgels containing hydrolysable acetal moieties in the crosslinkers for the encapsulation and acid-triggered release of proteins [170]. Figure 3.9 depicts the followed concept.

Similar acid-degradable microgels containing ovalbumin as an example of protein-based vaccines prepared in the same group were demonstrated to release their payload upon degradation under mildly acidic conditions in the phagosomes

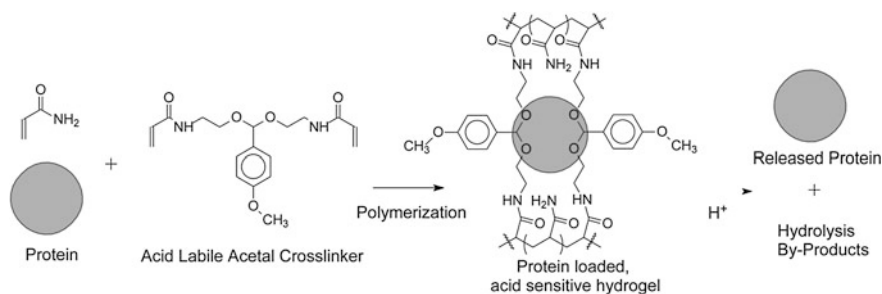


Fig. 3.9 Schematic representation of the concept of microgels containing acid-degradable crosslinkers. Loading of proteins in situ during microgel formation and their release upon acid-catalyzed hydrolysis of crosslinking points. Reproduced with permission from [170]. Copyright 2002 American Chemical Society

of antigen-presenting cells. The release of the protein was shown to activate ovalbumin-specific cytotoxic T lymphocytes in vitro [171]. By increasing the hydrophilicity of the labile crosslinker structure the loading efficiency and the resulting antigen presentation levels could be dramatically enhanced. Moreover, preliminary in vivo experiments proved enhanced survival rates for tumor-challenged mice [172]. In addition, the versatility towards the encapsulation of different biologically active macromolecules such as e.g. plasmid DNA [173] clearly demonstrates the great potential of these delivery systems. Especially the divinyl functionalization of the used crosslinkers enables their utilization in radical copolymerizations with a broad variety of monomers thus giving rise to the facile preparation of a multitude of acid-degradable polymeric microgels [174]. The concept of acid-labile crosslinkers can even be extended to more complex structures such as e.g. hollow microgel capsules prepared from polyvinylamine (PVAm) with ketal moieties containing crosslinks described by Shi et al. [175].

In addition to pH changes throughout the body, another biological relevant trigger is the presence of certain reducing agents in specific compartments. As an example, the accumulation of glutathione in the cytosol is worth mentioning [176]. Therefore, delivery vehicles based on functional groups cleavable in the presence of high reducing agents concentrations are particularly attractive for intracellular delivery [177]. In this context, the utilization of crosslinking molecules containing disulfide bonds hydrolysable in the presence of reducing agents have gained increasing interest for the preparation of degradable microgels [178]. Bromberg et al. prepared microgels based on poly(acrylic acid) covalently bonded to Pluronic (PEO-*b*-PPO-*b*-PEO) polyether copolymers [179]. Crosslinking of these microgels was achieved by permanent and stable ethylene-glycol-dimethacrylate (EGDMA) groups together with degradable *N,N'*-bis(acryloyl)cystamine. Degradation of the disulfide linkers upon the incubation with tris(2-carboxyethyl-phosphine) (TCEP) was found to result in an increased degree of swelling due to a decreased crosslinking density of the network. An additional advantage of disulfide based crosslinkers is their reversible formation/degradation, which can be used not only

for the release of functional compounds upon microgel degradation [180] but also for their entrapment based loading upon crosslinker formation. Regarding the latter, Ryu et al. recently described the formation of self-crosslinked polymer nanogels by chemically induced crosslinking of self assembled copolymers containing oligoethyleneglycol (OEG) and pyridyldisulfide (PDS) units [181]. Cleavage of a certain amount of PDS groups by dithiothreitol to the corresponding thiol functionalities and their subsequent reaction with uncleaved PDS groups leads to disulfide-crosslinks. Prepared microgels containing doxorubicin were found to release the drug in vitro, thus achieving cytotoxicity upon degradation of crosslinking points.

Microgels Containing Enzymatically Cleavable Crosslinkers

In the field of release applications, it is generally of interest to design carrier systems exhibiting a highly specific response to one particular stimulus. In this context, the utilization of enzymatically degradable microgels represents an attractive approach to ensure hydrolytic stability of the network—and thereby the prevention of leakage or degradation of the embedded functional compound—until the targeted site or time point is reached. Here, especially the localization of certain enzymes in distinct compartments of the body enables the design of materials with site specific stimulus-responsiveness. Based on these considerations, hydrogels containing enzymatically cleavable crosslinking points are investigated examples taking advantage of the presence of e.g. azoreductase in the colon [182]. While labile azobenzene moieties for covalent crosslinking are well examined for site specific drug delivery via macroscopic gels [183], the transfer of this concept to the micro-/nanometer scale is assumed to enhance the therapeutic efficacy due to a higher surface area of the carrier systems and a corresponding faster response to the trigger. Hatton and coworkers described the exploitation of 4,4'-di(methacryloylamino)azobenzene as crosslinker for the preparation of enzymatically degradable microgels consisting of a PAA network covalently bound to Pluronic polyether copolymers [179].

Another highly interesting approach to degradable (micro-)gels is based on the utilization of dextrans as naturally occurring polysaccharides that can be cleaved upon incubation with dextranase [184]. Covalent functionalization of dextran chains with either polymerizable vinyl groups [185] or thermal initiators [186] enables the formation of hydrogels by free radical (co)polymerization in aqueous media. The resulting networks can then be degraded by the addition of dextranase, inducing the release of embedded active compounds [17]. Here, the dextran polymer can be considered as a macromolecular crosslinker. Microgels based on dextran methacrylates have been investigated by Hennink and coworkers for the release of immunoglobulin G as a model protein [187]. In this case the co-entrapment of dextranase into the network renders the bulk-degradation of these gels rather an inherent feature than the response to an external trigger. As shown in

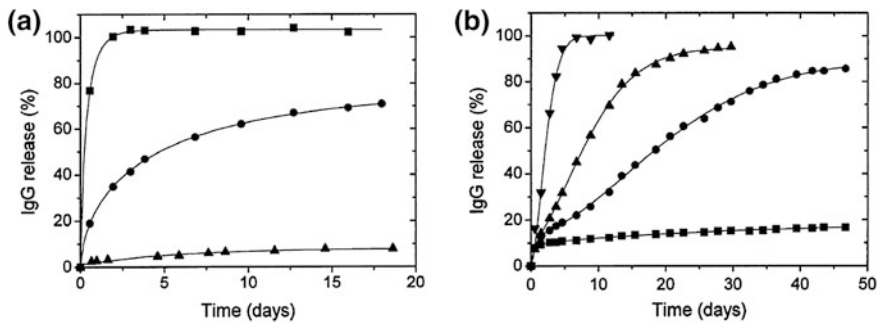


Fig. 3.10 Cumulative release of IgG versus time from degrading dextran microgels: **a** as a function of the DS: *DS* 4 (■), *DS* 7 (●) and *DS* 13 (▲); **b** as a function of the amount of incorporated dextran (*DS* 4): 2 U/g solid (▼), 0.7 U/g solid (▲), 0.2 U/g solid (●) and 0 U/g solid (■). Reproduced with permission from [187]. Copyright 1999 Elsevier

Fig. 3.10, it was observed that the rate of degradation and thereby the release of IgG is dependent on the degree of substitution (*DS*) (Fig. 3.10a) of the dextran chains with methacrylate groups as well as on the amount of embedded enzyme (Fig. 3.10b). Thus, a high loading efficiency as characterized by the reduction of the initial burst release to about 10 % was achieved by a high *DS*.

De Geest et al. further extend this concept and demonstrated that coating of these self-degrading microgels with a semi-permeable shell yields self-exploding capsules as promising materials for pulsatile release applications [188]. The degradation of the microgel core leads to an increase in the swelling pressure until the latter exceeds the tensile strength of the surrounding membrane, thus causing shell rupture and release of the payload.

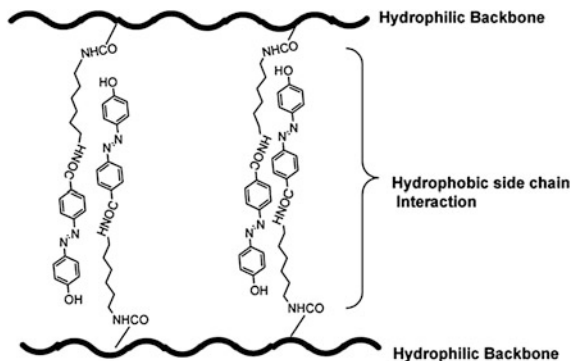
Another example for more complex microgel structures based on degradable dextrans is the combination of the enzyme-sensitive polysaccharide with thermo-responsive network-forming polymers. Kumashiro et al. demonstrated that the degradability of microgels containing dextrans covalently attached to PNIPAAm and poly(*N,N'*-dimethylacrylamide) (PDMAAm) is adjustable by temperature [189]. Since the network is swollen only at temperatures between the different LCSTs of PNIPAAm and PDMAAm, the enzymatic accessibility of the dextran chains (and thereby the overall degradability) is only given in this temperature range.

Microgels Containing Photo-Degradable Crosslinkers

Response mechanisms of microgels containing light-cleavable crosslinking points can generally be divided into two categories: (1) irradiation-induced cleavage of physical crosslinks and (2) photo-degradation of covalent crosslinking points.

Materials of the first category are typically crosslinked by physical aggregates of hydrophobic chromophores attached to a hydrophilic polymer backbone.

Fig. 3.11 Schematic representation of non-covalently crosslinked azo-dextran microgels. Reproduced with permission from [190]. Copyright 2007 Elsevier



Utilization of photo-reactive moieties able to change their polarity upon irradiation-induced isomerization renders these hydrophobic interactions sensitive to light as external trigger. Moreover, if the isomerization process is reversible, the crosslinking density can be reversibly adjusted as well. In general, several chromophores exhibiting the described features are reported in the literature. An example for the light-triggered changes in the physical crosslinking density of hydrophilic microgels was reported by Patnaik et al. by the utilization of azobenzenes as photo-reactive chromophores [190]. As shown in Fig. 3.11, microgel networks were prepared by the self aggregation of pre-formed azobenzene-dextran polymers due to hydrophobic interactions of *trans*-azobenzene groups attached to the hydrophilic polymer backbone.

As mentioned before, these molecules are able to undergo a *trans*-*cis* isomerization upon the irradiation with UV light. Since this change in configuration is accompanied by a change in the dipole moment of the molecule, the *cis*-isomer is significantly more hydrophilic, thus weakening the hydrophobic interactions responsible for network-formation. The resulting increase in the degree of swelling of these microgels corresponds to increased mesh sizes. Hence, the release of embedded compounds such as rhodamine and aspirin was found to proceed faster for irradiated microgels containing azobenzene moieties in the *Z*-configuration.

A similar approach was described by Akiyoshi and coworkers and is based on the microgel formation upon the self-assembly of spiropyran-bearing pullulan [191]. The physical crosslinks are formed by the aggregation of hydrophobic spiropyran groups. In analogy to the example described above, these molecules are known to undergo a light-triggered change in configuration to a hydrophilic zwitter-ionic merocyanine form, thereby reducing the hydrophobic interactions, destroying the physical crosslinking points and changing the solution properties of the microgels.

Regarding covalently crosslinked microgels, photo-dimerization reactions—especially [2+2] cycloaddition reactions—in combination with macroscopic polymeric gels are well established for the formation of crosslinks by the application of UV light [192, 193]. Transferring this concept to the nanoscale gives rise to a broad variety of interesting materials such as thermo- and pH-sensitive

microgels [194] prepared by e.g. photo-crosslinking of poly(*N,N'*-dimethylaminoethyl methacrylate-co-dimethylmaleimidoethyl methacrylate) [195]. Extending this concept by the exploitation of reversible photo-dimerization reactions, of e.g. cinnamoyl, anthracene and coumarin derivatives, is an attractive approach to both the light-triggered formation and cleavage of covalent crosslinks. The forward dimerization reaction of such chromophores is widely investigated for the preparation of (stimuli-responsive) [196] microgels by photo-crosslinking of e.g. cinnamoyl side groups in micellar aggregates of (amphiphilic) block copolymers [197] or photo-crosslinking of graft-copolymers containing the photo-reactive moieties in the polymer backbone [198].

Nevertheless, only little attention has been paid to the utilization of the photo-induced backwards reaction as light-cleavable crosslinks in microgels. Akashi et al. demonstrated the light-induced crosslinking and de-crosslinking of microgels prepared from poly(3,4-dihydroxycinnamaic acid-co-4-hydroxycinnamaic acid) [P(3,4DHCA-co-4-HCA)] copolymers containing cinnamates in the polymeric backbone [199]. As shown in Fig. 3.12, the reversibility of the photo-reaction was found to enable a controlled swelling/deswelling of the gel networks upon irradiation-induced adjustment of the crosslinking density.

In contrast to the non-degradable microgels prepared by photo-crosslinking of micellar (block) copolymer aggregates, the utilization of reversible photo-dimerization reactions in a similar approach allows to control the crosslinking density by light-induced formation/cleavage/re-formation of crosslinking points. As an example, thermo- and light-responsive nanogels were prepared by photo-crosslinking the core of hydrophilic block copolymer micelles containing a polymer displaying a LCST and bearing coumarin moieties [200]. After micelles were formed by heating a polymer solution above the LCST of the core forming block, crosslinking was achieved by the photo-dimerization of the chromophore upon illumination at λ_I . Upon cooling below the LCST crosslinked nanogels were

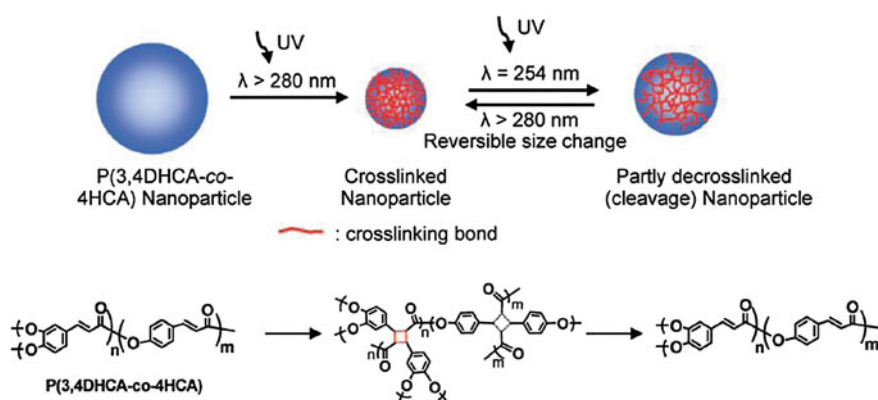


Fig. 3.12 Schematic representation of size change behavior of microgels with UV irradiation; chemical structure of UV-induced [2+2] cycloaddition formation (crosslinking) and deformation (cleavage). Reproduced with permission from [199]. Copyright 2008 American Chemical Society

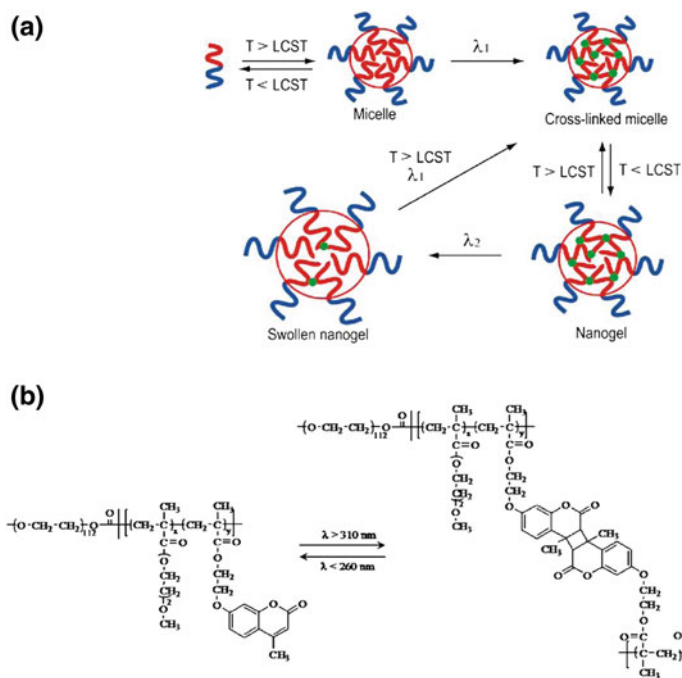


Fig. 3.13 a Schematic representation of the preparation and photo-controlled volume change of thermo- and light-sensitive microgels. b Designed diblock copolymer bearing coumarin side groups for the reversible photo-crosslinking reaction. Reproduced with permission from [200]. Copyright 2009 American Chemical Society

obtained. It was demonstrated that the degree of crosslinking can be reduced by irradiating a dispersion thereof at λ_2 leading to swelling of the gel network. Furthermore, the initial crosslinking density can be restored by photo-induced re-crosslinking at $T > LCST$. Figure 3.13 depicts the described concept.

Recently, this concept has been extended to pH- and light-responsive microgels following a similar approach which is based on exchanging the thermo-sensitive moieties in a comparable crosslinkable block with pH-sensitive 2-(diethylamino)-ethyl groups [201]. In addition, the utilization of a water soluble block copolymer containing pH-sensitive carboxylic acid moieties in one block and thermo-sensitive groups along with coumarin moieties in a second block led to multi-responsive microgels [202]. In dependency on the preparation route, either shell-crosslinked or core-crosslinked gel structures were obtained.

Even though these examples represent sophisticated approaches to controllable nanocarriers, cleavage of crosslinks obtained from [2+2] cycloadditions requires harsh irradiation conditions such as UV-C light ($\lambda = 200\text{--}280\text{ nm}$), thus limiting their application to fields where photo-degradability of functional compounds is not an issue [85].

3.4 Photochemistry in Polymeric Nanoscale Materials

The combination of photochemistry with the field of polymer chemistry has led to the development of materials whose properties can be modified upon the appliance of light. Since this behavior occurs as a response to an external field, the described concept is a special approach to stimuli-responsive materials which can be termed photo-sensitive.

3.4.1 *Light as a Trigger*

Among the broad variety of stimuli useful for changing the properties of polymeric materials such as e.g. pH or temperature, light represents an outstanding position due to various reasons. It can be applied in a very precise manner by adjusting the irradiation condition to the sensitivity of the incorporated chromophore. Thus, by selecting suitable wavelengths, intensities and polarization directions [203], unwanted side reactions or physical changes in co-existing non-reactive (polymeric) groups can be avoided [204]. Furthermore, light can be applied in a non-contact approach. This inherent feature renders photo-sensitive materials highly beneficial compared to approaches based on a response to changes in the chemical environment. Such systems being sensitive to e.g. variations in the pH, enzyme concentration or solvent composition require either the addition of a specific compound or the localization of the respective material in the specific environment. Light in contrast, can be applied to closed reaction systems and polymers in the dry state as well. In addition, light offers the possibility to change the polymer properties in very confined spaces by using for instance confocal or holographic methods [205]. This feature can not only be applied to create patterns with nanometric precision in polymer thin films [193], but also renders photo-sensitive materials especially interesting for applications in the nanoscale [193, 206]. Finally, light-sensitive materials are not only characterized by the high spatial resolution of their response but also by the increased resolution of their response time. In contrast to other stimuli-induced processes, photo-reactions mostly occur only if light is applied and come to a stop in the dark. This feature gives rise to kinetically controlled or stepwise response mechanisms.

3.4.2 *Photoreactions in Polymers*

Regarding photo-sensitive materials, tailoring the precise location and the photo-induced process of the photo-active chromophore in the material are the key requirements to effectively incorporate and fully exploit the designed properties of the material with respect to the desired application. In general the desired

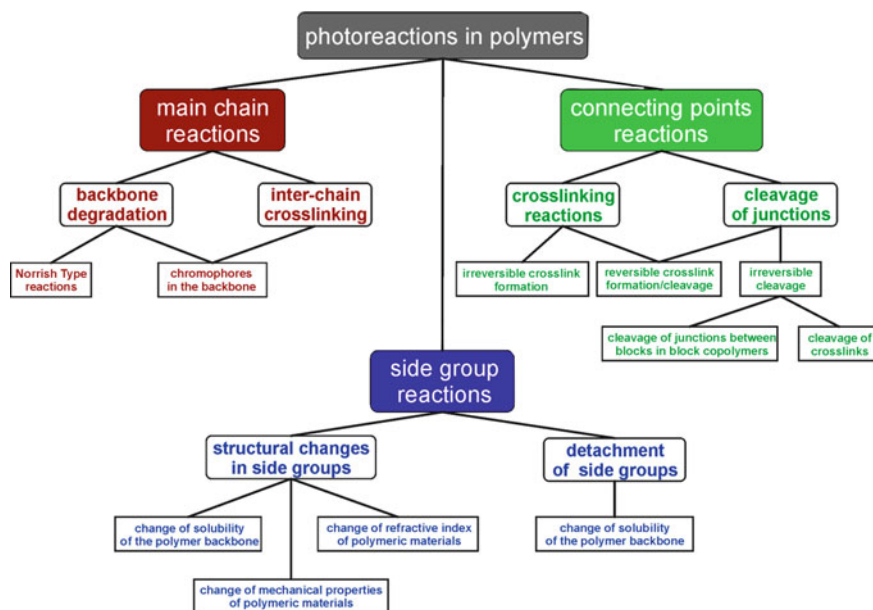


Fig. 3.14 Photoreactions in polymers: classification with respect to type and location of the light-induced process

photo-sensitivity of polymeric materials can be achieved by two different concepts. On one hand, this can be realized by the incorporation of photo-active guest molecules into a polymeric matrix. Here, the characteristics of the polymer are changed due to an altered interaction between matrix and inserted chromophores before and after irradiation. On the other hand, the properties of polymers can be directly tailored by their interaction with photons. To this extent, photo-reactive moieties are covalently incorporated into the polymer structure as either side groups or reactive moieties in the back bone. As shown in Fig. 3.14 depending on the incorporated chromophore and its location in the polymeric material, a wide span of different types of response mechanisms in photo-sensitive polymers can be distinguished.

3.4.2.1 Types of Chromophores in Polymeric Materials

While Fig. 3.14 gives a schematic overview of the general design parameters for photo-sensitive materials and their influence on the polymer properties, a more detailed insight in photo-activated reactions is the focus of this section. The most common photo-sensitive processes used to obtain different light-induced responses could be classified into the following categories:

- a) *cis*–*trans* isomerizations
- b) ionization reactions
- c) molecular switches
- d) dimerization reactions
- e) radical formation
- f) bond cleavage reactions.

***cis*–*trans* Isomerizations.** Probably the most prominent chromophores undergoing light-induced *cis*–*trans* isomerizations are azobenzene derivatives. Here, the irradiation with light of short wavelengths (λ_1) induces the transformation from the *trans* to the *cis* configuration. Of special interest is the reversibility of this reaction which can be induced either by thermal relaxation or the appliance of light of longer wavelengths (λ_2). Various materials for several applications are based on different inherent features of this isomerization. The accompanied change in the dipole moment renders the *cis* state more hydrophilic. If bound to a polymeric backbone, this alteration of the chromophore thus enables to adjust the overall hydrophilicity of the polymer [150, 207]. In combination with the structural change in the molecule, initial hydrophobic aggregates of azobenzene moieties are broken up, therefore giving rise to the reversible formation/cleavage of physical crosslinks [190]. Moreover, the change in the alignment of these chromophores upon irradiation is investigated for the preparation of materials for optical data storage [208–210]. Finally, the bending of the molecule can be used to induce shape changes in nematic liquid–crystal elastomers which represents a fascinating example for the alteration of macroscopic changes in a material controlled on a molecular level [203].

Ionization reactions. Several chromophores are known to exhibit a light-induced reversible dissociation into ion pairs which can be used for different types of applications. The variation of the electrostatic repulsion of tertiary carbon cations and anions such as e.g. hydroxide ions from triphenylmethane leuco derivatives enable the photo-induced expansion and shrinkage of polymers or gels [203]. In a more indirect approach, photo acid generators (PAGs)—mostly based on triphenylsulfonium triflates—are commonly used for chemically amplified or cascade reactions. Examples include the cleavage of acid-labile crosslinking points in polymeric gels or films via the in situ generation of protons by the irradiation of incorporated PAGs [211, 212] or the chemically amplified activation of pH-sensitive dye molecules in a polymeric matrix [213]. Since the latter case gives rise to changes in the refractive index of the materials, this concept can be used for optical data storage applications [214].

Molecular switches. Chromophores that can be classified as molecular switches are based on a light-induced isomerization process which is often accompanied by a change in the polarity of the chromophore. In this context, spiropyranes represent well examined compounds since they are capable of undergoing a reversible transformation from a hydrophobic closed spiropyran form to an open mesoionic merocyanine conformation. This light-induced change of polarity can be transferred to a polymeric chain, thus triggering its solubility [215, 216]. Incorporation of

spiropyranes into amphiphilic block copolymers enables the reversible triggering e.g. the disruption/formation of micellar aggregates by changing the polarity of the block containing the chromophore [217]. Similar applications are based on the utilization of diazonaphthoquinone (DNQ) derivatives which are well known from the DNQ Novolac photo-resist material. The irreversible transformation of hydrophobic 2-diazo-1,2-naphthoquinone into the hydrophilic 3-indenecarboxylate has found application e.g. in the degradation of micellar aggregates based on PEG chains containing the chromophore as head group [218]. In contrast, polymeric 1-iminopyridinium-ylides represent an example for an irreversible transformation from the initial mesoionic hydrophilic state to hydrophobic 1,2-diazepanes. This behavior can be used to create hydrophobic patterns in hydrophilic polymer films [219]. Another highly interesting category of applications exploits the light-induced changes in the absorption spectra of such molecular switches for optical data storage in polymeric materials [220].

Dimerization reactions. Photo-dimerization is a bimolecular light-activated process that involves an electronically excited unsaturated molecule which undergoes an addition reaction with an unexcited molecule of the same species, thus forming the dimer. [2+2] and [4+4] photo-cycloadditions are certainly the most common photo-dimerization reactions. Among the broad variety of different types of molecules which are known to undergo these photoreactions, cinnamate, coumarin or anthracene derivatives are probably the most prominent representatives. If these chromophores are attached as side groups to a polymeric backbone, irradiation can be used to form either macroscopic [193, 221–223] or nanoscale [195, 197, 200] crosslinked materials. Of special interest is the light-induced reversibility of these processes which enables to adjust the crosslinking density by the appliance of light of a different wavelength as the one used for the crosslinking [201, 202, 222]. Alternatively to the utilization of these chromophores as polymeric side groups, their incorporation into a polymeric back bone allows to crosslink the independent chains directly [199].

Radical formation and reactions from excited states. In the context of radical formation upon irradiation, benzophenones have gained very much attraction since the excited triplet state easily undergoes hydrogen atom abstraction reactions [224]. Therefore, the attachment of such moieties to polymers serves as a facile approach to photo-crosslinked materials [225] such as e.g. hydrogel thin films [226].

Bond cleavage reactions. Probably the simplest chromophore known to undergo bond cleavage reactions upon irradiation are the ester group. Here, Norrish type reactions (usually defined for aldehydes and ketones) are known to result in the side group cleavage (Norrish type I) but also in the degradation of polymeric backbones of e.g. PMMA (Norrish type II). [227, 228] Since these reactions require harsh irradiation condition such as UV-C light, much effort has been paid to increase the photo-sensitivity of ester groups by the introduction of several chromophores. As an example, the attachment of pyrenylmethanol to polymeric backbones via an ester bond is worth mentioning. Irradiation of these materials leads to the detachment of the chromophore and leaves a carboxylic acid group on the polymer. The resulting change from a hydrophobic to a hydrophilic

polymer can be used for the disruption of micellar aggregates from initially amphiphilic diblock copolymers [229]. A similar approach to the photolytic detachment of hydrophobic protection groups from carboxylic acids is based on the utilization of *o*-nitrobenzyl esters and derivatives. While their connection to a polymer as side groups gives rise to photo-resist materials [230] or light-cleavable micelles [231], incorporation of these moieties into the backbone results in completely photo-degradable polymers [232].

3.4.2.2 Photoreactions of *o*-nitrobenzyl Derivatives

As mentioned above, photolytic bond cleavage reactions have gained considerable interest in the field of nanoscale materials since they give rise to a broad variety of response mechanisms. Especially *o*-nitrobenzyl derivatives such as esters, carbonates or carbamates have been extensively examined since their discovery in 1901 [233] and are known to be cleaved fast and quantitatively upon irradiation with UV-A light ($\lambda > 300$ nm). Detailed investigations on the underlying mechanism of the light-induced bond cleavage in *o*-nitrobenzyl esters were performed by Schnabel and co-workers in the late 1980 s and the proposed pathway is depicted in Fig. 3.15 [234].

The light-induced bond cleavage of *o*-nitrobenzyl esters (3.1) yields the respective nitroso ketone or –aldehyde along with the carboxylic acid (3.6). The reaction mechanism contains the following steps. At first, the nitronic acid (3.3) is formed either from the excited singlet or the triplet state of **1** via an intramolecular hydrogen-transfer process including the biradical (3.2) as proposed intermediate. While the presence of **3** could easily be evidenced spectroscopically [235, 236], the decay mechanism of this compound to yield **5** and **6** has been subject to modifications along the investigations of Schnabel and co-workers. Finally, the

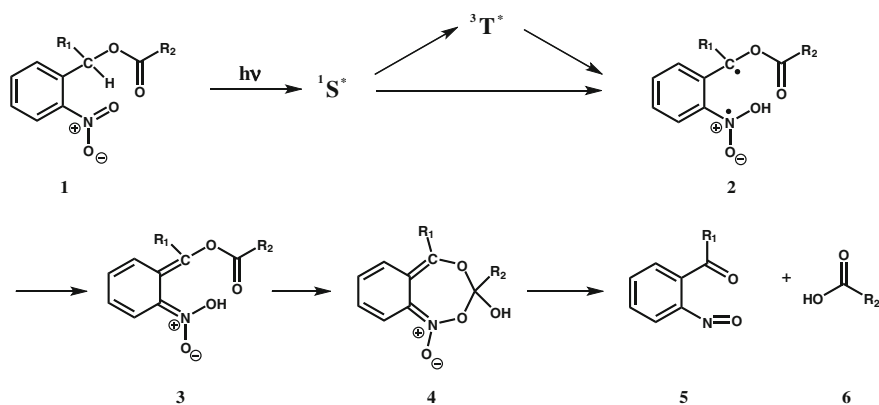


Fig. 3.15 Mechanism of the photoreaction of *o*-nitrobenzyl esters as proposed by Wong et al. [234]

intermediate of **5** has been evidenced in aqueous solution by changes in the electrical conductivity [235, 236].

Since these early detailed examinations, further investigations on the photolytic cleavage of various types of *o*-nitrobenzyl derivatives revealed the potential to easily adjust the photolytic characteristics by the molecular structure of the chromophore. In particular, the introduction of an α methyl group to the benzylic carbon of the *o*-nitrobenzyl core was found to increase the rate of photolysis significantly [234]. This effect can be explained by considering the abstraction of a benzylic proton by the photo-activated nitro group as the rate limiting step in the photolysis of the *o*-nitrobenzyl group, whereby the additional methyl group increases the acidity of this proton [237–239]. Moreover, the introduction of alkoxy substituents in the *o*-nitrobenzylic core results in a modified electronic structure of the chromophore which is known to result in a considerably increased UV absorption for $\lambda > 315$ nm compared to the unsubstituted core [239]. Since irradiations in this spectral region (UV-A light) represent relatively mild conditions with negligible corrupting influence on co-existing functional groups and molecules, the use of these moieties in biomedical related applications is strongly facilitated [204]. Further investigations on varying the molecular structure of these chromophores and their connection to functional groups or molecules gave rise to e.g. *o*-nitrobenzyl amines forming carboxamides upon irradiation [239, 240] and [2-(2-nitrophenyl)ethoxy]carbonyl (NPEOC) groups as new type of photo-labile functions [241].

The good cleavage properties of these different chromophores have been employed in various fields such as photo-labile supports for solid phase organic synthesis [239, 240, 242–244], linkers for chemical proteomics [245] or degradable linkers to bridge fluorophores to DNA [246]. Another group of applications is based on the use of *o*-nitrobenzyl derivatives to protect functional groups. Here, early investigations were based on the photo-generation of organic bases [247] or carboxylic acids [248]. More recently, possible applications as protection groups in biological active molecules and in nucleoside and nucleotide chemistry were gaining increasing interest [204]. In these cases, the photolytic deprotection can be used to activate a certain biological function upon deblocking e.g. an active centre or functionality [249].

Transferring the concept from solution based applications to the solid state, it is beneficial that high photolysis rates of the chromophore are maintained in polymeric matrices [230, 234] and even in the dry state [248]. This inherent feature gives rise to the light-induced patterning of surfaces via either the application as photo-labile protection group in the head groups of self-assembled silane monolayers [206, 250] or the preparation of photo-resist materials by the attachment of *o*-nitrobenzyl ester side groups to a polymer [230, 251]. The latter allows the surface patterning by UV light-induced solubility changes. In extension to dry polymer films, hydrogels in the macroscopic size range containing *o*-nitrobenzyl groups as crosslinking points allowed the formation of 3 dimensional channels upon focused irradiation [252].

The particular good performance of the photoreaction under various conditions represents a versatile tool for more complex applications in the nanometer size range as well. Recently investigated approaches include the design of targeting nanoparticles [253] and the preparation of photo-responsive nanocarriers using *o*-nitrobenzyl esters as capping groups on dendrimers [254] or hyperbranched polyglycerol nanocapsules [255]. Furthermore, Kim and co-workers lately prepared mesoporous silica particles with photo-responsive cyclodextrin gate functions connected via a cleavable *o*-nitrobenzyl moiety to the particle [256].

References

1. Klinger, D., Landfester, K.: *Polymer* **53**(23), 5209–5231 (2012)
2. Carothers, W.H.: *Chem. Rev.* **8**(3), 353–426 (1931)
3. Flory, P.J.: *J. Am. Chem. Soc.* **63**, 3083–3090 (1941)
4. Peppas, N.A., Huang, Y., Torres-Lugo, M., Ward, J.H., Zhang, J.: *Annu. Rev. Biomed. Eng.* **2**, 9–29 (2000)
5. South, A.B., Lyon, L.A.: *Angew. Chem. Int. Ed.* **49**(4), 767–771 (2010)
6. Qiu, Y., Park, K.: *Adv. Drug Del. Rev.* **53**(3), 321–339 (2001)
7. Peppas, N.A., Leobandung, W.: *J. Biomater. Sci. Polym. Ed.* **15**(2), 125–144 (2004)
8. Tokarev, I., Minko, S.: *Adv. Mater.* **22**(31), 3446–3462 (2010)
9. Tokarev, I., Tokareva, I., Gopishetty, V., Katz, E., Minko, S.: *Adv. Mater.* **22**(12), 1412–1416 (2010)
10. Alvarez-Lorenzo, C., Guney, O., Oya, T., Sakai, Y., Kobayashi, M., Enoki, T., Takeoka, Y., Ishibashi, T., Kuroda, K., Tanaka, K., Wang, G.Q., Grosberg, A.Y., Masamune, S., Tanaka, T.: *Macromolecules* **33**(23), 8693–8697 (2000)
11. Beloshenko, V.A., Varyukhin, V.N., Voznyak, Y.V.: *Russ. Chem. Rev.* **74**(3), 265–283 (2005)
12. Yeghiazarian, L., Arora, H., Nistor, V., Montemagno, C., Wiesner, U.: *Soft Matter* **3**(8), 939–944 (2007)
13. Yoshida, R.: *Adv. Mater.* **22**(31), 3463–3483 (2010)
14. Hennink, W.E., van Nostrum, C.F.: *Adv. Drug Del. Rev.* **54**(1), 13–36 (2002)
15. Wichterle, O., Lim, D.: *Nature* **185**(4706), 117–118 (1960)
16. Edman, P., Ekman, B., Sjöholm, I.: *J. Pharm. Sci.* **69**(7), 838–842 (1980)
17. Franssen, O., Vos, O.P., Hennink, W.E.: *J. Controlled Release* **44**, 237–245 (1997)
18. Yeh, P.Y., Kopeckova, P., Kopecek, J.: *J. Polym. Sci. Part A Polym. Chem.* **32**(9), 1627–1637 (1994)
19. Peppas, N.A., Benner, R.E.: *Biomaterials* **1**(3), 158–162 (1980)
20. Bigi, A., Cojazzi, G., Panzavolta, S., Rubini, K., Roveri, N.: *Biomaterials* **22**(8), 763–768 (2001)
21. Kim, S.W., Bae, Y.H., Okano, T.: *Pharm. Res.* **9**(3), 283–290 (1992)
22. Bezemer, J.M., Radersma, R., Grijpma, D.W., Dijkstra, P.J., Feijen, J., van Blitterswijk, C.A.: *J. Controlled Release* **64**(1–3), 179–192 (2000)
23. Chenite, A., Chaput, C., Wang, D., Combes, C., Buschmann, M.D., Hoemann, C.D., Leroux, J.C., Atkinson, B.L., Binette, F., Selmani, A.: *Biomaterials* **21**(21), 2155–2161 (2000)
24. Eagland, D., Crowther, N.J., Butler, C.J.: *Eur. Polym. J.* **30**(7), 767–773 (1994)
25. Miyata, T., Asami, N., Urugami, T.: *Macromolecules* **32**(6), 2082–2084 (1999)
26. Kopecek, J.: *J. Polym. Sci. Part A Polym. Chem.* **47**(22), 5929–5946 (2009)
27. Staudinger, H., Husemann, E.: *Ber. Dtsch. Chem. Ges.* **68**, 1618–1634 (1935)

28. Funke, W., Okay, O., Joos-Muller, B.: *Microencapsul. Microgels Iniferters* **136**, 139–234 (1998)
29. Flory, P.J.: *Principles of polymer chemistry*. Cornell University Press, Ithaca (1953)
30. Millar, J.R., Kressman, T.R., Smith, D.G., Marr, W.E.: *J. Chem. Soc.*, 218 (1963)
31. Millar, J.R., Marr, W.E., Smith, D.G., Kressman, T.R.: *J. Chem. Soc.*, 2779 (1963)
32. Zhou, X., Liu, B., Yu, X., Zha, X., Zhang, X., Chen, Y., Wang, X., Jin, Y., Wu, Y., Chen, Y., Shan, Y., Chen, Y., Liu, J., Kong, W., Shen, J.: *J. Controlled Release* **121**(3), 200–207 (2007)
33. Xu, Y.M., Du, Y.M.: *Int. J. Pharm.* **250**(1), 215–226 (2003)
34. Balthasar, S., Michaelis, K., Dinauer, N., von Briesen, H., Kreuter, J., Langer, K.: *Biomaterials* **26**(15), 2723–2732 (2005)
35. Landfester, K., Musyanovych, A.: *Hydrogels in miniemulsions*. In: Pich, A.R.W. (ed.) *Chemical Design of Responsive Microgels*, vol. 234, pp. 39–63 (2010)
36. Downey, J.S., Frank, R.S., Li, W.H., Stover, H.D.H.: *Macromolecules* **32**(9), 2838–2844 (1999)
37. Li, K., Stover, H.D.H.: *J. Polym. Sci. Part A Polym. Chem* **31**(13), 3257–3263 (1993)
38. Li, K., Stover, H.D.H.: *J. Polym. Sci. Part A Polym. Chem* **31**(10), 2473–2479 (1993)
39. Fitch, R.M.: *J. Elastomers Plast.* **3**, 146–156 (1971)
40. Croucher, M.D., Winnik, M.A.: *In scientific methods for the study of polymer colloids and their applications*. In: Candau, F., Ottewill, R.H. (eds.) pp. 35–72. Kluwer Academic Publishers, Dordrecht (1990)
41. Duracher, D., Elaissari, A., Pichot, C.: *J. Polym. Sci. Part A Polym. Chem* **37**(12), 1823–1837 (1999)
42. Boyko, V., Pich, A., Lu, Y., Richter, S., Arndt, K.F., Adler, H.J.P.: *Polymer* **44**(26), 7821–7827 (2003)
43. Pich, A., Karak, A., Lu, Y., Ghosh, A.K., Adler, H.J.P.: *Macromol. Rapid Commun.* **27**(5), 344–350 (2006)
44. Nayak, S., Lyon, L.A.: *Angew. Chem. Int. Ed.* **44**(47), 7686–7708 (2005)
45. McPhee, W., Tam, K.C., Pelton, R.: *J. Colloid Interface Sci.* **156**(1), 24–30 (1993)
46. Boyko, V., Richter, S., Pich, A., Arndt, K.F.: *Colloid Polym. Sci.* **282**(2), 127–132 (2003)
47. Hoare, T., Pelton, R.: *Langmuir* **20**(6), 2123–2133 (2004)
48. Kratz, K., Hellweg, T., Eimer, W.: *Colloids Surf. Physicochem. Eng. Aspects* **170**(2–3), 137–149 (2000)
49. Hazot, P., Chapel, J.P., Pichot, C., Elaissari, A., Delair, T.: *J. Polym. Sci. Part A Polym. Chem* **40**(11), 1808–1817 (2002)
50. Debord, J.D., Lyon, L.A.: *Langmuir* **19**(18), 7662–7664 (2003)
51. Lopez-Leon, T., Ortega-Vinuesa, J.L., Bastos-Gonzalez, D., Elaissari, A.: *J. Phys. Chem. B* **110**(10), 4629–4636 (2006)
52. Jones, C.D., Lyon, L.A.: *Macromolecules* **33**(22), 8301–8306 (2000)
53. Nayak, S., Gan, D.J., Serpe, M.J., Lyon, L.A.: *Small* **1**(4), 416–421 (2005)
54. Gan, D.J., Lyon, L.A.: *J. Am. Chem. Soc.* **123**(31), 7511–7517 (2001)
55. Pich, A., Tessier, A., Boyko, V., Lu, Y., Adler, H.-J.P.: *Macromolecules* **39**(22), 7701–7707 (2006)
56. Braun, O., Selb, J., Candau, F.: *Polymer* **42**(21), 8499–8510 (2001)
57. Juranicova, V., Kawamoto, S., Fujimoto, K., Kawaguchi, H., Barton, J.: *Angew. Makromol. Chem.* **258**, 27–31 (1998)
58. Candau, F., Zekhnini, Z., Heatley, F., Franta, E.: *Colloid Polym. Sci.* **264**(8), 676–682 (1986)
59. Corpart, J.M., Candau, F.: *Colloid Polym. Sci.* **271**(11), 1055–1067 (1993)
60. Neyret, S., Vincent, B.: *Polymer* **38**(25), 6129–6134 (1997)
61. Landfester, K.: *Adv. Mater.* **13**(10), 765–768 (2001)
62. Landfester, K.: *Macromol. Rapid Commun.* **22**(12), 896–936 (2001)
63. Lorenz, M.R., Kohnle, M.-V., Dass, M., Walther, P., Hoecherl, A., Ziener, U., Landfester, K., Mailaender, V.: *Macromol. Biosci.* **8**(8), 711–727 (2008)

64. Schreiber, E., Ziener, U., Manzke, A., Plettl, A., Ziemann, P., Landfester, K.: *Chem. Mater.* **21**(8), 1750–1760 (2009)
65. Urban, M., Musyanovych, A., Landfester, K.: *Macromol. Chem. Phys.* **210**(11), 961–970 (2009)
66. Weiss, C.K., Landfester, K.: In *hybrid latex particles: Preparation with, VanHerck, A.M.L.K. (ed.) vol. 233*, pp. 185–236 (2010)
67. Landfester, K.: Synthesis of colloidal particles in miniemulsions. *Annu. Rev. Mater. Res.* **36**, 231–279 (2006)
68. Landfester, K.: *Angew. Chem. Int. Ed.* **48**(25), 4488–4507 (2009)
69. Landfester, K., Bechthold, N., Forster, S., Antonietti, M.: *Macromol. Rapid Commun.* **20**(2), 81–84 (1999)
70. Landfester, K., Bechthold, N., Tiarks, F., Antonietti, M.: *Macromolecules* **32**(16), 5222–5228 (1999)
71. Kobitskaya, E., Ekinci, D., Manzke, A., Plettl, A., Wiedwald, U., Ziemann, P., Biskupek, J., Kaiser, U., Ziener, U., Landfester, K.: *Macromolecules* **43**(7), 3294–3305 (2010)
72. Landfester, K., Willert, M., Antonietti, M.: *Macromolecules* **33**(7), 2370–2376 (2000)
73. Oh, J.K., Bencherif, S.A., Matyjaszewski, K.: *Polymer* **50**(19), 4407–4423 (2009)
74. Capek, I.: *Cent. Eur. J. Chem.* **1**(3), 291–304 (2003)
75. Ethirajan, A., Schoeller, K., Musyanovych, A., Ziener, U., Landfester, K.: *Biomacromolecules* **9**(9), 2383–2389 (2008)
76. Baier, G., Musyanovych, A., Dass, M., Theisinger, S., Landfester, K.: *Biomacromolecules* **11**(4), 960–968 (2010)
77. Kazakov, S., Kaholek, M., Kudasheva, D., Teraoka, I., Cowman, M.K., Levon, K.: *Langmuir* **19**(19), 8086–8093 (2003)
78. Chu, L.-Y., Kim, J.-W., Shah, R.K., Weitz, D.A.: *Adv. Funct. Mater.* **17**(17), 3499–3504 (2007)
79. Karg, M., Pastoriza-Santos, I., Perez-Juste, J., Hellweg, T., Liz-Marzan, L.M.: *Small* **3**, 1222–1229 (2007)
80. Sorrell, C.D., Carter, M.C.D., Serpe, M.J.: *Adv. Funct. Mater.* **21**(3), 425–433 (2011)
81. Debord, J.D., Lyon, L.A.: *J. Phys. Chem. B.* **104**(27), 6327–6331 (2000)
82. Hellweg, T., Dewhurst, C.D., Bruckner, E., Kratz, K., Eimer, W.: *Colloid Polym. Sci.* **278**(10), 972–978 (2000)
83. Jeong, B., Gutowska, A.: *Trends Biotechnol.* **20**(7), 305–311 (2002)
84. Malmsten, M., Bysell, H., Hansson, P.: *Curr. Opin. Colloid Interface Sci.* **15**(6), 435–444 (2010)
85. Zha, L., Banik, B., Alexis, F.: *Soft Matter* **7**(13), 5908–5916 (2011)
86. Hamidi, M., Azadi, A., Rafiei, P.: *Adv. Drug Del. Rev.* **60**(15), 1638–1649 (2008)
87. Kamphuis, M.M.J., Johnston, A.P.R., Such, G.K., Dam, H.H., Evans, R.A., Scott, A.M., Nice, E.C., Heath, J.K., Caruso, F.: *J. Am. Chem. Soc.* **132**(45), 15881–15883 (2010)
88. Vinogradov, S.V.: *Curr. Pharm. Des.* **12**(36), 4703–4712 (2006)
89. Park, T.G., Hoffman, A.S.: *J. Biomed. Mater. Res.* **24**(1), 21–38 (1990)
90. Welsch, N., Ballauff, M., Lu, Y.: Microgels as nanoreactors: applications in catalysis. In: Pich, A.R.W. (ed.) *Chemical Design of Responsive Microgels*, vol. 234, pp. 129–163. Springer, Berlin (2010)
91. Lu, Y., Mei, Y., Drechsler, M., Ballauff, M.: *Angew. Chem. Int. Ed.* **45**(5), 813–816 (2006)
92. Ballauff, M., Lu, Y.: *Polymer* **48**(7), 1815–1823 (2007)
93. Lin, C.-C., Metters, A.T.: *Adv. Drug Del. Rev.* **58**(12–13), 1379–1408 (2006)
94. Peppas, N.A., Keys, K.B., Torres-Lugo, M., Lowman, A.M.: *J. Controlled Release* **62**(1–2), 81–87 (1999)
95. Canal, T., Peppas, N.A.: *J. Biomed. Mater. Res.* **23**(10), 1183–1193 (1989)
96. Mason, M.N., Metters, A.T., Bowman, C.N., Anseth, K.S.: *Macromolecules* **34**(13), 4630–4635 (2001)
97. Amsden, B.: *Macromolecules* **31**(23), 8382–8395 (1998)

98. Peppas, N.A.: *Hydrogels in Medicine and Pharmacy*, vol. 1–3. CRC Press, Boca Raton (1986)
99. Masaro, L., Zhu, X.X.: *Prog. Polym. Sci.* **24**(5), 731–775 (1999)
100. Lustig, S.R., Peppas, N.A.: *J. Appl. Polym. Sci.* **36**(4), 735–747 (1988)
101. Cheung, R.Y., Ying, Y.M., Rauth, A.M., Marcon, N., Wu, X.Y.: *Biomaterials* **26**(26), 5375–5385 (2005)
102. Hennink, W.E., Talsma, H., Borchert, J.C.H., DeSmedt, S.C., Demeester, J.: *J. Controlled Release* **39**(1), 47–55 (1996)
103. Brazel, C.S., Peppas, N.A.: *Biomaterials* **20**(8), 721–732 (1999)
104. Siepmann, J., Peppas, N.A.: *Adv. Drug Del. Rev.* **48**(2–3), 139–157 (2001)
105. Das, M., Zhang, H., Kumacheva, E.: *Annu. Rev. Mater. Res.* **36**, 117–142 (2006)
106. Griset, A.P., Walpole, J., Liu, R., Gaffey, A., Colson, Y.L., Grinstaff, M.W.: *J. Am. Chem. Soc.* **131**(7), 2469–2471 (2009)
107. Haag, R., Kratz, F.: *Angew. Chem. Int. Ed.* **45**(8), 1198–1215 (2006)
108. Khandare, J., Minko, T.: *Prog. Polym. Sci.* **31**(4), 359–397 (2006)
109. Heller, J.: *Biomaterials* **1**(1), 51–57 (1980)
110. Ehrbar, M., Metters, A., Zammaretti, P., Hubbell, J.A., Zisch, A.H.: *J. Controlled Release* **101**(1–3), 93–109 (2005)
111. Rice, M.A., Sanchez-Adams, J., Anseth, K.S.: *Biomacromolecules* **7**(6), 1968–1975 (2006)
112. Anseth, K.S., Metters, A.T., Bryant, S.J., Martens, P.J., Elisseeff, J.H., Bowman, C.N.: *J. Controlled Release* **78**(1–3), 199–209 (2002)
113. Kawaguchi, H.: *Prog. Polym. Sci.* **25**(8), 1171–1210 (2000)
114. Pich, A., Richtering, W., *Chemical Design of Responsive Microgels*, vol. 234, pp. 1–37. Springer, Berlin (2010)
115. Kubota, K., Fujishige, S., Ando, I.: *J. Phys. Chem.* **94**(12), 5154–5158 (1990)
116. Dusek, K., Patterso, D.: *J. Polym. Sci. Part B: Polym. Phys.* **6**(7PA2), 1209–12120 (1968)
117. Wu, C., Zhou, S.Q.: *Macromolecules* **30**(3), 574–576 (1997)
118. Pelton, R.H., Chibante, P.: *Colloids Surf.* **20**(3), 247–256 (1986)
119. Zha, L., Hu, J., Wang, C., Fu, S., Elaissari, A., Zhang, Y.: *Colloid Polym. Sci.* **280**(1), 1–6 (2002)
120. Gao, J., Frisken, B.J.: *Langmuir* **19**(13), 5212–5216 (2003)
121. Zhang, Q., Zha, L., Ma, J., Liang, B.: *Macromol. Rapid Commun.* **28**(1), 116–120 (2007)
122. Ge, H., Ding, Y., Ma, C., Zhang, G.: *J. Phys. Chem. B.* **110**(41), 20635–20639 (2006)
123. Meyer, D.E., Shin, B.C., Kong, G.A., Dewhirst, M.W., Chilkoti, A.: *J. Controlled Release* **74**(1–3), 213–224 (2001)
124. Nolan, C.M., Gelbaum, L.T., Lyon, L.A.: *Biomacromolecules* **7**(10), 2918–2922 (2006)
125. Nayak, S., Lee, H., Chmielewski, J., Lyon, L.A.: *J. Am. Chem. Soc.* **126**(33), 10258–10259 (2004)
126. Gao, H.F., Yang, W.L., Min, K., Zha, L.S., Wang, C.C., Fu, S.K.: *Polymer* **46**(4), 1087–1093 (2005)
127. Lee, Y., Park, S.Y., Kim, C., Park, T.G.: *J. Controlled Release* **135**(1), 89–95 (2009)
128. Vihola, H., Laukkanen, A., Tenhu, H., Hirvonen, J.: *J. Pharm. Sci.* **97**(11), 4783–4793 (2008)
129. Owens, III, D.E., Jian, Y., Fang, J.E., Slaughter, B.V., Chen, Y.-H., Peppas, N.A.: *Macromolecules* **40**(20), 7306–7310 (2007)
130. Bouillot, P., Vincent, B.: *Colloid Polym. Sci.* **278**(1), 74–79 (2000)
131. Yang, M., Liu, C., Li, Z., Gao, G., Liu, F.: *Macromolecules* **43**(24), 10645–10651 (2010)
132. Echeverria, C., Lopez, D., Mijangos, C.: *Macromolecules* **42**(22), 9118–9123 (2009)
133. Schmaljohann, D.: *Adv. Drug Del. Rev.* **58**(15), 1655–1670 (2006)
134. Eichenbaum, G.M., Kiser, P.F., Shah, D., Simon, S.A., Needham, D.: *Macromolecules* **32**(26), 8996–9006 (1999)
135. Eichenbaum, G.M., Kiser, P.F., Dobrynin, A.V., Simon, S.A., Needham, D.: *Macromolecules* **32**(15), 4867–4878 (1999)
136. Wells, L.A., Sheardown, H.: *Eur. J. Pharm. Biopharm.* **65**(3), 329–335 (2007)

137. Dou, H., Jiang, M.: *Polym. Int.* **56**(10), 1206–1212 (2007)
138. Ojugo, A.S.E., McSheehy, P.M.J., McIntyre, D.J.O., McCoy, C., Stubbs, M., Leach, M.O., Judson, I.R., Griffiths, J.R.: *NMR Biomed.* **12**(8), 495–504 (1999)
139. Van Dyke, R.W.: *Subcell. Biochem.* **27**, 331 (1996)
140. Das, M., Mardiyani, S., Chan, W.C.W., Kumacheva, E.: *Adv. Mater.* **18**(1), 80–83 (2006)
141. Tan, J.P.K., Tam, K.C.: *J. Controlled Release* **118**(1), 87–94 (2007)
142. Vinogradov, S., Batrakova, E., Kabanov, A.: *Colloids Surf. B. Biointerfaces* **16**(1–4), 291–304 (1999)
143. Lin, C., Zhong, Z., Lok, M.C., Jiang, X., Hennink, W.E., Feijen, J., Engbersen, J.F.J.: *Bioconjug. Chem.* **18**(1), 138–145 (2007)
144. Vinogradov, S.V., Bronich, T.K., Kabanov, A.V.: *Adv. Drug Del. Rev.* **54**(1), 135–147 (2002)
145. Deka, S.R., Quarta, A., Di Corato, R., Falqui, A., Manna, L., Cingolani, R., Pellegrino, T.: *Langmuir* **26**(12), 10315–10324 (2010)
146. Zhang, H., Mardiyani, S., Chan, W.C.W., Kumacheva, E.: *Biomacromolecules* **7**(5), 1568–1572 (2006)
147. Moniruzzaman, M., Fernando, G.F., Talbot, J.D.R.: *J. Polym. Sci. Part A Polym. Chem.* **42**(12), 2886–2896 (2004)
148. Kungwachakun, D., Irie, M.: *Makromol. Chemie. Rapid Commun.* **9**(4), 243–246 (1988)
149. Chen, L., Li, S.G., Zhao, Y.P., Wang, Y.C., Wang, Q.W.: *J. Appl. Polym. Sci.* **96**(6), 2163–2167 (2005)
150. Jochum, F.D., Theato, P.: *Chem. Commun.* **46**(36), 6717–6719 (2010)
151. Alvarez-Lorenzo, C., Bromberg, L., Concheiro, A.: *Photochem. Photobiol.* **85**(4), 848–860 (2009)
152. Li, M.-H., Keller, P.: *Soft Matter* **5**(5), 927–937 (2009)
153. Suzuki, A., Ishii, T., Maruyama, Y.: *J. Appl. Phys.* **80**(1), 131–136 (1996)
154. Nayak, S., Lyon, L.A.: *Chem. Mater.* **16**(13), 2623–2627 (2004)
155. Rodriguez-Fernandez, J., Fedoruk, M., Hrelescu, C., Lutich, A.A., Feldmann, J.: *Nanotechnology* **22**(24), 245708 (2011)
156. Oishi, M., Hayashi, H., Uno, T., Ishii, T., Iijima, M., Nagasaki, Y.: *Macromol. Chem. Phys.* **208**(11), 1176–1182 (2007)
157. Kawano, T., Niidome, Y., Mori, T., Katayama, Y., Niidome, T.: *Bioconjug. Chem.* **20**(2), 209–212 (2009)
158. Das, M., Sanson, N., Fava, D., Kumacheva, E.: *Langmuir* **23**(1), 196–201 (2007)
159. Gorelikov, I., Field, L.M., Kumacheva, E.: *J. Am. Chem. Soc.* **126**(49), 15938–15939 (2004)
160. Daniel, M.C., Astruc, D.: *Chem. Rev.* **104**(1), 293–346 (2004)
161. Nakamura, T., Tamura, A., Murotani, H., Oishi, M., Jinji, Y., Matsuishi, K., Nagasaki, Y.: *Nanoscale* **2**(5), 739–746 (2010)
162. Wu, W., Shen, J., Banerjee, P., Zhou, S.: *Biomaterials* **31**(29), 7555–7566 (2010)
163. Hoare, T., Pelton, R.: *Macromolecules* **37**(7), 2544–2550 (2004)
164. Berndt, I., Richtering, W.: *Macromolecules* **36**(23), 8780–8785 (2003)
165. Kiser, P.F., Wilson, G., Needham, D.: *Nature* **394**(6692), 459–462 (1998)
166. Franssen, O., Vandervennet, L., Roders, P., Hennink, W.E.: *J. Controlled Release* **60**(2–3), 211–221 (1999)
167. Moore, A., McGuirk, P., Adams, S., Jones, W.C., McGee, J.P., Ohagan, D.T., Mills, K.H.G.: *Vaccine* **13**(18), 1741–1749 (1995)
168. Kim, K.S., Graham, N.B.: *J. Ind. Eng. Chem.* **4**(3), 221–225 (1998)
169. Jhaveri, S.B., Carter, K.R.: *Macromolecules* **40**(22), 7874–7877 (2007)
170. Murthy, N., Thng, Y.X., Schuck, S., Xu, M.C., Frechet, J.M.J.: *J. Am. Chem. Soc.* **124**(42), 12398–12399 (2002)
171. Murthy, N., Xu, M.C., Schuck, S., Kunisawa, J., Shastri, N., Frechet, J.M.J.: *Proc. Natl. Acad. Sci. USA* **100**(9), 4995–5000 (2003)

172. Standley, S.M., Kwon, Y.J., Murthy, N., Kunisawa, J., Shastri, N., Guillaudeu, S.J., Lau, L., Frechet, J.M.J.: *Bioconjug. Chem.* **15**(6), 1281–1288 (2004)
173. Goh, S.L., Murthy, N., Xu, M.C., Frechet, J.M.J.: *Bioconjug. Chem.* **15**(3), 467–474 (2004)
174. Bulmus, V., Chan, Y., Nguyen, Q., Tran, H.L.: *Macromol. Biosci.* **7**(4), 446–455 (2007)
175. Shi, L., Berkland, C.: *Macromolecules* **40**(13), 4635–4643 (2007)
176. Bernkop-Schnurch, A.: *Adv. Drug Del. Rev.* **57**(11), 1569–1582 (2005)
177. Sivakumar, S., Bansal, V., Cortez, C., Chong, S.-F., Zelikin, A.N., Caruso, F.: *Adv. Mater.* **21**(18), 1820–1824 (2009)
178. Chong S.-F., Chandrawati, R., Staedler, B., Park, J., Cho, J., Wang, Y., Jia, Z.V., Davis, T.P., Zelikin, A.N., Caruso, F.: *Small* **5**(22), 2601–2610 (2009)
179. Bromberg, L., Temchenko, M., Alakhov, V., Hatton, T.A.: *Langmuir* **21**(4), 1590–1598 (2005)
180. Oh, J.K., Siegwart, D.J., Matyjaszewski, K.: *Biomacromolecules* **8**(11), 3326–3331 (2007)
181. Ryu, J.-H., Chacko, R.T., Jiwanich, S., Bickerton, S., Babu, R.P., Thayumanavan, S.: *J. Am. Chem. Soc.* **132**(48), 17227–17235 (2010)
182. Pradny, M., Kopecek, J.: *Makromol. Chemie-Macromol Chem. Phys.* **191**(8), 1887–1897 (1990)
183. Ghandehari, H., Kopeckova, P., Kopecek, J.: *Biomaterials* **18**(12), 861–872 (1997)
184. Franssen, O., vanOoijen, R.D., deBoer, D., Maes, R.A.A., Herron, J.N., Hennink, W.E.: *Macromolecules* **30**(24), 7408–7413 (1997)
185. Franssen, O., van Ooijen, R.D., de Boer, D., Maes, R.A.A., Hennink, W.E.: *Macromolecules* **32**(9), 2896–2902 (1999)
186. Abdurrahmanoglu, S., Firat, Y.: *J. Appl. Polym. Sci.* **106**, 3565–3570 (2007)
187. Franssen, O., Stenekes, R.J.H., Hennink, W.E.: *J. Controlled Release* **59**(2), 219–228 (1999)
188. De Geest, B.G., De Koker, S., Demeester, J., De Smedt, S.C., Hennink, W.E.: *Polym. Chem.* **1**(2), 137–148 (2010)
189. Kumashiro, Y., Ooya, T., Yui, N.: *Macromol. Rapid Commun.* **25**(8), 867–872 (2004)
190. Patnaik, S., Sharma, A.K., Garg, B.S., Gandhi, R.P., Gupta, K.C.: *Int. J. Pharm.* **342**(1–2), 184–193 (2007)
191. Hirakura, T., Nomura, Y., Aoyama, Y., Akiyoshi, K.: *Biomacromolecules* **5**(5), 1804–1809 (2004)
192. Kuang, G.-C., Ji, Y., Jia, X.-R., Li, Y., Chen, E.-Q., Zhang, Z.-X., Wei, Y.: *Tetrahedron* **65**(17), 3496–3501 (2009)
193. Connal, L.A., Vestberg, R., Hawker, C.J., Qiao, G.G.: *Adv. Funct. Mater.* **18**(20), 3315–3322 (2008)
194. Kuckling, D., Vo, C.D., Wohlrab, S.E.: *Langmuir* **18**(11), 4263–4269 (2002)
195. Gupta, S., Kuckling, D., Kretschmer, K., Choudhary, V., Adler, H.-J.: *J. Polym. Sci. Part A Polym. Chem* **45**(4), 669–679 (2007)
196. Yusa, S.-I., Sugahara, M., Endo, T., Morishima, Y.: *Langmuir* **25**(9), 5258–5265 (2009)
197. Tao, J., Liu, G.J., Ding, J.F., Yang, M.L.: *Macromolecules* **30**(14), 4084–4089 (1997)
198. Shi, D., Matsusaki, M., Akashi, M.: *Bioconjug. Chem.* **20**(10), 1917–1923 (2009)
199. Shi, D.J., Matsusaki, M., Kaneko, T., Akashi, M.: *Macromolecules* **41**(21), 8167–8172 (2008)
200. He, J., Tong, X., Zhao, Y.: *Macromolecules* **42**(13), 4845–4852 (2009)
201. Jin, Q., Liu, G., Li, J.: *Eur. Polym. J.* **46**(11), 2120–2128 (2010)
202. Jin, Q., Liu, X., Liu, G., Ji, J.: *Polymer* **51**(6), 1311–1319 (2010)
203. Jiang, H.Y., Kelch, S., Lendlein, A.: *Adv. Mater.* **18**(11), 1471–1475 (2006)
204. Mayer, G., Heckel, A.: *Angew. Chem. Int. Ed.* **45**(30), 4900–4921 (2006)
205. Day, D., Gu, M., Smallridge, A.: *Adv. Mater.* **13**(12–13), 1005–1007 (2001)
206. del Campo, A., Boos, D., Spiess, H.W., Jonas, U.: *Angew. Chem. Int. Ed.* **44**(30), 4707–4712 (2005)
207. Wang, G., Tong, X., Zhao, Y.: *Macromolecules* **37**(24), 8911–8917 (2004)
208. Haeckel, M., Kador, L., Kropp, D., Schmidt, H.-W.: *Adv. Mater.* **19**(2), 227–231 (2007)
209. Hagen, R., Bieringer, T.: *Adv. Mater.* **13**(23), 1805–1810 (2001)

210. Ruhmann, R.: *Polym. Int.* **43**(2), 103–108 (1997)
211. Shirai, M., Tsunooka, M.: *Bull. Chem. Soc. Jpn.* **71**(11), 2483–2507 (1998)
212. Yamaoka, T., Watanabe, H.: *J. Photopolym. Sci. Technol.* **17**(3), 341–359 (2004)
213. Yamashita, T., Nara, A., Fujimoto, T., Okano, K.: *J. Photopolym. Sci. Technol.* **22**(6), 783–787 (2009)
214. Belfield, K.D., Schafer, K.J.: *Chem. Mater.* **14**(9), 3656–3662 (2002)
215. Ito, Y., Sugimura, N., Kwon, O.H., Imanishi, Y.: *Nat. Biotechnol.* **17**(1), 73–75 (1999)
216. Irie, M., Iwayanagi, T., Taniguchi, Y.: *Macromolecules* **18**(12), 2418–2422 (1985)
217. Lee, H.-I., Wu, W., Oh, J.K., Mueller, L., Sherwood, G., Peteanu, L., Kowalewski, T., Matyjaszewski, K.: *Angew. Chem. Int. Ed.* **46**(14), 2453–2457 (2007)
218. Goodwin, A.P., Mynar, J.L., Ma, Y.Z., Fleming, G.R., Frechet, J.M.J.: *J. Am. Chem. Soc.* **127**(28), 9952–9953 (2005)
219. Klinger, D., Nilles, K., Theato, P.: *J. Polym. Sci. Part A Polym. Chem.* **48**(4), 832–844 (2010)
220. Corredor, C.C., Huang, Z.-L., Belfield, K.D., Morales, A.R., Bondar, M.V.: *Chem. Mater.* **19**(21), 5165–5173 (2007)
221. Zheng, Y.J., Mieie, M., Mello, S.V., Mabrouki, M., Andreopoulos, F.M., Konka, V., Pham, S.M., Leblanc, R.M.: *Macromolecules* **35**(13), 5228–5234 (2002)
222. Chen, Y., Geh, J.L.: *Polymer* **37**(20), 4481–4486 (1996)
223. Chen, Y., Geh, J.L.: *Polymer* **37**(20), 4473–4480 (1996)
224. Rabek, J.F.: *Mechanisms of photophysical process and photochemical reactions in polymer.* Wiley, New York (1987)
225. Wang, J.Z., Nayak, B.R., Creed, D., Hoyle, C.E., Mathias, L.J.: *Polymer* **46**(18), 6897–6909 (2005)
226. Beines, P.W., Klosterkamp, I., Menges, B., Jonas, U., Knoll, W.: *Langmuir* **23**(4), 2231–2238 (2007)
227. Braun, D., Berger, J.: *Kolloid Z. Z. Polym.* **250**(2), 142–147 (1972)
228. Conforti, P.F., Garrison, B.J.: *Chem. Phys. Lett.* **406**(4–6), 294–299 (2005)
229. Jiang, J.Q., Tong, X., Zhao, Y.: *J. Am. Chem. Soc.* **127**(23), 8290–8291 (2005)
230. Katz, J.S., Doh, J., Irvine, D.J.: *Langmuir* **22**(1), 353–359 (2006)
231. Jiang, J.Q., Tong, X., Morris, D., Zhao, Y.: *Macromolecules* **39**(13), 4633–4640 (2006)
232. Macdonald, S.A., Willson, C.G.: *ACS Symp. Ser.* **184**, 73–81 (1982)
233. Ciamician, G., Silber, P.: *Ber. Dtsch. Chem. Ges.* **34**, 2040–2046 (1901)
234. Wong, W.K., Schupp, H., Schnabel, W.: *Macromolecules* **22**(5), 2176–2181 (1989)
235. Schupp, H., Wong, W.K., Schnabel, W.: *J. Photochem.* **36**(1), 85–97 (1987)
236. Zhu, Q.Q., Schnabel, W., Schupp, H.: *J. Photochem.* **39**(2), 317–332 (1987)
237. Gravel, D., Giasson, R., Blanchet, D., Yip, R.W., Sharma, D.K.: *Can. J. Chem.* **69**(8), 1193–1200 (1991)
238. Yip, R.W., Wen, Y.X., Gravel, D., Giasson, R., Sharma, D.K.: *J. Phys. Chem.* **95**(16), 6078–6081 (1991)
239. Holmes, C.P.: *J. Org. Chem.* **62**(8), 2370–2380 (1997)
240. Holmes, C.P., Jones, D.G.: *J. Org. Chem.* **60**(8), 2318–2319 (1995)
241. Buhler, S., Lagoja, I., Giegrich, H., Stengele, K.P., Pfeleiderer, W.: *Helv. Chim. Acta.* **87**(3), 620–659 (2004)
242. Rodebaugh, R., FraserReid, B., Geysen, H.M.: *Tetrahedron Lett.* **38**(44), 7653–7656 (1997)
243. Whitehouse, D.L., Savinov, S.N., Austin, D.J.: *Tetrahedron Lett.* **38**(45), 7851–7852 (1997)
244. Yoo, D.J., Greenberg, M.M.: *J. Org. Chem.* **60**(11), 3358–3364 (1995)
245. Piggott, A.M., Karuso, P.: *Tetrahedron Lett.* **46**(47), 8241–8244 (2005)
246. Bai, X.P., Li, Z.M., Jockusch, S., Turro, N.J., Ju, J.Y.: *Proc. Natl. Acad. Sci. U.S.A.* **100**(2), 409–413 (2003)
247. Cameron, J.F., Frechet, J.M.J.: *J. Am. Chem. Soc.* **113**(11), 4303–4313 (1991)
248. Reichmanis, E., Smith, B.C., Gooden, R.: *J. Polym. Sci. Part A Polym. Chem.* **23**(1), 1–8 (1985)

249. Lemke, E.A., Summerer, D., Geierstanger, B.H., Brittain, S.M., Schultz, P.G.: *Nat. Chem. Biol.* **3**(12), 769–772 (2007)
250. Alvarez, M., Best, A., Pradhan-Kadam, S., Koynov, K., Jonas, U., Kreiter, M.: *Adv. Mater.* **20**(23), 4563–4567 (2008)
251. Barzynski, H., Sanger, D.: *Angew. Makromol. Chem.* **93**, 131–141 (1981)
252. Kloxin, A.M., Kasko, A.M., Salinas, C.N., Anseth, K.S.: *Science* **324**(5923), 59–63 (2009)
253. Dvir, T., Banghart, M.R., Timko, B.P., Langer, R., Kohane, D.S.: *Nano Lett.* **10**(1), 250–254 (2010)
254. Li, Y., Xinru, J., Min, G., Kuang, G., Wei, Y.: *J. Polym. Sci. Part A Polym. Chem.* **48**, 551–557 (2010)
255. Burakowska, E., Zimmerman, S.C., Haag, R.: *Small* **5**(19), 2199–2204 (2009)
256. Park, C., Lee, K., Kim, C.: *Angew. Chem. Int. Ed.* **48**(7), 1275–1278 (2009)

Chapter 4

Outline

The focus of this work lies on investigations on the following three approaches to irradiation-dependent response mechanisms: first, the light-sensitivity can be achieved by the utilization of photo-cleavable crosslinking points which represents a method for decreasing the crosslinking density until complete decomposition of the network upon irradiation. Second, the attachment of a functional drug molecule to a microgel network via a photo-cleavable linker enables to trigger its release by the appliance of light. Third, hydrophobic nanoparticles consisting of a photo-resist polymer change their hydrophilicity upon the light-induced detachment of the photo-labile chromophore, thus resulting in particle swelling and complete dissolution. Different approaches and concepts have been realized in this thesis:

Photo-sensitive microgels based on light-cleavable crosslinkers. The aim of this approach is the development of two classes of photo-sensitive microgels: (1) polymeric gel nanoparticles swellable and degradable in organic solvents and (2) hydrogel nanoparticles swellable and degradable in aqueous media. In order to realize this concept, novel photo-labile divinyl functionalized monomeric crosslinkers based on *o*-nitrobenzyl derivatives are designed to enable a light-induced degradation of the resulting polymeric networks. While the systematic variation of the molecular structure is assumed to result in different degradation rates depending on the irradiation conditions, the specific hydrophilicity of these divinyl functionalized molecules is characterized by medium polarity and, therefore, enables their versatile utilization in either direct or inverse miniemulsion copolymerizations. This behavior gives rise to the preparation of either PMMA or hydroxyl functionalized PHEMA microgels swellable and degradable in organic solvents. Moreover, by the introduction of anionic MAA moieties into PHEMA microgels, this concept can be transferred to double stimuli-responsive p(HEMA-*co*-MAA) hydrogel nanoparticles exhibiting a pH-dependent swelling and light-induced degradation behavior in aqueous media. This sensitivity to two orthogonal triggers is proposed to combine a pH-induced *post-formation* loading mechanism with a pH- and light-triggered release.

In addition, the concept of double-stimuli responsive hydrogel nanoparticles can be extended by the development of a new class of enzyme- and light-sensitive microgels based on (meth-)acrylate functionalized dextrans as photo- and enzymatically degradable macromolecular crosslinkers. The sensitivity to light can be achieved by introducing a photo-labile linker between the dextran chain and the polymerizable vinyl moieties. In contrast to the light-sensitive p(HEMA-*co*-MAA) microgels, the water solubility of the macromolecular crosslinkers is assumed to enable an in situ loading approach of hydrophilic functional compounds, thus extending the concept of photo-sensitive hydrogel nanoparticles.

Light-sensitive microgel-drug conjugates. The underlying concept of this approach is the development of a novel functional monomer consisting of a doxorubicin molecule covalently attached to a radically polymerizable methacrylate group via a photo-labile linker. Copolymerization of this doxorubicin-photo-labile linker-methacrylate (Dox-PL-MA) moiety with HEMA and MAA in inverse miniemulsion is designed to yield anionic microgels as well defined carrier systems for the light-induced delivery of doxorubicin. Here, the drug molecule is covalently attached to the network-forming copolymer and therefore leakage is assumed to be hindered until the light-induced cleavage of the linker molecule enables the release.

Photo-resist nanoparticles. This approach deals with the development of hydrophobic nanoparticles consisting of a photo-resist polymer. The polymeric structure is based on a protected poly (methacrylic acid) that can be easily deprotected by the photolytic cleavage of light-sensitive *o*-nitrobenzyl esters. As a result, conversion of the initial hydrophobic polymer into hydrophilic PMAA induces in situ particle swelling and finally complete dissolution in water. Here, the initial hydrophobic nature of the particles which enables an in situ loading of functional hydrophobic substances is of special interest. In comparison to the previously mentioned microgels which are limited to the loading and release of hydrophilic compounds, the light-induced release of hydrophobic substances in aqueous medium dramatically extends the fields of potential applications for photo-sensitive carriers.

In addition to these three different light-induced response mechanisms of microgels and nanoparticles, further investigations in the field of (stimuli-responsive) microgels are part of this thesis. The respective concepts are briefly introduced in the following paragraph.

Towards stimuli-responsive core/shell nanoparticles. The introduction of a degradable/swellable (polymeric) shell around the respective microgel core is assumed to enhance the loading and release efficiency of stimuli-responsive microgels since the shell serves as a diffusion barrier to prevent leakage of embedded functional compounds. Thus, investigating potential synthetic pathways for the formation of multiple stimuli-responsive core/shell nanoparticles containing a hydrogel core is of high interest. Preliminary studies on non-stimuli-responsive model systems include the shell formation around a preformed (microgel) core and the formation of the microgel core in a polymeric shell.

Surface modification of microgels with photo-reactive chromophores. The functionalization of microgels surfaces with photo-reactive moieties to trigger the particles interaction with different compounds or with each other is another interesting research area. Realization of this concept is based on the development of a synthetic protocol for the facile and effective surface modification of PHEMA and p(HEMA-*co*-MAA) microgels with cinnamoyl groups. The respective materials are designed as nanometric building blocks for the preparation of self-healing hydrogel thin films.

Chapter 5

Results and Discussion

5.1 Photo-Sensitive Microgels Based on Light-Cleavable Monomeric Crosslinkers

This chapter describes the development of two classes of photo-sensitive microgels: (i) polymeric gel nanoparticles swellable and degradable in organic solvents and (ii) hydrogel nanoparticles swellable and degradable in aqueous media. Both types of microgels are based on newly developed light-cleavable monomeric crosslinkers containing *o*-nitrobenzyl derivatives as the photo-reactive chromophores. The specific hydrophilicity of these divinyl functionalized molecules is characterized by a medium polarity and, therefore, enables their versatile utilization in either direct or inverse miniemulsion. In both cases, the dispersed phase can be formed by either dissolving the crosslinkers directly in the respective monomer(s) or by dissolving all polymerizable components in an organic solvent immiscible with the continuous phase. Free radical copolymerizations of the crosslinkers with different (functional) monomers yields then gel particles in the nanometer size range. Complete decomposition of the network structure can be achieved by cleaving the labile crosslinking points upon the appliance of light as external trigger and results in freely soluble polymer chains. The concept is schematically illustrated in Fig. 5.1.

5.1.1 Photo-Sensitive Polymeric Gel Nanoparticles

The use of cleavable crosslinking points in a gel is a method for triggering the complete decomposition of the network architecture using external stimuli. As mentioned before, light represents an outstanding position among different stimuli

Parts of this work are published in the paper “*Photo-Sensitive PMMA Microgels: Light-Triggered Swelling and Degradation*” Daniel Klinger, Katharina Landfester *Soft Matter*, **2011**, 7 (4), 1426. Reproduced from [9] by permission of the Royal Society of Chemistry.

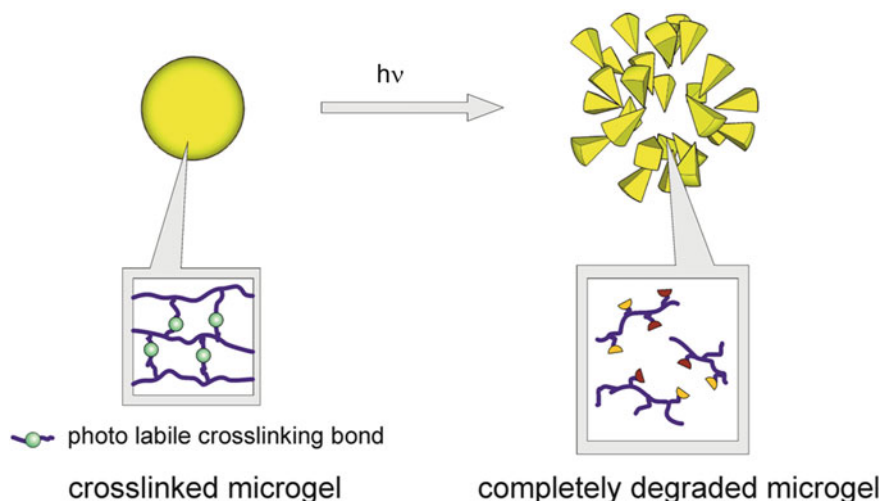


Fig. 5.1 Concept of photo-sensitive microgels based on light-cleavable monomeric crosslinkers

as it can be applied in a very precise manner by selecting suitable wavelengths, polarization directions, focus and intensities in a non-contact approach, respectively [1, 2]. Photochemistry in combination with polymeric gels is well established for the formation of crosslinks by the application of UV light [3, 4]. While e.g., the reversibility of the [2+2] cycloaddition reaction of coumarin, anthracene and cinnamoyl derivatives is well examined to prepare stimuli responsive macroscopic gels [5, 6], only little attention has been paid to the formation of photo-sensitive gel particles in the nano- or micrometer size range [7, 8]. In general, light-degradable (organo-) microgels represent a highly interesting class of materials that find applications in a broad variety of fields. Especially, microgels degradable in organic solvents could serve e.g., as carrier systems for catalytically active metal nanoparticles, whereat the accessibility of the catalyst can be triggered by the gel degradation.

In order to prepare photo-sensitive polymeric gel nanoparticles, novel photo-labile divinyl functionalized crosslinkers based on *o*-nitrobenzyl derivatives are designed to enable a light-induced degradation of the resulting polymeric networks. The systematic variation of the molecular structure is assumed to result in different degradation rates depending on the irradiation conditions. The work described in the following chapter deals with the preparation of photo-degradable PMMA microgels by free radical copolymerization of the crosslinkers with MMA in a direct miniemulsion polymerization process. In addition, utilization of the crosslinkers in a free radical copolymerization with HEMA as a hydrophilic monomer in inverse miniemulsion gives rise to hydroxyl functionalized light-sensitive microgels.

5.1.1.1 Photo-Sensitive PMMA Microgels: Light-Triggered Swelling and Degradation

The aim of this work is the synthesis of two classes (type A and type B) of novel photo-labile divinyl functionalized crosslinkers based on *o*-nitrobenzyl moieties, which will be used to build up photo-degradable PMMA microgels by free radical copolymerization with MMA in miniemulsion. The synthesized crosslinker structures were designed to exhibit two different degradation behaviors, thus influencing the swelling properties of the resulting PMMA gel particles upon irradiation in a good solvent for the polymer chains.

Investigations on the cleavage behavior will be focused on controlling the independent degradation of the different types of gel particles by means of irradiation wavelengths and times applied. A dissimilar photolytic reactivity of the crosslinkers should in principle enable the successive decomposition of one specific type of microgel after the other in a mixed dispersion of the two, thus giving access to the potential subsequent release of different functional compounds. The described concept is schematically illustrated in Fig. 5.2.

Irradiation of type B microgels with UV-A light of $\lambda > 315$ nm is proposed to result in either highly swollen, partially degraded gel networks or complete particle dissolution. In comparison, the structure of type A microgels is supposed to remain intact under the same conditions. Furthermore, distinct photolysis rates of the different crosslinker types should enable the independent time-controlled degradation of type B microgels using broadband UV light containing wavelengths of $\lambda < 315$ nm. Short irradiation times t_1 lead hereby selectively to the complete degradation of type B particles. Eventually, longer irradiation times $t_2 > t_1$ then enable the full particle degradation of type A microgels as well. In summary, either

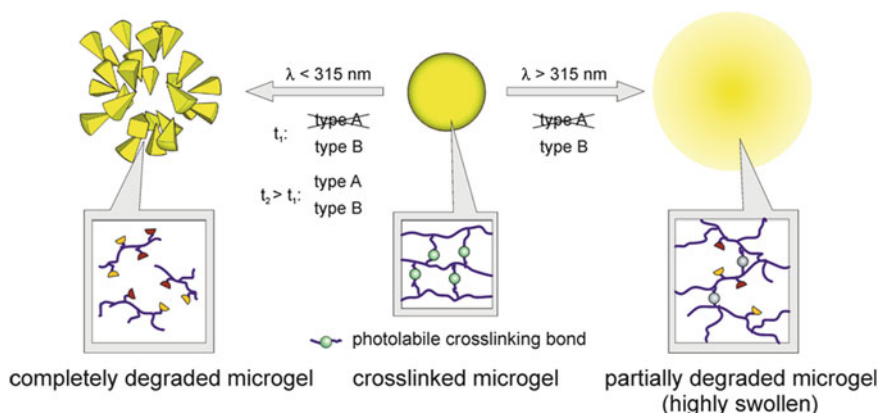


Fig. 5.2 Schematic representation of swelling and degradation behavior of type A and type B photo-degradable PMMA microgels upon UV irradiation with different wavelengths and for different irradiation times t_1 and t_2 . Reproduced from [9] by permission of the Royal Society of Chemistry

complete or partial particle degradation for both types of microgels is assumed to selectively be achieved by variation of the used UV light wavelengths and irradiation times (Fig. 5.2). Moreover, the low molecular weight structure of the crosslinkers should cause an initial small mesh size of the resulting gel, allowing the embedding of relatively small molecules.

Synthesis and characterization of photo-labile crosslinkers. In order to investigate the desired influence of the photo-labile chromophore on the photo-reaction of the resulting crosslinkers, two categories of molecules differing in their absorption spectra were synthesized and characterized regarding their photolysis. Figure 5.3 shows the synthetic pathway to four different photo-cleavable crosslinkers (CL-1A, CL-2A, CL-3A and CL-4B).

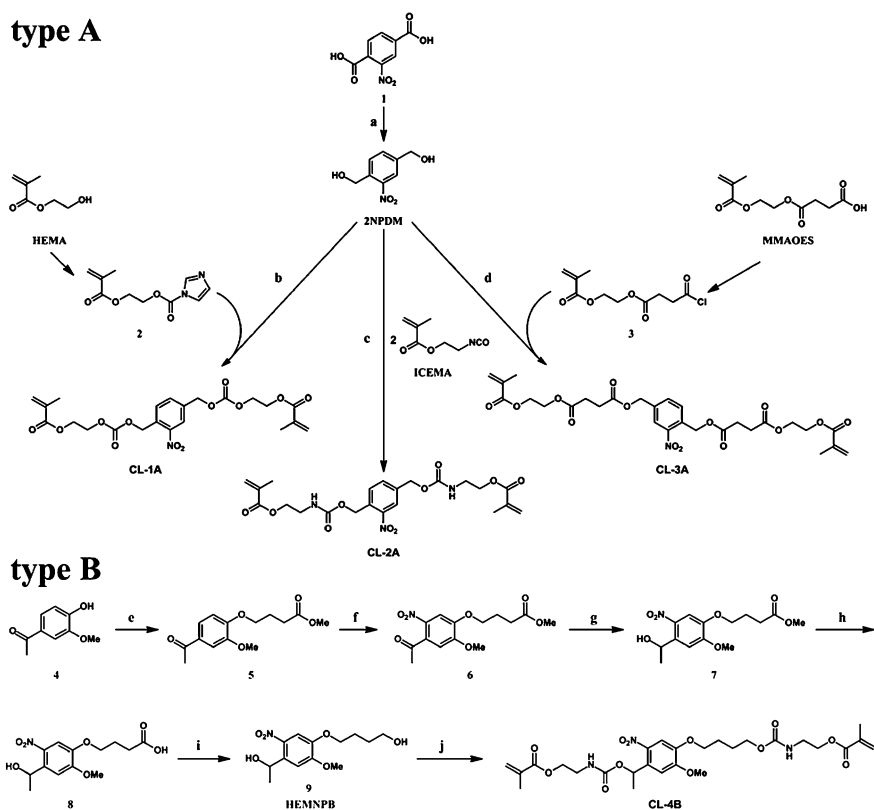


Fig. 5.3 Synthetic pathways to photo-cleavable crosslinkers of type A and B. Reagents and Conditions: **a** $\text{BH}_3^*/\text{THF}/\text{THF}$, 0 °C, 1 h then 40 °C, 18 h, 90 %; **b** (2), sodium ethanoate, THF (anhyd.), 25 °C, 5 day, 52 %; **c** 2-isocyanatoethyl methacrylate, THF (anhyd.), 65 °C, 24 h, 72 %; **d** (3), triethylamine, THF (anhy.), 25 °C, 16 h, 40 %; **e** methyl 4-bromobutyrate, $\text{K}_2\text{CO}_3/\text{DMF}$ (anhyd.), 25 °C, 16 h, quant.; **f** acetic anhydride/nitric acid (1:2, v/v), 0 °C, 3 h, 53 %; **g, h** $\text{NaBH}_4/\text{MeOH}/\text{THF}$, 25 °C, 16 h, NaOH , 25 °C, 7 h, 89 %; **i** $\text{BH}_3^*/\text{THF}/\text{THF}$, 0 °C, 1 h then 40 °C, 18 h, 86 %; **j** 2-isocyanatoethyl methacrylate, DBTDL (cat.)/THF, 65 °C, 48 h, 63 %

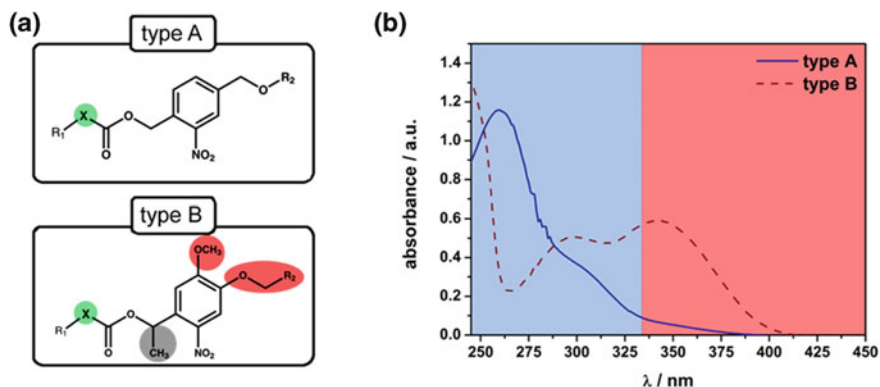


Fig. 5.4 Photo-labile crosslinking molecules CL-1A, CL-2A, CL-3A and CL-4B: **a** classification and **b** UV-vis spectra in THF. Adapted from [9] by permission of the Royal Society of Chemistry

CL-1A was synthesized by carbonyldiimidazole (CDI) activated coupling of 2 equivalents of hydroxyethyl methacrylate (HEMA) with 2NPDM using catalytic amounts of sodium ethanoate. The synthesis of CL-2A was achieved by a one step reaction of 2-isocyanatoethyl methacrylate with 2NPDM. For the synthesis of CL-3A, mono-2-(methacryloyloxy)ethyl succinate (MMAOES) was first converted to the acyl chloride by the reaction with oxalylchloride. The product was then allowed to react further with 2NPDM to the corresponding ester. CL-4B was synthesized according to the procedure for the synthesis of CL-2A whereas in this case, DBTDL was used to catalyze the reaction of the secondary hydroxyl group of the former prepared HEMNPB with the isocyanate. The classification of the respective crosslinking molecules and their absorption spectra are shown in Fig. 5.4.

Type A crosslinkers CL-1A, CL-2A and CL-3A are based on the (2-nitro-1,4-phenylene)dimethanol (2NPDM) group, whereas type B crosslinker CL-4B contains 4-(4-(1-hydroxyethyl)-2-methoxy-5-nitrophenoxy)butan-1-ol (HEMNPB) as the photo-reactive moiety. In the latter case, the introduction of a α -methyl group onto the benzylic carbon of the *o*-nitrobenzyl core is known to increase the rate of photolysis significantly [10]. This effect can be explained by considering the abstraction of a benzylic proton by the photo activated nitro group as the rate limiting step in the photolysis of the *o*-nitrobenzyl group, whereby the additional methyl group increases the acidity of this proton. Furthermore, the introduction of alkoxy substituents in the *o*-nitrobenzylic core results in a modified electronic structure of the chromophore which is known to result in a considerably increased UV absorption for $\lambda > 315$ nm compared to the 2NPDM moiety [11].

For the photolysis of the crosslinkers, the only requirement to the irradiation wavelength is to overlap with the absorption band of the photo-labile chromophore. However, to degrade the crosslinkers and the resulting PMMA gel particles in a controlled manner under mild conditions, Norrish-type side reactions, which primarily take place for irradiations with wavelengths of $\lambda < 300$ nm, should be

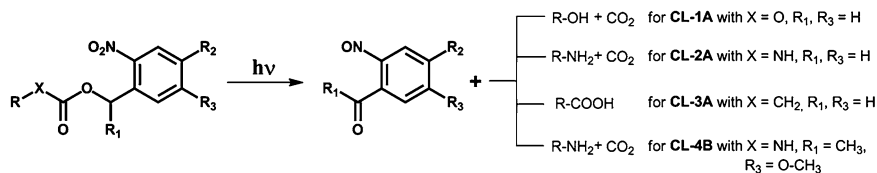


Fig. 5.5 Photoreactions of the degradable crosslinkers. Reproduced from [9] by permission of the Royal Society of Chemistry

avoided [12, 13]. UV–vis spectroscopy of the crosslinkers CL-1A–CL-3A shows in every case an absorption maximum at 260 nm accompanied by tailing up to 370 nm. In comparison, the spectrum of CL-4B shows the anticipated additional absorption maximum at 342 nm (see Fig. 5.4b). Here, the alkoxy substituents on the benzylic core exhibit a +M effect and therefore decrease the energy gap of the π – π^* transition, resulting in a bathochromic shift of the absorption maximum (see Fig. 5.4b). Thus, the crosslinker CL-4B shows a dramatically increased absorption in the targeted photolysis wavelength region of $\lambda > 315$ nm.

Photolysis of the cleavable crosslinkers in solution. Even though either type of crosslinker consists of a central *o*-nitrobenzylic group, the variation of the molecular attachment of the radically polymerizable methacrylate groups onto the photo-labile chromophore results in different photo-products with specific functional groups (Fig. 5.5). The photoreaction is based on a radical mechanism including the intramolecular benzylic hydrogen abstraction by a nitro group oxygen followed by a rearrangement and bond cleavage. Type A crosslinkers based on 2NPDM all generate a nitrosobenzaldehyde derivative together with either an alcohol for the carbonate derivative of CL-1A, an amine for the carbamate derivative of CL-2A or a carboxylic acid for the ester derivative of CL-3A. Crosslinker CL-4B however, degrades into an amine and a ketone, which is known to be less reactive towards possible imine formation with the free amino group. Regarding the incorporation of those compounds in swollen PMMA gel particles, a partial degradation of the gel does not only result in a more highly swollen state but also in the formation of previously protected functional groups covalently bound to the polymeric network, thus enabling further chemical modification.

The photo-degradation behavior of the crosslinkers was first investigated by analyzing the products of the photoreaction upon irradiating crosslinker solutions in THF ($3.0 \cdot 10^{-3}$ mol/L) for 8 h with UV light ($\lambda = 315$ – 390 nm, $I = 17$ mW/cm²). ¹H-NMR analysis of the crude reaction mixture showed a reduction of the peaks assigned to the benzylic proton(s) next to the respective carbonate, carbamate or ester group for every crosslinker. Hence, successful degradation was confirmed.

Furthermore, time-dependent UV–vis measurements of the crosslinker solutions in THF were conducted and their resulting irradiation time-dependent spectra are shown in Fig. 5.6. Since the absorption spectra of type A crosslinkers were

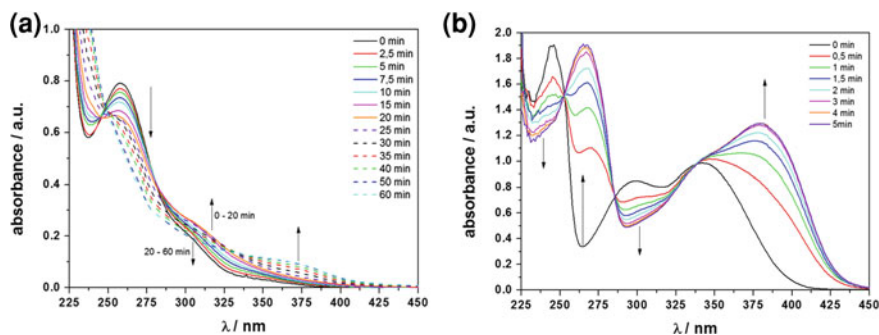


Fig. 5.6 Investigations on the photolysis of photo-cleavable crosslinkers in THF solution. Irradiation time-dependent UV-vis spectra of: **a** type A CL-1A crosslinker and **b** type B CL-4B crosslinker. Reproduced from [9] by permission of the Royal Society of Chemistry

found to be similar for CL-1A, CL-2A and CL-3A, Fig. 5.6a depicts the spectra of CL-1A exemplarily for all type A molecules.

Irradiation of either type A or type B crosslinkers with UV light of the wavelengths of $\lambda = 315\text{--}390$ nm resulted in every case in a red shift of the absorption maxima. Even though these light-induced changes of the spectra point towards successful photoreactions, the spectra of the crosslinkers CL-1A–CL-3A did not show well defined isosbestic points, thus indicating the simultaneous formation of side products in addition to the reaction shown in Scheme 2. Especially in the case of CL-1A and CL-3A, the secondary evolution of an additional absorption band at $\lambda > 350$ nm can be observed for irradiation times of more than 20 min (Fig. 5.6a), hence suggesting subsequent follow-up reactions of the primary photo products to the generation of *o,o'*-dicarboxyazobenzenes which are known to be formed by dimerization of the primary nitroso groups at longer irradiation times [11, 14]. Type B crosslinker CL-4B shows defined isosbestic points over the complete irradiation time scale (Fig. 5.6b). Nevertheless, the large red shift of the absorption band to $\lambda_{\text{max}} = 385$ nm and its high extinction coefficient hinder the accurate determination of the formation possible side products absorbing light in the same spectral region. Molecular structures and exact masses of the proposed secondary dimeric photo products are shown in Fig. 5.7.

In a next step, FD-MS measurements of the irradiated samples for the $^1\text{H-NMR}$ investigations were performed to investigate the formed photo products. All crosslinkers still showed the decreased characteristic molecule peak M^+ of the starting compounds. In addition, the appearance of the M^+ peaks corresponding to the formed nitrosobenzaldehyde photo products for type A crosslinkers and the respective keto compound for CL4 was observed and therefore proved successful cleavage. The subsequent generation of dicarboxyazobenzenes upon irradiation was confirmed by the appearance of the respective M^+ peak at 642 m/z for CL-1A-D and the M^+ peak at 754 m/z for CL-3A-D. In the other cases, the M^+ peak at 656 m/z for CL-2A-D and the $[\text{M}-1]^+$ peak at 827 m/z for CL-4B-D could be assigned to the respective azoxy compounds which are known to be generated

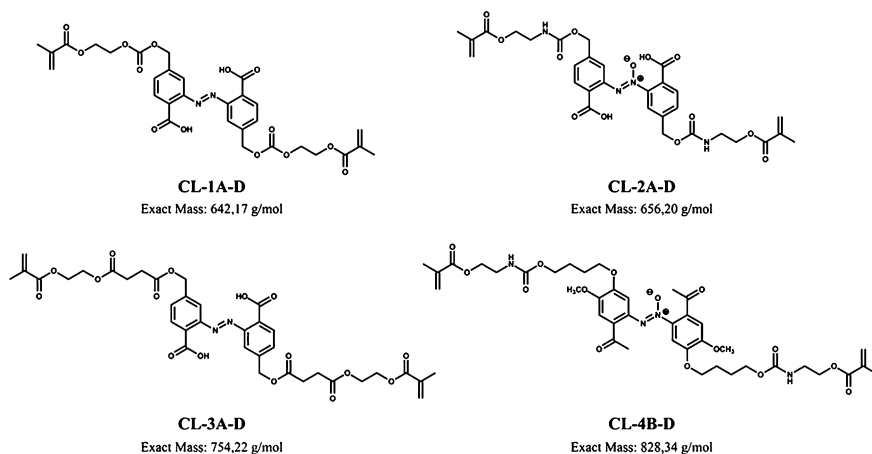


Fig. 5.7 Molecular structures of proposed dimeric side products of the photoreactions of the light-cleavable crosslinkers CL-1A–CL-4B. Reproduced from [9] by permission of the Royal Society of Chemistry

from azobenzenes [15, 16]. Carboxy or alkoxy radicals necessary for this reaction are assumed to be produced in small quantities by Norrish type side reactions of the crosslinkers upon irradiation of the non-degassed solution.

A quantitative time-dependent degradation analysis of the crosslinkers by UV absorption measurements was hindered by the formation of side products absorbing in the same spectral region. In this context, HPLC represents a powerful tool to examine the composition of the reaction mixtures at various times. Therefore, the kinetics of the photolysis of the photo-labile molecules were then investigated by monitoring the rate of disappearance of the starting compounds during irradiation. The presence of one defined peak in the elograms of the non-irradiated samples additionally confirmed excellent purity of the synthesized structures. The kinetic plots of $-\ln [CL]_t/[CL]_0$ versus time show all excellent linearity, indicating the expected first order kinetic with respect to the chromophore concentration (see Fig. 5.8b). Figure 5.8a presents an example of the time-dependent HPLC elution curves of the photoreaction of CL-4B and the kinetic plots for the calculation of the rate constants for all crosslinkers. The obtained results are listed in Table 5.1.

All newly synthesized crosslinkers were found to degrade completely upon irradiation with UV light of the wavelengths of $\lambda = 315\text{--}390$ nm. Elugrams of crosslinkers CL-1A–CL-3A showed the generation of multiple side products (data not shown) confirming the results obtained from UV-vis and FD-MS measurements. In contrast to the UV-vis measurements, CL-4B shows not only the formation of one main photo product, but also the dimeric azoxy side product verified by FD-MS can be detected as small peak in the elugram at ~ 4.4 min elution time (Fig. 5.8a). As expected, CL-4B shows a dramatically increased rate constant, in comparison to the type A crosslinkers. The enhanced absorption in the used

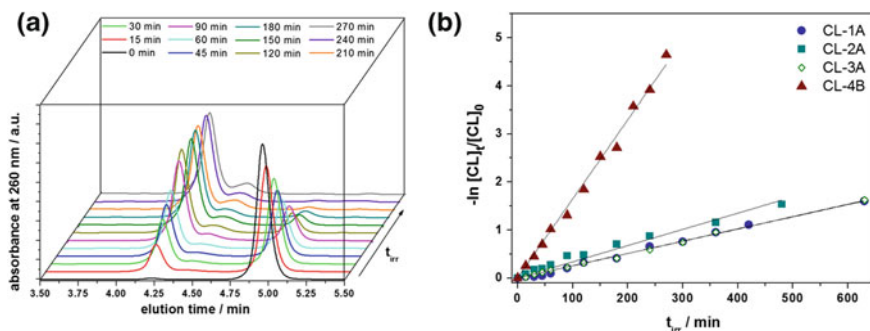


Fig. 5.8 Photolysis of degradable crosslinkers: **a** time-dependent HPLC elution curves of the photoreaction of CL-4B in THF; **b** kinetic plots for the calculation of the rate constants of the photoreaction. Reproduced from [9] by permission of the Royal Society of Chemistry

Table 5.1 Rate constants and half-life times for the photolysis of the synthesized degradable crosslinkers

Crosslinker	k/s^{-1}	$\tau_{1/2}/min$
CL-1A	$0.43 \bullet 10^{-4}$	270
CL-2A	$0.56 \bullet 10^{-4}$	206
CL-3A	$0.43 \bullet 10^{-4}$	271
CL-4B	$2.75 \bullet 10^{-4}$	42

photolysis wavelength region is accompanied by an increase of the acidity of the benzylic proton by the additional α methyl group. Hence, CL-4B reacts around 5 times faster than CL-2A and 6.4 times faster than CL-1A and CL-3A. Taking into account absorption of the products in the same spectral region as the wavelengths used for cleavage of the crosslinkers, the photoreaction is significantly slowed down. The less reactive molecules CL-1A–CL-3A are therefore more influenced by this effect than CL-4B and the difference of the photolysis rates is increased. This promising effect could enable a time-controlled and independent degradation of a specific type of particles using a definite wavelength of UV light. In addition, the divinyl groups present in either type of synthesized crosslinker enables the preparation of a broad variety of polymeric microgels by (co)-polymerization with different radical polymerizable monomers. In a first attempt, PMMA was chosen as well-known chemically inert polymer to examine the degradation behavior of the microgels.

Preparation and characterization of crosslinked photo-degradable PMMA gel particles by miniemulsion polymerization. With regard to potential release applications, the miniemulsion polymerization approach represents a big advantage compared to emulsion polymerization. Suppression of diffusion of compounds between droplets characterizes each droplet as a nanoreactor. Therefore, copolymerization with the respective crosslinking molecules or incorporation of active hydrophobic substances can easily be achieved during the polymerization. As no net diffusion takes place, the composition of the latex particles resembles the

Table 5.2 Nominal compositions of photo-degradable PMMA microgels

Sample	Crosslinker		
	Type	m/mg	mol-%
MG-0	DEGDMA	60.0	2.5
MG-X	DVB	33.0	2.5
MG-1A	CL-1A	124.0	2.5
MG-2A	CL-2A	123.0	2.5
MG-3A	CL-3A	152.0	2.5
MG-4B	CL-4B	149.0	2.5

composition of the monomer phase. Hence, all functionalities incorporated are equally distributed in each particle. In order to obtain photo-degradable PMMA microgels (MG), MMA was copolymerized with the crosslinkers CL-1A to CL-3A and CL-4B in miniemulsion. In addition, MG-0 microgels crosslinked with diethylene glycol dimethacrylate (DEGDMA) and MG-X microgels crosslinked with divinyl benzene (DVB) were synthesized as reference particles for the degradation experiments. In order to assure comparability of swelling and degradation behavior, 2.5 mol-% of crosslinker were used in every case. Table 5.2 lists the composition of the synthesized microgels.

After several washing steps, the number-weighted particle size distributions of the non-swollen particles in water were determined by DLS measurements. The obtained mean hydrodynamic diameters are shown in Fig. 5.11. All miniemulsion copolymerizations resulted in stable dispersions of non-swollen MGs in water with hydrodynamic diameters in the size range of 140–200 nm. The mean hydrodynamic diameters of particles synthesized with crosslinkers CL-2A and CL-4B were 204 nm (standard deviation ± 39 nm) and 174 ± 33 nm, whereas the crosslinkers DEGDMA, DVB, CL-1A and CL-3A yielded smaller particles of 141 ± 24 nm, 140 ± 19 nm, 149 ± 31 nm and 157 ± 29 nm, respectively. In all cases, representative SEM images showed spherical particles in the same size range (Fig. 5.9). Regarding the polydispersity of the microgels, it becomes obvious that the particle size is broadly distributed, which might be explained by the utilization of Lutensol AT-50 as non-ionic surfactant for stabilization of these miniemulsion. Compared to electrostatic stabilization by ionic surfactants, the sole steric effect by Lutensol AT-50 is here not as efficient. Even though particles with a more narrowly distributed particle size could be obtained by using anionic sodium dodecylsulfate (SDS), a non-ionic surfactant was chosen to assure best possible swellability in organic solvents. In contrast to the organic soluble Lutensol AT-50, this would be hindered by the presence of non-organic soluble SDS molecules on the particle surface.

Potential applications of the photo-degradable particles require stable dispersions in a good solvent for the polymer chains forming the network. Therefore, the freeze dried microgels were allowed to swell in THF for 3 days and the sol content was removed by additional washing steps. Evaporating the solvent under reduced pressure yielded the MGs as pale yellowish solids. Redispersion of the microgels could easily be achieved by swelling the dried samples in a good solvent such as

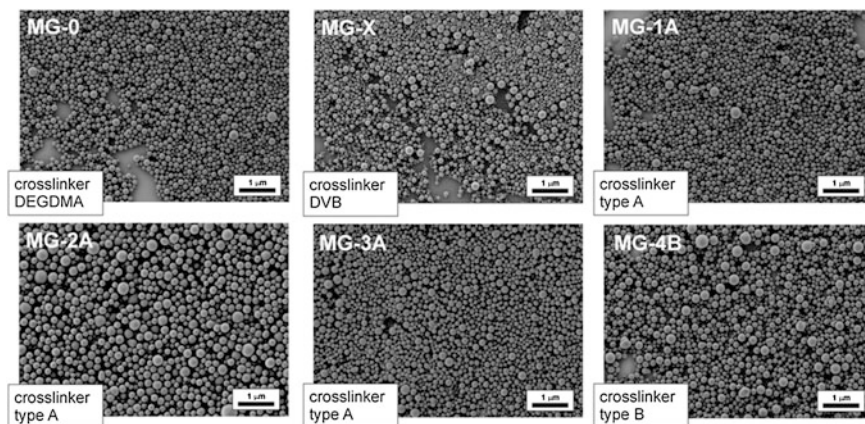


Fig. 5.9 Characterization of non-swollen PMMA gel particles prepared with different crosslinkers: Representative SEM images of microgels drop cast from aqueous dispersions on silicon wafers. Reproduced from [9] by permission of the Royal Society of Chemistry

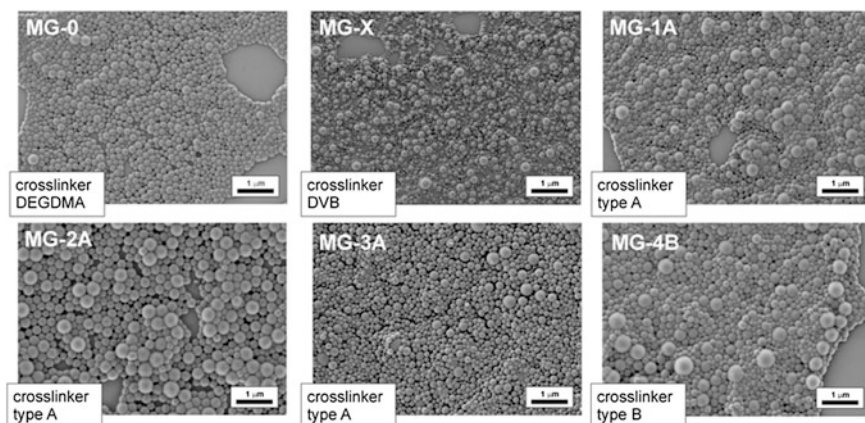


Fig. 5.10 Representative SEM images of crosslinked microgels after redispersion in chloroform (and drying). Reproduced from [9] by permission of the Royal Society of Chemistry

THF or chloroform over night. The obtained dispersions were sterically stabilized only by the dangling chains of the swollen outer layer of the microgels and no additional surfactant was needed. SEM showed still spherical particles after the redispersion indicating successful crosslinking in every case. Representative SEM images for the microgels after redispersion in chloroform are shown in Fig. 5.10.

Dynamic light scattering measurements yielded the hydrodynamic diameters of the swollen particles which showed a significant increase compared to the values obtained from dispersions in water. The degree of swelling (DGS), or the swelling ratio, was then calculated as $DGS = V_{\text{swollen}}/V_{\text{non-swollen}}$, thus representing the

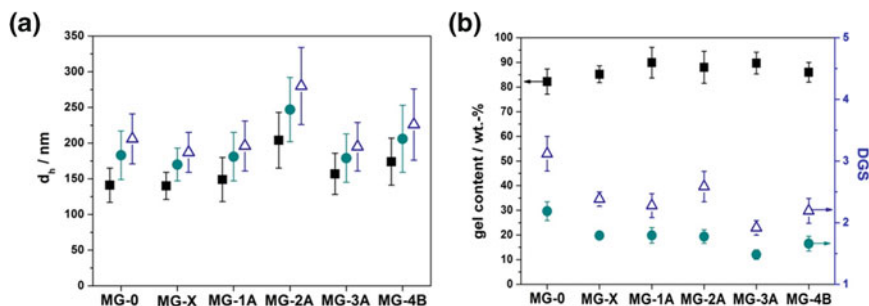


Fig. 5.11 Characterization of the PMMA MGs: **a** hydrodynamic diameters in (■) water, (●) THF and (△) chloroform; **b** (■) gel contents of the isolated MG particles and *DGS* in (●) THF and (△) chloroform. Reproduced from [9] by permission of the Royal Society of Chemistry

relative volume of included solvent. The obtained values are shown in Fig. 5.11 together with the hydrodynamic diameters of the swollen particles in THF and chloroform. Comparing the hydrodynamic diameters in the different solvents, the largest particle diameters are found for the dispersions in chloroform. Therefore, all particle degradation experiments were conducted in the highly swollen state of the microgels in chloroform.

Gravimetric analysis of the combined supernatants of the washing steps and the remaining particle dispersions afforded the sol/gel contents, which are shown in Fig. 3.5b. The gel contents are in the range of 83–90 % and did not vary significantly among the various microgels synthesized with different crosslinkers. The sol contents of 17–10 % may be explained by possible ring formation due to backbiting reactions of the crosslinking molecules [17].

While the determination of the sol/gel content in combination with the measured degree of swelling did not permit a quantitative evaluation of the crosslinking density or an absolute conclusion regarding the inner morphology, it allowed the expedient comparison of crosslinking efficiency of the different compounds among each other and relative to DEGDMA. Therefore, equally successful crosslinking and comparable distribution of crosslinks in the different microgels was presumed for all used crosslinkers.

Photo-degradation studies of the PMMA gel particles in chloroform. In general, photo-degradation of the microgel particles was conducted by irradiating 0.125 % (wt/v) dispersions of the microgels in chloroform by UV light of different wavelengths. At a first glance, a reduction in turbidity was detected for samples containing the photo-labile moieties. In contrast, a dispersion of the MG-0 reference particles showed no alteration. The reduced turbidity was attributed to a loosening of the network structure by degradation of cleavable crosslinking points, because a more swollen gel particle is characterized by a reduced contrast in the refractive indices between solvent and particle. As a result, the scattering intensity decreases, leading to an optically more transparent dispersion. A theoretic explanation for this phenomenon is based on the following equation for the

turbidity $\tau = cQ_{ext}3/(2d\rho)$ as described by Lechner [18]. Here, c is the mass concentration of the particles, Q_{ext} is the Mie extinction efficiency, d is the particle diameter and ρ the particle density. Here, the value of the parameter Q_{ext} is a function of the relative refractive index n_p/n_0 (n_p being the refractive index of the particles and n_0 the one of the solvent) and decreases with decreasing value of n_p/n_0 . The resulting influence on turbidity was described by Al-Manasir et al. and used to monitor the temperature dependent swelling of PNIPAAm microgels in water [19]. With the intention to follow the particle swelling or degradation, turbidity measurements were carried out in chloroform by measuring the intensity of the scattered light at 90° . In detail, the intensity count rates of the irradiated samples I_{irr} were determined relative to those of the non-irradiated samples I_0 . The values for the relative turbidity t_{rel} obtained from the equation $t_{rel} = (I_{irr}/I_0) \cdot 100 \%$, therefore reflect the relative degree of particle degradation.

In order to confirm the correlation between decreasing turbidity and increasing particle size, the reciprocal turbidity i.e., the transparency was plotted together with the corresponding hydrodynamic diameters against the time, for a dispersion of MG-4B upon irradiation with UV light ($\lambda = 315\text{--}390$ nm, $I = 17$ mW/cm²). The resulting graph in Fig. 5.12 shows a good agreement between the light-induced increase of particle swelling and the decrease in scattering intensity.

Wavelength-controlled selective degradation of MG-4B microgels. Kinetic turbidity measurements of the microgel dispersions were conducted to examine the influence of the different crosslinker photolysis rates on the time-dependent swelling behavior of the respective gel particles. It was expected that upon irradiation with wavelengths of $\lambda > 315$ nm, the faster photoreaction of CL-4B—due

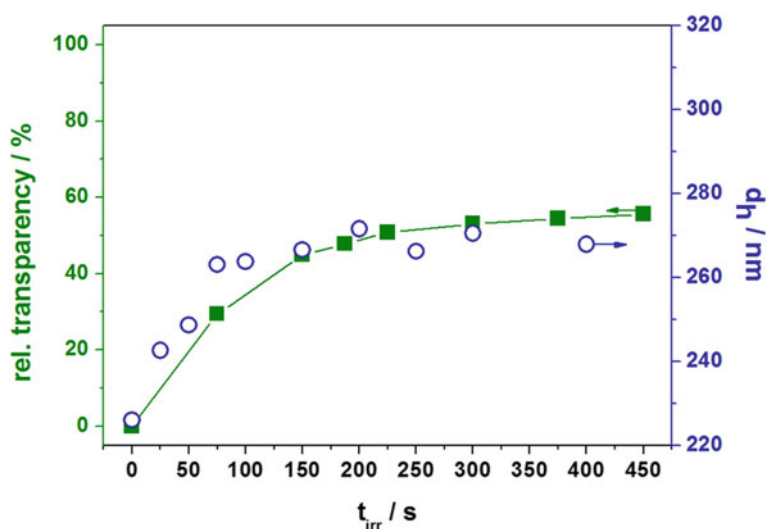


Fig. 5.12 Evolution of the irradiation time-dependent transparency and hydrodynamic diameters upon the irradiation of a dispersion of MG-4B in chloroform ($\lambda = 315\text{--}390$ nm; $I = 17$ mW/cm²). Reproduced from [9] by permission of the Royal Society of Chemistry

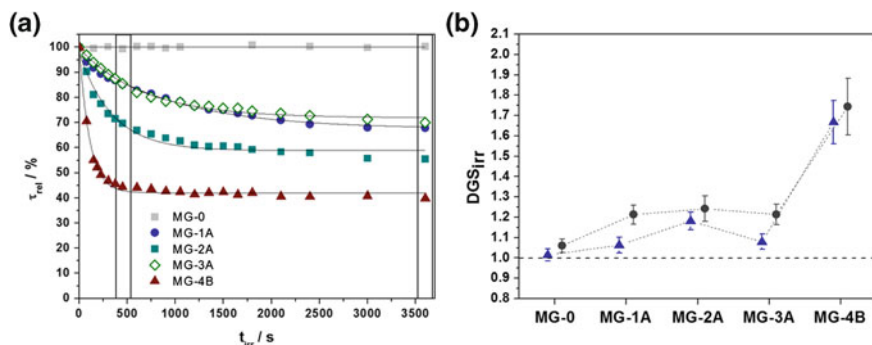


Fig. 5.13 Irradiation experiments of the PMMA MGs with $\lambda = 315\text{--}390$ nm and $I = 17$ mW/cm²: **a** time-dependent turbidity measurements; **b** DGS_{irr} , determined by DLS measurements after (▲) 400 s of irradiation and (●) 3600 s of irradiation. Reproduced from [9] by permission of the Royal Society of Chemistry

to the significantly higher absorption in this spectral region—also results in an accelerated increase of the corresponding gel particle size compared to the size change of particles synthesized with CL-1A to CL-3A. Irradiation experiments conducted with UV light of the wavelengths of 315–390 nm and an intensity of 17 mW/cm² confirmed this assumption, as can be seen in Fig. 5.13a. In the case of microgel particles containing photo-labile crosslinking points, the decrease in turbidity upon irradiation was found to follow an exponential decay to a constant level. In contrast, non-degradable MG-0 particles did not show any change of turbidity. As expected, MG-4B microgels are much more sensitive to light irradiation than MG-1A–MG-3A particles. It was assumed that the enhanced degradability of MG-4B microgels occurred due to the different photolytic reactivity of the crosslinkers. This should enable a selective degradation of MG-4B particles upon irradiation with UV-A light of wavelengths $\lambda > 315$ nm. Therefore, the different photolytic reactivity should in principle allow the successive decomposition of one specific type of microgel after the other in a mixed dispersion.

The turbidity of all the microgels containing either type A or type B photo-labile crosslinkers, decreases upon irradiation until a constant level is reached. The MG-4B microgels being the most sensitive for UV light of the spectral region over 300 nm, showed a decrease to a constant level of 42 %, whereas MG-2A reached 59 % and MG-1A and MG-3A still exhibited a reduced turbidity to around 70 %. Even much longer irradiation times of 3600 s did not result in a further decrease. It becomes obvious that even in the case of the most labile CL-4B crosslinker no complete particle degradation was achieved under the irradiation conditions used. During degradation of crosslinking points in the microgels, the photo products are probably still connected to a certain extent to the gel network. Therefore, the observed intermolecular formation of dimeric azobenzene or azoxybenzene moieties can take place to form new crosslinking points simultaneous to the cleavage of the photo-degradable crosslinkers. The resulting “steady state” is represented

by a constant maximum degree of swelling which can be seen as a plateau in the turbidity curves. In order to support this explanation and exclude polymer chain entanglement as a reason for incomplete particle degradation due to physical “crosslinks”, non-crosslinked PMMA particles were prepared analogue to the microgels MG-0. The freeze dried polymer particles dissolved readily in THF or chloroform as good solvents for PMMA and no particles could be detected either by DLS or SEM, suggesting that incomplete particle degradation is not a result of entanglements. Even though in the experiments conducted with the described wavelengths only partial degradation was observed in either case, an enlarged particle volume after irradiation represents an increase in solvent uptake, which correlates to a looser network structure in the gels. Thus, even partial degradation of the gel particles might be advantageous for delivery applications as diffusion out of the network proceeds faster.

In order to quantify the increase in swelling of the particles, DLS measurements of the particle dispersions in chloroform after different irradiation times were conducted. The degrees of swelling (DGS_{irr}) were then calculated as the volumes of irradiated particles relative to those of the non-irradiated ones in the same solvent. The DGS_{irr} of the samples after 3600 s irradiation time are shown in Fig. 5.13b. As expected, the MG-4B particles synthesized with type B crosslinker CL-4B showed a dramatically increased DGS_{irr} compared to the microgels containing CL-1A to CL-3A. Only the size of the reference particles MG-0 was not influenced at all. The kinetic turbidity measurements show that using shorter irradiation times increases the selectivity of MG-4B degradation. The degradation of MG-4B microgels already reaches a constant level after 400 s of irradiation, whereas the MG-1A to MG-3A particles still exhibit a higher turbidity compared to 3600 s irradiation time. Figure 3.7b shows the corresponding degrees of swelling after 400 s irradiation time which confirm an enhanced selectivity of MG-4B degradation.

The particle morphology of the irradiated samples was studied by SEM. Representative images of the MGs still showed the presence of spherical particles. However, the defined spherical morphology disintegrated to a certain extent and the particles are flattened on the surface. Here, the partial degradation of the crosslinking points led to a much softer gel material, which results in flattened particles, as can be seen exemplary for MG-4B in comparison to the non-influenced reference particles of MG-0 in Fig. 5.14.

Irradiation of the respective microgel dispersions with UV light of wavelengths in the spectral region above 350 nm should increase the difference in the swelling behavior of the type A and type B gel particles dependent on the irradiation time. Type B crosslinking molecules exhibit an absorption band with a maximum at 360 nm, whereas type A molecules show minor absorption in this spectral region. For this purpose, dispersions of the microgels in chloroform were irradiated with a UV-LED emitting at a discrete wavelength of 365 nm with an intensity of 60 mW/cm². Figure 5.15a shows the corresponding time-dependent turbidity measurements. The degrees of swelling after 200 s of irradiation are presented in Fig. 5.15b. In comparison to the irradiation experiments conducted with $\lambda = 315\text{--}390$ nm UV light and

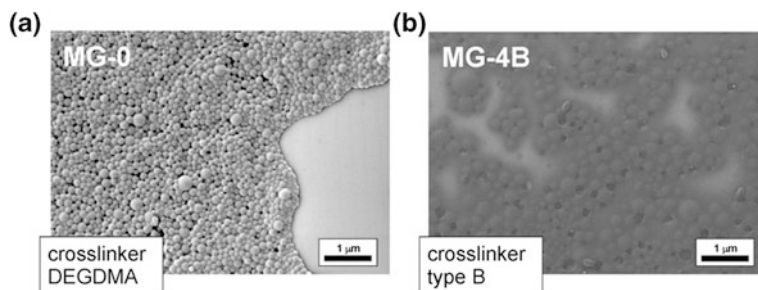


Fig. 5.14 SEM images of PMMA microgels after UV irradiation for 400 s ($\lambda = 315\text{--}390$ nm, $I = 17$ mW/cm²) in chloroform: **a** MG-0 out of CHCl₃; **b** MG-4B out of CHCl₃. Reproduced from [9] by permission of the Royal Society of Chemistry

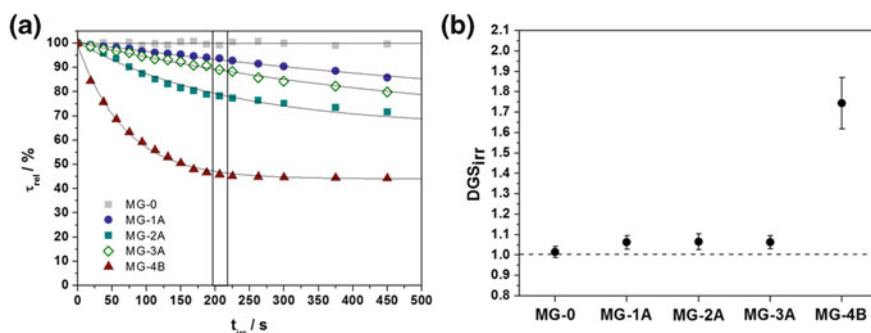


Fig. 5.15 Irradiation experiments of the PMMA MGs with $\lambda = 365$ nm and $I = 60$ mW/cm²: **a** time-dependent turbidity measurements; **b** DGS_{irr} determined by DLS measurements after 200 s of irradiation. Reproduced from [9] by permission of the Royal Society of Chemistry

the resulting DGS_{irr} (Fig. 5.13), it can be seen that the selective sensitivity of MG-4B microgels to irradiation can be drastically increased by adjusting the spectral region of the used UV light.

Furthermore, it is noteworthy that the time scale of degradation was significantly shortened compared to the use of 17 mW/cm² UV light of the wavelengths of $\lambda = 315\text{--}390$ nm. As expected, a higher light intensity causes an increase of the degradation rate of crosslinking points, which results in a faster swelling behavior of the microgels. This allows the control of particle degradation kinetics by adjustment of UV light intensity as an external trigger. In addition, an increase in light intensity does not result in a higher degree of swelling, thus confirming the presence of an equilibrium between crosslinker cleavage and new formation as described earlier.

Kinetically controlled selective degradation of MG-4B and complete degradation of microgels. Since a significant increase in swelling was already achieved upon irradiation with UV-A light in a reasonable time scale under mild conditions ($\lambda = 315\text{--}390$ nm, $I = 17$ mW/cm²; $\lambda = 365$ nm, $I = 60$ mW/cm²),

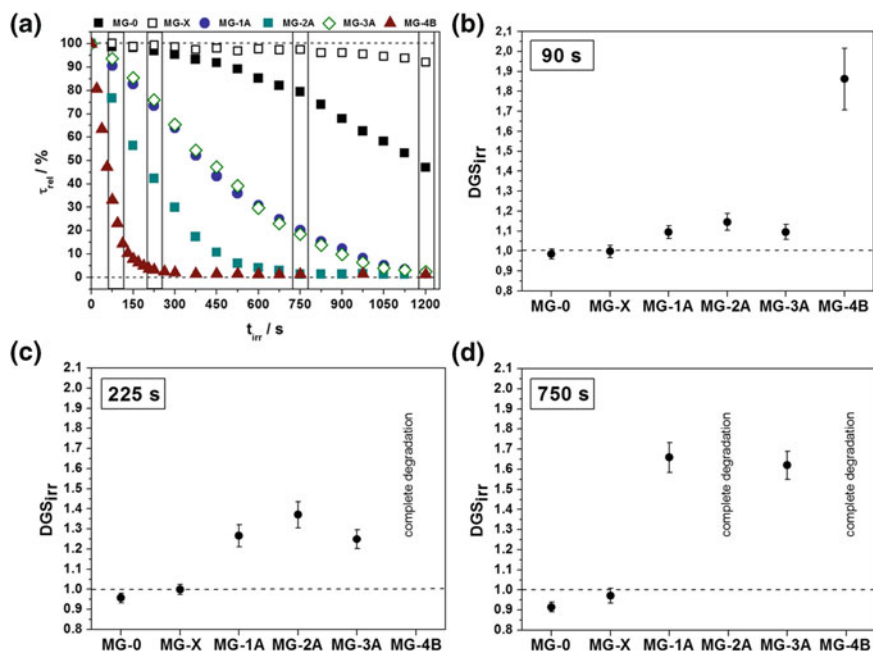


Fig. 5.16 Irradiation experiments of the PMMA MGs with $\lambda = 200\text{--}600$ nm and $I = 95$ mW/cm²: **a** time-dependent turbidity measurements; **b** DGS_{irr} determined by DLS measurements after 90 s of irradiation; **c** DGS_{irr} determined by DLS measurements after 225 s of irradiation; **d** DGS_{irr} determined by DLS measurements after 750 s of irradiation. Reproduced from [9] by permission of the Royal Society of Chemistry

further investigations with high intensity UV light of a broader spectral region were carried out to determine the possibility of complete particle degradation. For that purpose, dispersions of the microgels in CHCl₃ were irradiated with UV light of the wavelengths of $\lambda = 200\text{--}600$ nm and an intensity of 95 mW/cm². The time-dependent relative turbidity is shown in Fig. 5.16a. In contrast to the irradiation experiments with UV-A light, using broadband UV light leads to turbidity diminishments down to 1–2 % for the samples containing the photo-labile crosslinking points, implying complete particle degradation. This observation confirms the assumed presence of newly formed crosslinkers as dimeric side products of the irradiation. Whereas irradiation with wavelengths of $\lambda > 300$ nm does not influence those crosslinking points, the use of broadband UV light of $\lambda = 200\text{--}600$ nm is known to cleave azobenzene or azoxybenzene groups. Azoxybenzenes [15] as detected for CL-2A and CL-4B yield phenyl nitroxides by direct photolysis. Photo-degradation of azobenzenes [15, 16] (CL-1A-D and CL-3A-D, see Fig. 5.7) depends on the presence of radicals which are assumed to be generated in situ by Norrish type reactions upon irradiation.

Concerning the turbidity of the MG-0 reference particles, it becomes obvious that microgels with no photo-degradable crosslinker were also partially

disintegrated. This could be assigned to Norrish type side reactions, which are known to take place for wavelengths below 300 nm [12, 13]. In addition, the curve obtained for the MG-0 particles does not follow an exponential decay. In this case, a degradation mechanism based on Norrish type reactions is assumed, since the simultaneous occurrence of several non-defined photoreactions leads to a different degradation profile compared to the photo-labile microgels. It is further assumed that partial particle disintegration of the MG-0 particles crosslinked with DEGDMA occurs mainly due to photolytic Norrish type I cleavage reactions of the ester bonds present in this molecule, rather than due to Norrish type II PMMA main chain degradation reactions. The latter are known to dominate at shorter wavelengths (157 nm) [13] than the ones used in the described experiment (>200 nm). Microgels prepared with a crosslinker, not containing any labile ester bonds connecting two polymer chains, should therefore exhibit an enhanced photo stability. In order to prove this assumption and to increase the advantage of photo-degradable microgels, PMMA particles MG-X crosslinked with divinylbenzene (DVB) were synthesized analogue to the MG-0 particles. For irradiation of microgels MG-X in chloroform with UV light of the wavelengths of 200–600 nm, only a negligible decrease of turbidity was detected for irradiation times up to 1200 s. As a result only minor degradation of those particles was assumed and further proved by DLS and SEM measurements. SEM analysis showed still spherical particles and no loss of structural integrity was observed. The control particles therefore represent a photo-stable system, which exhibits only negligible amounts of Norrish type II PMMA main chain degradation.

With regard to a selective and independent degradation of MG-4B particles, the kinetic turbidity measurements reveal the additional possibility of an irradiation time controlled method. Compared to the wavelength selective approach, in this case a fixed UV light source can be used to achieve the selectivity.

After 90 s of irradiation MG-4B microgels exhibit already a decay of their turbidity down to 33 %. In contrast, the turbidity of the microgel MG-2A only decreased down to 77 % and those of the microgels MG-1A and MG-3A even just to 91–94 %. Determination of the DGS_{irr} after 90 s of irradiation confirms the selective swelling of MG-4B particles which show a significantly increased particle volume compared to the microgels MG-1A to MG-3A. The respective DGS_{irr} are presented in Fig. 5.16b. The selectivity of the irradiation time-controlled swelling of MG-4B microgels is characterized by the deviation between the DGS_{irr} of MG-4B and those of the type A microgels MG-1A to MG-3A. The observed differences are comparable to those obtained from the wavelength-controlled method, hence indicating equal selectivity. In comparison, no significant decrease in turbidity or increase in particle size (represented by the DGS_{irr} in Fig. 5.16b) was detected for the reference particles of MG-X and even for the MG-0 microgels, which are based on DEGDMA as crosslinker, thus rendering those particles stable under the irradiation conditions used.

Further irradiation experiments were conducted to investigate the selective complete degradation of MG-4B microgels. In this case, an irradiation time of 225 s yielded a turbidity of ~ 0 % which was assumed to correlate with complete

particle disintegration. As a matter of fact, no spherical structures but a polymer film were observed by SEM analysis of the irradiated MG-4B microgels (see Fig. 5.17b). In contrast, DLS measurements of the MG-1A to MH-3A gel particles treated the same way revealed only partial degradation, characterized by an increase in particle size. The resulting degrees of swelling after irradiation are shown in Fig. 5.16c. Even though MG-1A to MG-3A particles are also partially degraded, their relatively small volume changes clearly demonstrate the possible selective complete degradation of type B MG-4B microgels. Regarding the MG-0 and MG-X microgels, no significant particle degradation was observed. In both cases, turbidity measurements did not show any considerable decrease as well as DLS measurements did not reveal any changes in the DGS_{irr} . Therefore, the reference microgels are stable under the used conditions to completely degrade MG-4B particles.

In order to examine the light induced degradation of microgels containing crosslinkers of type A subsequent to the selective swelling or disintegration of type

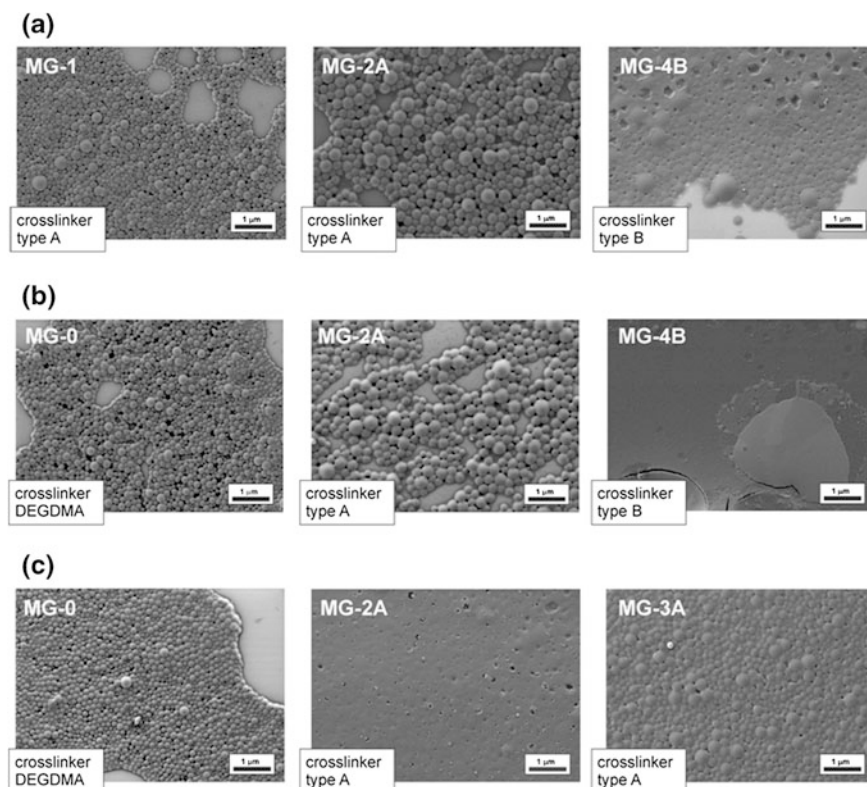


Fig. 5.17 Representative SEM images of PMMA MGs after irradiation in chloroform ($\lambda = 200\text{--}600\text{ nm}$, $I = 95\text{ mW/cm}^2$): **a** 90 s irradiation **b** 225 s irradiation; **c** 750 s irradiation. Reproduced from [9] by permission of the Royal Society of Chemistry

B MG-4B particles, DLS measurements were conducted to determine the DGS_{irr} at longer irradiation times. Here, 750 and 1200 s represent the points in time corresponding to a decay of turbidity to almost 0 %. Therefore, complete particle disintegration was assumed for those irradiation times. The resulting data from DGS_{irr} determination is shown in Fig. 5.16d. At an irradiation time of 750 s the microgels MG-2A were completely decomposed and no particle size could be determined by DLS. In contrast, the MG-1A and MG-3A particles showed an increasing DGS_{irr} with increasing irradiation time and still exhibited a spherical structure consisting of highly swollen gel networks (see Fig. 5.17c). Turbidity measurements of irradiation experiments of the non-photo-labile reference particles revealed also partial degradation for MG-0 microgels at longer irradiation times. As mentioned above, this effect, which results from Norrish type I ester cleavage side reactions of the DEGDMA crosslinker, can be avoided by using DVB as a crosslinker. As can be seen from turbidity measurements and DGS_{irr} values, the respective MG-X microgels exhibited a good stability even for longer irradiation times. Therefore, the impact of photo-degradable microgels is dramatically enhanced.

Complete degradation for all microgels containing either type of photo-labile crosslinker could be observed by SEM after 1200 s of irradiation (data not shown). The DGS_{irr} of the MG-0 reference particles seems to decrease with increasing irradiation time. It was assumed that degradation reactions and crosslinking reactions based on radical recombination and transfer reactions take place simultaneously and therefore do not result in a defined degradation of the microgel particles. In addition MG-X reference particles exhibit only a minor decrease of turbidity and DGS_{irr} , therefore representing photo-stable microgels.

All irradiated samples were further characterized with respect to the particle morphology using SEM. After 90 s of irradiation, the presence of spherical particles could still be observed in all cases, as can be seen in Fig. 5.17a. Similar to the irradiation experiments with UV-A light, the flattened particles on the silica surface result from the disintegration of the defined spherical morphology of MG-4B due to the cleavage of crosslinking points. However, for longer irradiation times of 225 s no particles were detected anymore for MG-4A. Figure 5.17b shows the representative images of the polymer film resulting from the complete degradation of MG-4B and exemplary for type A MGs, the flattened spherical structures of the swollen MG-2A particles. MG-0 reference microgels treated similarly are shown as an example of non-light-sensitive particles. In Fig. 5.17c images are presented which show the resulting structures after 750 s of UV irradiation. The MG-2A microgels were completely degraded, whereas MG-1A and MG-3A particles only disintegrated to a certain extent and can be identified as flattened spherical structures on the surface. Representative for type A microgels, MG-3A particles are shown in comparison to the MG-0 reference. Even though MG-0 reference particles still exhibit a defined spherical structure as well, MG-X microgels represent reference particles of increased photo stability, as can be seen from SEM analysis (data not shown), the turbidity measurements and the DGS_{irr} discussed above. In the case of longer irradiation times of 1200 s, all particles

containing either type of photo-labile crosslinker were completely decomposed (data not shown), whereas the MG-0 and MG-X reference particles still exhibited a spherical structure (data not shown).

In conclusion, depending on the used UV wavelengths and intensities, either partial and selective photolysis of the crosslinking points or complete degradation of the gel particles was achieved as is schematically summarized in Fig. 5.2.

Conclusion

In summary, a new system for controlled light-triggered release applications based on photo-degradable microgels was developed. The concept is based on the application of two classes (type A and type B) of newly synthesized photo-labile crosslinkers. The crosslinkers were designed to exhibit significant differences in the photolysis rates depending on the irradiation conditions, therefore enabling their successive and independent cleavage by adjusting the irradiation wavelengths and times. The divinyl functionality of the crosslinkers offers the possibility for the preparation of a broad range of photo-degradable (micro-)gels by radical copolymerization with different vinyl functionalized monomers. Investigating photo-degradable PMMA microgels as a model system for possible future materials for light-triggered release applications, it was shown that independent and successive degradation of the microgels containing type A or type B crosslinkers can be achieved by either a wavelength-controlled or an irradiation-time controlled approach. This specific performance in organic solvents represents a great potential for the controlled release of two different functional compounds embedded in two types of microgels out of a mixed dispersion thereof. In this context, e.g., the embedding of metallic nanoparticles as possible functional compounds would give rise to new light-triggered catalytic materials.

5.1.1.2 Photo-Sensitive PHEMA Microgels: Light-Triggered Swelling

The newly synthesized photo-cleavable crosslinking molecules described in the previous chapter are characterized by their specific solubility behavior in organic solvents of medium polarity (e.g. THF, acetone, ethyl acetate, DMSO, etc.). Their insolubility in water and good solubility in MMA as monomer/solvent enabled the formation of photo-sensitive PMMA microgels by copolymerization in direct miniemulsion; the dispersed droplets consisted of a solution of the crosslinkers in the monomer.

In general, the transformation of the concept of photo-sensitive microgels to water swellable gel nanoparticles is of high interest. A common approach to hydrogel nanoparticles is based on copolymerizations of crosslinkers and monomers in inverse miniemulsion [20]. In this method, the droplets mostly consist of an aqueous solution of crosslinkers and monomers. However, the water insolubility of the photo-cleavable crosslinking molecules hinders the preparation of hydrogel nanoparticles by this synthetic route. Nevertheless, the utilization of a hydrophilic monomer as solvent for the crosslinkers is assumed to be an alternative pathway to hydrogel nanoparticles based on an inverse miniemulsion process.

Necessary requirements have to be matched. A good solubility of the crosslinkers in the respective monomer in order to form the dispersed phase without water as solvent has to be ensured. Additionally, the crosslinking molecules have to be insoluble in the continuous phase, generally consisting of a non-polar solvent such as e.g., cyclohexane.

Based on these considerations, the aim of the work described in this chapter is the utilization of the photo-cleavable crosslinkers for the preparation of polymeric microgels by free radical copolymerization with a hydrophilic monomer in inverse miniemulsion. 2-Hydroxyethyl methacrylate (HEMA) was chosen as comonomer since its molecular structure is closely related to the formerly used MMA thus enabling a good solubility of the crosslinkers in the monomer. By this, the high versatility of the newly synthesized photo-cleavable crosslinkers regarding their application in different processing routes to polymeric microgels (their utilization in either direct or inverse miniemulsion) is assumed to be demonstrated. In addition, the utilization of HEMA as a monomer containing a hydroxyl group gives rise to gel networks with included functional groups thus allowing a further post polymerization modification. Moreover, by investigating the swelling behavior of the resulting photo-sensitive PHEMA microgels in water, the proposed inverse miniemulsion processing route to light-degradable hydrogel nanoparticles is to be examined.

Preparation of photo-sensitive PHEMA microgels by free radical copolymerization in inverse miniemulsion. The synthesized photo-cleavable crosslinkers were readily soluble in HEMA and not soluble in cyclohexane. This characteristic enabled the application of the inverse miniemulsion technique for the preparation of light-degradable PHEMA microgels. The dispersed phase consisted of a solution of the crosslinkers in the monomer (2.5 mol-%). A solution of the non-ionic surfactant KLE in cyclohexane was used as the continuous phase. After polymerization and washing the obtained dispersions, the particles were investigated with regard to their hydrodynamic diameters by DLS and particles morphologies were examined by SEM. Figure 5.18 shows representative SEM images of the microgels drop cast from cyclohexane dispersions and the d_h values from DLS.

The free radical copolymerization of HEMA with different crosslinkers in inverse miniemulsion afforded in all cases microgels with hydrodynamic diameters around 100 nm of well defined spherical structures. Therefore, it was demonstrated that the specific medium polarity of the newly synthesized photo-cleavable crosslinkers (CL-1A to CL-4B, see Sect. 5.1.1.1) enables their utilization for the preparation of a broad range of light-sensitive microgels by either direct (Sect. 5.1.1.1) or inverse miniemulsion polymerization.

Investigations on the swelling behavior of photo-sensitive PHEMA microgels. Besides investigating the versatility of the crosslinkers regarding their application in different processing routes of microgels, the photo-sensitive PHEMA microgels were prepared in order to examine the potential of transferring the concept of light-degradable microgels to hydrogel nanoparticles. To this extent, the prepared microgels were freeze dried and their swelling behavior in water was

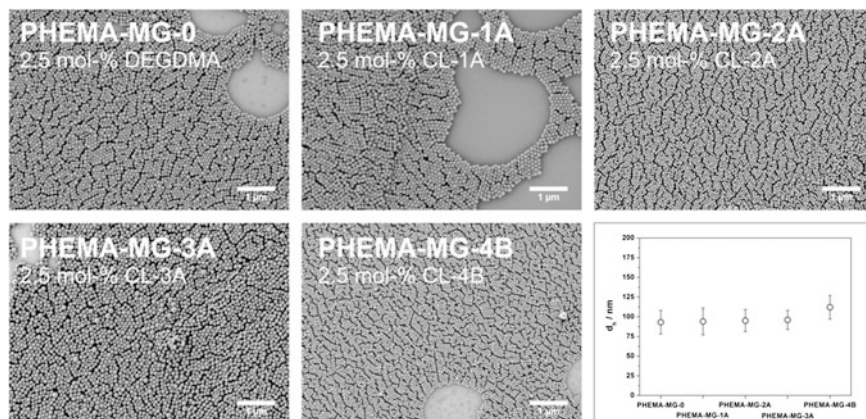


Fig. 5.18 Characterization of non-swollen photo-sensitive PHEMA gel nanoparticles with different crosslinkers. Representative SEM images and hydrodynamic diameters obtained by dynamic light scattering

investigated. It was found that all PHEMA microgels were not swellable in aqueous medium independent of temperature and concentration. At first view, this behavior was unexpected since HEMA as hydrophilic monomer is readily soluble in water. On the other hand, the water solubility of the resulting polymer is well known to crucially depend on the molecular weight of PHEMA [21, 22]. As the described microgels were prepared by free radical copolymerization, no control over the molecular weight of PHEMA was achieved. As a consequence, the resulting lengths of the polymeric chains of the gel network were assumed to be in the range of restricted water solubility and thus hindering particles swelling in aqueous medium. However, further swelling experiments of the prepared photo-sensitive microgels revealed a good swellability of the materials (0.5 % w/v) in a chloroform/methanol (1/1 v/v) mixture (visual inspection).

Investigations on the light-induced particles degradation. Even though the prepared photo-sensitive PHEMA microgels did not exhibit the expected water swellability, the utilization of HEMA as a monomer bearing functional hydroxyl groups renders the prepared PHEMA-MG-1A–PHEMA-MG-4B microgels—in addition to the light-sensitive PMMA polymeric gel nanoparticles described in the previous chapter—as second highly interesting class of photo-degradable nano-scaled materials. In order to test the proposed light-induced particle swelling/degradation, dispersions of the swollen microgels (0.125 % w/v) in chloroform/methanol were irradiated with UV light ($\lambda = 315\text{--}390\text{ nm}$; $I = 17\text{ mW/cm}^2$). The particle swelling/degradation was monitored by turbidity analogously to the experiments conducted on photo-sensitive PMMA microgels (Sect. 5.1.1.1). The resulting turbidity curves in dependency on the irradiation time are shown in Fig. 5.19.

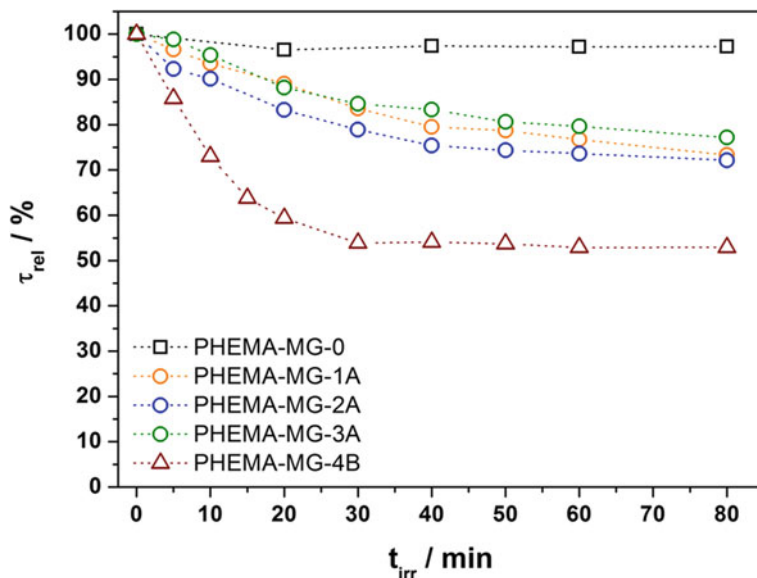


Fig. 5.19 Irradiation experiments of PHEMA microgels dispersed in chloroform/methanol (1/1 w/v): irradiation time-dependent turbidity measurements

It was found that the turbidity of all microgels containing either type A or type B photo-labile crosslinkers decreased upon irradiation until a constant level was reached. The observed turbidity profiles exhibited the same trend as observed for the photo-sensitive PMMA microgels described in the previous chapter. PHEMA-MG-4B microgels being the most sensitive for UV light of the spectral region over 300 nm showed the most pronounced decrease in turbidity down to a constant level of around 50 %. In comparison, PHEMA-MG-1A–PHEMA-MG-3A exhibited a decrease in turbidity to only 70–80 %. The PHEMA-MG-0 nanoparticles as reference particles containing DEGDMA as photolytically stable crosslinker were not influenced by the irradiation with UV light. It becomes obvious that in all cases no complete particle degradation (as characterized by a turbidity reduced to approximately 0 %) was achieved. This effect is based on the same considerations as described in the previous chapter. Formation of polymer bound dimeric side products of the photoreaction of the crosslinkers hinders the complete particle dissolution due to the formation of new crosslinking points. Nevertheless, the reduced turbidity is assumed to base on an increased degree of swelling of the particles correlating to a looser network structure of the gels. This behavior is assumed to be advantageous for release applications as diffusion from the network proceeds faster for increased mesh sizes.

Conclusion

As described in this chapter, the successful preparation of photo-sensitive PHEMA microgels was achieved by free radical copolymerization of the newly

synthesized photo-cleavable crosslinkers (CL-1A to CL-4B) with HEMA in inverse miniemulsion. The specific medium hydrophilicity of the crosslinking molecules was found to render those compounds highly versatile regarding different processing routes (direct and inverse miniemulsion) to light-sensitive microgels consisting of a broad variety of (functional) monomers. Even though the prepared PHEMA microgels were not swellable in aqueous medium, the expected light-induced particle swelling was successfully demonstrated by irradiation time-dependent turbidity measurements in organic solvents.

In addition, the incorporation of hydroxyl groups into the polymeric network represents a very promising approach to functional light-sensitive polymeric gel nanoparticles. In this context, by taking advantage of potential coupling reactions of functional compounds with the hydroxyl groups (e.g., esterifications, ether formations, etc.) a post polymerization functionalization of the network could be envisioned.

5.1.2 Photo-Sensitive Hydrogel Nanoparticles

Having demonstrated the successful development of photo-sensitive microgels swellable and degradable in organic solvents, transferring this approach to aqueous media renders them highly interesting for a broad variety of applications such as sensors [23], optics [24], colloidal crystals [25, 26], and biomedical fields [27–29]. In the latter, the controlled delivery of pharmaceutically active substances holds promise to be a key concept for future treatment of diseases. Regarding drug delivery applications, various types of polymeric carrier systems have been developed over the past years. Compared to macromolecular approaches such as polymer-drug conjugates [30, 31], particulate drug delivery systems are characterized by an enhanced protection of embedded active compounds against the body's defense mechanisms, therefore enabling the delivery of drugs to diseased sites in high doses with minimal damage to healthy tissue [32, 33]. In this context, micellar aggregates of amphiphilic block copolymers have been well established but are mainly applied for the incorporation of hydrophobic drugs into the hydrophobic micellar cores [34]. In contrast, microgels as intermolecularly crosslinked hydrophilic polymeric nanoparticles allow the incorporation of water-soluble drugs, including proteins and nucleic acids, in the network. Furthermore, the utilization of biocompatible and nonantigenic materials enhances the protection of the payload from hostile enzymes until the delivery to targeted tissues [35]. Additional advantages include the ease of preparation, high stability, and the good dispersibility in water [35–37].

Parts of this work are published as: “Dual Stimuli-Responsive Poly(2-hydroxyethyl methacrylate-co-methacrylic acid) Microgels Based on Photo-cleavable Crosslinkers: pH-dependent Swelling and Light-Induced Degradation” Daniel Klinger, Katharina Landfester, *Macromolecules* **2011**, *44* (24), 9758. Reprinted with permission from [38]. Copyright 2011 American Chemical Society.

This chapter first describes the development of pH-sensitive p(HEMA-*co*-MAA) microgels as model systems for biomedical release applications. In the second part the introduction of light-cleavable crosslinking points in these materials results in double stimuli-responsive hydrogel nanoparticles exhibiting pH-dependent swelling and light-induced degradation in water.

5.1.2.1 Anionic Hydrogel Nanoparticles Containing Methacrylic Acid Groups

Investigations described in the previous chapter revealed a good solubility of the newly synthesized photo-cleavable crosslinking molecules (CL-1A to CL-3A and CL-4B) in HEMA as hydrophilic monomer. This characteristic enabled the formation of light-degradable PHEMA microgels by free radical copolymerization in inverse miniemulsion. However, the swellability of the resulting gel particles was found to be restricted to organic solvents due to the limited solubility of PHEMA in water. It is assumed that transferring the concept of light-degradable microgels to water swellable hydrogel particles can be achieved by improving the swellability of PHEMA based microgels in water upon introducing methacrylic acid groups into the gel network. Since the dispersed phase during particle preparation in inverse miniemulsion mainly consists of HEMA, this particular composition is assumed to ensure a good solubility of the photo-cleavable crosslinkers. In addition, the introduction of methacrylic acid groups represents a widely investigated approach to render microgels containing even hydrophobic comonomers (e.g. MMA) [39, 40] water swellable, thus enabling to transfer the concept of photo-sensitive gels to hydrogels. Moreover, the introduction of carboxylic acid groups into the gel networks renders the degree of swelling of the particles sensitive to pH and ionic strength. Regarding possible loading and release applications, the introduction of this second stimuli-responsiveness is of high interest.

This chapter describes the development of non-photo-sensitive p(HEMA-*co*-MAA) microgels as model system for release applications of light-degradable hydrogel nanoparticles in biomedical fields. At first, particle preparation by free radical copolymerization in inverse miniemulsion is optimized to yield microgels exhibiting a swelling profile dependent on the pH and the ionic strength of the surrounding medium. Secondly, by exploiting the pH dependency of the networks, loading and release of myoglobin as a model protein is studied. At last, biocompatibility of fluorescently labeled microgels is investigated by cell tests.

p(HEMA-*co*-MAA) Microgels: pH-Dependent Swelling in Aqueous Media

The aim of the work presented here is the synthesis of non-photo-sensitive water swellable anionic p(HEMA-*co*-MAA) hydrogel nanoparticles in inverse miniemulsion. Further points of interest are the influence of the composition of the network forming copolymer (i.e., the HEMA/MAA feed ratio) on the swelling behavior of the resulting microgels as well as the dependency of the reversible volume phase transition on the pH and the ionic strength of the surrounding aqueous medium.

Preparation of crosslinked p(HEMA-*co*-MAA) microgels by inverse mini-emulsion polymerization. Crosslinked p(HEMA-*co*-MAA) microgels were prepared by free radical terpolymerization of 2-hydroxyethyl methacrylate (HEMA) with methacrylic acid (MAA) as comonomer and diethylene glycol dimethacrylate (DEGDMA) as crosslinker in inverse miniemulsion. Dispersed phases consisted of mixtures of HEMA, MAA and DEGDMA without solvent. While the ratio of HEMA/MAA was varied, the amount of crosslinker was kept constant to 2.5 mol-% thus enabling to investigate differences in the pH dependent swelling behavior solely dependent on the amount of ionizable methacrylic acid groups. In total four types of different microgels were synthesized and the compositions of the dispersed phases are shown in Table 5.3.

After polymerization, all dispersions were repeatedly washed with cyclohexane to remove excess surfactant. The purified particles were characterized with respect to the particles sizes by DLS and SEM was used to investigate the morphology of the non-swollen gel particles. Hydrodynamic diameters obtained from DLS measurements are listed in Table 5.3 and Fig. 5.20 depicts representative scanning electron micrographs of the microgels.

It can be seen that for all different HEMA/MAA feed ratios microgels of hydrodynamic diameters around 150 nm with relatively narrow size distributions were prepared. In the investigated range of HEMA/MAA feed ratios, the composition of the dispersed phase did not influence the stability of the miniemulsion and resulting particles exhibited well defined spherical structures. In comparison, the incorporation of a hydrophilic comonomer into microgels by preparation methods based on precipitation polymerization from aqueous solutions is limited to a certain amount [41]. Hence, it can be concluded that the inverse miniemulsion approach represents a facile and versatile method for the preparation of anionic p(HEMA-*co*-MAA) microgels of various compositions.

The purified microgels in cyclohexane were freeze dried and transferred to aqueous media by swelling the dried particles in water (0.5 % w/v) with a pH adjusted to 11. The resulting dispersions were washed repeatedly with deionized water to remove the sol content of the crosslinking polymerization (i.e., unreacted monomers and non-crosslinked polymers and oligomers). The purified dispersions in water were stable without any additional surfactant due to sterical stabilization of dangling chains of the outer swollen particle layer.

Table 5.3 Nominal compositions and hydrodynamic diameters of p(HEMA) and p(HEMA-*co*-MAA) microgels

Sample	HEMA (wt.-%)	MAA (wt.-%)	DEGDMA (mol.-%) ^a	d_h^b (nm)
MG-A	100	0	2.5	154 ± 25
MG-B	95	5	2.5	157 ± 26
MG-C	90	10	2.5	184 ± 31
MG-D	85	15	2.5	127 ± 23

^a w.r.t. total amount of monomers; ^b Determined by DLS in cyclohexane

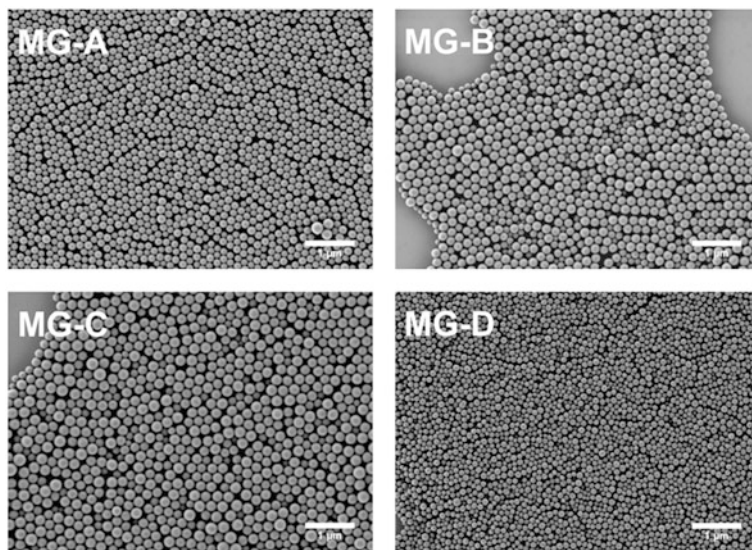


Fig. 5.20 Representative SEM images of MG-A–MG-D microgels on silica drop cast from cyclohexane dispersions

Characterization of the swelling behavior of p(HEMA-co-MAA) in dependency on pH and ionic strength. The prepared particles were designed to exhibit a good water swellability in combination with a pH dependent swelling profile. Deprotonation of the carboxylic acid groups increases the hydrophilicity of the network and results in an increase of the degree of swelling of the particles. This effect is even enhanced by the electrostatic repulsion of the generated anionic groups at higher pH values.

With the aim to investigate the influence of the amount of MAA in the networks on the maximum degree of swelling, the pH values of the aqueous microgel dispersions (0.125 % w/v) were adjusted to pH 8.5 thus ensuring complete deprotonation of all carboxylic acid groups. The hydrodynamic diameters of the particles were determined by DLS and the respective degrees of swelling were calculated. The resulting values in dependency on the amount of MAA are plotted in Fig. 5.21.

Regarding the swellability of the microgels in basic aqueous medium, it becomes obvious that for MG-B to MG-D particles the degree of swelling increases with the amount of incorporated methacrylic acid groups. The observed behavior follows the anticipated trend, since more (deprotonated) MAA groups in the gel result in an overall enhanced hydrophilicity of the network in combination with an increased electrostatic repulsion. In comparison, experiments to transfer MG-A particles to the water phase did not yield stable dispersions of swollen particles. It can be concluded that the incorporation of MAA represents a successful approach to improve the water swellability of PHEMA based networks.

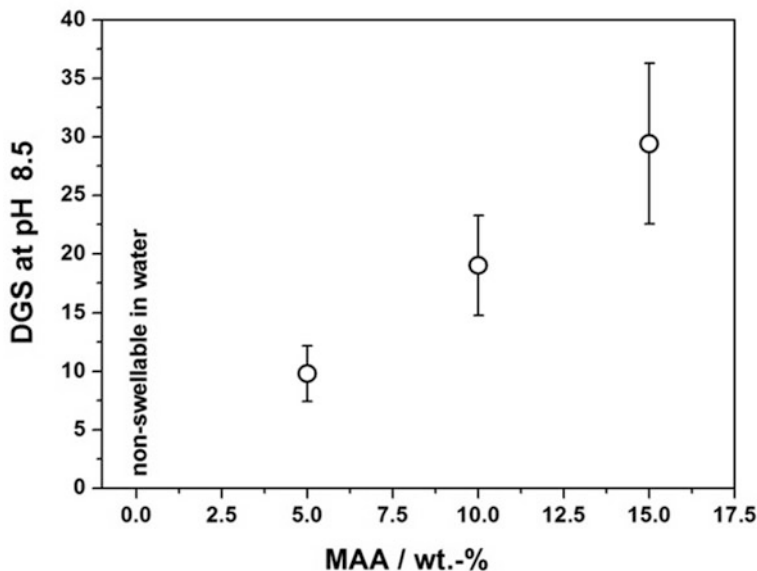


Fig. 5.21 Characterization of p(HEMA) (MG-A) and p(HEMA-*co*-MAA) (MG-B–MG-D) microgels: *DGS* at pH 8.5 in dependency on the amount of methacrylic acid groups

Since the prepared p(HEMA-*co*-MAA) microgels were designed to serve as model systems for pH-triggered loading and release applications, a large response to the respective stimulus is favorable. As shown in Fig. 5.21, this requirement is best fulfilled by MG-D microgels exhibiting the most pronounced increase in the particles diameters upon transfer to a basic aqueous medium, thus representing the most promising candidate for further examinations regarding the loading and release of functional compounds. With the aim to investigate the complete pH dependent swelling profile, the pH value of a MG-D dispersion was varied step-wise from pH 3.5 to pH 12 by adding diluted sodium hydroxide solution. Subsequently, after each titration step, the hydrodynamic diameters of the particles were measured by DLS. Figure 5.22a shows the obtained plot of d_h in dependency on pH. The pH-induced volume phase transition is assumed to be reversible by protonation/deprotonation of carboxylic acid groups in the network. To examine the proposed behavior, four cycles of varying the pH from 8.5 to 4.5 and subsequently measuring the hydrodynamic diameters were conducted. The resulting plot is shown in Fig. 5.22b.

The pH dependent swelling profile in Fig. 5.22a shows a critical swelling transition at a pH value of around pH 6. Starting from pH 3.5, the majority of the carboxylic acid groups became deprotonated above pH 6.0 and the average particle diameters increased dramatically by about 240 nm. The maximum degree of

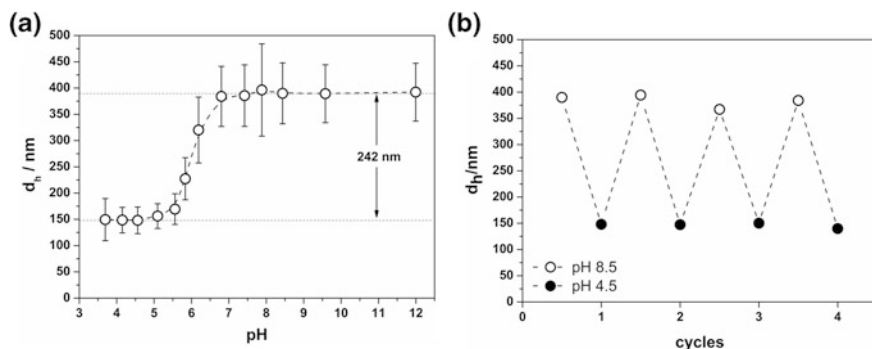


Fig. 5.22 Characterization of the pH dependent swelling profiles of MG-D microgels: **a** pH dependency of hydrodynamic diameters of the particles; **b** reversibility of the pH-induced volume phase transition

swelling was reached at pH around 7.5 and is mainly caused by the electrostatic repulsion of the strongly anionic carboxylate moieties. For pH values below pH 5.0, the network forming polymer chains were protonated, thus rendering the gel more hydrophobic. As a result of the absence of inner charges, the microgels are collapsed and behave like conventional latex particles. Lowering the pH under 3.5 resulted in coagulation of the particles due to the lack of sterical stabilization of dangling chains. The reversibility of the described pH-induced volume phase transition is shown in Fig. 5.22b and was found to be complete for 4 investigated cycles of pH transitions from pH 8.5 to pH 4.5.

It is well known that the pH sensitivity of ionic microgels is strongly influenced by the ionic strength of the surrounding medium. The presence of counterions to the ionizable groups in the network forming polymers shields the electrostatic repulsion resulting in a decreased degree of swelling [39, 40]. This effect was investigated for MG-D microgels by adding aliquots of an aqueous sodium chloride solution to a dispersion of the microgels in water at pH 8.0. After every NaCl addition step the hydrodynamic diameters were measured and the obtained values are plotted against the sodium ion concentration in Fig. 5.23.

The plot in Fig. 5.23 clearly shows a decrease of the MG-D hydrodynamic particle diameter with increasing concentration of sodium ions. As mentioned above, electrostatic interactions between anionic groups in the network and cationic counterions enable the penetration of sodium ions into the network. Consequently, the electrostatic repulsion between the anionic carboxylate groups is shielded by the cationic sodium ions thus resulting in a decreased degree of swelling.

Conclusion

In summary, free radical terpolymerization of HEMA, MAA, and DEGDMA in inverse miniemulsion represents a facile approach for the preparation of p(HEMA-co-MAA) microgels. The incorporation of methacrylic acid groups into the network resulted in a well defined and pronounced pH-sensitive reversible volume phase transition of the gel particles. In combination with the additional dependency of the

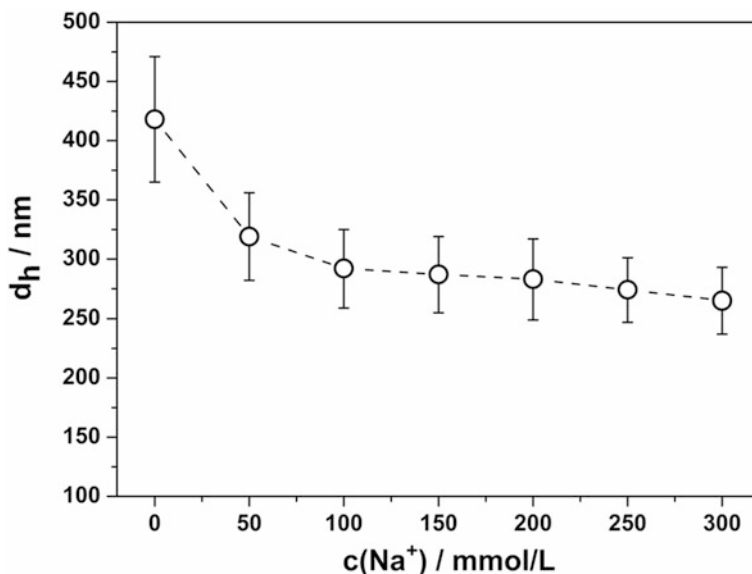


Fig. 5.23 Dependency of the hydrodynamic diameters of MG-D particles on the ionic strength of the dispersion (i.e., the concentration of sodium ions). The dotted line is a guide to the eyes

degree of swelling on the ionic strength of the dispersion this behavior is highly promising for loading and release applications of functional compounds.

Moreover, the hydrogel particles were prepared from HEMA/MAA mixtures as dispersed phases in the inverse miniemulsions. As the photo-labile crosslinkers described in the previous chapter showed a good solubility in HEMA as the main ingredient of the mixtures, the investigated synthetic approach is assumed to be transferable to the preparation of water swellable light-degradable microgels by copolymerization of HEMA with MAA in the presence of the photo-cleavable crosslinkers.

p(HEMA-co-MAA) Microgels: Loading and Release of Myoglobin

Having demonstrated the occurrence of a well defined pH-dependent swelling profile of p(HEMA-co-MAA) MG-D microgels, their potential utilization for the loading and release of functional compounds is of high interest. Moreover, as the photo-degradable analogues are assumed to be prepared by the same procedure, MG-D microgels serve as model compounds in order to gain insight into potential loading of the light-sensitive particles with functional compounds.

Concerning potential delivery applications, loading of microgels can be achieved by embedding functional substances either in situ during gel formation [42, 43] or by *post-formation* methods [45, 46]. In both approaches, an effective loading is characterized by the prevention of leakage of the functional compound until the targeted site or time point is reached. This can be realized, e.g., by

hindering the diffusion due to mesh sizes smaller than the hydrodynamic radii of the functional substances (e.g., proteins, enzymes, catalytic metal nanoparticles) [47, 48], by electrostatic interactions of e.g., small molecules with the polymeric matrix [39, 40] or by embedding compounds into collapsed networks [49], thus excluding water from the gel interior and preventing diffusion.

Since particle synthesis was carried out by polymerization of HEMA/MAA/DEGDMA mixtures (without an additional solvent) in droplets of an inverse miniemulsion at 72 °C, in situ embedding of (sensitive) water soluble functional compounds, such as e.g., proteins, is not applicable. Nevertheless, the stimuli-responsive behavior of the material is assumed to enable a *post-fabrication* loading of the microgels by exploiting the reversible volume-phase transition in combination with electrostatic interactions between the polymeric network and the payload. This approach generally bears the advantage of avoiding potential side reactions of the embedded compound during the polymerization.

A proposed loading and release mechanism of anionic p(HEMA-*co*-MAA) microgels is based on the following considerations which are schematically illustrated in Fig. 5.24. The gel particles are highly swollen in aqueous medium of pH values higher than pH 6.0 and consist of negatively charged networks of large pore sizes. Immersing the microgels in a solution of a substance with a hydrodynamic diameter smaller than the mesh sizes of the gel and positively charged at the respective pH, enables the diffusion of the functional compound into the network. Loading by electrostatic interactions between the different ionic groups can therefore be achieved [50] (see Fig. 5.24a and b). From this point on, two different release mechanisms depending on the size of the functional compound are imaginable. On one hand, for small molecules embedded in the network, the protonation of the anionic groups of the network forming copolymer upon lowering the pH reduces the electrostatic interactions between the positively charged payload and the network. In combination with the exclusion of water from the gel, this behavior induces the release following a “squeeze out” mechanism [51] (see Fig. 5.24a-ii). On the other hand, a deswelling of the gel corresponds to a decrease of the pore sizes of the network. For substances of a hydrodynamic diameter larger than the pore sizes of the collapsed gel, their diffusion from the network is hindered [46] even though the electrostatic interactions are weakened as well [52]. This approach is assumed to result in an entrapment of the respective compound (see Fig. 5.24b-i). In this case, leakage of the payload from the collapsed microgels at low pH values is prevented. A release can then be induced by increasing the pH to a value at which both the functional compound and the carboxylic acid groups in the network are negatively charged. Therefore, the reduced electrostatic interactions between embedded substance and network in combination with the increased pore sizes of the swollen gel induce the release (see Fig. 5.24b-ii).

This chapter focuses on investigations on the loading of p(HEMA-*co*-MAA) MG-D microgels with myoglobin by the described approach of entrapment upon deswelling of the particles and the subsequent release induced by reswelling. Myoglobin was chosen as a model protein since it fulfills certain important criteria for the successful loading. The isoelectric point of myoglobin of $I_p = 7.0$ was

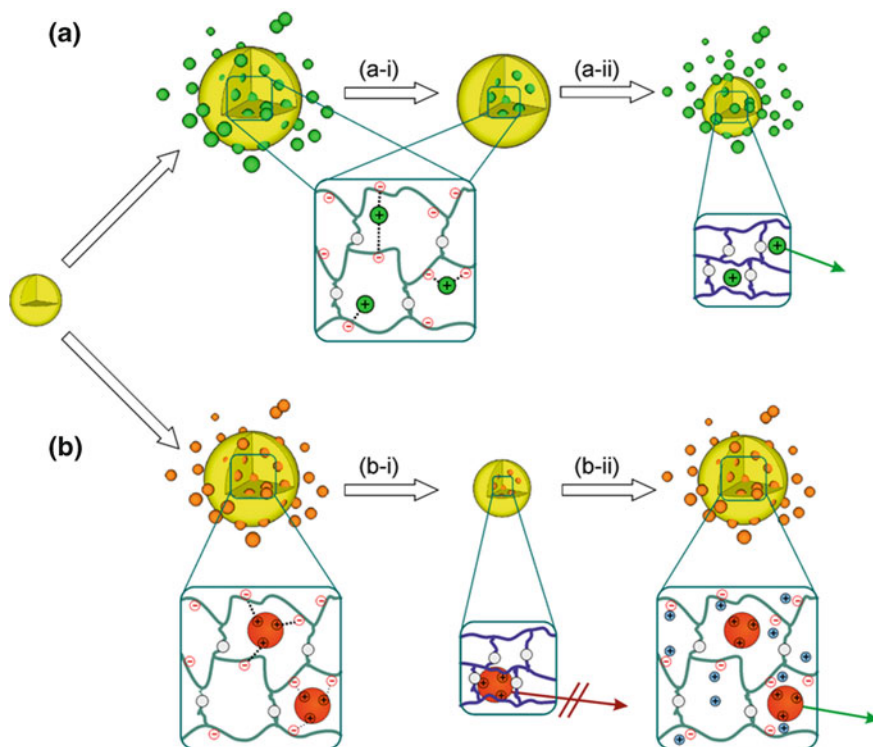


Fig. 5.24 Schematic illustrations of different loading and release strategies of p(HEMA-co-MAA) microgels: **a** loading of small cationic molecules into the anionic gel; **a-i** washing of the loaded microgels; **a-ii** release upon pH induced deswelling; **b** loading of large cationic functional compounds into the anionic gel; **b-i** entrapment by pH induced deswelling; **b-ii** release by reswelling in PBS

shown to enable the successful loading into anionic microgels containing methacrylic acid groups at pH 6.75 [40]. At this pH value it was demonstrated that the MG-D microgels are highly swollen due to the presence of anionic charges in the network-forming copolymer (see previous chapter). In addition, this particular pH value lower than the isoelectric point of the protein renders the latter positively charged, thus enabling an efficient loading due to electrostatic interactions with the negatively charged gel. Moreover, the relatively large hydrodynamic diameter of around 4.4 nm of the globular protein (molecular weight of around 17 kDa) is assumed to facilitate the entrapment in the microgels upon deswelling. Another beneficial characteristic is the UV absorption maximum at $\lambda_{max} = 410$ nm, which permits both the determination of loading efficiencies and the monitoring of the release by UV-vis spectroscopy.

Examining the potential loading and release pathway by investigating the degree of swelling of MG-D p(HEMA-co-MAA) microgels. As mentioned above, loading of p(HEMA-co-MAA) MG-D microgels with myoglobin and the

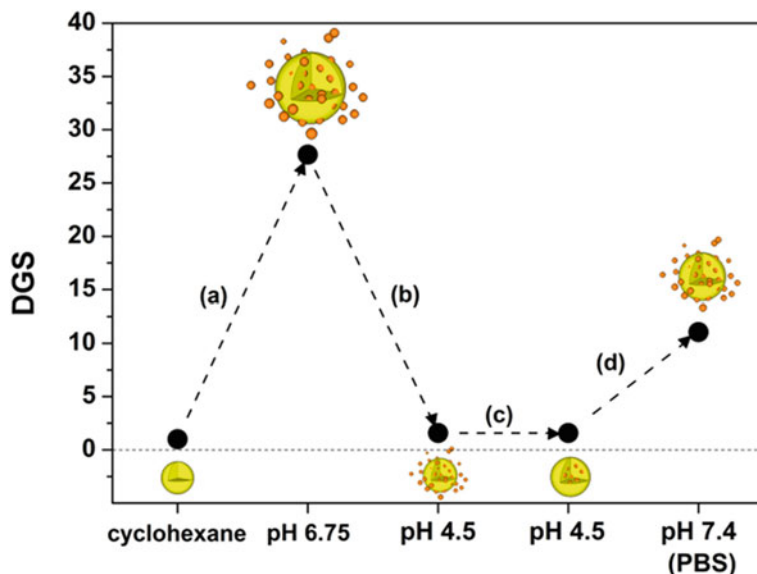


Fig. 5.25 *DGS* values of MG-D microgels for every step of the proposed loading and release pathway. The respective steps are schematically illustrated: **a** loading of myoglobin; **b** entrapment of myoglobin; **c** purification; **d** release of myoglobin. *Note* investigated samples did not contain myoglobin, cartoons are shown to clarify the proposed loading and release mechanism

subsequent release is based on exploiting electrostatic interactions between protein and network in combination with the pH-dependent swelling profile of the gel particles. In a first attempt, the pH-dependent swelling response of MG-D microgels without myoglobin was investigated according to the proposed loading and release strategy. Figure 5.25 shows the degrees of swelling for every step of the described pathway including schematical illustrations of the proposed pathway.

The swelling behavior of MG-D microgels depicted in Fig. 5.25 follows the anticipated profile and gives rise to the potential embedding and release of myoglobin following the depicted pathway of: (a) loading by swelling the microgels in a myoglobin solution of pH 6.75; (b) entrapping the protein by deswelling the microgels upon lowering the pH to a value of 4.5; (c) purifying the loaded microgels by washing with water of pH 4.5 and finally: (d) release of myoglobin by transferring the loaded microgels to phosphate buffer solution (PBS) of pH 7.4. Please note that in the last step, even though the pH of PBS is higher than the apparent pK_a of the microgels, the degree of swelling varies dramatically from the one obtained for microgels in pH 6.75. As investigated in the previous chapter, this effect is based on the ionic strength of the buffer solution which influences the swelling behavior of the microgels. Nevertheless, a smaller increase in the *DGS* is assumed to result in a slower release over a longer period of time. Regarding delivery applications, this profile is generally of high interest.

Loading of MG-D p(HEMA-co-MAA) microgels with myoglobin. Following a procedure described by Eichenbaum et al. [39], loading of anionic p(HEMA-co-MAA) MG-D microgels with myoglobin was performed by immersing the gel particles over night in a solution of the protein at pH 6.75. As mentioned above, the loading mechanism is based on the electrostatic interaction of the positively charged myoglobin molecules with the negatively charged polymeric gel in combination with the large pore sizes of the network. After equilibration, the pH of the dispersion was adjusted to pH 4.5 in order to collapse the microgels and entrap the embedded protein. Afterwards, the microgel particles were separated by centrifugation, the supernatant was removed and the particles were redispersed in water with pH 4.5. After repeatedly washing the loaded particles, the microgels were finally redispersed in PBS. The loading process was monitored by UV-vis spectroscopy. Figure 5.26 shows the UV-vis spectra of a myoglobin reference solution (of the same concentration as used for the loading experiments) at pH 4.5 in comparison to the UV-vis spectra of the supernatants after the first centrifugation- and the following washing steps.

Comparing the UV-vis spectrum of the myoglobin reference solution to the spectrum of the supernatant (after centrifugation of the collapsed microgels dispersed in the myoglobin solution), it can be seen that the intensity of the absorbance at $\lambda_{max} = 410$ nm decreased significantly. The observed difference can be attributed to a removed amount of myoglobin from the solution therefore indicating successful loading of the protein into the microgels by entrapment. The subsequent washing steps were conducted to remove excess myoglobin. By

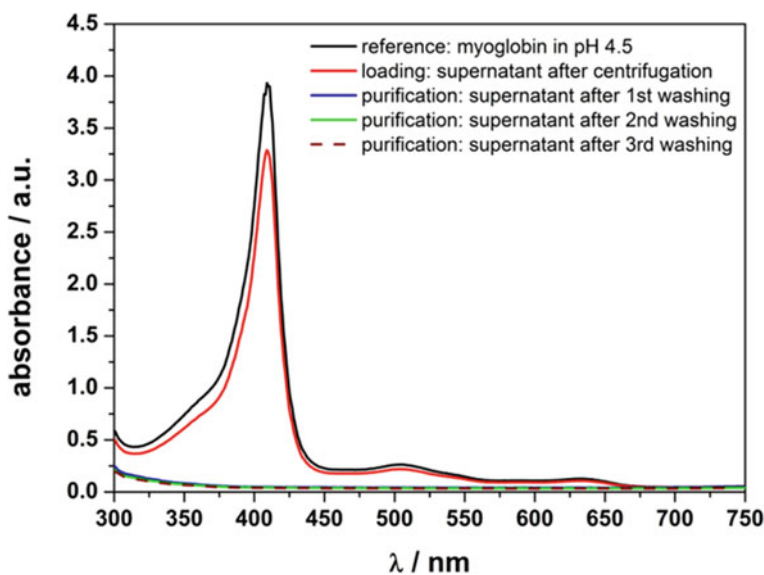


Fig. 5.26 UV-vis spectroscopic examination of the loading process of MG-D microgels with myoglobin

adjusting the pH value of the surrounding medium to pH 4.5, carboxylic acid groups are protonated and the electrostatic interaction with the positively charged myoglobin is weakened. While protein molecules in the microgel interior are entrapped due to the decreased pore sizes of the gel network, loosely adsorbed myoglobin molecules on the particles surface are assumed to be liberated. Therefore, multiple washing steps with water of pH 4.5 were conducted to remove physically adsorbed proteins. The UV–vis spectra of the supernatants of the performed washing steps did not show a significant absorbance in the wavelength region of λ_{max} of myoglobin. Hence it was concluded that myoglobin was mainly incorporated into the microgels interior rather than adsorbed on the particles surface. Moreover, the absence of myoglobin in the washing phases points towards an efficient entrapment accompanied by the successful suppression of leakage at the respective low pH value of 4.5. After the last centrifugation step, the microgels were redispersed in PBS.

Two important benchmarks of loading experiments are the loading efficiency (*LE*) and the embedding efficiency (*EE*). The loading efficiency represents the mass ratio of incorporated functional compound to carrier and can in this case be calculated by the following equation:

$$LE = \frac{m_{\text{embedded}}(\text{myoglobin})}{m_{\text{total}}(\text{microgels})}$$

The embedding efficiency describes the mass ratio of incorporated functional compound to the total mass of functional compound available for embedding. For the experiments described, it can be calculated using the following equation:

$$EE = \frac{m_{\text{embedded}}(\text{myoglobin})}{m_{\text{total}}(\text{myoglobin})}$$

Both parameters, embedding and loading efficiency, were determined by comparing the absorbance intensities at $\lambda_{max} = 410$ nm of the loaded microgels dispersed in PBS to a calibration curve of myoglobin in PBS. In order to take potential scattering influences of the microgels into account, all samples of varying myoglobin concentrations used for the calibration curve contained the same amount of dispersed “empty” MG-D microgels as in the loaded sample. Figure 5.27a shows the UV–vis spectrum of the loaded MG-D microgels in PBS and Fig. 5.27b depicts the calibration curve obtained from the absorbance intensities at $\lambda_{max} = 410$ nm.

Calculation of loading and embedding efficiency afforded the values of $EE = 6.9 \pm 0.6$ % and $LE = 62.3 \pm 5.0$ %. Regarding the high loading efficiency of 62.3 % it can be concluded that the investigated approach of loading myoglobin upon entrapment of the protein in collapsed MG-D microgels is a highly efficient process. The relatively low embedding efficiency of 6.9 % can be assigned to a huge excess of myoglobin with respect to the amount of microgels. Nevertheless, the examined loading strategy allows the recycling of not

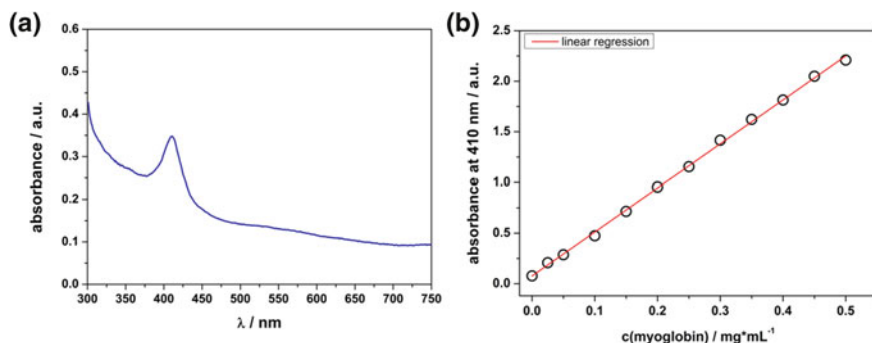


Fig. 5.27 Determination of loading- and embedding efficiency of myoglobin in MG-D microgels: **a** UV-vis spectrum of loaded MG-D microgels dispersed in PBS; **b** calibration curve of myoglobin in PBS containing the same amount of “empty” MG-D microgels as in **a**

incorporated myoglobin since the microgels were easily removed from the solution by centrifugation.

Release of myoglobin from p(HEMA-co-MAA) MG-D microgels. Having demonstrated the efficient loading of myoglobin in MG-D microgels, in a next step the subsequent release of the protein was investigated by transferring the loaded microgels from water of pH 4.5 to phosphate buffer solution of pH 7.4. The resulting microgel dispersion was shaken at 37 °C and samples were taken after predetermined time intervals. After removal of the microgels by centrifugation of each sample, the released amount of myoglobin in the supernatant was determined by comparing the UV absorbance at $\lambda_{max} = 410$ nm to a calibration curve of myoglobin in PBS. Figure 5.28a shows the measured time-dependent UV-vis spectra of the release experiment and Fig. 5.28b depicts the cumulative release of the protein in dependency on the incubation time.

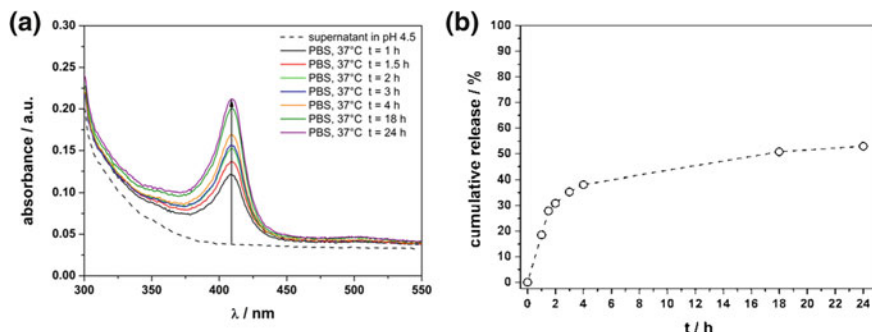


Fig. 5.28 Investigations on the release of myoglobin from p(HEMA-co-MAA) MG-D microgels in PBS at 37 °C: **a** time-dependent UV-vis spectra; **b** cumulative release in dependency on the incubation time. *Dotted line* is a guide to the eyes

The increasing absorbance at $\lambda_{max} = 410$ nm in the time-dependent UV-vis spectra clearly demonstrates an increase of the concentration of myoglobin in the supernatants after centrifugation. By transferring the loaded collapsed particles from pH 4.5 to PBS of pH 7.4, the loaded myoglobin is assumed to be released due to a combination of different factors. At first, the particles exhibit an increased degree of swelling in the medium of increased pH, therefore consisting of larger pore sizes which enable a diffusion of the protein from the network. Secondly, even though the carboxylic acid groups in the network forming copolymer are assumed to be protonated at pH 7.4, this pH value is higher than the isoelectric point of myoglobin ($I_p = 7.0$). Thus, the protein is mainly negatively charged as well. The resulting electrostatic repulsion between the anionic groups in the network and on the protein results in the release from the gel. Third, the high ionic strength of the buffer solution induces a shielding of anionic groups in the network. Moreover, the sodium counterions are assumed to displace electrostatic interactions between remaining positive charges of the protein and anionic carboxylate groups of the gel network therefore minimizing attractive physical interactions.

Based on the UV-vis spectroscopic investigations, the cumulative release was calculated. The observed release profile (see Fig. 5.28b) was found to follow an initial burst release of around 35 % of myoglobin during the first 3 h of incubation in combination with a slow release of additional about 18 % of embedded protein in a time span of 21 h. Since the maximum release after 24 h of incubation was determined to be 53 % of the loaded amount, it can be stated that a quantitative release was not achieved by this investigation method. It is assumed that this behavior is based on the equilibration between the release of myoglobin and the repenetration/diffusion of myoglobin into the highly swollen networks. Since the surrounding medium was not changed, a thermodynamic equilibrium was allowed to adjust. It is further proposed that the release profile depends on the concentration of myoglobin in the local environment of the microgels. As outlook, further investigations on this assumption are of high interest. As an example, the removal of the surrounding medium after predetermined release times and redispersion of the microgels in fresh PBS is supposed to shift the equilibrium towards complete release.

Conclusion

In summary, p(HEMA-co-MAA) MG-D microgels were successfully loaded with myoglobin as a model protein by electrostatic interactions of the positively charged myoglobin molecules with the negatively charged polymeric gel in combination with large pore sizes of the swollen network. Subsequent entrapment of the compound by pH induced deswelling of the particles resulted in a high loading efficiency of $LE = 62$ %, thus rendering this approach highly effective. The observed release profile upon swelling the particles under physiological conditions (PBS, 37 °C) followed an initial burst release of 38 % in combination with a slow release of additional 16 % of loaded myoglobin over a prolonged period of time, thus representing a saturation profile. It can be concluded that the observed release profile is very promising for applications where a fast provision

of a high concentration of the compound (as result of the response to a trigger) in combination with a subsequent steady supply for a longer period of time is wanted.

p(HEMA-co-MAA) Microgels: Fluorescent Labeling and Cell Tests

The newly developed and highly efficient procedure for loading MG-D microgels with myoglobin in combination with the observed release profile renders those materials interesting for delivery applications in biomedical fields. Nevertheless, a crucial point regarding their potential usage as carrier systems for *in vivo* treatments is the interaction with human cells. Therefore, the *in vitro* uptake of p(HEMA-co-MAA) microgels into human cells as well as the cytotoxicity are crucial parameters to be studied [53].

While uptake routes into cells have been described for small molecules and macromolecules [54, 55], the uptake mechanisms of larger particles in the size range of hundreds of nanometers have not been clarified. Possible mechanisms include, among others, pinocytosis, non-specific endocytosis and receptor-mediated endocytosis [56, 57]. Especially receptor-mediated uptake is a widely investigated approach to targeting of specific cell types [58, 59]. Since most types of carcinogenic cells are characterized by an increased expression of folate receptors, functionalization of nanometric delivery systems with folic acid on the surface results in an enhanced uptake of the respective vehicles in carcinogenic cells rather than in healthy cells [60].

The work presented in this chapter describes the preparation of p(HEMA-co-MAA) microgels (synthesized analogously to MG-D gel particles but marked with a fluorescent dye covalently incorporated into the network) and the investigation of their interaction with HeLa cells. In addition, since these materials represent model compounds for the aimed preparation of photo-degradable p(HEMA-co-MAA) microgels that will be introduced in Sect. 5.1.2.2, the results obtained from these investigations are assumed to be of high importance to predict the biocompatibility of the light-sensitive analogues.

Preparation and characterization of fluorescent p(HEMA-co-MAA) microgels. The incorporation of fluorescent markers into nanoparticles is a key requirement in order to investigate their cellular uptake by either flow cytometry or confocal laser scanning microscopy (CLSM). The incorporation of the fluorescent functionality into p(HEMA-co-MAA) microgels can be achieved by copolymerization of the described monomers with a methacryl-functionalized bodipy dye (bodipy-1) (synthesized by Dr. Andrey Turshatov). In comparison to hydrophobic polymeric nanoparticles where fluorescent dyes such as perylene monoimide (PMI) can be included physically into the particles, the swollen network structure of microgels would result in the leakage of these types of dyes. As a consequence, the described covalent attachment of the dye to the network is necessary. An additional beneficial characteristic of the used fluorescent marker is the high stability of the bodipy chromophore against photo bleaching upon fluorescence spectroscopy.

Table 5.4 Nominal composition and characterization data of fluorescent FL-MG microgels

Sample	Composition				Characterization		
	HEMA (wt.-%)	MAA (wt.-%)	DEGDMA (mol.-%) ^a	bodipy-1 (wt.-%)	d_h (CH) ^b (nm)	d_h (PBS) ^c (nm)	DGS (PBS)
FL-MG	85	15	2.5	0.93	124 ± 15	287 ± 34	12 ± 2

^a w.r.t. total amount of monomers; ^b determined by DLS in cyclohexane; ^c determined by DLS in PBS

Fluorescent p(HEMA-*co*-MAA) microgels FL-MG containing bodipy-1 were synthesized analogous to MG-D particles described in the previous chapter. After purification in cyclohexane the particles were examined with regard to the hydrodynamic diameters by DLS and the particles morphologies by SEM. After transfer to PBS, the swollen microgels were investigated by DLS and fluorescence spectroscopy. Table 5.4 shows the nominal composition of the FL-MG microgels, their hydrodynamic diameters in cyclohexane and PBS as well as the calculated degree of swelling in PBS. A representative SEM image of the particles from cyclohexane dispersion, the respective fluorescence spectrum in PBS and the molecular structure of bodipy-1 are shown in Fig. 5.29.

The prepared microgels were found to consist of well defined spherical structures with hydrodynamic diameters of 124 nm in cyclohexane. The particles dispersion in PBS showed a profound fluorescence emission upon excitation with light of the wavelength of $\lambda_{exc} = 488$ nm (matching the excitation wavelength used in FACS and CLSM), thus demonstrating the successful incorporation of the bodipy-1 dye. Comparing the particle sizes and their swelling behavior to the MG-D microgels, similar values were obtained. As a consequence, the utilization of FL-MG microgels as model systems for the prediction of the behavior of MG-D particles is enabled.

Cell tests: cytotoxicity and cellular uptake. *All cell tests were performed by Melanie Dröge.* Regarding the potential utilization of p(HEMA-*co*-MAA) microgels for delivery applications in biomedical fields, a basic requirement for the materials is a good biocompatibility as expressed by a low immunogenicity. In this

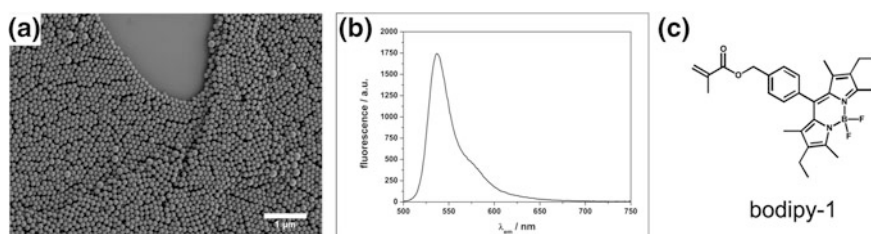


Fig. 5.29 Characterization of fluorescent p(HEMA-*co*-MAA) FL-MG microgels: **a** representative SEM image of the particles drop cast from cyclohexane dispersion; **b** fluorescence emission spectrum of the microgels in PBS ($\lambda_{exc} = 488$ nm); **c** molecular structure of the incorporated bodipy-1 fluorescent dye

context, several microgel nanoparticles are known to be characterized by a hindered opsonisation from macrophages. Here, a hydrophilic particle surface impedes the phagocytosis based on adhesion and induces a “stealth” behavior of the latexes [61]. Considering the p(HEMA-co-MAA) microgels as biocompatible compounds, their potential for *in vivo* applications still strongly depends on their cytotoxicity. This parameter was investigated by incubation (24 h) of HeLa cells with particle dispersions in PBS of increasing concentrations and staining with 7-aminoactinomycin (7-AAD) as fluorescent apoptosis marker. Investigations on the incubated cells by flow cytometry revealed three populations (viable, apoptotic, dead) by using negative controls and the apoptotic and dead cells present in cell cultures. The relative amounts of the respective populations dependent on the concentration of added microgels are shown in Fig. 5.30.

As can be seen from the data presented in Fig. 5.30, the FL-MG p(HEMA-co-MAA) microgels had no cytotoxic effect on the HeLa cells after incubation for 24 h. Even for drastically increased particle concentrations, the viability was always above 88 %.

The proposed potential of the described microgels as carrier systems for the delivery of functional compounds into cells is based on their successful cellular uptake. In this context, especially the efficient uptake without the need for a transfection agent or targeting vector is of high interest and was studied by incubation of HeLa cells with increasing concentrations of FL-MG particles. The fluorescent labeling of the microgels enabled to determine the uptake by flow

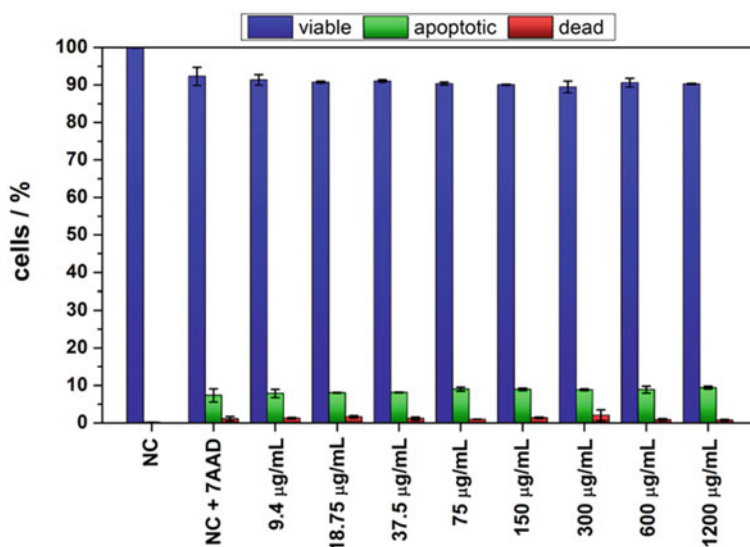


Fig. 5.30 Cytotoxicity tests of HeLa cells incubated with FL-MG dispersions of varying concentrations (NC represents the negative control of pure HeLa cells). Data obtained by M.Dröge

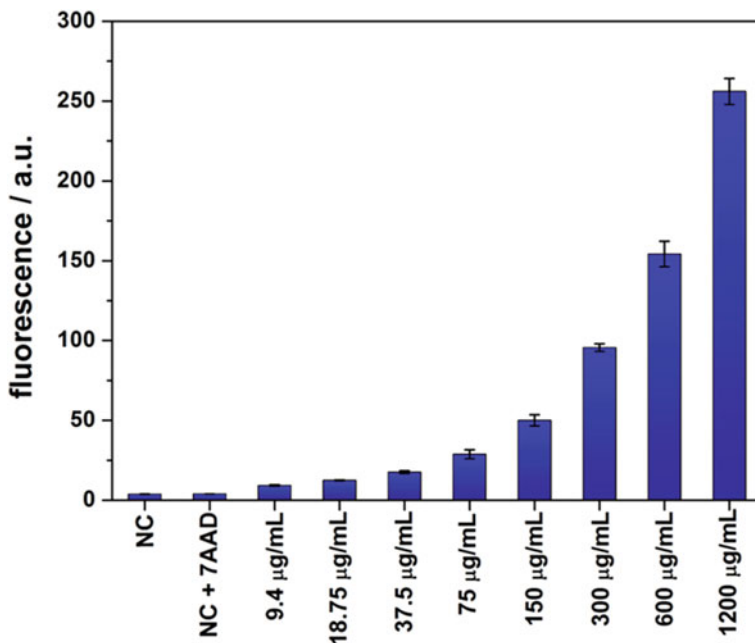


Fig. 5.31 Characterization of cellular uptake of FL-MG microgels by flow cytometry: median of nFL1 fluorescence for different particles concentrations. Data from M.Dröge

cytometry measurements. The cells were selected on a forward/sideward scatter plot, thereby excluding cell debris. Further analysis of the FL1 channel ($\lambda_{exc} = 488$ nm) afforded the median from 1D histograms corresponding to the amount of nanoparticles taken up by or associated with individual cells (analysis was performed by Melanie Dröge). The results obtained from the flow cytometry experiments are shown in Fig. 5.31.

By comparing the intensities obtained from cells incubated with different amounts of microgels to the negative controls (without and with 7-AAD), it can be seen that the fluorescence signals for the microgels containing samples were significantly increased. Moreover, the signal intensity increased dramatically with increasing microgel feed concentration. While the observed behavior clearly points towards an attractive interaction between HeLa cells and the FL-MG microgels, the performed flow cytometry measurements do not allow distinguishing between a successful cellular uptake and the adsorption of particles to the cell surface. Confocal laser scanning microscopy (cLSM) studies were performed in order to investigate the localization of the microgels in/at the cells (conducted in cooperation with Daniela Baumann). Figure 5.32 shows the obtained cLSM images of HeLa cells incubated with two different concentrations of FL-MG microgels in comparison to the negative control.

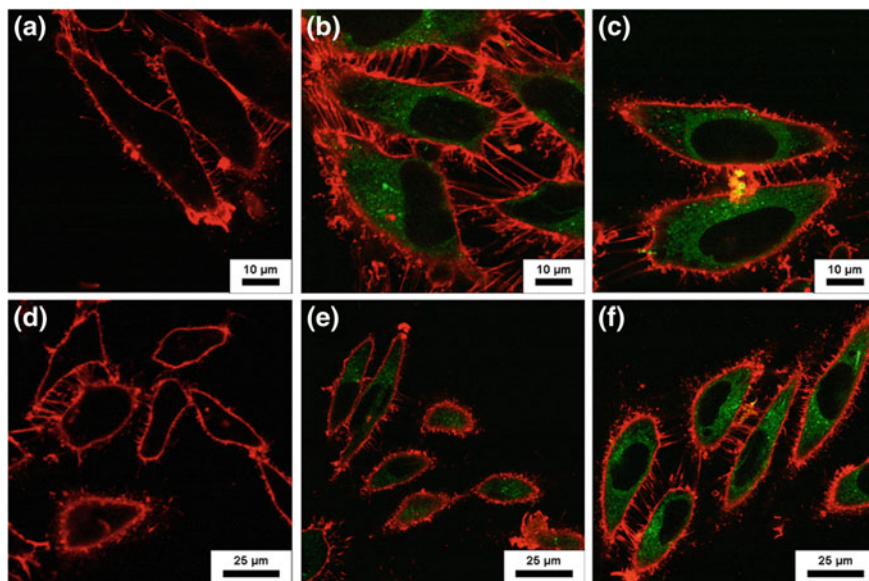


Fig. 5.32 cLSM images of HeLa cells incubated with different concentrations of FL-MG microgels: **a, d** negative control without gel nanoparticles; **b, e** incubated with 800 $\mu\text{g/mL}$; **c, f** incubated with 1200 $\mu\text{g/mL}$. Images from D. Baumann

It becomes obvious that incubation with FL-MG microgels does not induce any morphological changes of the cells compared to the untreated negative control shown. As can be seen from the green fluorescence in the images of Fig. 5.32 the microgel particles are not attached to the cell membrane but are successfully incorporated into the cells. Moreover, the fluorescence is rather diffuse than spatially well confined. This effect is assumed to stem from the swollen state of the microgel particles in aqueous medium thus rendering the particles structure more diffuse.

Conclusion

In summary, it was found that fluorescently labeled FL-MG microgels did exhibit a good cellular uptake by HeLa cells in combination with a negligible cytotoxicity. This performance is assumed to be an inherent feature of the p(HEMA-co-MAA) microgels with a specific particles size and swelling behavior. As a consequence, the utilization of FL-MG microgels as model systems for the prediction of the biocompatibility of loaded MG-D particles is enabled. In addition, since these materials represent model compounds for the aimed preparation of photo-degradable p(HEMA-co-MAA) microgels, the results obtained from the described investigations are assumed to be transferable to the light-sensitive analogues.

5.1.2.2 Dual Stimuli-Responsive p(HEMA-*co*-MAA) Microgels: pH-Dependent Swelling and Light-Induced Degradation

Having demonstrated in the previous chapters the great potential of non-light-sensitive p(HEMA-*co*-MAA) microgels for loading and release applications in biomedical fields, the combination of these pH-sensitive materials with the developed concept of light-degradable microgels is highly interesting.

Regarding particulate delivery systems solely based on pH-sensitive materials, either degradation- or swelling-induced release occurs as a response to the H^+ concentration of the local environment, thus rendering those particles “smart”. Such concepts are investigated for drug delivery applications by exploiting the acidic pH of malignant tissue and lysosomes [48, 62]. Nevertheless, these systems require the addition of protons or the localization in acidic milieus. In comparison, inducing the release of a payload by applying an external trigger without a change in the chemical composition of the surrounding media bears the advantage of an on-demand delivery. Concerning this point, light represents an outstanding position as it can be applied in a very precise manner by selecting suitable wavelengths, polarization directions and intensities in a non-contact approach [1, 63]. In addition, light offers the possibility to change the polymer properties in very confined spaces and time scales [64, 65].

The aim of this work is the preparation of dual stimuli-responsive p(HEMA-*co*-MAA) microgels to exhibit a pH-dependent volume phase transition due to ionizable MAA groups in the network-forming polymer and the ability to complete particle disintegration upon irradiation due to light-cleavable crosslinking points. The particular combination of the mentioned stimuli is designed to exhibit two different degradation profiles as shown in Fig. 5.33.

In both cases, particles are highly swollen for pH values higher than the pK_a of the microgels, whereas decreasing the pH leads to a deswelling of the networks. The disintegration of the collapsed particles by direct irradiation represents a one-

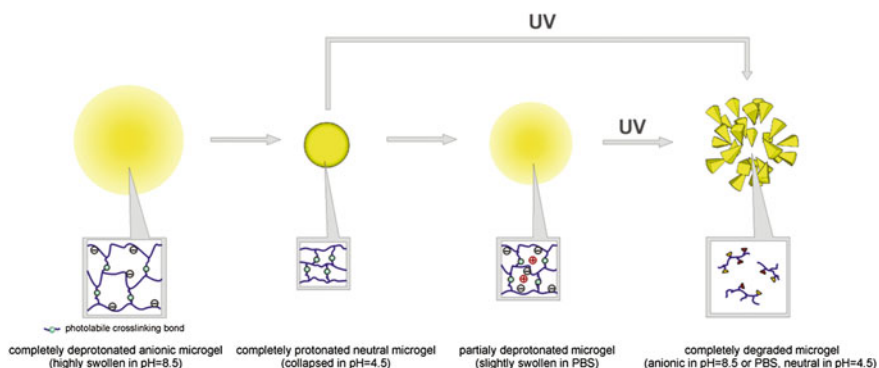


Fig. 5.33 Schematic representation of the double stimuli-responsive character of the photo-degradable p(HEMA-*co*-MAA) microgels. Reprinted with permission from [38]. Copyright 2011 American Chemical Society

step degradation profile. In contrast, by transferring the collapsed particles to phosphate buffer solution, slightly swollen particles are obtained, which subsequently can be degraded by the application of UV light, therefore characterizing a two-step swelling/degradation profile.

Realization of the described concept is based on the formerly developed preparation method of light-sensitive PHEMA microgels. As the photo-labile crosslinkers described in the previous chapters exhibited a good solubility in HEMA as the main ingredient of the mixtures, the investigated synthetic approach is assumed to be transferable to the preparation of pH-sensitive and light-degradable microgels by copolymerization of HEMA with MAA in the presence of photo-cleavable crosslinkers in inverse miniemulsion.

Synthesis and characterization of photo-labile crosslinkers. Investigations on photo-sensitive PMMA polymeric gel microgels revealed the synthesized crosslinker CL-4B as the compound exhibiting the best photolytic properties under mild irradiation conditions [9]. Based on these considerations concerning the utilized chromophore, a new crosslinker CL-5B was synthesized in order to investigate the influence of the molecular structure on the degradation behavior of the hydrogel particles. The synthetic pathway to CL-5B in comparison to CL-4B is shown in Fig. 5.34 together with the reaction conditions.

Both structures are based on 4-(4-(1-hydroxyethyl)-2-methoxy-5-nitrophenoxy)butanoic acid (HEMNPBA) which was synthesized accordingly to a previous publication [9]. Briefly, acetovanillone was reacted with methyl 4-bromobutyrate to the corresponding keto ester (5) under basic conditions. A subsequent nitration of the crude product was achieved by the reaction with acetic anhydride and nitric acid. In the next step, the reduction of the keto group of (6) with excess borohydride was conducted and directly followed by inducing the ester cleavage by the addition of NaOH in water yielding HEMNPBA (8). CL-4B was synthesized by first reducing the acid group of (8) to the corresponding alcohol and then reacting (9) with two equivalents of 2-isocyanatoethyl methacrylate in the presence of catalytic amounts of DBTDL to form the carbamate. In the case of CL-5B, HEMNPBA (8) was reacted with an excess amount of methacryloyl chloride to form the *o*-nitrobenzyl ester of (10). The symmetric crosslinker CL-B was then prepared by DCC coupling of two equivalents of (10) with ethylene diamine.

CL-4B and CL-5B crosslinkers are both based on nitroveratryloxycarbonyl derivatives as the photo-reactive moieties thus representing crosslinkers of type B, as introduced in Sect. 5.1.1.1. The particular chromophore was demonstrated to be characterized by a fast photoreaction due to the α -methyl group on the benzylic carbon of the *o*-nitrobenzyl core. Moreover, its high extinction coefficient for $\lambda > 315$ nm enables the degradation of the crosslinkers and the resulting p(HEMA-*co*-MAA) gel particles in a controlled manner under mild conditions (UV-A light of wavelengths $\lambda > 315$ nm). Meaning, Norrish-type side reactions, which primarily take place for irradiations with wavelengths of $\lambda < 300$ nm [12, 13] and undesirable side effects in biological applications should be avoided. UV-vis spectroscopy of the crosslinkers CL-4B and CL-5B showed in every case an absorption maximum at 300 nm and an additional absorption maximum at

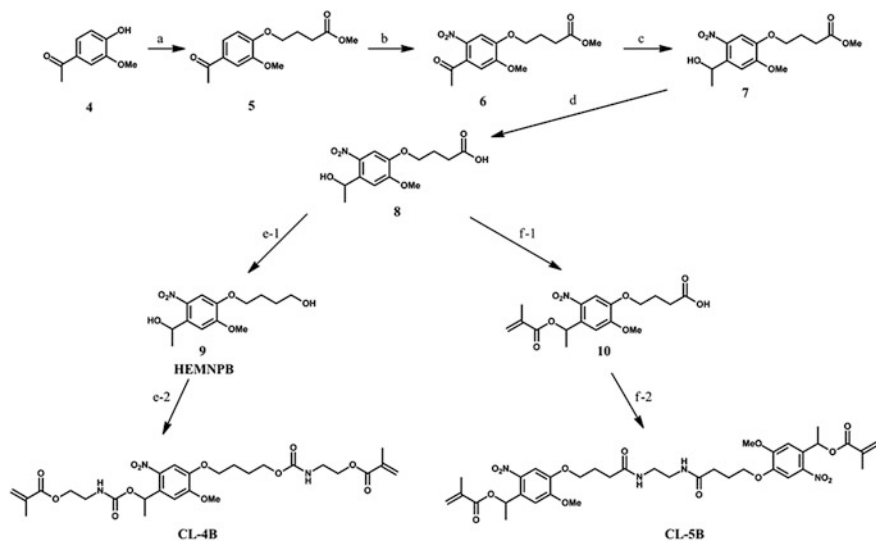


Fig. 5.34 Synthesis of photo-cleavable crosslinkers. Reagents and conditions: **a** methyl 4-bromobutyrate, $\text{K}_2\text{CO}_3/\text{DMF}$ (anhyd.), 25 °C, 16 h, quant.; **b** acetic anhydride/nitric acid (1:2, v/v), 0 °C, 3 h, 53 %; **c**, **d** $\text{NaBH}_4/\text{MeOH}/\text{THF}$, 25 °C, 16 h, NaOH , 25 °C, 7 h, 89 %; **e-1** $\text{BH}_3^*\text{THF}/\text{THF}$, 0 °C, 1 h then 40 °C, 18 h, 86 %; **e-2** 2-isocyanatoethyl methacrylate, DBTDL (cat.)/THF, 65 °C, 48 h, 63 %; **f-1** methacryloyl chloride, NEt_3/DCM , 0–25 °C, 15 h, 42 %; **f-2** ethylenediamine, DCC, DMAP (cat.)/DCM, 0–25 °C, 15 h, 53 %. Reprinted with permission from [38]. Copyright 2011 American Chemical Society

342 nm. Thus, both crosslinkers exhibit a high absorption coefficient in the targeted photolysis wavelength region of $\lambda > 315$ nm.

Photolysis of the cleavable crosslinkers in solution. Although either type of crosslinker consists of one or two central *o*-nitrobenzylic group(s), the variation of the molecular attachment of the radically polymerizable methacrylate moieties onto the photo-labile chromophore results in different photo-products with specific functional groups. The carbamate derivative of crosslinker CL-4B degrades into an amine and a ketone, whereas irradiation of the ester of CL-5B generates two carboxylic acid groups and two ketone moieties. Earlier investigations on the photolysis of CL-4B revealed that upon longer irradiation times with UV light of the wavelengths of $\lambda > 300$ nm, dimeric azoxybenzene compounds are formed from the primary photo-products in THF solution. As shown for photo-degradable PMMA microgels, the covalent attachment of those side products to the polymer backbone hinders complete particle degradation due to the formation of new crosslinking points in the respective gels [9]. Even though a dramatic increase in the degree of swelling for those particles could be detected for the mentioned irradiation conditions, complete microgel disintegration enhances the potential for delivery applications. Therefore, the symmetric molecular structure of CL-5B was designed to generate only carboxylic acid groups on the polymer backbone by photolytic cleavage of the *o*-nitrobenzyl ester bonds. The separated middle part of

the crosslinking molecule contains both of the chromophore cores and is not connected to the gel-forming polymers any more. Thus, a possible formation of dimeric side products of the photo-product is assumed to result in liberated molecules not hindering the particle degradation. In addition, the formed methacrylic acid groups for CL-5B in the polymer backbone are supposed to enhance the swelling of the anionic gels whereas the amine groups generated upon photolysis of CL-4B are—due to electrostatic interactions and dependent on the pH—able to form physical crosslinks with the methacrylic acid groups in the p(HEMA-co-MAA) copolymer.

In comparison to the studies performed on CL-4B [9], the photo-degradation behavior of the crosslinker CL-5B in equimolar THF solution was first investigated by irradiation time-dependent UV-vis measurements. The respective plot of CL-5B is shown in Fig. 5.35.

Irradiation of either the CL-4B (see Sect. 5.1.1.1) or the CL-5B crosslinker with UV light of the wavelengths $\lambda = 315\text{--}390$ nm resulted in every case in a red shift of the absorption maxima to $\lambda_{max} = 385$ nm. These light-induced changes of the absorption spectra point towards successful photo-reactions. However, the formation of possible side products absorbing light in the same spectral region could not be excluded. In the case of CL-4B, no further changes in the absorption spectra were detected after an irradiation time of 5 min indicating no further conversion of the photo-reaction. In comparison, more than 10 min of irradiation were necessary to complete the light-induced cleavage of the CL-5B molecule. Comparing the

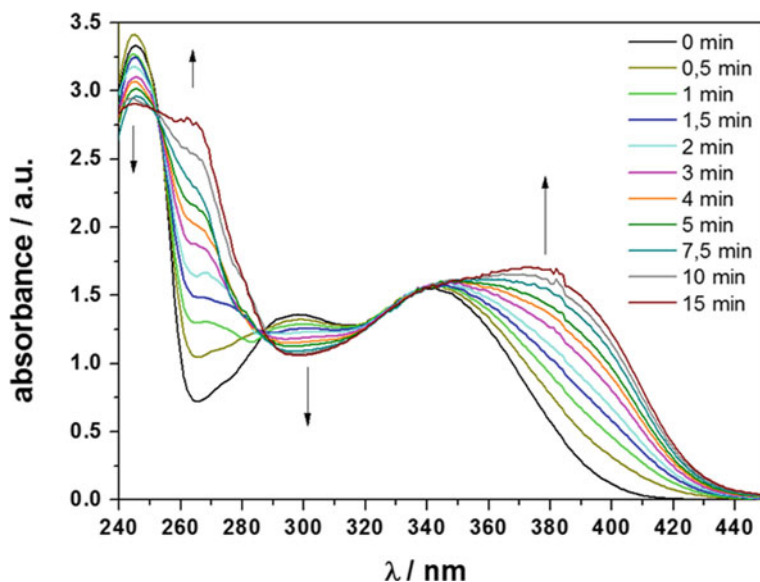


Fig. 5.35 Investigations on the photolysis of photo-cleavable crosslinker CL-5B in THF solution: Irradiation time-dependent UV-vis spectra. Adapted with permission from [38]. Copyright 2011 American Chemical Society

molecular structure of CL-4B to CL-5B, it becomes obvious that for the same molar concentration in THF, in the latter case two chromophores per molecule have to be cleaved. As a result, the required irradiation time is increased.

In order to perform a quantitative time-dependent degradation analysis of the crosslinkers, HPLC measurements were conducted to examine the composition of the reaction mixtures at various irradiation times. The kinetics of the photolysis of the photo-labile molecules was therefore investigated by monitoring the rate of disappearance of the starting compounds during irradiation. Kinetic plots of $-\ln [CL]_t/[CL]_0$ versus time show all excellent linearity, indicating the expected first order kinetic with respect to the chromophore concentration (see Fig. 5.36b). Figure 5.36 presents an example of the time-dependent HPLC elution curves of the photo-reaction of CL-B and the kinetic plots for the calculation of the rate constants for both crosslinkers. The obtained half-life times and rate constants are listed in Fig. 5.36b.

Both crosslinkers were found to degrade completely upon irradiation with UV light of wavelengths with $\lambda = 315\text{--}390$ nm. As shown before [9], the elugram of crosslinker CL-4B exhibits the direct formation of one main photo-product accompanied by the generation of the dimeric azoxybenzene side product. In comparison, the elugram of CL-5B displays the formation of an intermediary compound (peak at 6.6 min) during irradiation in addition to the main photo-product (peak at 5.0 min). The intermediate was assigned to the compound generated by the unilateral cleavage of one *o*-nitrobenzyl ester group of the symmetric bifunctional molecule. Further irradiation leads to the complete cleavage of both chromophore units and therefore results in one main photo-product, which was assigned to the peak at 5.0 min. It was demonstrated that the variation of the molecular structures of the crosslinkers CL-4B and CL-5B results in different degradation profiles whereas CL-4B reacts around 1.5 times faster than CL-5B. Taking into account absorption of the (intermediary) photo-products in the same spectral region as the wavelengths used for the cleavage of the crosslinkers,

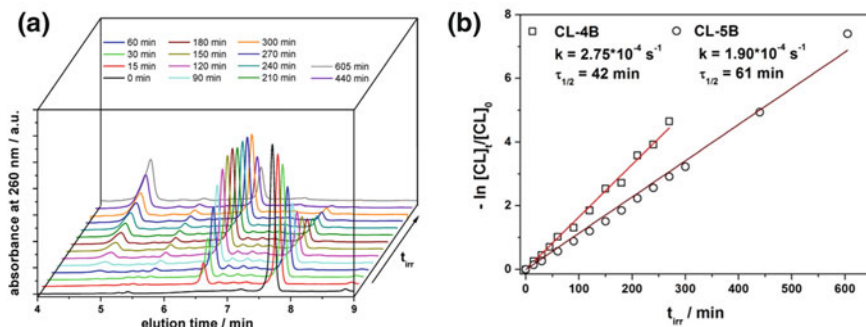


Fig. 5.36 Kinetic investigations on the photolytic crosslinker degradation: **a** irradiation time-dependent HPLC measurements of CL-5B; **b** kinetic plots of $-\ln [CL]_t/[CL]_0$ versus irradiation time for CL-4B and CL-5B, respective rate constants and half times. Adapted with permission from [38]. Copyright 2011 American Chemical Society

the photo-reaction of the two chromophores containing CL-5B is significantly slowed down compared to CL-4B. Nevertheless, even an unilateral cleavage of the CL-5B molecule is assumed to already enable the degradation of a polymeric network. In addition, the complete cleavage of CL-5B for longer irradiation times does not generate any polymer bound dimeric side products, which is expected to facilitate the complete particle degradation under mild conditions.

Preparation and characterization of crosslinked photo-degradable p(HEMA-co-MAA) hydrogel nanoparticles by inverse miniemulsion copolymerization. Photo-degradable p(HEMA-co-MAA) microgels were prepared by the copolymerization of HEMA, MAA, and the respective crosslinkers in inverse miniemulsion. Thereby, the successfully developed method of preparing light-sensitive PHEMA microgels by inverse miniemulsion copolymerization is transferred to water swellable pH-sensitive p(HEMA-co-MAA) hydrogel microgels (HG-MGs).

In order to assure comparability between the individual gel particles regarding their swelling and degradation behavior, 2.5 mol-% of crosslinkers were used in every case. The nominal compositions of the dispersed phases are shown in Table 5.5.

For the HG-MG-4B-I microgels, the crosslinking molecule CL-4B was readily soluble in the monomer mixture, so no further solvent was used to form the dispersed phase prior to polymerization. Solubility restrictions of CL-5B in the same monomer composition hindered analogous reaction conditions. Therefore, in order to form HG-MG-5B-II microgels, 20 wt.-% of DMSO were added to assure complete crosslinker solubility. Analogously, HG-MG-4B-II gel particles were prepared using crosslinker CL-4B. In addition, particles containing no crosslinking molecules were prepared as reference particles for the swelling and degradation experiments. P(HEMA-co-MAA) HG-MG-0-I nanoparticles were polymerized analogously to HG-MG-4B-I gel particles without any additional solvent for the dispersed phase. In contrast, HG-MG-0-II particles, polymerized using 20 wt.-% DMSO as solvent, represent the reference particles to the HG-MG-4B-II and HG-MG-5B-II microgels. To remove excess surfactant, all particle dispersions were repeatedly washed with cyclohexane after polymerization yielding stable dispersions. Hydrodynamic diameters of the non-swollen MGs were determined by DLS measurements in cyclohexane and were found to be in the size range of around 130 nm for HG-MG-0-I and HG-MG-4B-I particles and about 85 nm for HG-MG-0-II, HG-MG-4B-II and HG-MG-5B-II microgels. For the miniemulsions

Table 5.5 Nominal compositions of (photo-sensitive) p(HEMA-co-MAA) HG-MGs

Sample	DMSO m/mg	Crosslinker		
		Type	m/mg	mol-%
HG-MG-0-I	–	–	–	–
HG-MG-4B-I	–	CL-4B	185	2.5
HG-MG-0-II	375	–	–	–
HG-MG-4B-II	375	CL-4B	185	2.5
HG-MG-5B-II	375	CL-5B	235	2.5

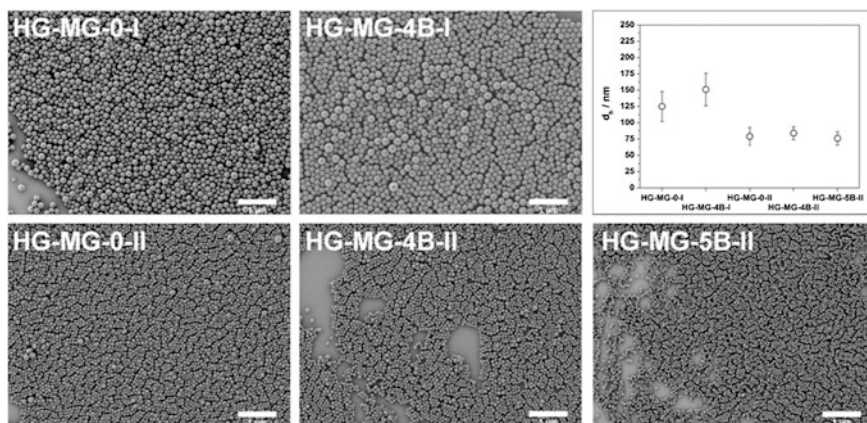


Fig. 5.37 Representative SEM images of p(HEMA-*co*-MAA) microgels drop cast from cyclohexane dispersions and hydrodynamic diameters obtained from DLS measurements in cyclohexane. Reprinted with permission from [38]. Copyright 2011 American Chemical Society

including DMSO as solvent for the dispersed phase, smaller particles were obtained after polymerization. This effect might be either explained by a changed surface tension or a decreased viscosity in this system. Figure 5.37 shows representative SEM pictures of the drop cast cyclohexane dispersions on silica wafers together with the hydrodynamic diameters obtained from DLS measurements.

In order to transfer the prepared microgels to the aqueous phase, the freeze-dried samples were allowed to swell in water (solid content 5.0 % (w/v)) adjusted to pH 12. Here, complete deprotonation of the carboxylic acid groups was achieved as could be monitored by the decrease of the pH to about pH 8 for all samples. After titration with diluted hydrochloric acid to pH 7, the swollen microgels were washed 3 times with deionized water to remove formed sodium chloride, unreacted monomers and non-crosslinked free polymer chains and oligomers. Freeze-drying of the purified dispersions yielded the microgels as slightly yellow colored powders which can be stored in the dried state and transferred to water by simple swelling. Resulting aqueous dispersions are stable without any additional surfactant due to sterical stabilization by dangling chains of the swollen outer layer of the microgels.

The retention of the particulate structure for the crosslinked particles dispersed in aqueous media of pH 8.5 was confirmed by SEM analysis. Figure 5.38 shows representative pictures. Due to the highly swollen state of the microgels, the particles can be identified as flattened spheres on the wafer. Non-crosslinked reference particles HG-MG-0-I and HG-MG-0-II completely dissolved in water and SEM analysis only showed polymer films but no spherical structures (data not shown).

Investigations on the pH-dependent swelling behavior of the microgels. The prepared microgels are designed to exhibit a pH-dependent swelling behavior due to the anionic network-forming p(HEMA-*co*-MMA) copolymer. Deprotonation of

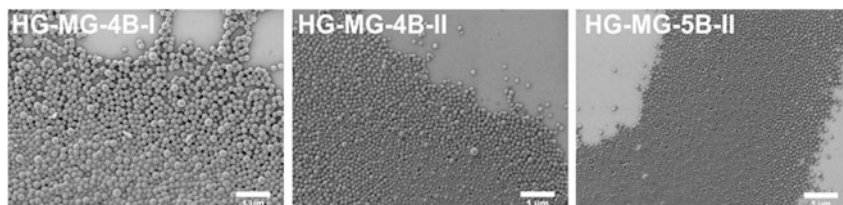


Fig. 5.38 Representative SEM images of photo-degradable p(HEMA-co-MAA) microgels drop cast from aqueous dispersions at pH 8.5. Reprinted with permission from [38]. Copyright 2011 American Chemical Society

the carboxylic acid groups increases the hydrophilicity of the network, thus inducing an enlargement of the degree of swelling of the particles. This effect is even enhanced by electrostatic repulsion of the generated anionic groups at higher pH values.

With the aim to investigate the described behavior, the pH values of microgel dispersions in water were varied from pH 4 to pH 12 by adding an aqueous NaOH solution, and hydrodynamic diameters (d_h) of the particles were measured by DLS for every pH value. The resulting graphs of plotting d_h against pH are shown in Fig. 5.39a–c. Figure 5.39d additionally shows the resulting degrees of swelling calculated as $DGS = V_{swollen}/V_{non-swollen}$, where $V_{non-swollen}$ represents the values obtained for the particle dispersions in cyclohexane.

As expected, all microgels exhibited pH-dependent swelling properties with critical swelling transitions at pH values between 6.0 and 8.5. The majority of the carboxylic acid groups became deprotonated above pH 6.0 and the average particle diameters increased dramatically. In all cases a maximum degree of swelling was reached at about pH 9, represented by electrostatic repulsion of the strongly anionic chains. Regarding pH values below 5.5, the network forming polymer chains were protonated, thus rendering the gels more hydrophobic. As a result of the absence of inner charges, the microgels are collapsed and behaved like conventional latex particles. Lowering the pH below 3.75 resulted in coagulation of the particles due to the lack of any steric stabilization of dangling chains.

Comparing the actual relative volumes of the different particles, it is noteworthy that all microgels dispersed in phosphate buffer solution (PBS) with pH 7.4 showed a lower swelling degree compared to the identical particles in water of the same pH (see Fig. 5.39d). Cationic electrolytes present in the buffer solution shield the generated anionic groups in the network, thus resulting in a reduced electrostatic repulsion. In this context it becomes obvious that the observed degrees of swelling in PBS are lower than in the case of MG-D and FL-MG particles described in previous chapters. This effect is assumed to be the result of the more pronounced hydrophobic nature of the photo-cleavable crosslinkers in comparison to DEGDMA. Therefore, the overall hydrophilicity of the network is reduced. Furthermore, it becomes obvious that the DGS values of HG-MG-4B-II and HG-MG-5B-II enlarged with increasing pH to a similar steady value of $DGS_{max} = 11$ at pH 8.5. In contrast, at the

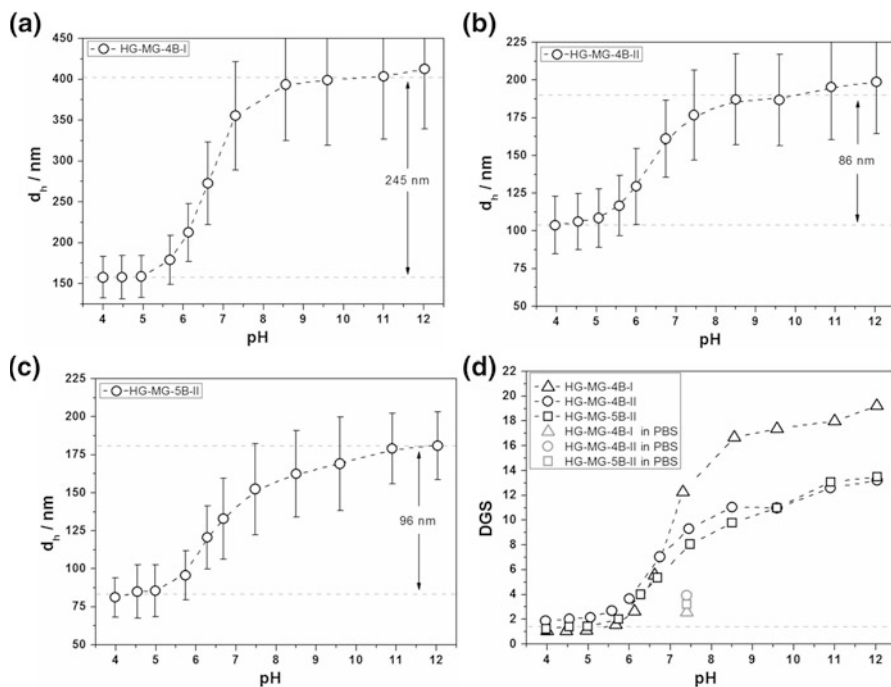


Fig. 5.39 Investigations on the pH-dependent swelling behavior of photo-degradable p(HEMA-co-MAA) microgels: **a–c** hydrodynamic diameters measured by DLS of aqueous dispersions of HG-MG-4B-I, HG-MG-4B-II and HG-MG-5B-II dependent on the pH; **d** degrees of swelling in dependency on pH and additional values for PBS as medium. Adapted with permission from [38]. Copyright 2011 American Chemical Society

same pH, HG-MG-4B-I is swollen to a much greater extent, as characterized by a higher maximum degree of swelling of $DGS_{\max} = 17$. As HG-MG-4B-I and HG-MG-4B-II only differ in their preparation, namely their initial composition of the dispersed phase before the polymerization, it is assumed that this parameter either influences the amount of included crosslinker or the incorporation ratio of HEMA/MAA in the final network.

UV-vis measurements of microgel dispersions in DMSO were conducted to determine the amount of incorporated crosslinking molecules. For quantification, spectra of the swollen photo-degradable microgels were compared to spectra of solutions of the respective crosslinkers in dispersions of non-photo-degradable p(HEMA-co-MAA) microgels. By this, in contrast to pure crosslinker solutions, scattering effects can be taken into account. The relative quantity of incorporated crosslinker was determined with respect to HEMA and MAA amounts before polymerization as mol-% of theory. Whereas in the case of HG-MG-4B-II and HG-MG-5B-II 73 and 82 mol-% of CL-4B and CL-5B were incorporated into the respective microgels, for HG-MG-4B-I a value of 117 mol-% integration of CL-4B was determined. Considering the pH-dependent swelling profile of the different

microgels, an increased DGS_{\max} of HG-MG-4B-I in combination with a higher amount of incorporated crosslinker (>100 mol% of theory) is assumed to base on an enhanced incorporation of MAA into the network. Since the similar crosslinker incorporation efficiencies into the microgels, polymerized using additional DMSO as solvent (HG-MG-4B-II and HG-MG-5B-II), were found to vary significantly from the value for HG-MG-4B-I, it is assumed that the composition of the dispersed phase during polymerization influences both parameters mentioned above: the crosslinker incorporation and the HEMA/MAA ratio in the network forming polymer. In general, non-quantitative conversions of the polymerization reactions yielded sol contents consisting of unreacted monomers, crosslinkers and non-crosslinked oligomer- or polymer chains. Removal of the sol during gel purification therefore resulted in crosslinker incorporation efficiencies depending on the composition of the respective sol content and differing from the theoretical amount.

In order to investigate the proposed enhanced incorporation of MAA into HG-MG-4B-I microgels, potentiometric titration experiments were conducted. The pH values of the different aqueous microgel dispersions (0.5 % w/v) were adjusted to about pH 4 by adding diluted hydrochloric acid (0.05 N). The resulting mixture was allowed to equilibrate for 1 h and was then titrated to around pH 10 by adding NaOH (0.05 N). After every base addition step, the dispersions were allowed to equilibrate for 15 min under stirring and ultrasonicated for 2 min. Titration curves for the different microgels are shown in Fig. 5.40.

In every case three different inflection points were observed at about pH 4.7, 6.3 and 8.3. The lowest inflection point at about pH 4.7 is the first equivalence point of the titration, meaning the neutralization of all excess HCl. The highest inflection point at about pH 8.3 is the second equivalence point and corresponds to the point of complete deprotonation of all methacrylic acid groups [66]. The respective contents of ionizable groups Q in the microgels were determined from the difference in amount of OH^- between these points. In addition the third inflection point at about pH 6.3 represents the half equivalence point and denotes the $\text{p}K_a$ values of the microgels. From the calculated values for Q , the MAA incorporation efficiency IE (MAA) was determined relative to the theoretical amount assuming 100 % incorporation of monomers and crosslinkers into the latex particles. The obtained values are listed in Table 5.6.

It was demonstrated that for all samples the amount of integrated MAA groups in the microgels differs from the theoretical amount of 100 %. Keeping in mind that the final composition of the polymeric gels is influenced by the conversion of the polymerization, this effect can be explained by removal of the sol content during the purification procedure which resulted in the observed deviations from the theoretical values. Nevertheless, HG-MG-4B-I with $Q = 1.26 \cdot 10^{-3}$ mol/g clearly contains a higher percentage of acid groups than microgels MG-2A and MG-2B with $Q = 1.17 \cdot 10^{-3}$ and $1.16 \cdot 10^{-3}$ mol/g, thus resulting in a higher degree of swelling despite an also enhanced incorporation of crosslinking points. The observed $\text{p}K_a$ values are in all cases in good agreement with the observed swelling profiles.

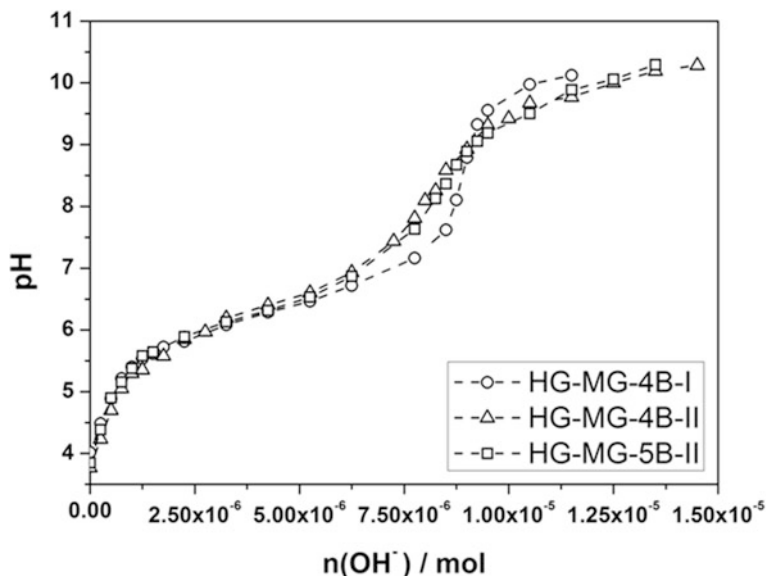


Fig. 5.40 Determination of the amount of ionizable groups in photo-degradable p(HEMA-co-MAA) microgels: titration curves. Reprinted with permission from [38]. Copyright 2011 American Chemical Society

Table 5.6 Determination of the amount of methacrylic acid in photo-degradable p(HEMA-co-MAA) microgels: obtained values for the content of ionizable groups Q , the incorporation efficiency IE of MAA and the pK_a values

Sample	$Q/10^{-3}$ mol/g	IE (MAA)/%	pK_a
HG-MG-4B-I	1.26	81	6.30
HG-MG-4B-II	1.17	77	6.28
HG-MG-5B-II	1.16	75	6.27

Photo-degradation experiments of p(HEMA-co-MAA) microgels in aqueous media. Photo-degradation of the different microgels in water was examined by irradiating 0.125 % (w/v) dispersions in various aqueous media with UV light. The light-induced swelling/degradation was monitored by turbidity of the samples. Analogously to irradiation studies of photo-degradable PMMA particles, turbidity was measured as the relative scattering intensity at 90° [9]. The cleavage of crosslinking points leads to a looser network structure, thus decreasing the contrast in the refractive indices between solvent and particle [18, 19].

In a first attempt, dispersions of highly swollen microgels at pH 8.5 were irradiated with UV light of varying wavelengths and intensities. Figure 5.41 shows the resulting turbidity curves.

As can be seen in Fig. 5.41a, irradiation of HG-MG-4B-I microgels with UV light of the wavelengths of 315–390 nm and an intensity of 17 mW/cm^2 does only

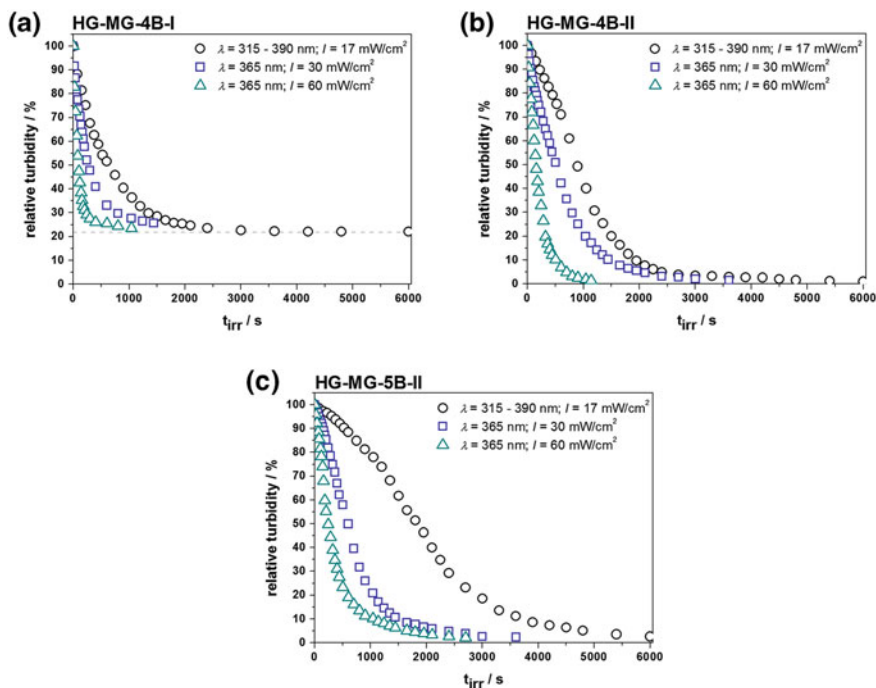


Fig. 5.41 Investigations on the light-induced particle degradation at pH 8.5 by turbidity measurements for different light intensities and wavelengths for: **a** HG-MG-4B-I; **b** HG-MG-4B-II and **c** HG-MG-5B-II. Adapted with permission from [38]. Copyright 2011 American Chemical Society

result in a decay of the turbidity down to a constant level of about 21 %, therefore indicating only increased particle swelling due to incomplete degradation. In contrast, HG-MG-4B-II and HG-MG-5B-II both exhibit a decrease in scattering intensity to almost 0 % of the initial value being a sign of complete particle disintegration. Furthermore, using a discrete irradiation wavelength of 365 nm and increasing the UV light intensity up to 30 and 60 mW/cm² results in a faster degradation for all microgels but does not influence the constant turbidity level >0 % of HG-MG-4B-I. In general, this behavior allows controlling the degradation rate via the light intensities used.

The differences of the degradation profiles of HG-MG-4B-I and HG-MG-4B-II microgels, both based on crosslinker CL-4B, are dependent on their respective polymerization conditions. Whereas in the case of HG-MG-4B-I no additional solvent was used during polymerization, HG-MG-4B-II microgels were prepared by adding DMSO to the dispersed phase. As discussed above, this parameter influences the composition of the final gels in terms of amount of MAA groups in the network-forming copolymer and incorporated crosslinker molecules. As a higher crosslinker content was determined for HG-MG-4B-I particles compared to

HG-MG-4B-II gels, the observed retardation of light induced particle disintegration can be explained. Nevertheless, increasing the irradiation light intensity does not affect the constant turbidity level observed for HG-MG-4B-I latexes, therefore indicating the influence of another parameter. Irradiation of CL-A crosslinking molecules is known to form dimeric azoxybenzene side products. As shown for PMMA-gel particles, those side products are bound to the polymer backbone, therefore forming new crosslinking points hindering complete particle disintegration [9]. It is assumed that this effect also occurs in HG-MG-4B-I microgels but is suppressed in the case of HG-MG-4B-II. It is assumed that a higher degree of chain entanglement in combination with a higher amount of incorporated crosslinker in HG-MG-4B-I microgels retards the diffusion of cleaved polymer chains in the gels, thus rendering the formation of dimers by the encounter of two polymer bound chromophores more likely. In this context, the use of additional DMSO as solvent for the dispersed phase of HG-MG-4B-II is assumed to influence the resulting molecular weight of the gel forming polymers by restraining the Trommsdorff effect due to a higher dilution of the polymerization mixture. Even though reference particles HG-MG-0-I and HG-MG-0-II were completely soluble and disintegrated at pH 8.5, the determination of the molecular weights of the polymers by GPC analysis yielded values of $M_n = 235,000$ g/mol (PDI = 4.3) and $M_n = 53,000$ g/mol (PDI = 2.0) for HG-MG-0-I and HG-MG-0-II, respectively. The about five times increased molecular weight of the polymers formed without additional DMSO as well as the dramatically increased polydispersity point towards the occurrence of a gelation effect during the polymerization. It is concluded that incomplete particle degradation of HG-MG-4B-I originates in the distinct photolysis behavior of CL-4B in correlation with polymer entanglement of the network-forming copolymer.

Regarding possible release applications for the double stimuli-responsive microgels, a direct degradation of the collapsed particles at pH 4.5 would enable a one-step release, whereas the degradation of slightly swollen microgels in PBS would combine a slow diffusion-based release with a subsequent irradiation-based degradation, thus representing a two-step release profile.

In order to examine light-triggered particle disintegration in dependency of the pH, irradiation experiments with UV light of $\lambda = 365$ nm and $I = 60$ mW/cm² were conducted in different aqueous media and reactions were monitored again by turbidity measurements. The obtained curves are shown in Fig. 5.42.

The irradiation of HG-MG-4B-I microgels in aqueous media at different pH resulted in every case in a decay of turbidity down to a constant level higher than 0 %. Comparing the results obtained for pH 8.5 and 10.5, no differences in the turbidity curves were observed, thus confirming that incomplete particle degradation is a result of newly formed crosslinks as side products of the photolysis of CL-4B. Physical crosslinks between the formed amine groups of cleaved CL-4B and the carboxylic acid groups of the network-forming copolymer can be excluded due to the absence of protonated amine moieties at this pH value. Measurements in PBS buffer at pH 7.4 and aqueous medium at pH 4.5 resulted in an increase of the constant turbidity levels up to 32 and 60 % respectively. Here, analogously to the

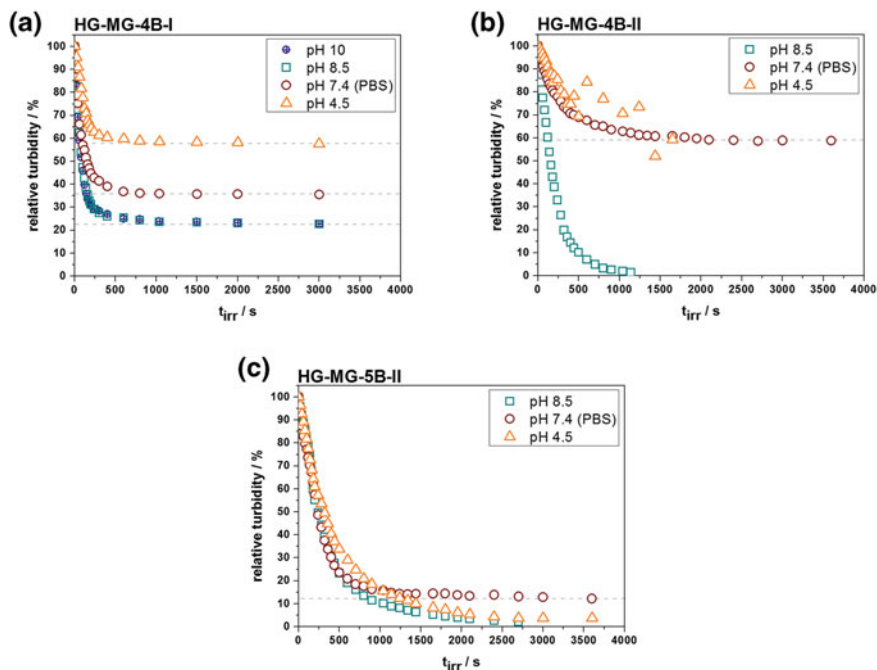


Fig. 5.42 Investigations on the light-induced ($\lambda = 365$ nm; $I = 60$ mW/cm²) particle degradation by turbidity measurements at different pH values for: **a** HG-MG-4B-I; **b** HG-MG-4B-II and **c** HG-MG-5B-II. Adapted with permission from [38]. Copyright 2011 American Chemical Society

experiments in basic media, irradiation of the microgels causes the cleavage of CL-4B molecules and the formation of new crosslinks as side reactions resulting in swollen gel particles rather than free polymer chains. The final degree of swelling after irradiation correlates to the constant turbidity level and is influenced by two parameters: (a) the ratio of CL-4B cleavage to dimeric side product formation and (b) the pH-dependent swelling properties of the gels. An initial low degree of swelling due to a lower pH favors in this context the formation of new crosslinks. A more confined space enhances the reaction probability of two polymer bound groups thus hindering particle swelling.

Experiments conducted on HG-MG-4B-II microgels confirm the conclusions derived above. While complete degradation was observed for a high initial degree of swelling at pH 8.5, irradiations in PBS or pH 4.5 resulted in incomplete particle disintegration, characterized by final constant turbidity values of about 60%. At pH 8.5, in contrast to HG-MG-4B-I latexes, reduced entanglement of the shorter polymer chains enables the generated photolysis products to diffuse apart sufficiently fast enough not to form dimeric side products. By lowering the pH and thereby reducing the initial degree of swelling, the spatial concentration of the photolysis products in the less swollen gels is increased, thus enabling the

formation of new dimeric crosslinks and resulting in swelling of the particles or formation of macroscopic aggregates rather than complete degradation.

Regarding HG-MG-5B-II gel particles crosslinked with CL-5B—independent of the pH of the media—the turbidity of the samples decreased upon irradiation in every case down to almost 0 %, therefore indicating complete particle degradation. In contrast to HG-MG-4B-I and HG-MG-4B-II particles crosslinked with CL-4B, CL-5B—used to crosslink HG-MG-5B-II—was designed to be cleaved upon irradiation without generating polymer bound chromophores. As a result, photolytic generation of dimeric side products prohibits the formation of new crosslinks. The excellent and fast degradation behavior of HG-MG-5B-II independent on the pH of the aqueous phase renders those particles highly interesting for possible release applications.

Investigations on the double stimuli-responsive behavior of the p(HEMA-*co*-MAA) hydrogel nanoparticles. Depending on the specific properties of the active compound to be delivered, the loading and release mechanisms due to an externally induced volume transition can vary significantly. As described in the case of non-photo-sensitive p(HEMA-*co*-MAA) particles, while collapsing a microgel can induce the release of embedded low molecular weight compounds electrostatically adsorbed to the former swollen network [51], a similar volume transition can be used to entrap high molecular weight compounds such as e.g., proteins in the gel [46, 67]. Here, the swollen state enables the diffusion of active compounds with a hydrodynamic diameter smaller than the mesh size of the swollen network in- and out of the gel. Deswelling of the network is characterized by an effective decrease of the mesh size, therefore entrapping the active compound due to hindered diffusion. Subsequent swelling results then in the release of the captured compound. Following this concept, the successful loading and release of myoglobin into- and out from non-photo-sensitive p(HEMA-*co*-MAA) was demonstrated in Sect. p(HEMA-*co*-MAA) Microgels: Loading and Release of Myoglobin.

Regarding the potential of the dual stimuli-sensitive photo-degradable p(HEMA-*co*-MAA) microgels for release applications, pH-dependent swelling/deswelling of the gels should be combined with subsequent photo-degradation. Figure 5.43 demonstrates the investigated responses in terms of the degree of swelling of the different microgel particles. It becomes obvious that all microgel particles can easily be transferred from the cyclohexane phase to aqueous media by swelling freeze dried samples at pH values higher than pH 8. Lowering the pH to around 4.5 resulted in every case in deswelling of the microgels, therefore giving rise to a potential entrapment of active compounds in the network. Collapsed particles can then follow either a direct degradation or a two-step swelling/degradation profile. Whereas the direct case represents the light-triggered degradation of the collapsed particles in acidic medium, the two-step profile can be realized by slightly swelling the particles in PBS which is then followed by (complete) particle degradation upon irradiation.

It was demonstrated that in the case of microgel particles HG-MG-4B-I and HG-MG-4B-II crosslinked with CL-4B, the direct photolytic degradation of the

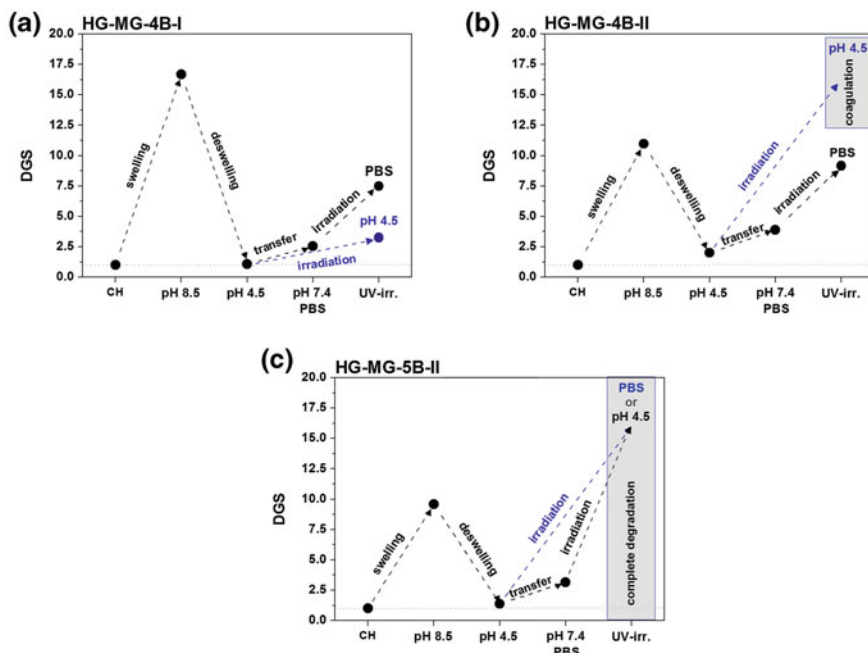


Fig. 5.43 Investigations on the double stimuli-responsive behavior of photo-degradable p(HEMA-co-MAA) microgels: pH-induced swelling and light-triggered (partial) degradation in different media. Plots of *DGS* in dependency on different stimuli for: **a** HG-MG-4B-I; **b** HG-MG-4B-II and **c** HG-MG-5B-II. Adapted with permission from [38]. Copyright 2011 American Chemical Society

collapsed particles is hindered by the formation of new crosslinks and results only in slightly swollen particles or macroscopic coagulates. Nevertheless, swelling of these microgels in PBS is characterized by an initial small increase in the degree of swelling up to a *DGS* of about 3. Subsequent irradiation leads then to dramatic increases in the particle volumes to a *DGS* of about 8. This pronounced difference is assigned to increased mesh sizes, thus increasing the diffusion coefficients of potential embedded compounds in the swollen state. In contrast, due to the specific designed photolytic behavior of CL-5B crosslinking molecules, HG-MG-5B-II microgels can be fully degraded upon UV light irradiation either in acidic aqueous phase or in PBS. In summary, this versatile behavior is assumed to be highly interesting for potential release applications.

Conclusion

The concept of light-degradable microgels was successfully transferred from gel particles swellable in organic solvents (Sect. 5.1.1) to water swellable hydrogel nanoparticles. Novel photo-degradable p(HEMA-co-MAA) microgels were prepared by free radical inverse miniemulsion copolymerization of HEMA and MAA

with two newly synthesized photo-labile crosslinking molecules. The introduction of anionic MAA moieties into the gel renders the microgels double stimuli-responsive as they exhibited a pH-dependent swelling and light-induced degradation behavior. The particular combination of the mentioned stimuli was found to exhibit two different degradation profiles. In both cases, particles were highly swollen for pH values higher than the pK_a of the microgels, whereas decreasing the pH led to a deswelling of the networks. The disintegration of the collapsed particles by direct irradiation represents a one-step degradation profile. In contrast, by transferring the collapsed particles to phosphate buffer solution, slightly swollen particles were obtained, which were subsequently degraded by the application of UV light, therefore characterizing a two-step swelling/degradation profile.

The preparation and characterization of the described microgels reveals their versatile behavior representing a great potential for delivery applications in materials science or biomedical fields. As outlook, three possible loading and release pathways are imaginable: (i) The pH-induced volume transition in combination with the ionization/deionization of the network gives rise to a potential loading with functional small cationic compounds due to electrostatic interactions with the polymeric matrix at high pH. A triggered release of these substances would be induced by decreasing the electrostatic interactions and deswelling the network upon adjusting the pH below the apparent pK_a value of the gel—i.e., transferring the gels from pH 7.4 to pH 5.0. (ii) In addition, the pH-dependent volume transition and the associated reduction of effective mesh sizes could be applied to entrap functional compounds of large hydrodynamic diameters upon lowering the pH to a medium value (i.e., transfer from pH 8.5 to phosphate buffer solution with pH 7.4) at which small cationic molecules are still embedded. The described double-stimuli responsive character would enable the combination of the pH-dependent release of electrostatically loaded small substances at pH 5 with an orthogonal light-induced fast on-demand release of large sterically entrapped compounds upon irradiation at the same pH. (iii) The pH-induced volume transition could be applied to entrap active compounds of large hydrodynamic diameters by deswelling the gels (e.g., transfer from $pH > 7$ to $pH < 6$). By subsequent increasing the pH, a first pH-dependent swelling controlled release profile could then be combined with either a subsequent or substitutional degradation induced release. This concept was successfully investigated for non-photo-sensitive p(HEMA-co-MAA) microgels (see Sect. p(HEMA-co-MAA) Microgels: Loading and Release of Myoglobin). Especially due to the good cellular uptake and the negligible cytotoxicity of these model compounds (see Sect. p(HEMA-co-MAA) Microgels: Fluorescent Labeling and Cell Tests), the light-sensitive analogues represent highly interesting potential carriers for delivery applications. Even though this concept has yet to be studied, the results described in this chapter renders those materials highly promising.

5.2 Photo-Sensitive Hydrogel Nanoparticles Based on Light-Cleavable *Polymeric* Crosslinkers

The work described in this chapter deals with the development of a new class of enzyme- and light-sensitive microgels based on (meth-)acrylate functionalized dextrans as photo- and enzymatically degradable macromolecular crosslinkers. An important feature of these modified polysaccharides is their highly hydrophilic nature that enables their utilization for microgel preparation in inverse mini-emulsion processes. In comparison to the previously described light-cleavable low molecular weight crosslinkers which require the addition of an organic solvent for the formation of the dispersed phase, the water solubility of the dextran based crosslinkers is designed to enable the dispersed phase to be formed by dissolving the crosslinker and additional comonomer(s) in water as solvent immiscible with the continuous phase. This water solubility of the dextran based crosslinkers is assumed to give rise to a potential in situ embedding of functional water soluble compounds (e.g., proteins) already during microgel formation by free radical (co)polymerization in the aqueous droplets [43]. In comparison, the p(HEMA-co-MAA) based materials described in the previous chapter require the addition of an organic solvent for the formation of the dispersed phase, thus restricting loading of (solely water soluble) functional compounds to *post-formation* methods. Hence, the development of dextran containing photo-sensitive microgels expands the versatility of preparation routes to light-degradable hydrogel nanoparticles for release applications dramatically.

Regarding the described macromolecular crosslinkers, a sensitivity to light can be achieved by introducing a photo-labile linker between the dextran chain and the polymerizable vinyl moieties. Upon irradiation, cleavage of the connecting points between the dextran backbone and the network-forming polymer leads to freely soluble dextrans and the respective polymer chains. As the dextran backbone can be cleaved by dextranase, the resulting microgels are designed to be also enzymatically degradable, thus representing double stimuli-responsive materials. The proposed concept is schematically illustrated in Fig. 5.44.

In order to realize the described approach, free radical copolymerizations of methacrylated dextrans with acrylamide in inverse miniemulsion are investigated to demonstrate the adaptability of the functionalized polysaccharides as crosslinkers for the preparation of enzymatically degradable microgels. Subsequently, this newly developed concept is expanded to the formation of enzymatically- and light-degradable microgels as double stimuli-responsive materials.

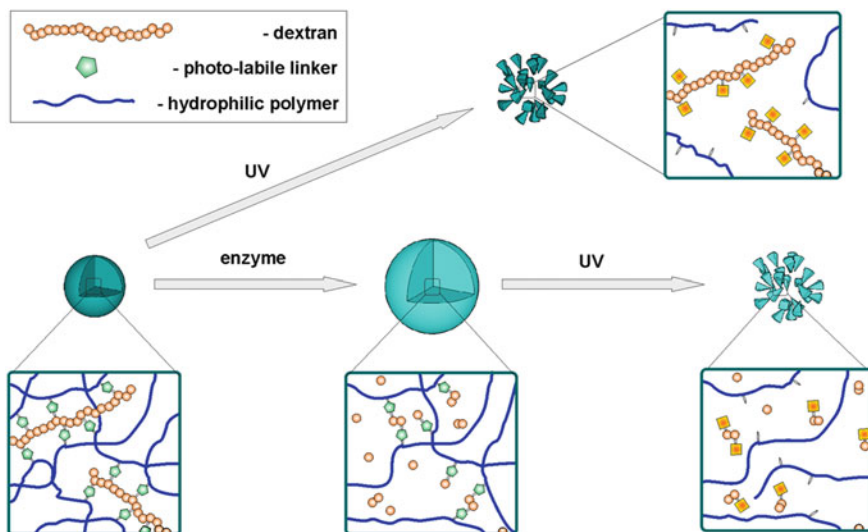


Fig. 5.44 Schematic illustration of the concept of enzymatically- and light-degradable microgels based on functionalized dextrans as macromolecular crosslinkers. Adapted from [44] by permission of the Royal Society of Chemistry

5.2.1 Enzymatically Degradable Nanogels Based on Dextran-Methacrylates as Macromolecular Crosslinkers

A highly interesting approach to degradable (micro-) gels is based on the utilization of dextrans as naturally occurring polysaccharides, that can be cleaved upon incubation with dextranase [68]. Covalent functionalization of dextran chains with either polymerizable vinyl groups [69] or thermal initiators [70] enables the formation of hydrogels by free radical (co)polymerization in aqueous solutions. The resulting networks can then be degraded by the addition of dextranase, inducing the release of embedded active compounds [71]. Microgels based on dextran methacrylates have been investigated for the release of immunoglobulin G as a model protein [42].

Investigated routes to enzymatically degradable microgels containing functionalized dextrans are so far based on precipitation polymerizations from aqueous solutions. This preparation method is generally a widely used approach to microgel formation but is limited by some serious drawbacks. On one hand the

Parts of this work are published as: “Enzymatically Degradable Nanogels by Inverse Miniemulsion Copolymerization of Acrylamide with Dextran-Methacrylates as Crosslinkers” Daniel Klinger, Eugen M. Aschenbrenner, Clemens K. Weiss and Katharina Landfester, *Polym. Chem.* **2012**, 3, 204. Reproduced from [75] by permission of the Royal Society of Chemistry.

microgels reported in the literature are in the size ranges of 4–10 μm [42, 72] and thus comparably large in diameter. On the other hand, introduction of a second comonomer is limited by its hydrophilicity [41]. To ensure successful particle precipitation upon polymerization, very hydrophilic comonomers can only be incorporated to a certain extent thus restricting the versatility of this approach and these materials. Compared to the described method of precipitation polymerization, the inverse miniemulsion technique is advantageous. Since the only main requirement for copolymerization of different hydrophilic monomers is their immiscibility with the continuous phase, this approach is very tolerant to a broad variety of materials [73]. A second advantageous point is the good control over the size of the particles obtained by inverse miniemulsion polymerizations. Particle sizes are generally in the sub-micron range and can be adjusted by the choice and concentration of surfactant from roughly 100 to ~ 500 nm [74].

In this chapter, the preparation of enzymatically degradable poly(acrylamide-*co*-dextran methacrylate) nanogels by free radical copolymerization from aqueous solutions of acrylamide (AAm) and dextran methacrylate (Dex-MA) in inverse miniemulsion is presented. Acrylamide as a highly water soluble monomer was chosen as a model compound to demonstrate the versatility of the inverse miniemulsion polymerization process towards the choice of monomers. In addition, the multiple methacrylation of dextran leads to water soluble dextran methacrylates which are used as enzymatically degradable macromolecular crosslinking molecules. Even though this sensitivity depends on a change in the chemical composition of the respective surrounding media, it gives rise to a potential release of compounds in aqueous media of a broad range of pH values, therefore representing an alternative approach to predominantly used acid-labile crosslinkers.

Important properties of the resulting nanogels such as the initial degree of swelling and the sol content are assumed to be adjustable by varying the amount of methacrylate units available for crosslinking. Systematic investigations on this parameter are part of this study and are expected to give insight in the crosslinking performance of the Dex-MA molecules. In this context, another important focus of the work presented is to optimize the synthetic parameters (i.e., the Dex-MA/AAm feed ratio) in order to yield nanogels which combine a high crosslinking density (i.e., small mesh sizes) and -efficiency for ambient polymerization temperatures with a good enzymatic degradability. Nanogels fulfilling these criteria are assumed to be highly interesting materials for potential release applications.

Synthesis of dextran-methacrylates (Dex-MA). (*Reactions were performed by Eugen Aschenbrenner*) Dextran was functionalized using a modification of the protocol presented by Kim et al. [76]. In brief, the polysaccharide was functionalized with methacrylate groups by coupling of hydroxyl moieties at the polymer backbone with methacrylic anhydride. The *DS* was evaluated from $^1\text{H-NMR}$ spectra by calculating the ratio of the peak areas of the olefinic peak at 6.2 ppm relative to the anomeric proton of dextran assigned to the peak at 4.9 ppm by using the formula:

$$DS(\text{Dex} - \text{MA}) = \frac{A[\text{olefinic} - H @ 6.2 \text{ ppm}]}{A[\text{anomeric} - H @ 4.9 \text{ ppm}]}$$

The calculated values are listed in Table 5.7.

Synthesis and characterization of p(AAm-co-Dex-MA) nanogels. As mentioned above, important properties of the hydrogels, such as the initial swelling ratio and the crosslinking efficiency are assumed to strongly depend on the amount of crosslinking points, i.e., methacrylate groups in the network and their distribution therein. Those parameters were adjusted by the variation of: (i) the ratio of Dex-MA/AAm for a fixed *DS* of Dex-MA; (ii) the *DS* of Dex-MA for a fixed ratio of Dex-MA/AAm and (iii) the molecular weight of the Dex-MA for analogous *DS*. Moreover, a fixed value of methacrylic groups in the network was achieved by a combined variation of the Dex-MA/AAm ratio and the *DS* of the respective Dex-MA. Table 5.7 shows the respective compositions of the synthesized enzymatically degradable microgels (E-MG).

The continuous phase consisted of a 1 % (w/v) solution of the nonionic surfactant Lubrizol U in cyclohexane. Dispersed phases contained mixtures of Dex-MA and acrylamide dissolved in aqueous 0.5 M NaCl solution with 50 % (w/v) monomer. Polymerizations were either initiated from the continuous phase by using V-59 at 70 °C or V-70 at 37 °C or from the dispersed phase by using KPS/TEMED at room temperature or VA-044 at 45 °C. After polymerization (16 h) the resulting particles were repeatedly washed with cyclohexane to remove excess surfactant. The resulting dispersions in cyclohexane represent the nanogel particles in their collapsed (non-swollen) state. SEM was used to investigate the particles morphologies. Figure 5.45 shows representative micrographs of nanogels E-MG-1A, E-MG-2A and E-MG-3A.

In a first attempt, Dex-MAs based on dextran of $M_n = 40,000$ g/mol with different *DS* were used to form nanogels E-MG-1A to E-MG-3D. In comparison, gel particles E-MG-4A–E-MG-6A were synthesized using functionalized dextrans of 6,000 g/mol with *DS* and Dex-MA/AAm weight ratios analogous to E-MG-1A, E-MG-2A and E-MG-3A. The non-swollen gel particles were investigated regarding their hydrodynamic diameters by DLS. Figure 5.46 shows the obtained values in dependency on the amount of methacrylic groups.

As shown in Fig. 5.46a, for fixed Dex-MA/AAm ratios, the variation of the total amount of MA-units available for crosslinking is realized by using dextran methacrylates with different degrees of substitution. It becomes obvious that gel particles of analogous Dex-MA weight contents exhibit similar hydrodynamic diameters, independent of either the degree of substitution or the Dex-MA molecular weight (Fig. 5.46b).

Furthermore, upon increasing the Dex-MA/AAm ratio, an increased particle size results. Sizes of nanogels containing 5 wt.-% Dex-MA are in the range of 130 nm (Fig. 5.46a, b), particles containing 17.5 wt.-% Dex-MA (Fig. 5.46a) exhibit hydrodynamic diameters of 145 nm and in the case of 30 wt.-% Dex-MA (Fig. 5.46a) d_h values of 165 nm were detected. This effect was assigned to the increased viscosities (visual inspection) of the dispersed phases for increased

Table 5.7 Synthetic details for the preparation of p(AAm-co-Dex-MA) nanogels by free radical inverse miniemulsion copolymerization

Sample	Dex-MA type	M_w (Dex) (g/mol)	DS (Dex) ^a	Dex-MA content (wt.-%) ^b	MA-units (mol.-%) ^c	Initiator type	T_{polym} (°C)
E-MG-1A	Dex-MA1	40,000	0.12	5.0	0.24	V-59	70
E-MG-1B	Dex-MA1	40,000	0.12	17.5	0.90	V-59	70
E-MG-1C	Dex-MA1	40,000	0.12	30.0	1.69	V-59	70
E-MG-2A	Dex-MA2	40,000	0.17	5.0	0.33	V-59	70
E-MG-2B	Dex-MA2	40,000	0.17	17.5	1.25	V-59	70
E-MG-2C	Dex-MA2	40,000	0.17	22.0	1.62	V-59	70
E-MG-2D	Dex-MA2	40,000	0.17	30.0	2.34	V-59	70
E-MG-3A	Dex-MA3	40,000	0.33	5.0	0.59	V-59	70
E-MG-3B	Dex-MA3	40,000	0.33	13.0	1.63	V-59	70
E-MG-3C	Dex-MA3	40,000	0.33	17.5	2.27	V-59	70
E-MG-3D	Dex-MA3	40,000	0.33	30.0	4.28	V-59	70
E-MG-4A	Dex-MA4	6,000	0.09	5.0	0.18	V-59	70
E-MG-5A	Dex-MA5	6,000	0.19	5.0	0.36	V-59	70
E-MG-6A	Dex-MA6	6,000	0.29	5.0	0.48	V-59	70
E-MG-1Ab	Dex-MA1	40,000	0.12	30.0	1.69	V-70	37
E-MG-2Ab	Dex-MA2	40,000	0.17	30.0	2.34	V-70	37
E-MG-3Ab	Dex-MA3	40,000	0.33	30.0	4.28	V-70	37
E-MG-7Ab	Dex-MA7	40,000	0.05	30.0	0.72	V-70	37
E-MG-1Db	Dex-MA1	40,000	0.12	100.0	12.0	V-70	37
E-MG-8Aa	Dex	40,000	–	30.0	–	V-59	70
E-MG-8Ab	Dex	40,000	–	30.0	–	V-70	37
E-MG-8Ac	Dex	40,000	–	30.0	–	KPS/TEMED	30
E-MG-8Ad	Dex	40,000	–	30.0	–	VA-044	45

^a Calculated as DS = amount of functionalized glucopyranosyl groups/total amount of glucopyranosyl groups^b w.r.t. to mass of Dex-MA + AAm^c w.r.t. to monomer units of AAm + glucopyranosyl groups

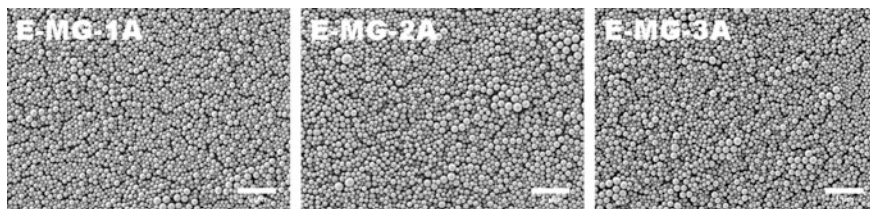


Fig. 5.45 SEM images of nanogels E-MG-1A, E-MG-2A and E-MG-3A dropcast from cyclohexane dispersions. Reproduced from [75] by permission of the Royal Society of Chemistry

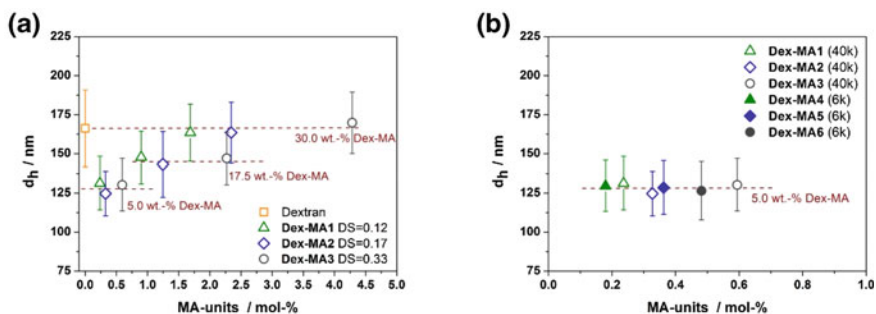


Fig. 5.46 Hydrodynamic diameters in cyclohexane of p(AAm-co-Dex-MA) nanogels containing various amounts of functionalized dextrans of different DS : **a** $M_n(\text{Dex-MA}) = 40,000$ g/mol; **b** $M_n(\text{Dex-MA}) = 6,000$ g/mol in comparison to $M_n(\text{Dex-MA}) = 40,000$ g/mol with similar DS . Reproduced from [75] by permission of the Royal Society of Chemistry

Dex-MA contents prior to polymerization. Miniemulsification is achieved by applying high shear forces by ultrasonication, where a fission and fusion process results in the formation of stable droplets of a narrow size distribution. This process is influenced by the viscosity of the dispersed phase yielding bigger droplets for dispersed phases of higher viscosities.

All nanogels described above were synthesized by initiation with V-59 from the continuous phase at 70 °C. Regarding the possibility of embedding active compounds such as e.g., proteins in the gel networks during polymerization, mild conditions for the gel formation have to be applied in order to ensure the integrity of the compound to be delivered. Therefore, experiments to investigate different initiation and polymerization conditions were conducted. In a first attempt, non-crosslinked reference particles for the degradation studies were synthesized by inverse miniemulsion polymerization of acrylamide in the presence of non-functionalized dextrans of $M_n = 40,000$ g/mol. E-MG-8Aa was polymerized by initiation with V-59 at 70 °C from the continuous phase analogously to particles E-MG-1A–E-MG-3D. The resulting particles exhibited a similar hydrodynamic diameter of 165 nm in cyclohexane. Particle formation reactions with unfunctionalized dextran at lower temperatures were carried out by using oil soluble V-70

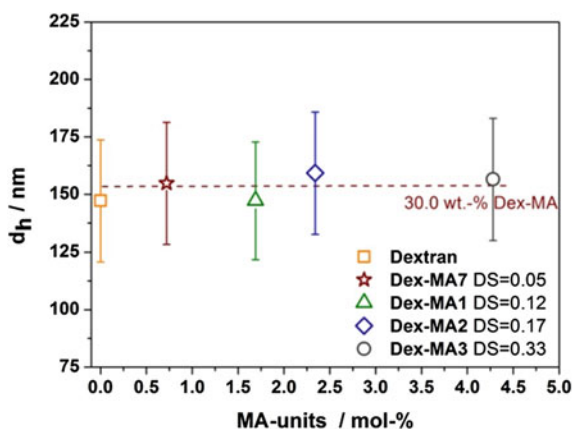
for initiation from the continuous phase at 37 °C (E-MG-8Ab), water soluble VA-044 for initiation from the dispersed phase at 45 °C (E-MG-8Ad) and water soluble KPS for initiation from the dispersed phase upon adding tetramethylethylenediamine (TEMED) to the continuous phase at room temperature (E-MG-8Ac). In case of initiation by KPS/TEMED no stable dispersions were obtained whereas utilization of either V-70 or VA-044 resulted without exception in stable dispersions of dextran-containing PAAm particles in cyclohexane. Resulting hydrodynamic diameters were in the same range (165 nm) as those of particles with 30 wt.-% of functionalized dextrans (see Fig. 5.47 for initiation with V-70, data for initiation with VA-044 not shown).

Since initiation with V-70 required the lowest polymerization temperatures, the respective conditions were used to synthesize E-MG-1Ab–E-MG-7Ab p(AAm-co-Dex-MA) microgels with weight contents of 30 wt.-% Dex-MA of different *DS* analogously to E-MG-1A–E-MG-3D particles. As shown in Fig. 5.47, resulting particles in cyclohexane exhibited hydrodynamic diameters of ~165 nm similar to the nanogels obtained from polymerizations at 70 °C.

Investigations on further increasing the amount of Dex-MA in the nanogels revealed that at very high Dex-MA contents (60 wt.-%), increasing polydispersity and ill-defined morphologies resulted (data not shown). In this case, a dramatically increased viscosity (visual inspection) hinders homogenization of the pre-emulsion by ultrasonication. In addition, the high amount of the functionalized dextran is assumed to influence the stability of the droplets due to the interfacially active character of the amphiphilic Dex-MA. Since attempts to form nanogels from pure Dex-MA1 (E-MG-1Db) did not yield stable miniemulsions, the presence of a second comonomer seems to be a crucial requirement for the formation of enzymatically degradable gel particles by inverse miniemulsion polymerization.

Summarizing the preparation of p(AAm-co-Dex-MA) nanogels, it can be concluded that the free radical copolymerization in inverse miniemulsion allows the formation of stable dispersions consisting of well defined spherical particles. The applied synthetic approach is highly versatile with respect to the

Fig. 5.47 Hydrodynamic diameters in cyclohexane of p(AAm-co-Dex-MA) nanogels containing various amounts of functionalized dextrans ($M_n = 40,000$ g/mol) of different *DS*. Polymerizations were carried out at 37 °C using V-70 as initiator. Reproduced from [75] by permission of the Royal Society of Chemistry



polymerization conditions (i.e., initiating mechanism and temperature). Moreover, increasing the Dex-MA/AAm feed ratio was found to result in stable dispersions for Dex-MA contents up to 30 wt.-%. Resulting particle sizes were found to depend on the amount of Dex-MA in the dispersed phase prior to polymerization and were in the nanometer size range. The obtained nanogels were then further investigated with regard to their respective gel properties by transferring them to aqueous media.

Investigations on the relative crosslinking efficiency and the swelling behavior of p(AAm-co-Dex-MA) nanogels in water. Subsequent to particle purification by washing with cyclohexane, all dispersions were freeze dried yielding the nanogels as white powders. In order to investigate the gel properties of the prepared p(AAm-co-Dex-MA) hybrid particles, dispersions in aqueous medium were obtained by simply dispersing and swelling the freeze dried samples in water. Purification was achieved by repeated centrifugation and redispersion in water. The resulting dispersions of the swollen nanogels were stable without any additional surfactant. This effect is assumed to occur due to sterical stabilization by hydrated dangling chains of the swollen outer particle layer. Determination of the hydrodynamic diameters by DLS allowed calculating the degrees of swelling (*DGS*), or the swelling ratios, which were calculated as $DGS = V_{swollen}/V_{non-swollen}$. The washed nanogel dispersions were assumed to consist solely of p(AAm-co-Dex-MA) networks, i.e., the gel content of the crosslinking copolymerization. The combined supernatants of the washing steps represent the sol content consisting of unreacted monomers, non-crosslinked polymer chains and non-incorporated oligomers. Freeze drying of both fractions was followed by gravimetric analysis and afforded the sol/gel content for every sample.

While the determination of the sol/gel content in combination with the measured degree of swelling did not permit a quantitative evaluation of the crosslinking density or an absolute conclusion regarding the inner morphology, it allowed the expedient comparison of important properties, such as the initial swelling ratio and the relative crosslinking efficiency. As mentioned above, those parameters strongly depend on the amount and distribution of crosslinking points—i.e., methacrylate groups—in the network and can be adjusted by the variation of: (i) the ratio of Dex-MA/AAm for a fixed *DS* of Dex-MA; (ii) the *DS* of Dex-MA for a fixed ratio of Dex-MA/AAm and (iii) the molecular weight of the Dex-MA for analogous *DS*. Moreover, a fixed value of methacrylic groups in the network can be achieved by a combined variation of the Dex-MA/AAm ration and the *DS* of the respective Dex-MA.

Figure 5.48 shows the resulting *DGS*s and sol contents for nanogels polymerized at 70 °C with various amounts of Dex-MA1 (Fig. 5.48a), Dex-MA2 (Fig. 5.48b) and Dex-MA3 (Fig. 5.48c), thus representing three different classes of nanogels. Each class is characterized by a particular degree of substitution of the used Dex-MA. The amount of methacrylate groups was varied in every class by changing the ratio of Dex-MA/AAm. It becomes obvious that both *DGS* and sol content decrease with an increasing amount of Dex-MA i.e., a higher number of methacrylate groups, thus indicating enhanced crosslinking efficiency.

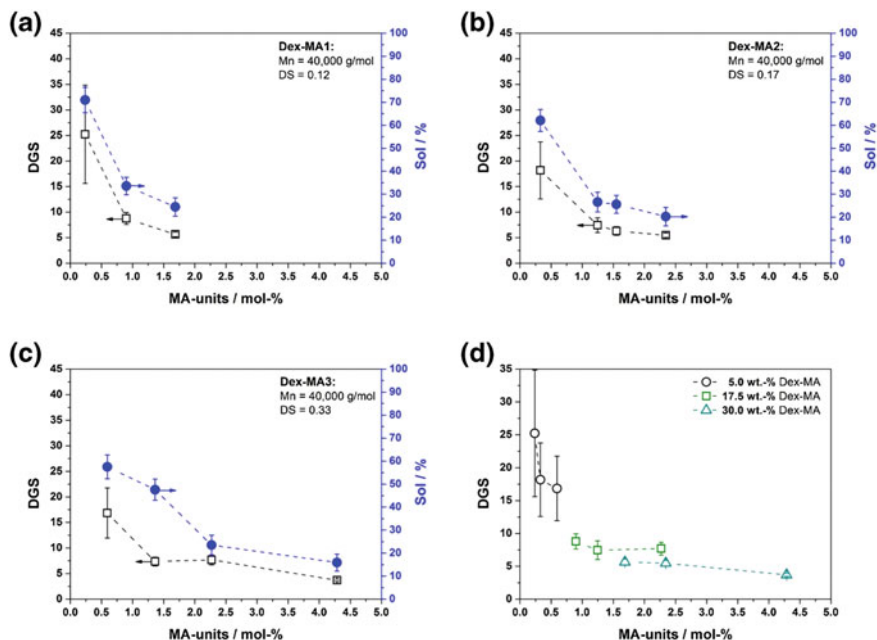
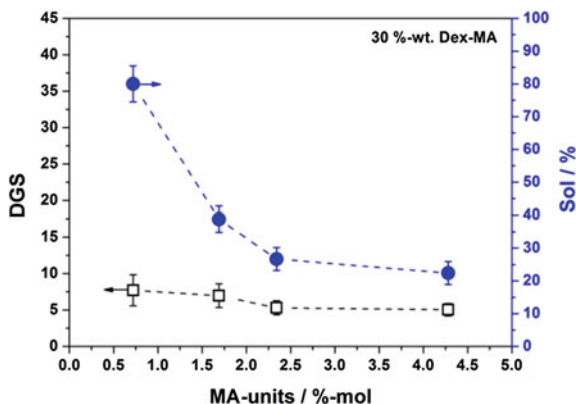


Fig. 5.48 *DGS* and sol contents of p(AAm-co-Dex-MA) nanogels (prepared at 70 °C) in dependency on the amount of polymerizable MA units: **a** Nanogels polymerized with various amounts of Dex-MA1; **b** nanogels polymerized with various amounts Dex-MA2; **c** nanogels polymerized with various amounts Dex-MA3; **d** comparison of *DGS* of nanogels polymerized with various amounts of Dex-MA1, Dex-MA2 and Dex-MA3. Reproduced from [75] by permission of the Royal Society of Chemistry

As shown in Fig. 5.48d, the same effect can be observed by comparing the *DGS*s of nanogels polymerized with the same Dex-MA/AAm ratio but containing Dex-MA crosslinkers with different degrees of substitution. Here as well, higher amounts of methacrylate units (realized by increased *DS*) result in lower initial degrees of swelling and consequently increased crosslinking efficiencies. Independent on the degree of substitution, all nanogels polymerized with 30 wt.-% of various types of Dex-MA exhibit *DGS* in the same order of magnitude. It is concluded that the swelling behavior not only depends on the amount of polymerizable methacrylate units but also on the Dex-MA/AAm ratio. This suggests that also the amount of dextran chains in the network strongly influences the swelling behavior due to different interaction parameters of the hydrophobically functionalized dextran and poly acrylamide with water. The composition of the hybrid nanogels therefore represents an additional crucial parameter.

Figure 5.49 shows the values for the *DGS* and sol contents for p(AAm-co-Dex-MA) nanogels containing 30 wt.-% Dex-MA of various *DS* (Dex-MA1, Dex-MA2, Dex-MA3 and Dex-MA4) polymerized at 37 °C initiated with V-70 from the oil phase.

Fig. 5.49 Characterization of the gel properties of p(AAm-co-Dex-MA) nanogels polymerized at 37 °C with 30 wt.-% of Dex-MAs with various degrees of substitution: *DGS* and sol contents in dependency on the amount of polymerizable MA units. Reproduced from [75] by permission of the Royal Society of Chemistry



Analogously to nanogels polymerized at 70 °C, 1.69 mol-% of MA-units correspond to the number of the MA moieties introduced with 30 wt.-% of Dex-MA1. Similarly, 2.34 mol-% correspond to Dex-MA2 and 4.28 mol-% to Dex-MA3. In comparison to E-MG-1C, E-MG-2D and E-MG-3D, all samples exhibit similar initial swelling ratios and only slightly increased sol contents. Therefore, an equally effective crosslinking polymerization (network formation) is assumed. Regarding a potential embedding of active substances into the gels, this versatility of polymerization conditions represents a big advantage. Whereas in the case of E-MG-7Ab microgels (0.72 mol-% of MA-units by utilization of 30 wt.-% of Dex-MA7) a dramatic increase in the sol content can be observed, the initial degree of swelling does not vary significantly from the values for the microgels containing similar amounts of dextran methacrylates of higher degrees of substitution. As mentioned above, the *DGS* of the particles is assumed to not only be affected by the crosslinking density but also to depend on the Dex-MA/AAm ratio. It is assumed, that the swelling behavior of E-MG-7Ab microgels is dominated by the high amount of dextran methacrylate rather than the comparatively low crosslinking efficiency.

In general, the total amount of crosslinking points in a p(AAm-co-Dex-MA) gel can be varied by either changing the Dex-MA/AAm ratio for a Dex-MA of a fixed *DS* or by changing the *DS* of the dextran methacrylate for a fixed Dex-MA/AAm ratio. Another highly important factor which governs the properties of the hybrid microgels is the distribution of crosslinking points in the network. In order to investigate this parameter, microgels containing equal amounts of 1.5 mol-% methacrylate units but varying in the Dex-MA/AAm ratio were prepared using dextran methacrylates of different degrees of substitution. Similar contents of MA-units were realized by increasing the Dex-MA/AAm ratio with decreasing *DS* of the Dex-MA used. The resulting microgels were investigated with respect to their initial degree of swelling and their sol content. Figure 5.50a shows the obtained values of *DGS* in dependency on the Dex-MA/AAm ratio. Figure 5.50b depicts the dependency the sol contents on the degree of substitution of the Dex-MA used.

As can be seen, increasing the amount of Dex-MA simultaneously to decreasing the degree of substitution leads to reduced initial degrees of swelling

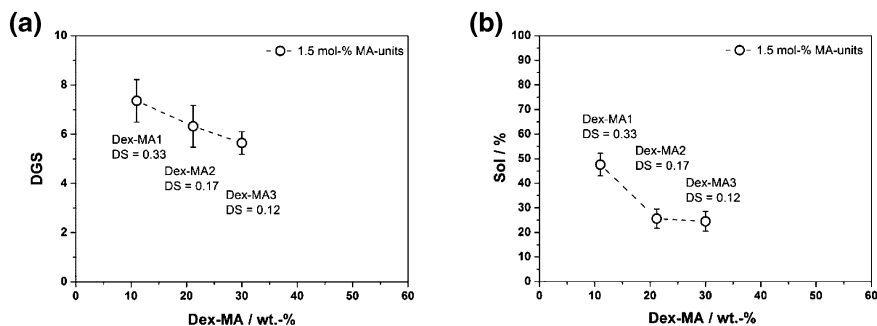


Fig. 5.50 Investigations on the gel properties of p(AAm-co-Dex-MA) nanogels synthesized with a fixed amount of 1.5 mol-% of methacryl units by changing the Dex-MA/AAm ratio and the *DS* of the Dex-MA: **a** *DGS* in dependency on the amount of different Dex-MAs; **b** sol contents in dependency on the amount of different Dex-MAs. Reproduced from [75] by permission of the Royal Society of Chemistry

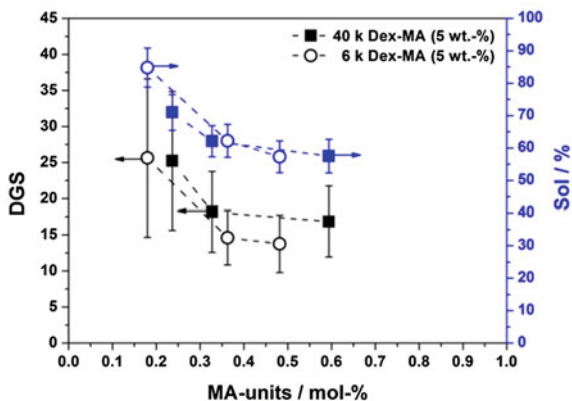
and lower sol contents. A reduced sol content can be assigned to a better crosslinking efficiency which is assumed to be caused by a better distribution of the crosslinking points in the gel network. The *DGS* exhibit a similar behavior (i.e., microgels polymerized with a higher amount of Dex-MA of a lower degree of substitution swell less). However, in this case the distribution of crosslinking points is not the single factor influencing the swellability of the hybrid gels. As mentioned above, the Dex-MA/AAm ratio also affects the swelling properties of the hybrid material due to different interactions of the modified dextran and polyacrylamide chains with water.

In order to further investigate the influence of the distribution of crosslinking points in the gel network, nanogel particles polymerized with dextran methacrylates based on dextran (molecular weight 6,000 g/mol, 6 k) were compared to the samples containing Dex-MA (40 k). In this experiment 6 k Dex-MA crosslinkers were synthesized to exhibit similar degrees of substitution as the 40 k analogues. Figure 5.51 shows the *DGS* and sol contents of the resulting microgels polymerized with each 5 wt.-% of different Dex-MAs of either 6 k or 40 k.

As can be seen, both the initial degrees of swelling and the sol contents are reduced to some extent for the nanogels containing the respective low molecular weight Dex-MA crosslinkers, therefore indicating a slightly better distribution of crosslinks in the gel network.

In summary, free radical copolymerization of acrylamide with dextran methacrylates as biodegradable crosslinkers in inverse miniemulsion was found to be highly versatile with regard to the polymerization conditions (initiation mechanism and -temperature) and the Dex-MA/AAm feed ratio. Increasing the amount of polymerizable methacrylate units available for crosslinking were carried out by either increasing the Dex-MA/AAm feed ratio for a fixed *DS* of Dex-MA or by increasing the *DS* of Dex-MA for a fixed Dex-MA/AAm feed ratio. As expected, a

Fig. 5.51 Investigations on the gel properties of p(AAm-co-Dex-MA) nanogels synthesized with 5 wt.-% of Dex-MAs of different DS: Comparison of *DGS* and sol contents for 40 k Dex-MAs with 6 k Dex-MAs of similar degrees of substitution. Reproduced from [75] by permission of the Royal Society of Chemistry



higher amount of MA-units correlates with a higher crosslinking efficiency as determined by low initial degrees of swelling and low sol contents.

Enzymatic degradation experiments. In order to investigate the behavior of the p(AAm-co-Dex-MA) nanogels in the presence of dextranase, aqueous particle dispersions were incubated with the enzyme at 37 °C for 24 h. The dispersions contained 0.0625 wt.-% of purified gels after removal of the sol fraction. Particle degradation was monitored by turbidity measurements in transmission. Keeping in mind potential applications of the microgels for release applications, a low initial degree of swelling represents a crucial parameter to prevent leakage of embedded compounds. Therefore, particles with high crosslinking efficiency and low sol content are of special interest. As discussed above, for particles containing 30 wt.-% of Dex-MA this criterion is fulfilled for all dextrans with different degrees of substitution. The relative turbidity curves shown in Fig. 5.52a thus enable the

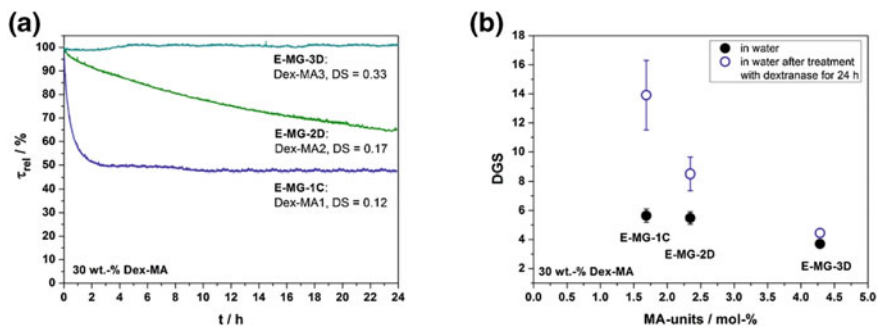


Fig. 5.52 Enzymatic degradation of p(AAm-co-Dex-MA) nanogels with various amounts of methacrylate units for a fixed Dex-MA content of 30 wt.-%: **a** time dependent turbidity measurements; **b** comparison of the degrees of swelling before and after the 24 h treatment with dextranase. Reproduced from [75] by permission of the Royal Society of Chemistry

investigation of the degradability in dependency on the total amount of crosslinking points and the DS of the used Dex-MAs for a fixed Dex-MA/AAm ratio.

The investigated nanogels E-MG-1C, E-MG-2D and E-MG-3D contained increasing numbers of crosslinking points due to an increasing DS of the Dex-MA used. Whereas the turbidity of E-MG-3D nanogels containing 4.48 mol-% of MA-units (30 wt.-% Dex-MA3; $DS = 0.33$) was not influenced by the addition of dextranase, nanogels E-MG-1C with 1.72 mol-% (30 wt.-% Dex-MA1; $DS = 0.12$) and E-MG-2D with 2.53 mol-% (30 wt.-% Dex-MA2; $DS = 0.17$) of crosslinking points showed a pronounced decrease in turbidity upon 24 h incubation down to 47 and 65 % respectively. This effect is based on the cleavage of dextran chains between the crosslinking points, covalently linking Dex-MA molecules to pAAm chains. As a result the gel structure is disintegrated and mesh sizes are increased, yielding particles with increased swelling ratios. The corresponding loosened network is characterized by a decreased difference of the refractive indices of polymer and solvent which is known to reduce the intensity of scattered light and therefore the relative turbidity [18, 19]. Measurements of particle sizes after enzymatic degradation yielded the DGS which are shown in Fig. 5.52b in comparison to the non-degraded particles. As can be seen, a decrease in turbidity is accompanied by an increased degree of swelling of the gel particles thus confirming successful cleavage of crosslinkers. The performed measurements clearly exhibit a dependency of the degradation profile on the amount of methacrylate units and the degree of substitution of the used Dex-MA crosslinkers. While it becomes obvious that a higher amount of crosslinking points results in a less pronounced degradation (Fig. 5.52), it could not be determined whether this effect is based on a smaller mesh size of the network in general (the total amount of crosslinking points) or the distribution of the methacrylate units along the dextran chains (the degree of substitution of the respective Dex-MA). The first parameter is assumed to influence the degradation by a decreased accessibility of dextran chains in the network due to hindered diffusion of the enzyme molecules into the network. A higher DS of Dex-MA as the second parameter could interfere with a successful dextran chain cleavage by sterical hindrance due to the connected PAAm chains.

To test these assumptions, microgels with similar contents of methacrylate units but various amounts of dextran methacrylates of different degrees of substitution were investigated with respect to their degradation behavior. Figure 5.53a shows the resulting turbidity curves and Fig. 5.53b the respective DGS obtained from particle sizes determined by DLS.

Turbidity measurements clearly demonstrate a decrease in the optical density for all samples which is assigned to network degradation upon cleavage of dextran chains. The DGS after enzymatic treatment indicate a pronounced increase of the swelling ratio for all degrees of substitution of Dex-MA.

Comparing the differences in the DGS after enzymatic treatment of E-MG-3B and E-MG-2C to the data obtained for microgels E-MG-3D and E-MG-2D (Fig. 5.52b) containing more Dex-MA with the same DS , it is observed that

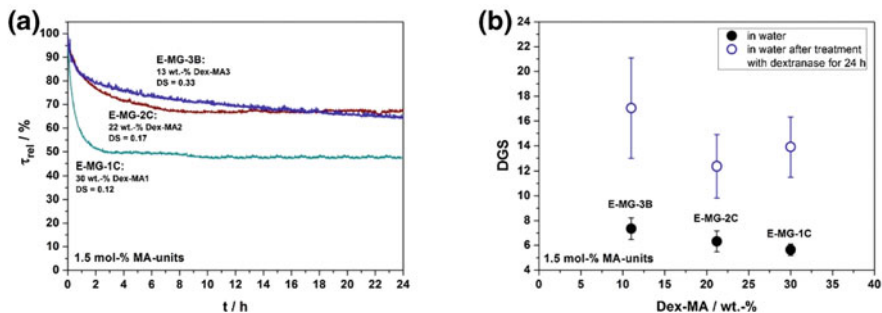


Fig. 5.53 Enzymatic degradation of p(AAm-co-Dex-MA) nanogels with various amounts of methacrylate units for a fixed Dex-MA content of 30 wt.-%: **a** time dependent turbidity measurements; **b** comparison of the degrees of swelling before and after the 24 h treatment with dextranase. Reproduced from [75] by permission of the Royal Society of Chemistry

decreasing the amount of methacrylate units (i.e., the amount of the respective Dex-MA) results in an enhanced degradability. While for E-MG-3D containing 30 wt.-% of Dex-MA3 only a negligible increase in DGS after treatment with dextranase was observed, the DGS for E-MG-3B containing 12 wt.-% of Dex-MA3 changed from the initial value of $DGS = 7.4$ to $DGS = 17$. A similar behavior was observed for microgels prepared with Dex-MA2. The measured increase of $DGS = 6.3$ before to $DGS = 12.3$ after enzymatic cleavage for E-MG-2C (containing 22 wt.-% of Dex-MA2) is much higher than the difference of $DGS = 5.5$ to $DGS = 8.5$ obtained for E-MG-2D (containing 30 wt.-% of Dex-MA2). Therefore, it is assumed that one crucial parameter for successful microgel degradation is the total amount of crosslinking points (MA-units) in the gel. This observation can be interpreted by a reduced accessibility of the dextran chains for dextranase with increasing amounts of crosslinking points. By investigating the enzymatic degradation of crosslinked dextran methacrylates, Franssen et al. proposed that the degradability is reduced due to the presence of interpenetrating networks and the fact that the dextran chains are severely strained [69]. Moreover, the diffusion of the enzyme in a more crosslinked network (i.e., more Dex-MA) is decreased as a result of a screening effect. A high density of crosslinking points correlates with small mesh sizes and would give access to the enzymatic degradation of the outer particle sphere due to an enhanced accessibility of the surface. In contrast, the relatively large size of the enzyme (44 kDa) is assumed to hinder its diffusion into the particle core due to comparably small mesh sizes thus resulting in incomplete particle degradation.

Besides the described screening effect, the interaction of the functionalized dextrans with the active sites of the enzyme can play an important role as well. As it is known from the literature [68], dextranase is capable of hydrolyzing a glycosidic bond between a substituted and an unsubstituted glucopyranose unit of dextran methacrylate in solution. In contrast, bonds between two adjacent

functionalized residues cannot be cleaved. Regarding the synthesis of Dex-MA crosslinkers, the functionalization with methacrylate groups is assumed to result in a statistical distribution of the latter along the dextran backbone. Thus, the probability of obtaining chain segments with two substituted glucopyranose units next to each other increases with increasing *DS*. In the resulting hydrogel matrix those segments covalently connect PAAm chains forming the network. Since degradation of those structural elements is hindered, incomplete particle degradation occurs.

Another important observation is the dependency of the degradation rate of the microgels on the *DS* of the Dex-MAs (for a fixed amount of MA-units in the gel). As can be seen in Fig. 5.53a, the rate of particle disintegration (measured by turbidity) decreases for an increasing degree of substitution of dextran. This effect can be assigned to a changed interaction of the Dex-MA with the active sites of the enzyme. Investigations made in the group of Hennink proposed that dextran methacrylates with a low degree of substitution can easily be cleaved by dextranase yielding isomaltose and methacrylated isomaltotriose as the main degradation products [68, 69]. In this case, the long unsubstituted segments of the dextran chains between two functionalized glucopyranose units are assumed to exhibit enough conformational freedom to fold correctly in the binding site of dextranase. Thus degradation by even multiple scissions of these segments results in degradation profiles similar to native dextran. In contrast, increasing the *DS* results in shorter unsubstituted chain segments which are restricted in their conformational freedom due to adjacent methacrylated glucopyranose units. Even though these chain segments can still bind to the active sites of the enzyme, the affinity and corresponding degradation rate is decreased. As the *DS* of the synthesized crosslinkers increases from Dex-MA1 to Dex-MA3, the corresponding decreases of the degradation rates are also assumed to be a result of the reduced affinity of Dex-MA to the binding sites of dextranase. This effect is even enhanced in the p(AAm-co-Dex-MA) nanogels since polyacrylamide chains grafted from the dextran molecules cause an additional sterical hindrance with respect to the interaction with the active sites of the enzyme.

In another attempt, microgels E-MG-8Aa containing 30 wt.-% of unfunctionalized dextran were transferred to aqueous medium in order to investigate the dissolution behavior of non-crosslinked particles. Even though no crosslinking methacrylate functionalities were present in this sample, a turbidity of 13 % relative to the initial turbidity of E-MG-1C microgels was observed. The detected value did not change upon 24 h of incubation with dextranase (data not shown). Therefore it is assumed that, in addition to the above discussed limitations of the enzymatic degradation, complete particle dissolution is also restricted by physical crosslinks due to entanglement of PAAm chains in the gels (as seen in pure PAAm hydrogel nanoparticles—data not shown).

Summarizing the statements made above, the observed degradation profiles are assumed to be based on a combination of four different parameters: (i) an increasing amount of crosslinking methacrylate groups reduces the accessibility of

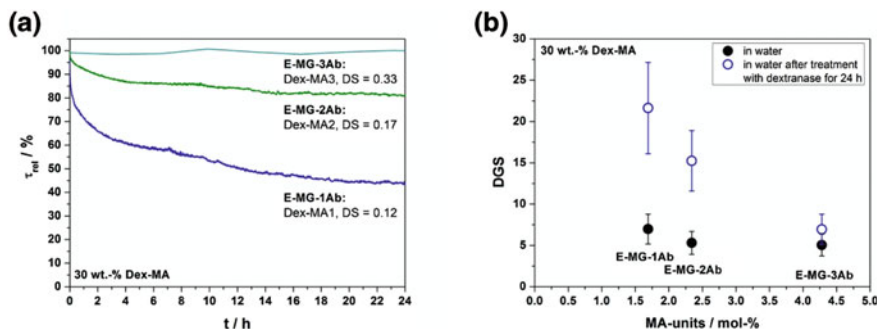


Fig. 5.54 Enzymatic degradation of p(AAm-*co*-Dex-MA) nanogels with various amounts of methacrylate units for a fixed Dex-MA content of 30 wt.-% polymerized at 37 °C: **a** time dependent turbidity measurements; **b** comparison of the degrees of swelling before and after the 24 h treatment with dextranase. Reproduced from [75] by permission of the Royal Society of Chemistry

dextran chains for the enzyme due to comparably small mesh sizes of the network; (ii) hindered cleavage of two neighboring substituted glucopyranose residues results in incomplete particle degradation and increases with the DS ; (iii) for increasing the DS the affinity of the Dex-MA to the binding site of the enzyme is reduced thus resulting in decreased degradation rates; (iv) PAAm chains grafted from the dextran backbone reduce the interaction of the polysaccharide with the enzyme due to sterical hindrance; (v) physical crosslinks due to entanglement of PAAm chains hinder complete particle dissolution, independent of the enzymatic degradability. Nevertheless, the observed increases in particle volumes after treatment with dextranase holds great potential for the release of functional compounds from the network, triggered by increasing mesh sizes.

In a last experiment the influence of the polymerization conditions on the degradability of the microgels was investigated. As discussed above, potential delivery applications require mild polymerization conditions in order to prevent embedded functional compounds from damage. Microgels E-MG-1Ab–E-MG-3Ab were polymerized at ambient temperatures of 37 °C to facilitate a potential embedding of sensitive functional compounds such as e.g., proteins. As their swelling behavior was found to be similar to the gels polymerized at 70 °C it is assumed that also the degradation profiles do not vary significantly from those of the respective microgels E-MG-1C, E-MG-2D and E-MG-3D. In Fig. 5.54 the time dependent turbidity measurements of the enzymatic treatment are shown as well as the DGS before and after 24 h of incubation with dextranase.

Compared to microgels of similar compositions polymerized at 70 °C, no significant deviations of the degradation profiles of the samples polymerized at 37 °C could be observed by turbidity measurements. In addition the DGS after

enzymatic treatment exhibit comparable increases in particle size upon dextran chain cleavage. Regarding potential release applications, MG-1Ab nanogels are the most promising candidates for a combination of reasons: (i) the low polymerization temperature gives rise to the potential embedding of sensitive compounds; (ii) the low initial degree of swelling and the low sol content point towards a high crosslinking efficiency and density, thus reducing leakage of potential embedded substances; (iii) enzymatic degradation proceeds comparably fast and is characterized by a substantial increase in *DGS*, hence enabling the release of a payload upon the treatment with dextranase. As a result, p(AAm-*co*-Dex-MA) gel particles represent a highly interesting class of nano-scaled hybrid materials, which are characterized by their partial biodegradability and simple and versatile processing routes.

Conclusion

In conclusion, free radical copolymerization of acrylamide with dextran methacrylates as biodegradable crosslinkers in inverse miniemulsion represents a facile approach to p(AAm-*co*-Dex-MA) gel particles in the nanometer size range. The investigated preparation method was found to be highly versatile with regard to the polymerization conditions (initiation mechanism and -temperature) and the Dex-MA/AAm feed ratio. Systematic investigations on increasing the amount of polymerizable methacrylate units available for crosslinking were carried out by either increasing the Dex-MA/AAm feed ratio for a fixed *DS* of Dex-MA or by increasing the *DS* of Dex-MA for a fixed Dex-MA/AAm feed ratio. As expected, a higher amount of MA-units correlates with a higher crosslinking efficiency as determined by low initial degrees of swelling and low sol contents. Enzymatic degradation profiles of the nanogels were examined by turbidity measurements and DLS. The investigations revealed a dependency of the degree and the rate of degradation on the crosslinking density (MA-units incorporated) of the gels and the *DS* of the used Dex-MAs.

The described adjustment of the gel properties by variation of the synthetic parameters revealed p(AAm-*co*-Dex-MA) nanogels as extremely interesting candidates for potential release systems in the nanometer size range. In this context, the combination of an ambient polymerization temperature with high crosslinking densities—as determined by low initial degrees of swelling and the low sol contents—gives rise to the potential embedding of sensitive compounds. Furthermore, enzymatic degradation proceeds comparably fast and is characterized by a substantial increase in *DGS*, hence enabling the release of a payload upon the treatment with dextranase.

As a result, p(AAm-*co*-Dex-MA) gel particles represent a very interesting class of nanoscale hybrid materials, which are characterized by their partial biodegradability and simple and versatile processing routes. Moreover, their sensitivity towards dextranase is of great advantage for release applications since it is an orthogonal approach to widely used pH- or temperature sensitive microgels.

5.2.2 *Enzymatically- and Light-Degradable Nanogels Based on Functionalized Dextran as Crosslinkers*

In the previous chapter, the successful preparation of enzymatically degradable microgels by free radical copolymerization of dextran methacrylates with acrylamide in inverse miniemulsion was demonstrated. Optimization of the synthetic parameters resulted in nanogels which combined a high crosslinking density (i.e., small mesh sizes) and -efficiency with a good enzymatic degradability. Even though the investigated materials were found to degrade only partially upon incubation with dextranase, the observed dramatic increases in the respective degrees of swelling are assumed to give rise to potential enzyme triggered release applications. Nevertheless, the described microgels require the addition of enzymes or the localization of the carrier system in specific milieus. In comparison, the release of a payload upon applying an external trigger without a change in the chemical composition of the surrounding media bears the advantage of an on-demand delivery. As mentioned before, light is especially interesting as stimulus since it offers the possibility to change the network properties in very confined spaces and time scales in a non-contact approach respectively.

Based on these considerations, the aim of the work presented in this chapter is to expand the newly developed concept of enzymatically degradable microgels to the preparation of double stimuli-responsive nanogels being degradable upon the addition of dextranase or the irradiation with light as an orthogonal second trigger. The presented approach to realize the described concept is based on free radical inverse miniemulsion copolymerization of acrylamide (AAm) with newly synthesized functional dextran crosslinkers containing acrylate moieties covalently attached to the backbone via a photo-labile linker (Dex-PL-A).

Enzymatically and photolytically degradable hybrid p(AAm-co-Dex-PL-A) nanogels were designed to alter their network structure upon the appliance of two different stimuli; i.e., the addition of dextranase or the irradiation with UV-light. While enzymatic degradation of the nanogels can be achieved by cleavage of the dextran backbone upon the addition of dextranase, irradiation of the hydrogel nanoparticles leads to photolytic cleavage of the covalent linkage of the polyacrylamide chains to the dextran chains and is assumed to yield freely soluble polyacrylamide and dextran chains. Both stimuli can be applied either separately or subsequently, thus enabling a good and versatile control over the swelling and degradation behavior. The described concept is schematically illustrated in Fig. 5.55.

Synthesis and characterization of dextran-photo-labile linker-acrylate (Dex-PL-A). Dextran-photo-labile linker-acrylate (Dex-PL-A) molecules were

Parts of this work are published in the paper: "Enzymatic- and Light-Degradable Hybrid Nanogels: Crosslinking of Polyacrylamide with Acrylate Functionalized Dextranes Containing Photo-Cleavable Linkers" Daniel Klinger, Katharina Landfester, *J. Polym. Sci.: Part A* **2012**, 50 (6), 1062. Reprinted with permission from [44]. Copyright 2011 Wiley Periodicals, Inc.

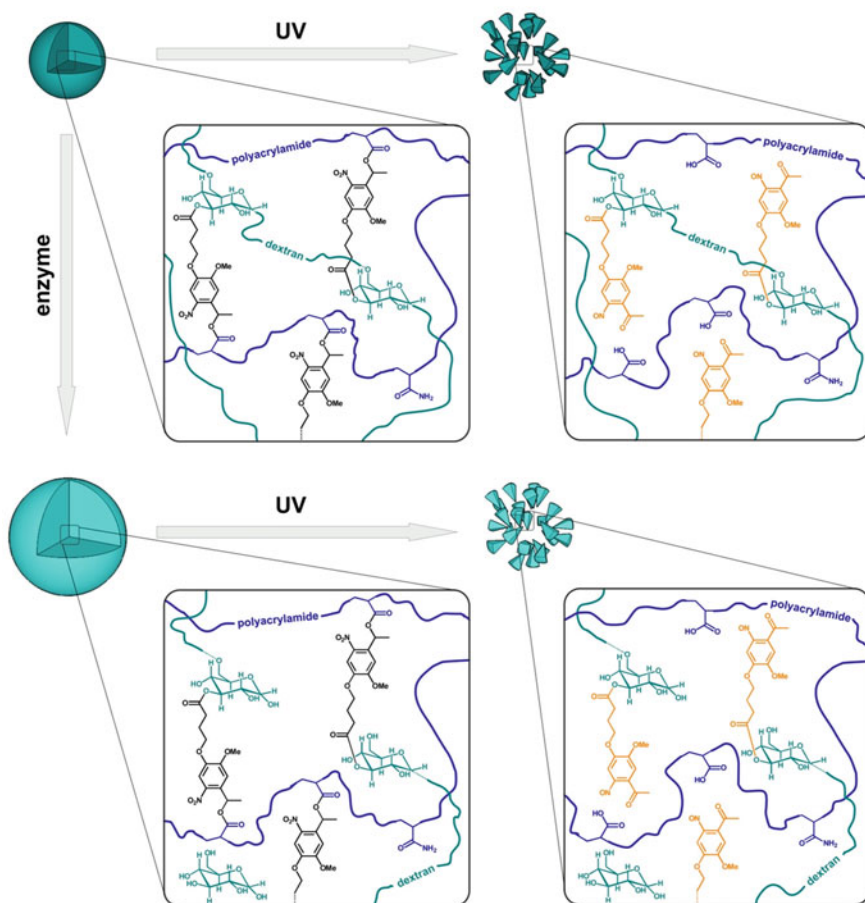


Fig. 5.55 Schematic representation of the double stimuli-induced degradation of hybrid p(AAm-co-Dex-PL-A) nanogels. Reprinted with permission from [44]. Copyright 2011 Wiley Periodicals, Inc

synthesized according to Fig. 5.56 in order to combine the enzymatic degradability of the dextran biopolymer with the photolytic properties of the *o*-nitrobenzyl ester groups in the photo-cleavable spacer between acrylate moieties and the polysaccharide backbone.

The carboxylic acid and hydroxyl functionalized photo-labile chromophore (8) was synthesized according to the procedure described earlier [9]. In brief, the ether formation of (4) with methyl 4-bromobutyrate was followed by nitration of the aromatic core with acetic anhydride/nitric acid. Reduction of the keto group of (6) and subsequent ester hydrolysis yielded (8) in good yields. In a next step, the hydroxyl group was reacted with acryloyl chloride to attach the polymerizable unit through a photo-labile *o*-nitrobenzyl ester bond. The carboxyl group of (11) was

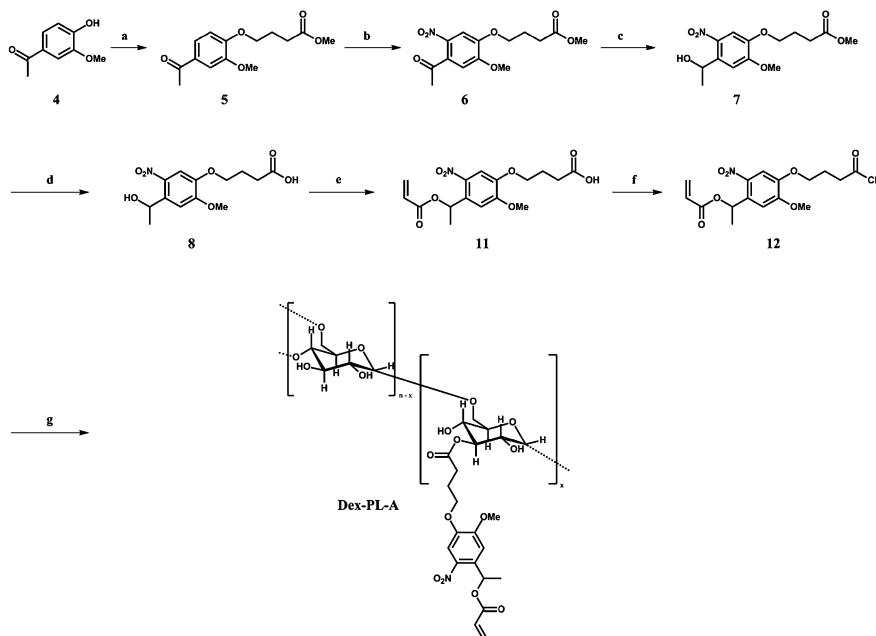


Fig. 5.56 Synthetic pathway to Dex-PL-A. Reagents and Conditions: **a** methyl 4-bromobutyrate, $\text{K}_2\text{CO}_3/\text{DMF}$ (anhyd.), 25 °C, 16 h, quant.; **b** acetic anhydride/nitric acid (1:2, v/v), 0 °C, 3 h, 53 %; **c, d** $\text{NaBH}_4/\text{MeOH}/\text{THF}$, 25 °C, 16 h, NaOH , 25 °C, 7 h, 89 %; **e** acryloyl chloride, NEt_3 , DCM , 0 °C to RT, 16 h, 65 %; **f** oxalyl chloride, DMF (cat.), DCM (anhyd.), 3 h, quant.; **g** dextran (6 k), NEt_3 , LiCl , DMF (anhyd.), RT, 16 h, 60 °C, 1 h, 58 %. Reprinted with permission from [44]. Copyright 2011 Wiley Periodicals, Inc

then activated by forming the respective carboxyloxy chloride with oxalylchloride. Finally, the crosslinking molecule Dex-PL-A was obtained by the reaction of hydroxyl groups of dextran with the activated carboxyl group of (12), thus covalently attaching the acrylate moieties to the dextran backbone via the photolabile linker. The obtained crosslinker was investigated with regards to the degree of substitution by means of $^1\text{H-NMR}$ measurements. Calculation of the peak area ratio of the 6 protons (aromatic, olefinic and tertiary benzylic) of the photo-labile linker to the one anomeric proton of dextran afforded a degree of substitution (*DS*) of $DS = 0.17$. In other words, on one dextran chain consisting of ~ 34 glucopyranosyl groups, 5–6 of these groups are functionalized. While a low degree of substitution is assumed to decrease the crosslinking efficiency, functionalization of the dextran with too many acrylate side groups could influence the enzymatic degradation behavior due to a reduced accessibility of the dextran backbone as a result of sterical hindrance. The medium degree of substitution of 0.17 should allow a sufficient crosslinking upon copolymerization with acrylamide while maintaining the enzymatic degradability. Additionally, a comparatively low molecular weight of 6,000 g/mol of the used dextran was chosen to enable a good

distribution of the crosslinking points in the resulting gel. Preliminary studies performed on PAAm nanogels crosslinked with dextran methacrylates confirmed this hypothesis (see Sect. 5.2.1).

As discussed in previous chapters, regarding the photolysis of the crosslinking molecules and the resulting nanogels, a fast and quantitative reaction under mild conditions is highly favored. The α -methyl group on the benzylic carbon of the *o*-nitrobenzyl was introduced into the photo-labile chromophore as it is known to increase the rate of photolysis significantly [10]. The introduction of alkoxy substituents in the *o*-nitrobenzylic core results in a modified electronic structure of the chromophore which is known to result in a considerably increased UV absorption for $\lambda > 315$ nm [11] and thus, allows for a more gentle decomposition with possible benefits for release applications of sensitive molecules. Figure 5.57 presents the UV–vis spectroscopic investigation of the Dex-PL-A crosslinker. It reveals an absorption maximum at 260 nm accompanied by the anticipated additional absorption maximum at 350 nm. Thus, the crosslinker exhibits a high absorption in the targeted photolysis wavelength region of $\lambda > 315$ nm.

Photolysis of the cleavable crosslinker in solution. In order to investigate the photolytic performance of the newly synthesized photo cleavable crosslinker, time dependent UV–vis measurements of Dex-PL-A in aqueous solution were performed. The respective spectra are shown in Fig. 5.57.

Irradiation with UV light of the wavelength of $\lambda = 365$ nm resulted in a red shift of the absorption maximum at 350 nm and the evolution of two new absorption bands at 235 and 270 nm. In addition, absorbance at 305 nm decreased upon irradiation as shown in magnification in the inset of Fig. 5.57a. Along with these light-induced changes in the spectra, the occurrence of well defined isosbestic points over the complete irradiation time scale points towards a successful cleavage of the chromophore which is supposed to be a first order reaction. As shown in Fig. 5.57b, the rate of decrease of the absorbance at 305 nm during irradiation followed an exponential decay to a constant level at 176 s. Kinetic analysis was performed by setting the value of the final absorbance at 245 s as

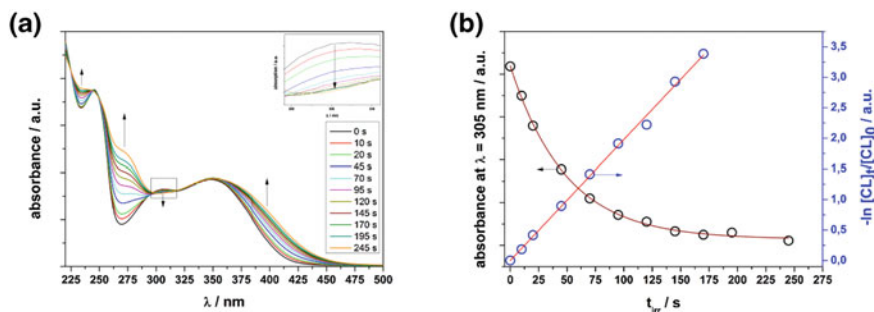


Fig. 5.57 Irradiation of Dex-PL-A in aqueous solution: **a** time dependent UV–vis spectra; **b** time dependent absorbance at $\lambda = 305$ nm and kinetic plot. Reprinted with permission from [44]. Copyright 2011 Wiley Periodicals, Inc

zero. The resulting kinetic plot of $-\ln [CL]_t/[CL]_0$ versus time shows excellent linearity, indicating the expected first order kinetic with respect to the chromophore concentration. The observed well defined photolytic cleavage in short time scales under mild irradiation conditions in combination with the polymerizable acrylate functionalities and the enzymatic degradable dextran backbone renders these newly synthesized molecules highly interesting as double stimuli-sensitive crosslinkers for the formation of degradable hydrogels from aqueous solutions.

Preparation and characterization of hybrid p(AAm-co-Dex-PL-A) gel nanoparticles by inverse miniemulsion copolymerization. In order to prepare hybrid p(AAm-co-Dex-PL-A) nanogel particles, acrylamide (AAm) and Dex-PL-A were dissolved in an aqueous sodium chloride solution and copolymerized in inverse miniemulsion by free radical polymerization. Table 5.8 lists the composition of the different nanogels in combination with the type of initiator. Two sets of experiments were performed to demonstrate the versatility of this preparation method. While hybrid nanogels HNG-1A–HNG-3A of set A were polymerized at 70 °C using V-59 as radical initiator, V-70 was used for the preparation of set B (HNG-1B–HNG-4B) by initiating the polymerization at a much lower temperature of 37 °C. With regard to a potential embedding of active compounds, a lower polymerization temperature holds promise for the embedding of labile biological compounds (e.g., proteins or enzymes) at mild conditions.

Another important factor to be considered during nanogel preparation is the crosslinking density of the resulting network. Especially in the context of potential carrier applications, the prepared nanogels should exhibit a low initial degree of swelling in order to prevent diffusion of embedded compounds from the network. Even though this parameter can be adjusted by increasing the Dex-PL-A/AAm ratio (i.e., the amount of crosslinking points on the dextrane), a balance between a low initial *DGS* and a good enzymatic degradability is of high importance. Incorporation of too many crosslinking points is known to hinder enzymatic degradation of the dextran chains due to a reduced accessibility caused by too small mesh sizes of the gel [69]. Hence, in every set of nanogels, the amount of Dex-PL-A crosslinker was varied with the intention to investigate the influence of the Dex-PL-A/AAm ratio on the properties of the resulting microgels. For polymerizations at 70 °C HNG-1A contained 5 wt.-%, HNG-2A 17.5 wt.-% and HNG-3A 30 wt.-% of Dex-PL-A respectively. Analogously, the gel particles HNG-1B–HNG-4B of set B contained 5.0, 17.5, 30 and 60 wt.-% of Dex-PL-A. All polymerizations were carried out over night and the resulting dispersions were washed repeatedly with cyclohexane to remove excess surfactant. The resulting stable dispersions of hybrid nanogels in cyclohexane were investigated with regard to the hydrodynamic diameter by DLS measurements and the particle morphologies and sizes were determined by SEM. Figure 5.58 shows representative SEM pictures of HNG-3 in comparison to HNG-3B as well as the respective number weighted size distributions obtained from DLS and SEM analysis. Figure 5.58b shows the hydrodynamic diameters of the particles in cyclohexane in dependency on the amount of acrylate groups available for crosslinking.

Table 5.8 Synthetic details for the inverse miniemulsion copolymerizations of hybrid nanogels

Classification	Sample	AAm m/g	Dex-PL-A m/g	m(Dex-PL-A)/ [m(Dex-PLA) + m(AAm)] (%)	Solvent f. dispersed phase		Initiator type
					Type	m/g	
Set A	HNG-1A	0.950	0.050	5.0	0.5 M NaCl	1.000	V-59
	HNG-2A	0.825	0.175	17.5	0.5 M NaCl	1.000	V-59
	HNG-3A	0.700	0.300	30	0.5 M NaCl	1.000	V-59
Set B	HNG-1B	0.950	0.050	5.0	0.5 M NaCl	1.000	V-70
	HNG-2B	0.825	0.175	17.5	0.5 M NaCl	1.000	V-70
	HNG-3B	0.700	0.300	30	0.5 M NaCl	1.000	V-70
	HNG-4B	0.400	0.600	60	0.5 M NaCl	1.000	V-70

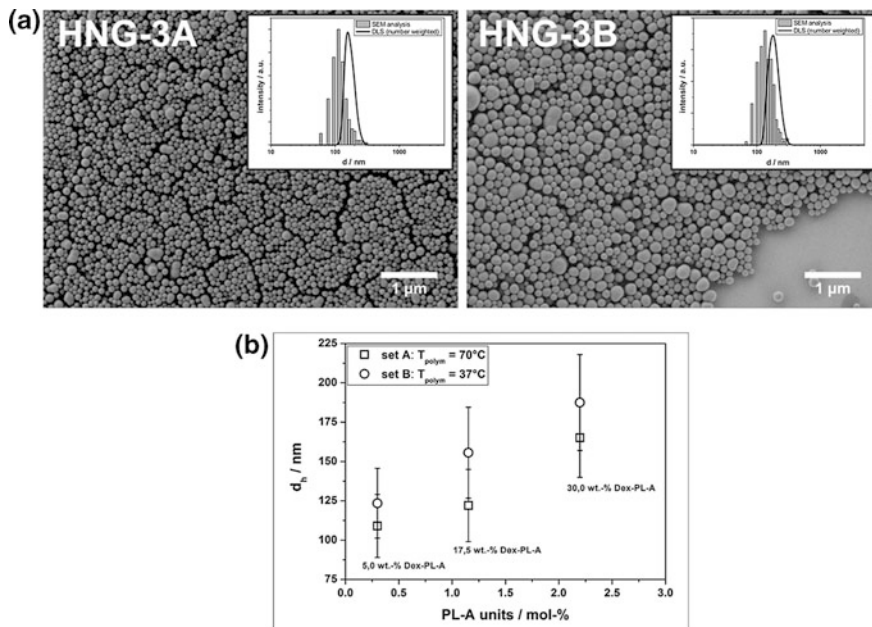


Fig. 5.58 **a** Representative SEM pictures HNG-3A and HNG-3B nanogels dropcast from cyclohexane dispersion and size distributions obtained from DLS measurements (number weighted) in comparison to diameters obtained from SEM analysis. **b** Hydrodynamic diameters of hybrid nanogels obtained from DLS measurements in cyclohexane dispersion after washing. Reprinted with permission from [44]. Copyright 2011 Wiley Periodicals, Inc

As can be seen from SEM pictures, inverse miniemulsion copolymerizations yielded well defined spherical hybrid gel particles with nanoscale dimensions. From the hydrodynamic particle diameters shown in Fig. 5.58b, it becomes obvious that for an increasing amount of polymerizable acrylate units—realized by increasing the Dex-PL-A/AAm ratio—the particle size also increases. Analogously to p(AAm-co-Dex-MA) nanoparticles described in the previous chapter, this effect is assumed to be based on an increased viscosity of the monomer phase for higher contents of functionalized dextrans. Comparing the hydrodynamic diameters obtained from DLS measurements to the diameters from SEM pictures (see Fig. 5.58), it becomes apparent that the values from light scattering in cyclohexane dispersion are larger than those obtained from the dried particles. As water was added as a solvent for the monomer phase, it is still present in the formed gel particles after polymerization. Compared to the collapsed dried particles observed by SEM, nanogels in cyclohexane dispersion consist of swollen networks resulting in increased particle diameters.

At very high Dex-PL-A contents (60 wt-%), increasing polydispersity and ill-defined morphologies were observed (data not shown). In this case, the high amount of the functionalized dextran is assumed to influence the stability of the

droplets due to the surface active character of the amphiphilic Dex-PL-A. Since attempts to form nanogels from pure Dex-PL-A did not yield stable miniemulsions, the presence of a second comonomer seems to be a crucial requirement for the formation of enzymatically- and light-degradable gel particles by inverse miniemulsion polymerization.

Transfer of the gel particles to the aqueous phase was easily achieved by immersing the freeze dried particles over night in water. Repeated washing of the swollen nanogels with deionized water removed the soluble fraction of the crosslinking polymerization reaction. Since a lower sol content reflects a higher crosslinking efficiency, its determination enables the relative evaluation of the performance of the crosslinking copolymerization. As mentioned above, the swelling ratio or the degree of swelling (*DGS*) is another important property of the nanogels. Similar to the sol content, this parameter is an indication for the efficiency of the crosslinking reaction, since a lower initial degree of swelling is based on a smaller mesh size of the network caused by the incorporation of more crosslinking points. Figure 5.59a shows the values for the sol contents and initial

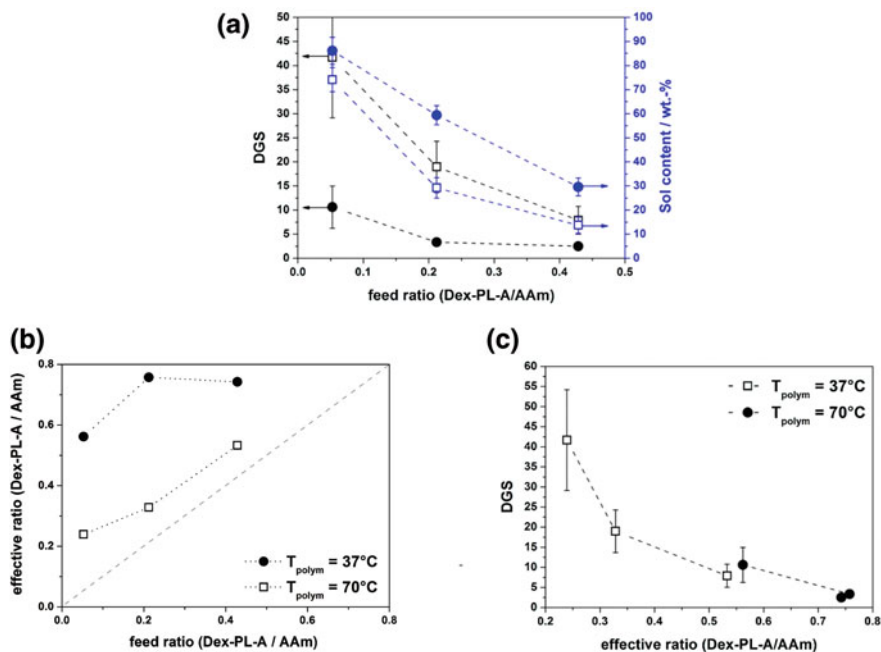


Fig. 5.59 Characterization of the gel properties of the hybrid $p(\text{AAm-co-Dex-PL-A})$ nanogels: **a** *DGS* and sol content values in dependency on the feed ratio of Dex-PL-A/AAm. Empty squares nanogels of set A polymerized at 70 °C, filled dots nanogels of set B polymerized at 37 °C; **b** effective ratio of Dex-PL-A/AAm in comparison to the respective feed ratio, the diagonal represents the ideal case of quantitative incorporation of both compounds and is a guide for the eye; **c** *DGS* values in dependency on the effective ratio of Dex-PL-A/AAm. Empty squares nanogels of set A polymerized at 70 °C, filled dots nanogels of set B polymerized at 37 °C. Reprinted with permission from [44]. Copyright 2011 Wiley Periodicals, Inc

*DGS*s obtained by gravimetric analysis and DLS measurements. Though determination of either parameter does not permit to draw quantitative conclusions regarding the crosslinking density or the inner morphology of the nanogels, it nevertheless allows the expedient relative comparison of the gel properties among the different samples.

Figure 5.59a shows the dependency of Dex-PL-A/AAM feed ratio to *DGS* values and sol contents. As expected, increasing the feed ratio of Dex-PL-A/AAM (i.e., the theoretical amount of polymerizable photo-labile linker acrylate (PL-A) groups) for a fixed polymerization temperature, reduces both the sol content and the initial degree of swelling. Both parameters indicate a higher copolymerization efficiency.

Comparing the properties of the gel particles polymerized at 70 °C to those of the nanogels polymerized at 37 °C it becomes obvious that for similar feed ratios of Dex-PL-A/AAM, a lower polymerization temperature resulted in increased sol contents and lower degrees of swelling. This effect can be assigned to comparably lower conversions of the polymerization reactions. The decreased reaction temperature hinders diffusion of monomers and increases the probability of termination reactions. Since ¹H-NMR analysis of the sol content (data not shown) revealed only negligible amounts of Dex-PL-A, quantitative incorporation of the crosslinking molecules is assumed. Based on the ensuing presumption that the sol content consisted only of unreacted AAM monomers and oligomers, the effective Dex-PL-A/AAM ratios were calculated. Figure 5.59b shows the calculated values plotted against the theoretical values; i.e., the feed ratios of Dex-PL-A/AAM. It is seen that for the same Dex-PL-A/AAM feed ratio, higher sol contents for the nanogels polymerized at 37 °C correlate with increased effective Dex-PL-A/AAM ratios compared to the samples polymerized at 70 °C.

Plotting the *DGS* values of the two sets of nanogels against the effective Dex-PL-A/AAM ratio shows the anticipated trend of decreasing degrees of swelling with increasing amounts of actually incorporated crosslinking molecules (Fig. 5.59c). The favored incorporation of functionalized dextran for the lower polymerization temperature (37 °C) is therefore expected to yield nanogels consisting of networks with smaller mesh sizes. Additionally, with increasing feed ratios of Dex-PL-A/AAM, a decreasing deviation of the effective ratios from the theoretical values is observed for both polymerization temperatures. This confirms a higher crosslinking efficiency if more Dex-PL-A crosslinking molecules are available.

The systematic variation of the Dex-PL-A/AAM ratio (Fig. 5.59a) revealed HNG-3B nanogels as the most promising candidates for potential release applications for three reasons: (i) The observed relatively low sol content of 29.6 wt.-% mainly consisted of AAM monomers and oligomers, therefore pointing towards a successful crosslinking copolymerization with an almost quantitative incorporation of Dex-PL-A crosslinking molecules. (ii) The low initial degree of swelling of 2.5 is potentially effective for the embedding of functional compounds. (iii) The substantially low polymerization temperature of 37 °C renders these synthetic parameters highly effective.

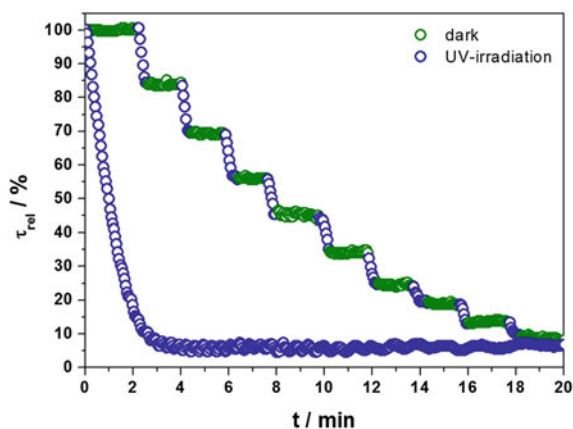
Photolytic and enzymatic degradation. Since hybrid p(AAm-co-Dex-PL-A) nanogels HNG-3B exhibited the desired gel properties, their degradation behavior upon irradiation and treatment with dextranase was investigated in order to demonstrate their potential for release applications. Degradation experiments were conducted in aqueous dispersions with a solid content of 0.0625 % consisting of purified nanogels.

Partial cleavage of crosslinking points by either photolytic disruption of the connecting bonds between polyacrylamide chains and dextrans or the enzymatic decomposition of the latter should result in a loosened network structure with increased mesh sizes, thus yielding gel particles of an increased degree of swelling. Further exposure to the respective stimuli is expected to form completely disintegrated networks consisting of freely soluble polymer chains and dextran oligomers. Generally, DLS measurements can be applied to determine increased particle sizes caused by the higher degree of swelling but are limited to the partial degradation regime. To investigate the complete degradation behavior, turbidity measurements can be used as they are capable of visualizing the complete time dependent photolytic and enzymatic particle disintegration as well.

First, the photolytic cleavage of the *o*-nitrobenzylester groups connecting polyacrylamide chains to dextrans was investigated. Two different experiments were performed: constant and stepwise irradiation of the sample with UV light. Figure 5.60 shows the resulting plots of turbidity versus time.

The plot clearly shows a profound decrease of the relative turbidity down to a constant level of almost 0 % after only ~ 3 min of continuous irradiation, thus indicating complete particle degradation in a short time scale under mild conditions. This observation was confirmed since attempts to perform DLS measurements on the resulting clear solution did not yield any results regarding particle sizes. The stepwise irradiation was performed by repeated cycles of irradiating the sample for each time 15 s and then keeping the sample in the dark for 2 min. Turbidity was monitored during the whole process and was found to decrease only during the appliance of light. Since turbidity—and therefore the degradation—is

Fig. 5.60 Turbidity measurements for the irradiation of an aqueous HNG-3B nanogel dispersion (0.0625 % w/v) with UV light ($\lambda = 365$ nm, $I = 30$ mW/cm²). Reprinted with permission from [44]. Copyright 2011 Wiley Periodicals, Inc



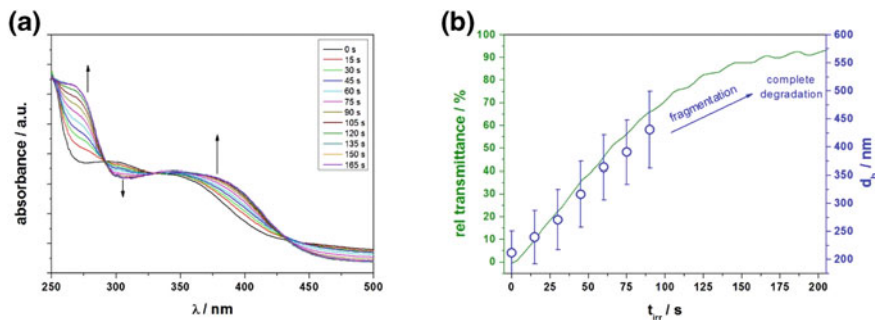


Fig. 5.61 **a** Irradiation time dependent UV–vis spectra of HNG-3B nanogels (normalized to $\lambda = 330$ nm at $t_{\text{irr}} = 165$ s); **b** Irradiation time dependent hydrodynamic diameters of HNG-3B nanogels in comparison to the relative transmittance of the respective aqueous dispersion. Reprinted with permission from [44]. Copyright 2011 Wiley Periodicals, Inc

not altered in the dark, the photolytic decomposition of the nanogels can be stopped at any desired degree, thus proving a highly controlled photo degradation profile.

The observed stepwise degradation allowed the detailed investigation of the photolytic decomposition at fixed time points of irradiation. Samples were withdrawn after every irradiation step and analyzed. The chromophore cleavage was investigated by UV–vis spectroscopy and the particle size assessed by means of DLS measurements. Figure 5.61a shows the respective normalized irradiation time dependent UV–vis spectra while Fig. 5.61b depicts the respective hydrodynamic diameters of the irradiated nanogels in comparison to the relative transmittance of the dispersion.

Irradiation time-dependent UV–vis measurements clearly show the successful cleavage of the photo-labile *o*-nitrobenzyl ester linkers. Compared to the photolysis of pure Dex-PL-A crosslinking molecules in solution, the spectra of the respective nanogels are influenced by scattering of the dispersion. As seen by turbidity measurements, the scattering intensity decreases upon irradiation and no isosbestic points were observed in the raw UV–vis spectra (data not shown). Nevertheless, the change in absorbance at 270 nm relative to the absorbance at 300 nm clearly points to a successful photoreaction. Since UV–vis spectroscopy of the irradiation of pure Dex-PL-A exhibited an isosbestic point at $\lambda = 330$ nm, normalizing the spectra of the nanogels to the final absorbance after 165 s of irradiation at this wavelength yielded the same well defined isosbestic points as well. Hence, it was concluded that the photoreaction is not influenced by the gel matrix.

DLS measurements of the irradiated samples clearly show the increase of particle sizes in dependency on the irradiation time. As expected the light-induced cleavage of covalent bonds between polyacrylamide and dextran chains results at first in highly swollen nanogels characterized by a loosened network structure and later in completely soluble polymer chains. While DLS measurements of irradiated

nanogels up to irradiation times of 90 s yielded well defined monomodal size distributions, the determination of hydrodynamic diameters for longer irradiation times exhibited multimodal distributions due to fragmentation of the gels. For even longer irradiation times, no results were obtained due to a too low scattering intensity. As speculated before, these results confirm that DLS characterization is indeed only possible in the partial degradation regime. In contrast, the performed turbidity measurements clearly are highly advantageous in order to investigate the full degradation profile. The correlation between increasing particle sizes and increasing transparency (i.e., decreasing scattering intensity) is confirmed by the plot in Fig. 5.61b.

In summary, the experiments demonstrate that the complete photolytic disintegration of the hybrid p(AAm-co-Dex-PL-A) network structure upon cleavage of the covalent bonds between PAAm and dextran can be achieved fast and quantitatively under mild irradiation conditions. Moreover, the well defined photoreaction even allows only partial degradation of crosslinking points and therefore nanogels of a desired specific degree of swelling can be obtained by adjusting the irradiation time accordingly.

To demonstrate the double stimuli-responsive character of the hybrid nanogels, further degradation experiments were conducted to investigate the enzymatic dextran chain cleavage upon the addition of dextranase. In principal, the degradation of the dextran backbone in the Dex-PL-A crosslinkers should lead to a disintegration of the polymeric network and result in either fully degraded gels or particles exhibiting an increased degree of swelling (for incomplete dextran chain cleavage). Investigations were carried out on aqueous dispersions of the purified HNG-3B gel particles (0.0625 % w/v) at 37 °C and turbidity of the sample was monitored after the addition of a dextranase solution. The resulting curve is shown in Fig. 5.62a.

The initial turbidity decreases as a function of incubation time until it reached a constant value of 50 % after circa 5 h. Even though no complete particle degradation—corresponding to a relative turbidity of around 0 %—was achieved, the

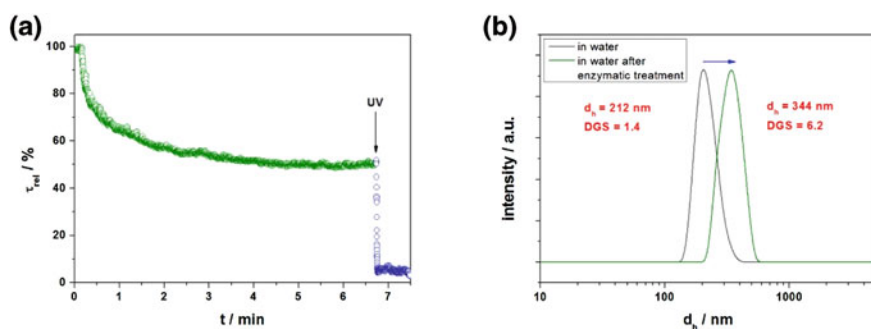


Fig. 5.62 Enzymatic and subsequent photolytic degradation of HNG-3B nanogels: **a** turbidity curve; **b** particle size distributions before and after enzymatic treatment measured by DLS. Reprinted with permission from [44]. Copyright 2011 Wiley Periodicals, Inc

drop in turbidity can be assigned to an increased degree of swelling of the hydrogel particles. The corresponding increased pore size of the network results from partial cleavage of the dextran backbones responsible for the crosslinking of gel. DLS measurements were conducted to confirm this assumption and the resulting size distributions before and after enzymatic treatment are shown in Fig. 5.62b. As expected, the particle size increased from an initial diameter of 212 to 344 nm, thus corresponding to a change in *DGS* from the low initial value of 1.4 to the final value of 6.2. Comparing the measured hydrodynamic diameter of 344 nm after enzymatic treatment—corresponding to a turbidity of 50 %—to the measured diameter of 364 nm after 60 s of UV irradiation—corresponding to a similar turbidity of about 50 %—the similar particle sizes once again demonstrate the good correlation between turbidity and degree of degradation (i.e. *DGS*). Moreover, these results point towards a comparable degradation mechanism including the increase in mesh sizes by cleavage of crosslinking points.

Since any treatment with the enzyme for longer times did not yield a further decay of the turbidity—i.e. breakage of dextran chains—the final value represents the crucial limit for enzymatic particle degradation. This observed limitation is in agreement with the results obtained from degradation experiments on p(AAm-*co*-Dex-MA) microgels as described in the previous chapter. In brief, incomplete microgel degradation upon treatment with dextranase is assumed to be based on: (i) the reduced accessibility of the dextran chains in the interpenetrating p(AAm-*co*-Dex-PL-A) network for the enzyme; (ii) the hindered cleavage of two neighboring substituted glucopyranose residues and (iii) the decreased affinity of the Dex-PL-A to the binding site of the enzyme due to the relatively high degree of substitution with PL-A moieties and (iv) grafted PAAm chains. Nevertheless, the observed 6 fold increase in particle volume after treatment with dextranase holds great potential for the release of functional compounds from the network triggered by increasing mesh sizes.

Having demonstrated partial enzymatic degradation, the question arises whether complete particle disintegration can be subsequently achieved by irradiation of the swollen nanogels. As shown in Fig. 5.62a, this pathway could indeed be used to realize a two step degradation profile. After the hybrid nanogel particles reached the maximal degree of swelling upon treatment with dextranase, irradiation of the swollen gel particles lead complete particle degradation as demonstrated by a measured turbidity of ~ 0 %. An additional advantage is the comparably much faster response to the trigger. Since enzymatic treatment can induce a continuous but slow degradation profile (~ 6 h), the photolytic degradation can be achieved in less than 2 min.

In order to verify the results presented above, SEM pictures of HNG-3B nanogel dispersions at different points of the two-step degradation were taken and are shown in Fig. 5.63.

The initial non-degraded particles can be identified as flattened spheres on the silica wafer (Fig. 5.63a). Even though drying of the particles from the swollen state resulted in film formation and flattened structures, the retention of the spherical morphology clearly hints again to the successful crosslinking of PAAm

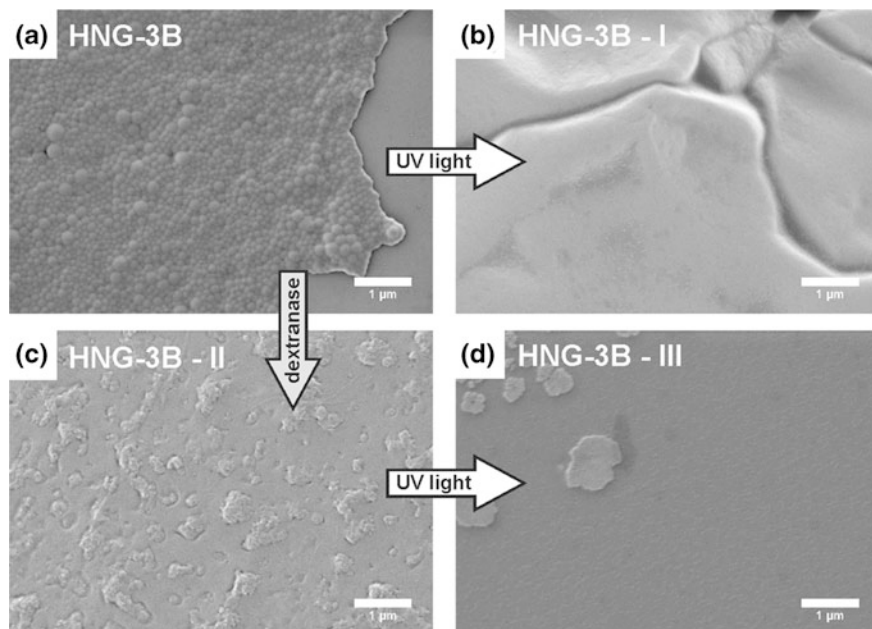


Fig. 5.63 SEM investigations on the stimuli-induced degradation behavior of HNG-3B: **a** swollen microgels in water; **b** completely degraded microgels after UV irradiation; **c** swollen and partially aggregated/fragmented microgels after treatment with dextranase; **d** completely degraded microgels after first enzymatic treatment and subsequent irradiation with UV light. Reprinted with permission from [44]. Copyright 2011 Wiley Periodicals, Inc

by Dex-PL-A. After irradiation with UV light no spherical structures were observed by SEM but a polymeric film (Fig. 5.63b), thus indicating complete particle degradation. As shown in Fig. 5.63c, after the enzymatic treatment partially aggregated/fragmented particular structures were still observed but an increasing film formation/flattening is visible, caused by the highly swollen state of the nanogels before drop casting. Finally, in Fig. 5.63d no particular structures were detected and the observed polymer film results from the completely degraded nanogels upon UV irradiation.

Summarizing the degradation behavior of the p(AAm-co-Dex-PL-A) hybrid nanogels three different degradation profiles were realized. At first, the exclusive photolytic cleavage of the photo-labile linkers between dextran and PAAm chains was successfully used to fully degrade the nanogels upon continuous irradiation in a short time span. Partial degradation of crosslinking points and therefore nanogels of a desired specific degree of swelling were obtained by adjusting the irradiation time accordingly. Second, partial enzymatic cleavage of the dextran backbones of the Dex-PL-A crosslinking molecules resulted in an increase of the degree of swelling of the nanogels up to a constant value. Third, the subsequent irradiation of those swollen hydrogel particles could be used to fully degrade the network

structure. Hence, by combining the two orthogonal stimuli a two-step degradation profile was realized rendering such hybrid nanogels highly versatile materials for potential release applications.

Conclusion

In conclusion, a new system for potential enzymatic- and light-triggered release applications based on degradable nanogels was successfully developed. Realization of this concept was achieved with newly synthesized water soluble cross-linking molecules consisting of vinyl functionalized dextrans. In addition to the inherent enzymatic cleavability of the dextran backbone upon incubation with dextranase, light-sensitivity was incorporated into the crosslinking structure by the covalent attachment of multiple radically polymerizable acrylate units via a photo-labile linker to the polysaccharide chains. The resulting dextran-photo-labile linker-acrylate (Dex-PL-A) structures are characterized by their good water solubility which—in combination with multiple vinyl groups per chain—offers the possibility for the preparation of a broad range of enzymatic- and light-degradable (nano-)gels by copolymerization with different vinyl functionalized monomers from aqueous solutions. As a first model system, acrylamide was copolymerized with Dex-PL-A in an inverse miniemulsion. High crosslinking efficiency of the resulting p(AAm-*co*-Dex-PL-A) nanogels was achieved by systematic increasing the Dex-PL-A/AAm ratio. It was shown that irradiation with UV light enabled either complete particle degradation or the adjustment of a desired specific degree of swelling by tuning the irradiation time accordingly. In addition, a two step degradation profile based on the subsequent appliance of the two orthogonal stimuli was realized by first generating highly swollen nanogels by partial enzymatic cleavage of the Dex-PL-A crosslinking molecules and their successive complete degradation upon irradiation. The facile way of preparation at ambient temperatures of 37 °C from aqueous solutions and the observed low initial degree of swelling is promising for the potential embedding of functional water soluble compounds already during the polymerization. In combination with the well defined degradation profiles, this feature renders these new materials highly interesting for triggered release applications in aqueous dispersions.

5.3 Light-Sensitive Microgel-Doxorubicin Conjugates: Labile Drug Attachment via a Photo-Cleavable Linker

In a previous chapter the great potential of p(HEMA-*co*-MAA) microgels for the triggered delivery of water soluble (biological) macromolecules was demonstrated by exploiting the pH-sensitivity of the polymeric network for the loading and release of myoglobin as a model protein. The pH-induced entrapment by a swelling-deswelling mechanism is suitable for the controlled release of *large* functional compounds.

In comparison, the loading efficiency of comparably *small* functional molecules into microgels is crucially limited by leakage of the active substances from the network. In this context, it is of high importance to ensure a successful retention of the functional molecule in the carrier system until the desired site or time point for its triggered release is reached. This can be achieved by several approaches.

On one hand, the embedding of hydrophobic drugs into non-swollen hydrophobic polymeric nanoparticles prevents their leakage in aqueous media. A triggered release can then be achieved e.g., by changing the hydrophilicity of the network-forming polymer from hydrophobic to hydrophilic. Hereby, the resulting swelling of the particles induces the release of the payload. This concept was recently described by Griset et al. for the delivery of paclitaxel from pH-sensitive expandable nanoparticles based on acetal protected polymers [77].

On the other hand, the covalent attachment of a drug to a hydrophilic polymeric carrier system is highly efficient to prevent its leakage. A triggered release can be achieved by the utilization of a specific linker molecule between drug and polymer which is cleavable upon the appliance of a certain trigger [78–81]. An interesting example to realize this concept was recently described by Choi et al. The investigated approach is based on a doxorubicin-PAMAM dendrimer conjugate where the hydrophilic drug is connected to the preformed dendrimer via a photo-cleavable linker [82]. As this was shown to be highly efficient for the release of doxorubicin upon irradiation, it is of great interest to extend this conception to a broad variety of polymeric carrier systems such as e.g., microgels. This would enable to study the delivery efficiency of the drug to cells in dependency on the used network-forming polymer. It is noteworthy that the functionalization of the previously mentioned dendrimers was achieved by attaching the linker-doxorubicin molecule to the preformed dendrimer via a subsequent esterification step. Utilization of this coupling reaction limits the versatility of this approach to polymeric materials containing either functional hydroxyl- or amine groups. Therefore, in order to ensure a versatile applicability of the described concept it is of high interest to develop a synthetic strategy which allows the incorporation of the doxorubicin-photo-labile linker moiety into a wider range of polymeric materials.

The aim of the work described in this chapter is the development of a novel functional monomer consisting of a doxorubicin molecule covalently attached to a radically polymerizable methacrylate group via a photo-labile linker. Generally, this doxorubicin-photo-labile linker-methacrylate (Dox-PL-MA) moiety is assumed to be copolymerizable with a broad variety of hydrophilic monomers, thus giving rise to a multitude of different delivery systems. Keeping in mind the observed good cellular uptake and negligible cytotoxicity of previously described p(HEMA-*co*-MAA) microgels, their great potential for delivery applications in biomedical fields is obvious. Therefore, in a first attempt to demonstrate the versatility of the Dox-PL-MA molecule, the copolymerization of the latter with HEMA and MAA in inverse miniemulsion is designed to yield anionic microgels as well defined carrier systems for the light-induced delivery of doxorubicin. Here, the drug molecule is covalently attached to the network-forming copolymer and

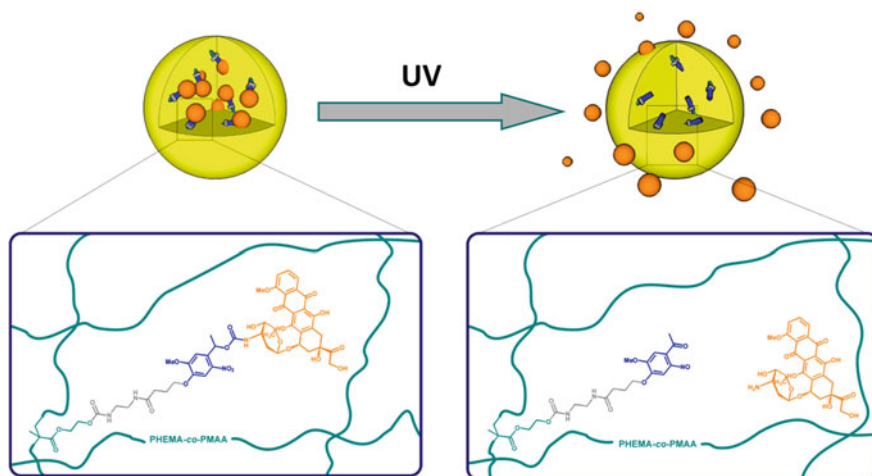


Fig. 5.64 Schematic illustration of the concept of light-sensitive microgel-doxorubicin conjugates

therefore leakage is hindered. Moreover, the embedding of the drug into the network efficiently shields the doxorubicin against the body's defense mechanisms. In contrast to previously described approaches based on network degradation, an effective release only at the targeted site can be induced by the light-induced cleavage of the linker molecule leaving the microgel structure intact. The described concept is schematically illustrated in Fig. 5.64.

Realization of the described concept starts with the synthesis of the Dox-PL-MA moiety. Here, an efficient synthetic route has to be developed and the resulting product has to be investigated with regards to the photolytic release of doxorubicin in solution. In a next step, a mild preparation method for p(HEMA-co-MAA) microgels should be elaborated. Finally, this is assumed to enable the incorporation of the Dox-PL-MA in situ during nanoparticles formation without damaging the drug molecule.

Synthesis and characterization of doxorubicin-photo-labile linker-methacrylate (Dox-PL-MA). Regarding the photolytic performance of the Dox-PL-MA molecule, two important considerations have to be taken into account: First, the doxorubicin molecule has to be coupled to the photo-cleavable linker in such a way that light-induced cleavage yields the free drug molecule leaving the photo-product of the chromophore attached to the polymeric network. This can be achieved by forming a carbamate bond between the amine group of the drug and the benzylic hydroxyl group of the chromophore. Second, the introduction of an α -methyl group in the chromophore was shown to enhance the rate of photolysis significantly. Therefore, in a first synthetic approach the route described by Choi et al. [82]. was modified accordingly. Figure 5.65 depicts the examined pathway.

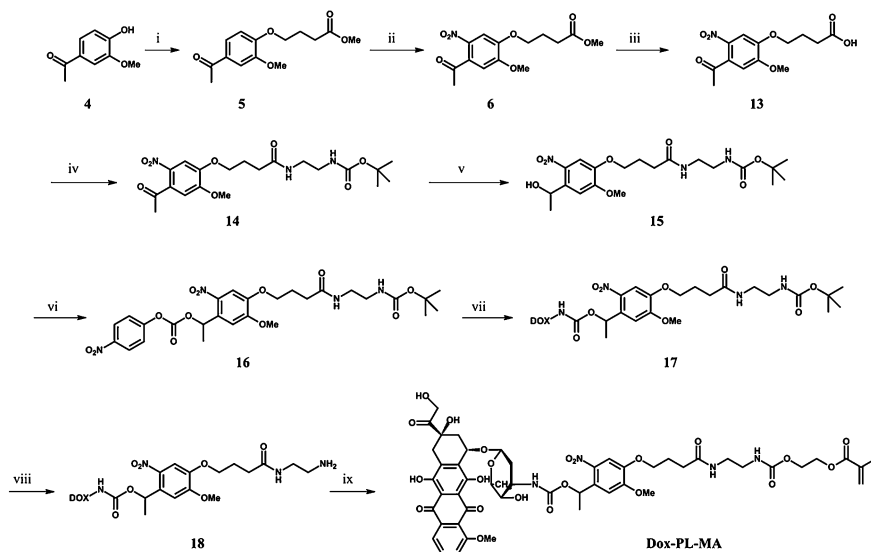


Fig. 5.65 Synthetic route A to Dox-PL-MA. Reagents and conditions: *i* methyl 4-bromobutyrate, K_2CO_3 /DMF, 25 °C, 16 h; *ii* acetic anhydride/nitric acid (1:2 v/v), 0 °C, 3 h; *iii* NaOH, THF/MeOH, 25 °C, 7 h; *iv* *N*-BOC-ethylenediamine, DCC, DMAP, DCM/DMF, 0 °C, 1 h then 25 °C, 24 h; *v* $NaBH_4$, THF/MeOH, 25 °C, 7 h; *vi* *p*-nitrophenyl chloroformate, DCM/DMF, 25 °C, 20 h; *vii* doxorubicin, DMF, triethylamine, 25 °C, 16 h; *viii* TFA, chloroform, 25 °C, 10 min; *ix* *p*-nitrophenyl chloroformate activated HEMA, triethylamine, DMF, 25 °C, 48 h

The synthesis starts with the preparation of the chromophore core of (6) analogous to the synthesis of the photo-labile crosslinkers CL-4B and CL-5B described in previous chapters. In a next step, the methyl ester is hydrolyzed and the resulting carboxylic acid (13) is coupled with mono BOC-protected ethylene diamine to yield (14). Subsequent reduction of the keto group produces the alcohol of (15) which exhibits two orthogonal addressable functionalities. Because the amine group is protected, efficient attachment of the drug molecule to the secondary hydroxyl group can take place. This is achieved by first activating the latter with *p*-nitrophenyl chloroformate to yield the reactive carbonate (16) and then forming the *o*-nitrobenzyl carbamate of (17) upon nucleophilic substitution of the *p*-nitrophenol by the amine group of doxorubicin. In analogy to the procedure described in the literature, in a next step, the deprotection of the amine group takes place by treatment with anhydrous trifluoroacetic acid (TFA). In contrast to the published procedure [82], this synthetic step was found not only to set free the BOC-protected amine group to generate (18), but also to degrade the glycosidic bond between the aromatic system and the pyranose unit in the doxorubicin molecule. Even though reactions were performed under extremely dry conditions, several attempts to follow this pathway failed to yield the desired product. Hence, a new synthetic route was designed to contain the coupling of the sensitive drug

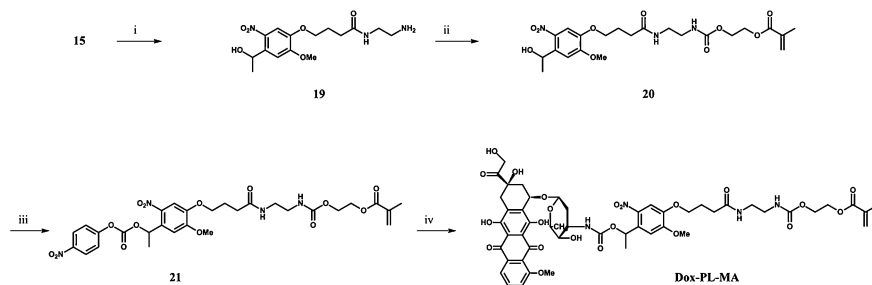


Fig. 5.66 Synthetic route B to Dox-PL-MA. Reagents and conditions: *i* TFA, chloroform, 25 °C, 10 min; *ii* *p*-nitrophenyl chloroformate activated HEMA, triethylamine, DMF, 25 °C, 48 h; *iii* *p*-nitrophenyl chloroformate, diisopropylethylamine, DMAP, DCM, THF, 25 °C, 24 h; *iv* doxorubicin, DMF, triethylamine, 25 °C, 16 h

molecule to a preformed photo-labile linker-methacrylate as the last step. The synthetic concept is illustrated in Fig. 5.66.

The alternative pathway (route B) starts with the previously described compound (15) containing a secondary hydroxyl group and a *N*-BOC-protected amine group as functional moieties for further modifications. While the former synthetic protocol route A was based on protecting the amine group during the coupling of the doxorubicin moiety to the alcohol, route B exploits the pronounced differences in the nucleophilicity of the secondary hydroxyl group and the deprotected amine of (19). Here, the selective reaction of the primary amine with *p*-nitrophenyl chloroformate activated HEMA yielded the photo-labile linker-methacrylate of (20). Subsequent attachment of the drug molecule was finally achieved by *p*-nitrophenyl chloroformate activated coupling of (21) with doxorubicin and resulted in Dox-PL-MA in good yield (57 %). Investigations on the product by ¹H- and ¹³C-NMR- as well as ESI mass spectroscopy confirmed the proposed structure (see experimental part).

The synthesized Dox-PL-MA molecule was examined with regard to its purity by HPLC measurements coupled with UV–vis spectroscopy. The obtained elution curve is shown together with the 3-dimensional plot of UV–vis absorbance in dependency on the elution time in Fig. 5.67.

Regarding the HPLC elution curve depicted in Fig. 5.67a, two distinctive peaks of similar peak areas were detected at elution times of 9.21 and 9.83 min. At first sight, this observation points towards an unsuccessful purification of the prepared Dox-PL-MA containing a side product. Nevertheless, the respective UV–vis spectra obtained for both peaks (see Fig. 5.67b) exhibited the same absorption bands at $\lambda_{max1} = 295$ nm, $\lambda_{max2} = 350$ nm and $\lambda_{max3} = 485$ nm. Therefore, it is assumed that the two different peaks can be assigned to two enantiomers of the Dox-PL-MA molecule which contains a chiral centre at the benzylic carbon coupling the doxorubicin moiety to the photo-labile linker-methacrylate. Consequently, it can be concluded that the desired product was obtained in high constitutional purity.

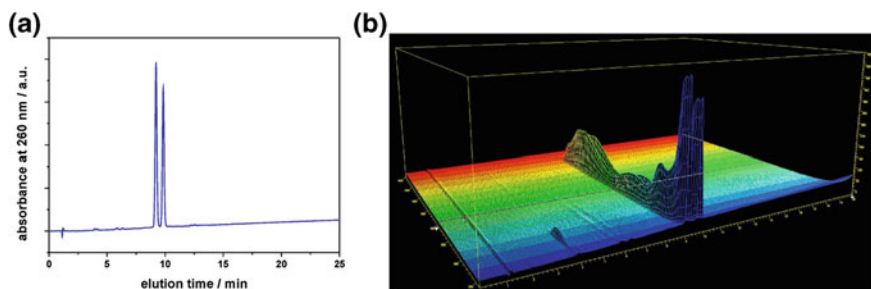


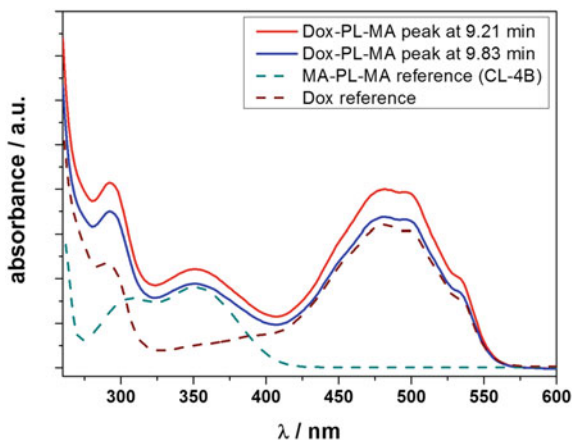
Fig. 5.67 HPLC investigations on the synthesized Dox-PL-MA molecule: **a** elution curve and **b** 3-D elution curves containing the respective UV-vis spectra

In order to further evaluate the spectroscopic properties of the Dox-PL-MA and demonstrate its successful preparation, UV-vis spectra of each fraction from HPLC (peak at 9.21 min and peak at 9.83 min of elution time) were compared to the spectra of pure doxorubicin and pure CL-4B crosslinker as model system for the carbamate based photo-labile linker. The resulting spectra are shown in Fig. 5.68.

As can be seen from the UV-vis spectra of the two enantiomers of Dox-PL-MA, in both samples the absorption band of pure doxorubicin ($\lambda_{max} = 485$ nm) is present in addition to the band of the photo-labile linker ($\lambda_{max} = 350$ nm), thus indicating a successful attachment of the drug to the polymerizable methacrylate unit via the photo-cleavable chromophore.

Regarding the light-induced release of doxorubicin under mild conditions by photolysis of the Dox-PL-MA molecules, it is of high importance that the chemical structure of the drug molecule is not influenced by the irradiation. A pre-requirement is a low extinction coefficient in the spectral region used for light-induced cleavage. Since the photo-labile linker molecule exhibits a high absorbance at $\lambda = 350$ nm, this wavelength was targeted for irradiation experiments. In comparison, the pure

Fig. 5.68 UV-vis spectroscopic investigations: Spectra of the 2 Dox-PL-MA enantiomers in comparison to the spectra of pure doxorubicin and CL-4B as carbamate based model compound for the pure photo-labile linker



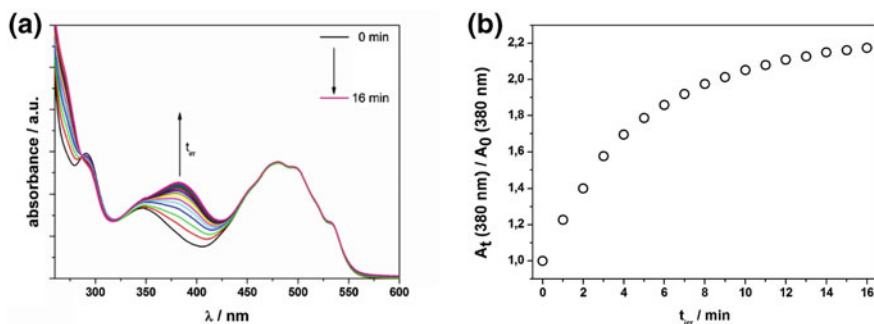


Fig. 5.69 Kinetic investigations on the photolytic degradation of Dox-PL-MA in THF solution: **a** irradiation time-dependent UV-vis spectra; **b** relative absorbance of Dox-PL-MA at $\lambda = 380$ nm in dependency on the irradiation time. Data obtained from M. Dröge

doxorubicin molecule features only a negligible absorbance at this wavelength. This characteristic should in principle enable the controlled drug detachment without light-induced changes in the biological active molecule.

Summarizing the observations described above, a novel functional monomer consisting of a doxorubicin molecule covalently attached to a methacrylate group via a photo-labile linker was successfully synthesized. Utilization of the incorporated radically polymerizable moiety is assumed to give rise to the preparation of a wide range of polymeric light-triggered delivery systems by copolymerization of the synthesized compound with different monomers. As mentioned above the incorporation of those molecules into water-swallowable microgels is of special interest. Moreover, since the attachment of the drug to the photo-labile linker-methacrylate molecule was the last step in the examined synthetic protocol, the activated precursor (12) is assumed to be modifiable with a multitude of functional compounds bearing either a hydroxyl- or amine group. Hence, the described synthetic concept is assumed to be transferable to the preparation of a broad variety of polymeric systems for light-triggered cleavage/release applications.

Photolysis of the cleavable Dox-PL-MA in solution. In comparison to studies performed on the photo-cleavable crosslinkers described in a previous chapter, the photo-degradation behavior of the Dox-PL-MA was first investigated by irradiation time-dependent UV-vis measurements in THF solution. Figure 5.69a depicts the recorded spectra.

Irradiation of Dox-PL-MA with UV light of the wavelength of $\lambda = 365$ nm resulted in red shift of the absorption maximum to $\lambda_{max} = 380$ nm. This light-induced change of the absorption spectra together with the observed well defined isosbestic points point towards a successful photoreaction. It is noteworthy that the absorbance band at $\lambda_{max} = 485$ nm assigned to the doxorubicin molecule did not change upon irradiation in the investigated time span. This is assumed to be a sign for the drug molecule not being influenced by the application of UV light of this particular wavelength.

Figure 5.69b shows the relative absorbance of the compound at 380 nm as a function of irradiation time (Abs_t/Abs_0), where Abs_0 and Abs_t are the absorbances at time zero (0) and a specific time (t). The relative absorbance value reached a plateau after an irradiation time of approximately 14 min thus indicating no further photoreaction.

Summarizing these experiments, the photolysis of the Dox-PL-MA molecules was demonstrated to proceed fast under mild irradiation conditions (UV-A light, low intensity). Especially the unaltered absorbance of the drug molecule, points towards a release of the intact drug molecule.

Synthesis and characterization of p(HEMA-co-MAA) microgels as model systems for Dox-PL-MA containing hydrogel nanoparticles. As mentioned above, the polymerizable methacrylate unit in the Dox-PL-A molecule is designed to enable the preparation of photo-sensitive polymeric carrier systems by copolymerization of the synthesized compound with a broad variety of functional monomers. Having demonstrated the good cellular uptake of p(HEMA-co-MAA) microgels in a previous chapter, incorporation of Dox-PL-MA into these materials represents a highly interesting approach to the light-triggered release of doxorubicin from water-swallowable microgels.

Incorporation of Dox-PL-MA into p(HEMA-co-MAA) microgels can be achieved in situ during nanoparticles formation by free radical copolymerization in inverse miniemulsion. Following this approach, a high loading efficiency is assumed since embedding of doxorubicin is realized by its covalent attachment to the network-forming copolymer rather than by electrostatic interactions between the drug molecule and the gel. As a result, leakage should be dramatically hindered. Nevertheless, as the stability of doxorubicin is known to be sensitive to its environment (e.g., pH, temperature) [83], microgel formation has to be conducted under mild conditions. Therefore, in a first attempt, a new “gentle” preparation route to p(HEMA-co-MAA) microgels was developed in order to ensure the stability of the drug during its incorporation.

In comparison to the previously reported procedure (see Sects. p(HEMA-co-MAA) microgels: pH-dependent swelling in aqueous media and Dual Stimuli-Responsive p(HEMA-co-MAA) Microgels:pH-Dependent Swelling and Light-Induced Degradation), the new route is based on forming the dispersed phase of the inverse miniemulsion from a solution of HEMA, DEGDMA and potassium methacrylate in PBS buffer. In contrast to using the free methacrylic acid, the pH of the dispersed phase is here adjusted by the buffer to a neutral value of 7.4. This is assumed to prevent an acid-induced degradation of the glycosidic bond [83] in the drug molecule. Moreover, by using V-70 as thermal initiator with a low decomposition temperature, the polymerization temperature can be dramatically lowered to 37 °C.

Based on these considerations, p(HEMA-co-MAA) model microgels M-MG-0 were prepared by free radical copolymerization in inverse miniemulsion. The molar amount of DEGDMA crosslinker and the molar ratio of K-MAA/HEMA were similar to FL-MG microgels (see Sect. p(HEMA-co-MAA) microgels: fluorescent

Table 5.9 Nominal composition of p(HEMA-*co*-MAA) model microgels prepared under mild conditions

Sample	Monomer				Solvent		Crosslinker		
	Type	m/mg	Type	m/mg	Type	m/mg	Type	m/mg	mol-% ^a
M-MG-0	HEMA	637.5	K-MAA	161.4	H ₂ O	150	DEGDMA	37.5	2.5
					PBS	150			

^a w.r.t. all monomers

labeling and cell tests) in order to retain the observed good cellular uptake and low cytotoxicity. Table 5.9 lists the used amounts for the dispersed phase.

After polymerization, the dispersion was repeatedly washed with cyclohexane to remove excess surfactant. The purified particles were characterized regarding the particles sizes by DLS and SEM was used to investigate the morphology of the non-swollen gel particles. Hydrodynamic diameters obtained from DLS measurements together with representative scanning electron micrographs of the microgels are shown in Fig. 5.70.

It can be seen that microgels of hydrodynamic diameters around 110 nm with relatively narrow size distributions were obtained. These observations are in good agreement with the results obtained for FL-MG microgels. Hence, it can be concluded that the particle sizes and morphologies are not influenced by this preparation method. Regarding the swellability of the microgels, in contrast to FL-MG microgels, no base addition was needed to achieve swollen particles. This is assumed to further enhance the stability of the pH-sensitive doxorubicin during the formation of the carrier system. DLS measurements of the swollen particle dispersions in PBS yielded hydrodynamic diameters of around 250 nm. The respective *DGS* of 12.4 is in good agreement with the value obtained for FL-MG microgels (*DGS* = 12.0).

It can be concluded, that the new mild microgel preparation method yielded well defined p(HEMA-*co*-MAA) M-MG-0 model particles. The respective

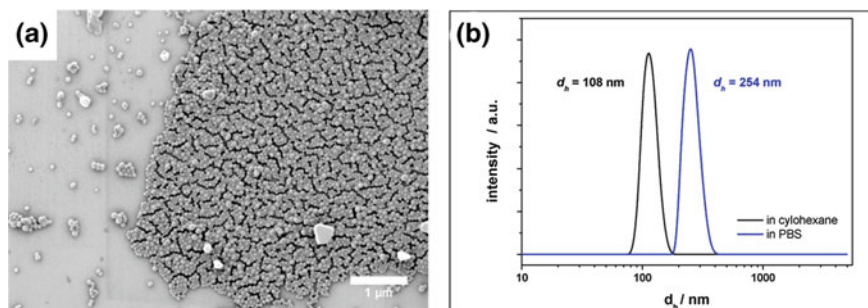


Fig. 5.70 Characterization of p(HEMA-*co*-MAA) model microgels prepared under mild conditions: **a** representative SEM image of the microgels drop cast from cyclohexane dispersion; **b** number weighted particles size distribution of particles in cyclohexane and PBS as determined by DLS

microgel properties did not vary significantly from those observed for FL-MG microgels. Consequently, it is proposed that the biocompatibility of the M-MG-0 particles does not vary from their FL-MG analogues.

Conclusion and outlook

Summarizing the results described in this chapter, it can be concluded that an efficient synthetic route to a novel functional monomer consisting of a doxorubicin molecule covalently attached via a photo-labile linker to a radically polymerizable methacrylate group was successfully developed. Copolymerization of the synthesized compound with different monomers is assumed to give rise to a wide range of polymeric light-triggered delivery systems. In this context, polymer-drug conjugates, polymeric micelles, hydrogels, hydrogel thin films or especially hydrogel nanoparticles are imaginable.

Moreover, the activated precursor (12) is assumed to be modifiable with a multitude of functional compounds bearing either a hydroxyl- or amine group. Hence, the described synthetic concept is assumed to be transferable to the preparation of a broad variety of polymeric systems for light-triggered cleavage applications. Further investigations following this approach might include the functionalization of the precursor with a bromine containing group serving as initiator for ATRP. Polymerization of this new monomer by a method orthogonal to the ATRP concept is assumed to yield a reactive polymer which can be further functionalized with polymeric arms by a grafting from approach. Irradiation with light is then assumed to detach the grafted polymers from the backbone.

With respect to the photolysis of the Dox-PL-MA molecules, the doxorubicin moiety is characterized by a minor extinction coefficient at the wavelength used for cleavage. As demonstrated by irradiation time-dependent UV-vis measurements, this characteristic enables the controlled drug detachment without light-induced changes in the pharmaceutically active molecule.

Generally, the doxorubicin-photo-labile linker-methacrylate (Dox-PL-MA) moiety is assumed to be copolymerizable with a broad variety of hydrophilic monomers. Having demonstrated the observed good cellular uptake and negligible cytotoxicity of p(HEMA-*co*-MAA) microgels, copolymerization of the Dox-PL-MA molecule with HEMA and MAA in inverse miniemulsion is assumed to yield anionic microgels as well defined carrier systems for the light-triggered delivery of doxorubicin. In a first step, a mild preparation method for p(HEMA-*co*-MAA) microgels was elaborated in order to ensure the potential incorporation of the Dox-PL-MA in situ during nanoparticles formation without damaging the drug molecule.

As outlook, transferring this newly developed mild preparation route for p(HEMA-*co*-MAA) microgels to the formation of analogous hydrogel nanoparticles containing the Dox-PL-MA conjugate is of high interest. Resulting microgels should be investigated with regard to the incorporation efficiency of doxorubicin, and the light-triggered release profile of the drug from the network in PBS. Moreover, cell tests should be performed in order to examine the cellular uptake of the prepared particles. In this context, it is assumed that drug loaded microgels incorporated into cells do not influence cell viability if kept in the dark. In contrast, the light-triggered

release of doxorubicin should result in a pronounced cytotoxicity. Control experiments of irradiating cells with incorporated non-loaded microgels should be performed in order to take potential light-induced damages into account.

5.4 Photo-Resist Nanoparticles: Light-Induced Degradation of Hydrophobic Polymers in Aqueous Dispersion

In the previous chapters, the preparation and characterization of novel light-sensitive microgels has been investigated. Examined approaches included among others: (a) crosslinked hydrophobic polymer lattices degradable in non-polar organic solvents and (b) hydrogel nanoparticles swellable and degradable in aqueous dispersion. Both concepts are based on exploiting the good solubility of the network-forming (co)polymer in the respective solvent. Here, particle degradation is achieved by cleaving photo-labile crosslinking points responsible for retention of the particulate structure of the swollen networks. By this, the investigated materials show great potential for the loading and release of functional compounds of a hydrophilicity similar to the gel network and the specific solvent.

In general, especially the development of carrier systems for the delivery of active substances in aqueous medium is of high interest for a broad variety of applications. The described concept of degradable hydrogel nanoparticles is nevertheless restricted to the loading and release of hydrophilic substances. In addition, it is of interest to be able to deliver hydrophobic substances in water as well, since it holds promise to widen the fields of application dramatically. Investigations to realize this concept are mainly based on micellar aggregates of amphiphilic block copolymers which enable the embedding of non-polar molecules in the hydrophobic core [34]. In comparison, polymeric nanoparticles are characterized by their outstanding ability to maintain their initial structural integrity in diverse environments [74, 84]. The combination of this characteristic with the ability to disassemble in a controlled fashion upon an applied stimulus is of high interest for a broad variety of applications including the fields of drug delivery [85], catalysis, optics and colloidal crystals [36, 41]. In this context, a novel approach for the embedding of hydrophobic drugs into non-swollen pH-sensitive hydrophobic nanoparticles based on acetal protected polymers was recently described by Griset et al. A triggered release was achieved by changing the hydrophilicity of the network-forming polymer from hydrophobic to hydrophilic. Hereby, the resulting swelling of the particles induced the release of the payload [77]. Another approach to degradable nanoparticles was investigated by

Parts of this work are published as “Polymeric Photo-Resist Nanoparticles: Light-Induced Degradation of Hydrophobic Polymers in Aqueous Dispersion” Daniel Klinger, Katharina Landfester, *Macromol. Rapid Comm.* **2011**, 32 (24), 1979. Reprinted with permission from [87]. Copyright 2011 Wiley Periodicals, Inc.

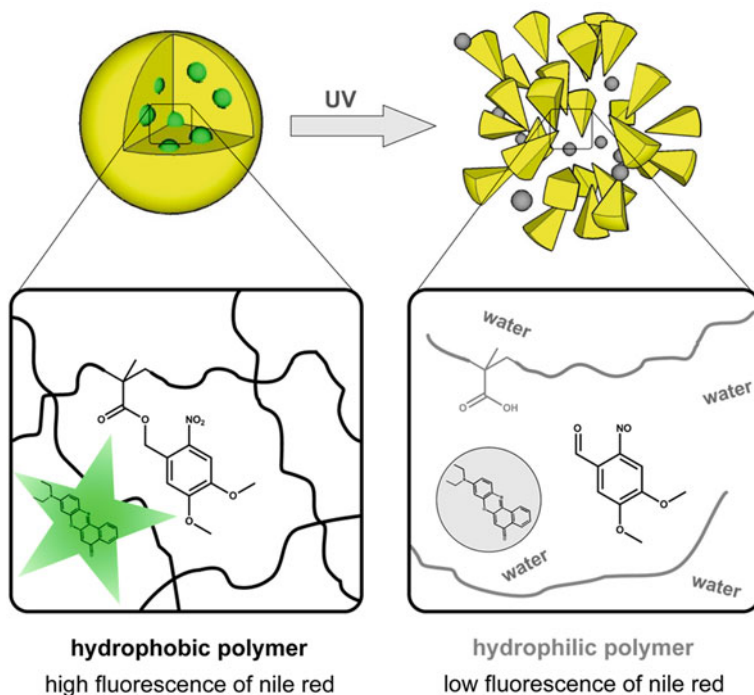


Fig. 5.71 Schematic illustration of the concept of light-degradable polymeric photo-resist nanoparticles. *Note* overlapping of schematic polymer chains in the initial particles refers to entanglement and not to crosslinking. Reprinted with permission from [87]. Copyright 2011 Wiley Periodicals, Inc

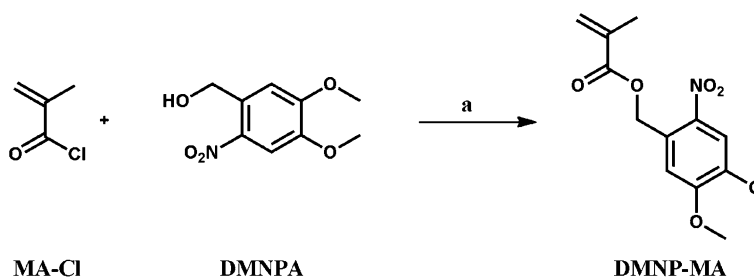


Fig. 5.72 Synthesis of DMNP-MA. Reagents and conditions: **a** triethylamine, DCM, 0 °C, 1 h then 25 °C, 16 h, 87 %

Fomina et al. Here, light-degradable nanoparticles were prepared by a solvent evaporation method from a preformed photo-degradable polymer. The examined polymer combined multiple light-sensitive triggering groups along the backbone

with quinine-methide self-immolative moieties [86]. A drawback however, is the complex preparation method including several extensive synthetic steps.

Based on these considerations, the work described in this chapter deals with the development of hydrophobic nanoparticles consisting of a photo-resist polymer. Particle preparation by free radical polymerization in miniemulsion represents a facile alternative to the concept described by Fomina et al. These lattices are designed to be degradable upon a light-induced change of the hydrophobicity of the respective material. The polymeric structure is based on a labile protected poly(methacrylic acid) (PDMNB-MA) that can be easily de-protected by the photolytic cleavage of the *o*-nitrobenzyl esters. As a result, conversion of the initial hydrophobic polymer into hydrophilic PMAA induces *in situ* particle dissolution in water. With the aim to investigate the potential of the described particles for release applications, Nile red was encapsulated as a model compound. Nile red as a hydrophobic dye bears the advantage of acting as a fluorescent probe due to its high fluorescence sensitivity toward changes in polarity. Thus, incorporation of Nile red into PDMNB-MA nanoparticles allows for studying not only the particle degradation process (via solubilization of *in situ* generated PMAA during photo-cleavage of PDMNB-MA), but also the possibility to perform controlled release experiments. The concept is schematically illustrated in Fig. 5.71.

Selection and synthesis of the monomer, (4,5-dimethoxy-2-nitrobenzyl methacrylate (DMNB-MA)). The monomer 4,5-dimethoxy-2-nitrobenzyl methacrylate (DMNB-MA) was synthesized by the modification of a reported procedure [88]. As shown in Fig. 5.72, the desired product can be obtained in good yield by a one-step reaction of methacryloyl chloride (MA-Cl) with 4,5-dimethoxy-2-nitrophenyl alcohol (DMNPA).

Regarding the light-induced cleavage of the photo-labile *o*-nitrobenzyl ester bond, irradiation conditions represent a crucial parameter. As mentioned in previous chapters, to avoid unwanted Norrish-type side reactions, the wavelength absorbance of the photo-cleavable moiety must be higher than 315 nm [12, 13]. Thus, the presence of methoxy groups in the aromatic core of the *o*-nitrobenzyl chromophore was necessary to shift the absorption to higher values [11]. The synthesized DMNB-MA monomer indeed showed an absorption band at $\lambda = 350$ nm thus enabling photolysis under mild conditions in a controlled way.

Nanoparticle preparation by miniemulsion polymerization. Due to the melting point of DMNB-MA above room temperature, suitable methods for nanoparticle formation are generally limited. Compared to emulsion polymerizations based on diffusion of liquid monomers, the miniemulsion process represents a big advantage as it can be used to prepare nanoparticles by polymerizing solid monomers in droplets of their respective solutions. In miniemulsions, suppression of diffusion between droplets characterizes each droplet as a nanoreactor. As a result, the incorporation of additional hydrophobic substances—e.g., Nile red as functional dye—is easily achieved [89, 90]. Since the composition of the final latex particles resembles the composition of the monomer phase, all functionalities incorporated are equally distributed in each particle.

The choice of solvent for the photo-labile monomer is limited to a non-water miscible liquid in order to form stable droplets in the miniemulsion. Furthermore, the solvent should enable a good solubility of both the monomer and the resulting polymer. If this would not be the case, phase separation during miniemulsion polymerization could lead to either capsular or non-spherical particle morphologies. Chloroform fulfills all the aforementioned criteria and bears the additional advantage of its ability to act as a chain transfer agent in radical polymerizations generating polymers of decreased molecular weights—compared to polymerizations without chain transfer—and thus increasing the polymer solubility. Since particle degradation is based on simply dissolving the deprotected PMAA polymer in water, a low molecular weight of the polymer is favorable.

Based on these considerations, two different photo-resist nanoparticles (PR-NP) were synthesized using chloroform as solvent for the dispersed phase following a previously reported method [9]. PR-NP1 particles consist of pure poly(DMNB-MA) while PR-NP2 additionally contains Nile red incorporated into the polymeric matrix. Furthermore, polystyrene reference particles without (PS-NP1) and with Nile red (PS-NP2) were prepared under analogous reaction conditions. Nominal feed compositions of the dispersed phases are depicted in Table 5.10.

After purification, the latexes were characterized with regard to the particles sizes and size distributions by DLS, the molecular weight of the polymer by GPC and the encapsulation efficiency (*EE*) of Nile red by fluorescence spectroscopy; results are shown in Table 5.11. The particle morphology was investigated by SEM and Fig. 5.73 exemplarily shows representative images for PR-NP1, PR-NP2, and PS-NP2. The insets depict the corresponding number weighted size distributions obtained from DLS measurements.

As can be seen from DLS data and SEM images, miniemulsion polymerizations yielded in all cases well defined spherical particles in the nanometer size range. As expected the polymerizations yielded polymers of relatively low molecular weights and polydispersities (see Fig. 5.73a).

As mentioned previously, Nile red was incorporated in PR-NP2 and PS-NP2 particles in order to monitor particle degradation and investigate the potential of the concept for release applications. Encapsulation efficiencies were determined by fluorescence spectroscopy. To this end, the fluorescence intensity of dissolved particles in DMSO for PR-NP2 and in 1,4-dioxane for PS-NP2 were compared to beforehand plotted calibration curves. Since fluorescence intensity of Nile red is known to be highly sensitive to the environment [91, 92], dissolved plain particles

Table 5.10 Synthetic parameters for the preparation of PR-NP and PS-NP nanoparticles by miniemulsion polymerization

Sample	Synthetic parameters		
	Monomer type	Dye	
		Type	m/mg
PR-NP1	DMNB-MA	–	–
PR-NP2	DMNB-MA	Nile red	0.500
PS-NP1	Styrene	–	–
PS-NP2	Styrene	Nile red	0.085

Table 5.11 Characterization of particles obtained from miniemulsion polymerization: Results of DLS measurements, the determination of encapsulation efficiencies and GPC measurements of the produced polymers

Sample	Results				
	Diameter ^a d_H /nm	Encapsulation of nile red		M_w (polym.) ^b g/mol	PDI ^b
		EE /% of theory	mol/mg (particles)		
PR-NP1	80 ± 14	–	–	3,954	1.89
PR-NP2	79 ± 15	3.52	2.17 · 10 ⁻¹⁰	3,706	1.77
PS-NP1	77 ± 13	–	–	10,319	2.62
PS-NP2	56 ± 11	6.23	1.67 · 10 ⁻¹⁰	10,777	2.21

^a Determined by DLS measurements; ^b determined by GPC in THF, standard polystyrene

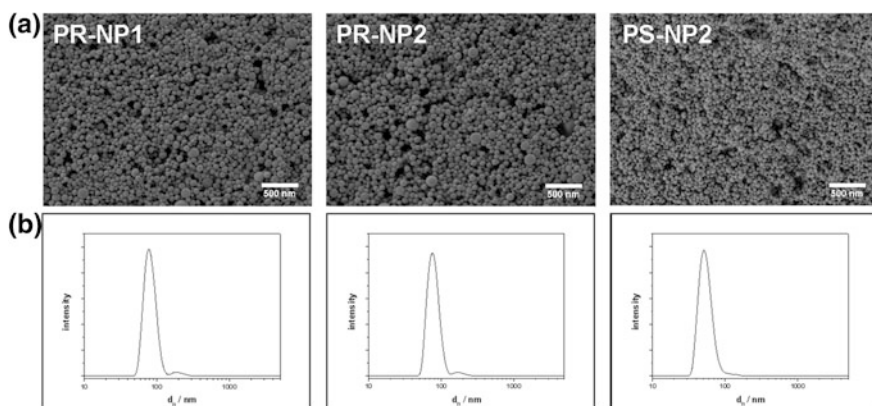


Fig. 5.73 Characterization of particles obtained from miniemulsion polymerization: **a** exemplary representative SEM images of PR-NP1, PR-NP2 and PS-NP2 particles and **b** number weighted size distributions obtained from DLS measurements. Reprinted with permission from [87]. Copyright 2011 Wiley Periodicals, Inc

(PR-NP1 or PS-NP1) in the same concentration as for the dye containing samples were added to every dye calibration solution in order to take the potential influence of the dissolved polymeric matrix into account. Results showed that the encapsulation efficiency of nile red strongly depends on the kind of polymer of the respective particles. While the theoretical incorporation of 0.5 mg of dye into poly(DMNB-MA) particles resulted in an actual EE of 3.52 %, an actual value of $EE = 20.23$ % was determined for polystyrene particles (PS-NP0, data not shown) polymerized under the same conditions. The discrepancies in the encapsulation efficiencies were assigned to differences in the hydrophilicity of the respective polymers. Since polystyrene is comparably less polar, the incorporation of the hydrophobic dye is favored. To ensure comparability of the influence of light on the fluorescence spectra between the different samples of PR-NP and PS-NP, a new polystyrene reference latex (PS-NP2) was synthesized. Adjusting the feed concentration of dye resulted in amounts of incorporated nile red similar to PR-NP2.

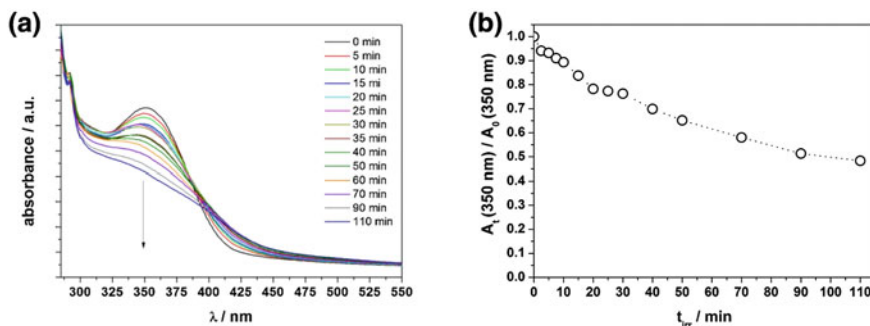


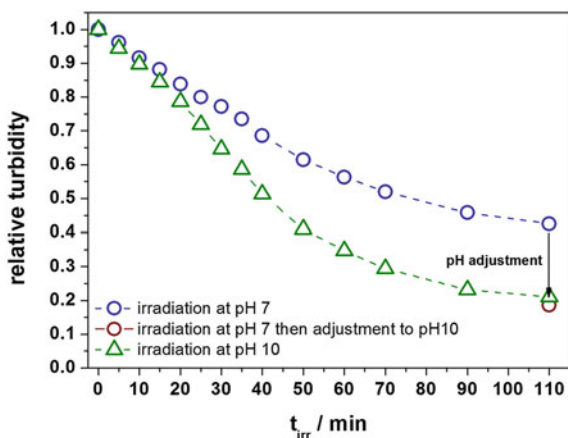
Fig. 5.74 Characterization of PR-NP2 nanoparticles upon irradiation with UV-light: **a** irradiation time dependent UV-vis spectra of the particle dispersion at pH 7; **b** relative UV absorbance at $\lambda_{max} = 350$ nm in dependency on the irradiation time. Reprinted with permission from [87]. Copyright 2011 Wiley Periodicals, Inc

Photolytic degradation experiments. Since well defined nanoparticles consisting of a polymeric photo-resist material were successfully prepared and loaded with Nile red, in the next step, the photolytic degradation behavior of these novel nanostructures was investigated. An aqueous dispersion of PR-NP2 (0.01 % w/v; pH 7) was placed in a quartz cuvette and irradiated with UV-A light ($\lambda = 315\text{--}390$ nm). Samples were taken at fixed time intervals and first investigated by UV spectroscopy. Figure 5.74 shows the obtained results.

As can be seen in Fig. 5.74a of the observed changes in the UV spectra—the initial absorbance at $\lambda = 350$ nm decreases with increasing irradiation time. This strongly suggests a successful photolytic cleavage of *o*-nitrobenzyl ester groups. Additionally, the occurrence of two isosbestic points at 300 and 400 nm evidences a well defined photolytic reaction with no side products. Plotting the relative absorbance intensity at 350 nm against time, the resulting graph in Fig. 5.74b follows an exponential decay down to a constant level, thus suggesting the expected first order kinetics regarding the chromophore concentration. Furthermore, the observed plateau shows that no further photo-cleavage occurs even for longer irradiation times.

Irradiation of the PR-NP2 was found to successfully trigger the photolytic detachment of the hydrophobic chromophore from the polymer backbone. The resulting light-induced transformation of the original hydrophobic p(DMNB-MA) polymer to the hydrophilic PMAA causes particle dissolution in water, which is assumed to follow a complex mechanism. In the early stages of irradiation, photolysis of the labile protecting groups renders the polymer hydrophilic, thus inducing swelling of the particles and formation of gel-like structures with increased diameters. Since PR-NP2 particles are not covalently crosslinked, the spherical structures can only be retained to a certain degree by physical crosslinks due to entanglement of polymer chains and/or hydrophobic interactions between not yet de-protected DMNB-MA moieties. Further irradiation leads to the diffusion of hydrophilic chains out of the particles and the complete spherical morphology disappears.

Fig. 5.75 Characterization of PR-NP2 nanoparticles upon irradiation with UV light. Relative turbidity in dependency on the irradiation time and the pH of the dispersion. Adapted with permission from [87]. Copyright 2011 Wiley Periodicals, Inc



Turbidity measurements can take both phenomena into account. An increase of the particle diameter due to a swollen gel-like structure results in a reduced scattering intensity caused by a reduced contrast between solvent and particle [18, 19]. In addition, the diffusion of free hydrophilic chains out of the particles represents particle degradation, yielding fragments with decreased sizes. As smaller fragments are characterized by a decreased scattering intensity, turbidity measurements are in this context highly advantageous compared to DLS. Irradiation time-dependent turbidity measurements performed on PR-NP2 dispersed in water adjusted to different pH values are shown in Fig. 5.75.

The decrease in turbidity upon irradiation time as shown in Fig. 5.75c demonstrates successful particle degradation (including both: swelling and dissolution). However, for pH 7 the observed values only drop to a constant level of around 40 % indicating incomplete degradation. As the irradiation experiments were carried out in deionized water at neutral pH and the hydrophilicity of the generated PMAA is strongly dependent on the pH, the resulting samples were basified with diluted NaOH to pH 10 and turbidity was measured again. The resulting drop in the relative scattering intensity to a value of around 17 % strongly suggests that both photo-cleavage and subsequent particle dissolution occurred favorably at basic pH values possibly due to deprotonation of the carboxylic acid groups of PMAA. Here, the electrostatic repulsion of the anionic groups generated under basic conditions, plus the enhanced solubility of the respective carboxylates in water, leads to complete dissolution.

In a next attempt, irradiation experiments of PR-NP2 in aqueous medium at pH 10 were conducted and the resulting turbidity curve is shown in Fig. 5.75. Compared to the irradiation carried out at pH 7, a direct decrease of the relative turbidity to 21 % was observed. The value is similar to the one of 17 % obtained for basification of the neutral dispersion after irradiation and corresponds as well to complete particle dissolution. As complete PR-NP2 particle dissolution was found to require basic conditions, it was demonstrated that this obligation could either be

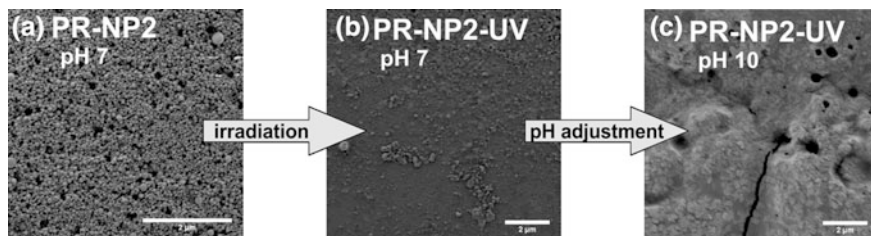


Fig. 5.76 Characterization of PR-NP2 nanoparticles upon irradiation with UV-light. Representative SEM images of PR-NP2 photo resin nanoparticles: **a** before and **b** after irradiation in pH 7; **c** after irradiation in pH 7 and titration to pH 10. Reprinted with permission from [87]. Copyright 2011 Wiley Periodicals, Inc

fulfilled by increasing the pH subsequent to irradiation at neutral pH or by directly irradiating particles dispersions at pH 10.

In order to visualize the particle degradation and investigate the proposed morphological changes in the PR-NP2 particles, SEM images were taken before and after 110 min of irradiation at different pH values. Figure 5.76 shows the obtained micrographs.

SEM images shown in Fig. 5.76 support the previous statement regarding the particle degradation. While pictures taken of the samples directly after irradiation in pH 7 (Fig. 5.76b) still show to some extent deformed particulate structures, micrographs of the same sample after adjusting the pH to pH 10 (Fig. 5.76) only depict a polymeric film. Moreover, a similar polymeric film was observed for the direct irradiation of PR-NP2 particles in pH 10 (data not shown).

Monitoring particle degradation by fluorescence spectroscopy of incorporated nile red. It is well known that the fluorescence of nile red strongly depends on the polarity of the matrix in which it is contained [91, 92]. While in apolar hydrophobic surroundings the dye is highly fluorescent, a hydrophilic environment significantly reduces its fluorescence to almost negligible values in water. This specific characteristic of nile red permitted the indirect study of the particle degradation by fluorescence measurements. Figure 5.77 shows irradiation time dependent fluorescence spectra of PR-NP2 and PS-NP2 lattices in aqueous dispersion.

From Fig. 5.77a it can be seen that the fluorescence intensity ($\lambda_{exc} = 555$ nm) of nile red in PR-NP2 decreases after only a few minutes of irradiation to an almost negligible value. Since photo-bleaching of the dye could occur due to the irradiation, photolytically stable polystyrene reference particles containing a similar amount of incorporated dye were irradiated in a control experiment. In this case the sample contained additional plain p(DMNB-MA) PR-NP1 particles in order to take the influence of the absorbance of the photo-cleavable chromophores into account. Comparing the resulting fluorescence spectra ($\lambda_{exc} = 530$ nm) in Fig. 5.77b to those of PR-NP2 in Fig. 5.77a, a minor loss of fluorescence intensity of nile red in the PS-NP2 particles was observed.

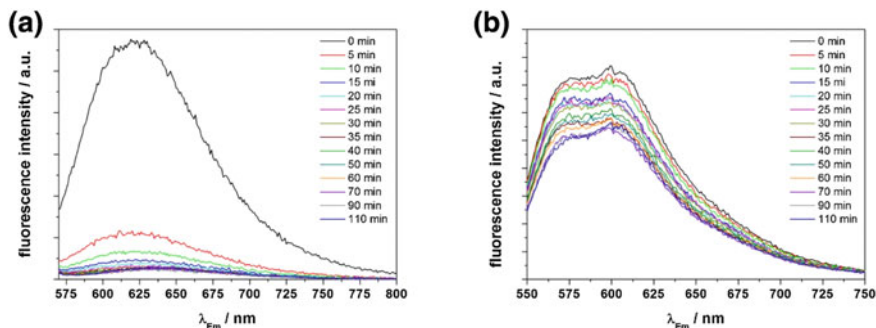
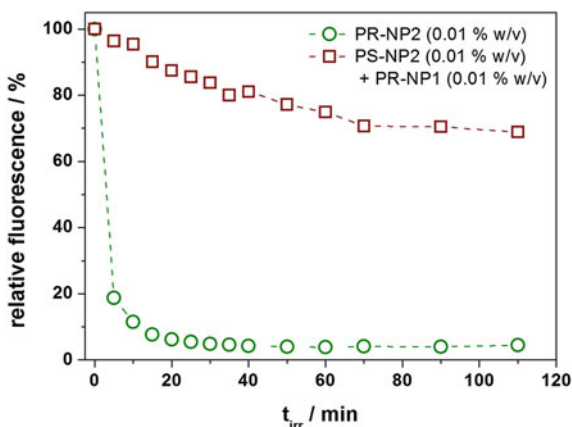


Fig. 5.77 Fluorescence measurements of Nile red containing particle dispersion upon irradiation with UV light: **a** emission spectra ($\lambda_{exc} = 555$ nm) of PR-NP2; **b** emission spectra ($\lambda_{exc} = 530$ nm) of a mixture of PS-NP2 reference particles and plain PR-NP1 lattices. Reprinted with permission from [87]. Copyright 2011 Wiley Periodicals, Inc

This comparison is further visualized by plotting the relative fluorescence intensities at the respective maxima ($\lambda_{em} = 628$ nm for PR-NP2 and $\lambda_{em} = 584$ nm for PS-NP2) with respect to the irradiation time (see Fig. 5.78).

The comparably much less pronounced decrease in intensity observed for the dye incorporated in a polystyrene matrix was assumed to be caused by photo-bleaching, whereas the decrease in the photo-resist matrix results from successful particle degradation. Therefore, the observed decrease within the first 15 min of irradiation suggests a successful change in the hydrophilicity of the polymeric matrix. Even though no complete particle degradation was observed for this stage by turbidity measurements, photolytic deprotection of MAA groups rendered the particle-forming polymer chains more hydrophilic which may result in a porous-like structure. This gel-like swollen state of the former hard spheres enables the penetration of water molecules into the matrix, thus quenching the fluorescence of the sensitive dye.

Fig. 5.78 Fluorescence measurements of Nile red containing particle dispersion upon irradiation with UV-light: irradiation time-dependent relative values of the fluorescence intensities at the respective maxima for PR-NP2 in comparison to PS-NP2. Reprinted with permission from [87]. Copyright 2011 Wiley Periodicals, Inc



It can be concluded that for potential release applications no complete particle degradation has to be achieved in order to enable the diffusion of compounds into or out from the particles. Nevertheless, appliance of longer irradiation times in combination with an increased pH can be used to completely degrade the particle structures due to photolytic inversion of the hydrophilicity of the particle forming polymer.

Conclusion

Nanoparticles consisting of a polymeric photo-resist material were successfully prepared in a facile way by direct miniemulsion polymerization of a newly synthesized light-sensitive monomer. Particle degradation in aqueous dispersion was achieved by irradiation with UV light and is based on the inversion of the hydrophilicity of the initial hydrophobic polymer. The successful incorporation of Nile red as a hydrophobic dye served as a probe to confirm particle degradation. Irradiation induced quenching of the fluorescence points towards the enabled diffusion of either water into- or Nile red out from the former hard sphere structures, therefore rendering the described nanoparticles very attractive for potential release applications of hydrophobic compounds in aqueous media. This concept—in combination with the previously described photo-degradable microgel approaches—dramatically widens the range of applications for photo-sensitive nanoscale materials. Moreover, the confinement of a photo-resist material to nanoscaled structures gives rise to potential new ways of surface patterning by e.g., colloidal lithography.

5.5 Towards Stimuli-Responsive Core/Shell Nanoparticles Containing a Microgel Core

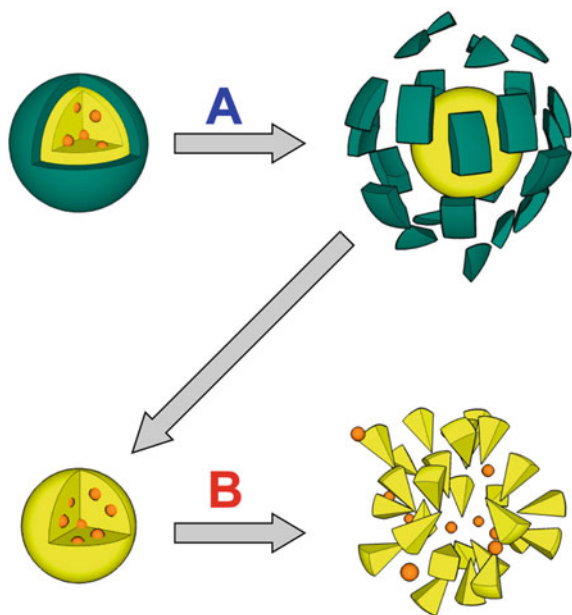
As described previously, the utilization of stimuli-responsive microgels for delivery applications is crucially governed by an efficient loading of the network with the functional compound to be released. Especially for small molecules the respective loading efficiency is strongly limited by the leakage of the active substances from the network [35, 93]. Therefore, it is of high importance to ensure a successful retention of the functional molecule in the carrier system until the desired site or time point for its triggered release is reached. This can be achieved by several approaches including, among others, the embedding of hydrophobic drugs into either non-swollen hydrophobic polymeric nanoparticles and their stimuli-induced swelling [77, 86] or into hydrophobic domains in hydrophilic microgels [94]. The covalent attachment of a drug to a hydrophilic polymeric carrier system via a cleavable molecule and the triggered degradation of the linker is another promising method [81, 82]. Investigations on light-sensitive materials based on both of the described concepts are part of this thesis and were described in previous chapters (see Sects. 5.3 and 5.4).

An alternative concept to enhance the loading and release efficiency of stimuli-responsive microgels is based on the introduction of a degradable/swellable (polymeric) shell around the respective microgel core [95–97]. Hereby, the shell serves as a diffusion barrier to prevent leakage of embedded functional compounds [98, 99]. Based on this consideration, the work described in this chapter deals with studies to investigate potential synthetic pathways for the formation of multiple stimuli-responsive core/shell nanoparticles containing a hydrogel core. A microgel core sensitive to a certain trigger B is designed to exhibit a specific stimuli-dependent release profile of an embedded functional compound. The introduction of a polymeric shell around this microgel core should enable a high loading efficiency since non-controlled diffusion from the network is hindered. By rendering the shell forming polymer sensitive to a second trigger A orthogonal to trigger B, a highly selective release profile can be realized. The overall release is then induced by first degrading/swelling the polymeric shell upon the appliance of trigger B, thus destructing the diffusion barrier. Secondly, the diffusion of the active compound from the microgel can subsequently be triggered by the trigger A. Figure 5.79 schematically illustrates the described concept.

The aim of the work described in this chapter is to investigate different synthetic routes for the preparation of non-stimuli-responsive core/shell nanoparticles as model compounds. Results from these experiments are expected to be transferable in a modified way to their stimuli-responsive analogues.

In general, different ways to core/shell nanoparticles are reported in the literature and can be divided into two different orthogonal pathways: (i) the shell formation around a preformed (microgel) core and (ii) the formation of the

Fig. 5.79 Schematic illustration of the concept of stimuli-responsive core/shell microgels for release applications: shell degradation upon appliance of trigger A and subsequent core disintegration upon appliance of trigger B, orthogonal to trigger A



microgel core in a polymeric shell, i.e., in a nanocapsule. Route (i) can be realized by either seeded precipitation/dispersion polymerization of a second monomer in the presence of seed particles representing the core [100, 101] or nanoprecipitation of a preformed polymer around preformed nanoparticles or liquid droplets [97, 102]. The orthogonal synthetic pathway (ii) can be realized by first forming nanocapsules through either polycondensation reactions [103] or nanoprecipitations of preformed polymers [102] on the surface of droplets containing monomers and crosslinkers polymerizable by a different mechanism. In a second step, microgel cores are then formed in the nanoreactors. Investigations on two of the mentioned orthogonal approaches based on polyacrylamide cores as non-stimuli-responsive model systems are subject of the following chapters.

5.5.1 PAAm/PMMA Core/Shell Nanoparticles by Seeded Dispersion Polymerization

Dispersion and precipitation polymerizations are typically based on initiating the polymerization of a solution of a monomer (and crosslinker) in a near θ solvent for the respective polymeric analogue [104–106]. While the polymerization proceeds, the monomer and formed oligomers are soluble until the growing chains reach a critical length. As a result of unfavorable polymer–solvent interactions, they phase-separate from the continuous medium by enthalpic precipitation, thus forming particle nuclei. In the case of crosslinkers present in the mixture, entropic precipitation occurs favorably. Here, crosslinking prevents the polymer and solvent from freely mixing even in good solvents for the polymer [107]. The resulting nuclei aggregate into larger particles that continue to grow by capturing other particles, by newly formed polymer chains or by absorption and polymerization of monomer. In this context, dispersion polymerizations are characterized by the addition of a steric stabilizer to control the size and narrow the distribution of the particles [108].

Based on this concept, the preparation of (crosslinked) core/shell nanoparticles can be achieved by a seeded dispersion polymerization which is based on a comparable mechanism. Here, the precipitation of formed oligomers of a critical chain length occurs preferentially on the surface of preformed seed particles present in the reaction mixture, thus forming core/shell particles [41, 109, 110]. An obligation for this concept, however, is the suppression of secondary nucleation, forming particles only consisting of the polymer proposed to form the shell. The formation of core/shell nanoparticles without secondary nucleation crucially depends on a high concentration of the seed particles [111]. Since a larger number of seed particles in the system corresponds to a larger surface area available for precipitation, secondary nucleation is hindered. Moreover, successful precipitation also depends on the interaction parameters between the shell forming polymer and the core. Since precipitation around the core is an enthalpy driven process, a

similar chemical nature/hydrophilicity of the two polymers is assumed to favor this mechanism. Regarding the preparation of core/shell nanoparticles from polymers exhibiting a very dissimilar interaction parameter with the solvent, incorporation of vinyl groups on the seed particle surface was shown to result in the formation of a shell due to capturing of formed oligomeric radicals [109].

Since the aim of this work is to build a polymeric shell around microgel cores in order to serve as diffusion barrier for potential embedded compounds, a requirement of the shell forming polymer is either an increased hydrophobicity or orthogonal swellability compared to the hydrogel core. Investigations described in this chapter focus on the utilization of a preformed crosslinked polyacrylamide core as seed particle and the formation of a poly(methyl methacrylate) shell by seeded precipitation polymerization of MMA. The described materials were chosen for two reasons: (a) the relatively hydrophobic nature of PMMA is assumed to give rise to a non-water-swellable shell, thus “sealing” the hydrogel core and (b) the chemical structure of PMMA resembles the structure of PAAm in such an extent that the enthalpic precipitation around the core is assumed to be enabled. Figure 5.80 schematically illustrates the proposed synthetic pathway.

Preparation of PAAm core nanoparticles (C-NP). PAAm microgels as core nanoparticles (C-NP) were prepared in analogy to a previously described method (see Sect. 5.2) by free radical copolymerization of AAm with DEGDMA (5 wt.-%) in inverse miniemulsion. After polymerization, the particles were washed repeatedly with cyclohexane in order to remove excess surfactant and characterized by means of the particle size and morphology by PCCS and SEM. Figure 5.81 shows representative SEM images of the particles dropcast from either

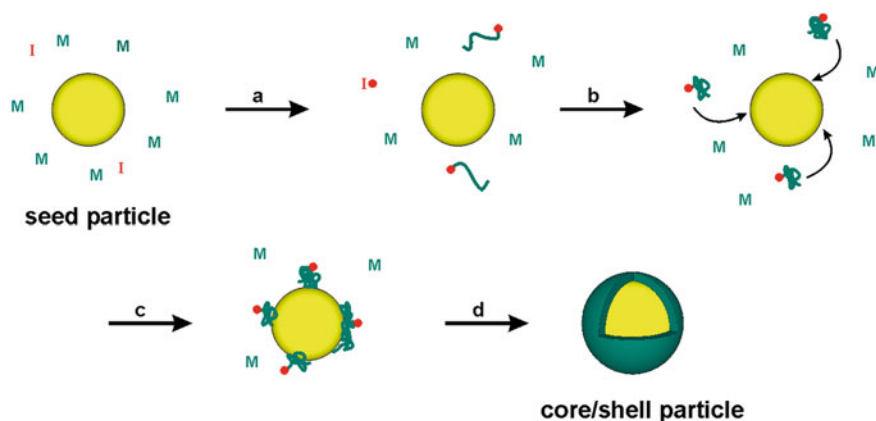
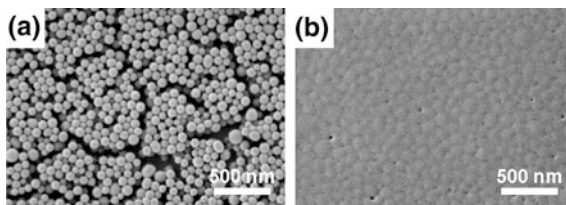


Fig. 5.80 Simplified schematic illustration of a seeded precipitation polymerization process containing several steps: **a** initiation and propagation of the shell-forming monomer to soluble oligomers, **b** growth of oligoradicals until critical chain length for precipitation is reached and precipitation around the seed particles, **c** chain growth on particle surface, **d** final core/shell particle. Note: This model is simplified and does not depict potential secondary nucleation

Fig. 5.81 Characterization of C-NP particles by SEM: **a** drop cast from cyclohexane dispersion and **b** drop cast from MeOH/H₂O 40/60 dispersion



cyclohexane or MeOH/H₂O (40/60) dispersions and the corresponding size distributions.

Investigations on the preparation of PAAm/PMMA core/shell nanoparticles (C/S-NP) by seeded precipitation polymerization. Successful preparation of core/shell nanoparticles by seeded precipitation polymerization crucially depends on various parameters such as: (i) the solvent, (ii) the seed particles concentration, (iii) the type and amount of initiator, (iv) the amount of monomer and (v) the amount and chemical nature of a potential surfactant. In order to get an insight into the formation possibilities of PAAm/PMMA core/shell nanoparticles, first experiments were conducted by keeping the parameters (i)–(iv) constant thus investigating the influence of an additional surfactant to the shell formation procedure.

The so defined system took the following considerations into account. Regarding (i), the used solvent has to fulfill three important criteria: (a) enabling a good colloidal stability of the microgel core particle, (b) enabling a good solubility of the monomer used for the preparation of the polymeric shell, and (c) enabling the precipitation of the shell forming polymer upon growing chain lengths. Keeping those requirements in mind, a solvent mixture of methanol/water (40/60 v/v) was found to be suitable. As mentioned above, another important principle to be considered is the suppression of secondary nucleation. This can be achieved by the utilization of a large number of seed particles. Based on investigations made by Jiang et al. [111], a seed particle concentration of $4.3 \cdot 10^{15}$ N_p/L was chosen for the conducted experiments. The next parameter (iii) defining the specific system is the type and amount of initiator. Here, KPS was chosen, since it showed a good solubility in the described solvent mixture. The concentration with respect to the MMA monomer was kept constant throughout all conducted experiments. As a last parameter (iv), in all seeded precipitation polymerizations, an amount of 10 weight equivalents of MMA with respect to the seed particles was used. By this, a shell with a diameter comparably large to the core is assumed to be formed. This is proposed to enable the visualization of the successful formation of the polymeric shell by determining the increase in the overall particle diameters by SEM.

Investigations on the influence of type and amount of surfactant. As mentioned above, having set all other parameters than the type and amount of surfactant to a constant value, this specific system allows to examine the uncoupled influence of the latter on the preparation method.

In a first attempt, the seed particles were dispersed in MeOH/water (40/60) without an additional surfactant. After the addition of MMA to the mixture, the

particles were found to macroscopically aggregate. This effect was assigned to a deswelling of the particles upon the addition of MMA as a non-solvent for the polyacrylamide chains. Since the microgel cores were sterically stabilized in the MeOH/water mixture by dangling chains of their outer swollen layer, a collapse of the particles upon changing the solvent polarity (by MMA addition) resulted in a lack of stabilization. As a result, it can be concluded that an additional surfactant/stabilizer is necessary in order to ensure colloidal stability of the seed particles.

In order to prevent aggregation of the deswollen C-NP in the solvent/MMA mixture, polyvinylpyrrolidone (PVP) (20 wt.-% w.r.t. seed particles + MMA) with a molecular weight of either $M_n = 10,000$ g/mol or $M_n = 30,000$ g/mol as sterical stabilizer was added to the PAAm microgel dispersion prior to the addition of MMA. It is assumed that the stabilizer not only prevents the collapsed seed particles from aggregation but also ensures colloidal stability of the resulting core/shell particles. It was found that after the addition of MMA, no macroscopic aggregation occurred (visual inspection). Nevertheless, to further investigate the proposed colloidal stability of C-NP in MeOH/H₂O/MMA, PCCS measurements were conducted. In comparison to DLS measurements conducted in previous chapters, this method allows one to examine the particles sizes in more concentrated dispersions; multiple scattering is not taken into account by the cross correlation method. As the investigated systems do not have to be diluted, these measurements allow to determine the particle sizes in the actual dispersion. It was found that even though the dispersions were stable after MAA addition, a bimodal distribution of increased particle diameters of 377 and 549 nm was detected by PCCS for the case of 10 k PVP. These increased diameters (in comparison to $d_h = 290$ nm in MeOH/water) are assumed to rather be the result of smaller particle aggregates than highly swollen particles, since MMA was found to induce a deswelling of the C-NP. In the case of 30 k PVP a similar trend was observed, thus indicating insufficient stabilization for this type of stabilizer.

In a next attempt, instead of a pure hydrophilic stabilizer such as PVP, the influence of amphiphilic surfactant molecules on the colloidal stability of C-NP was investigated. In contrast to anionic *SDS* which caused aggregation of the PAAm microgels, the addition of the non-ionic surfactant Lutensol AT-50 (2.8 wt.-% w.r.t. seed particles + MMA) was found to ensure good colloidal stability of the seed particles in the MeOH/water/MMA mixture. PCCS measurements exhibited a hydrodynamic diameter of 86 nm. This value is only slightly larger, than the average diameter of 70 nm obtained from SEM investigations of the dried particles, therefore indicating good stabilization of non-swollen C-NP particles.

Since the addition of Lutensol AT-50 prevented the PAAm seed particles from aggregation, the preparation of core/shell particles by precipitation polymerizations was investigated. Nevertheless, not only the colloidal stability of the core microgels prior to, but also the stability of the resulting core/shell particles during and after the polymerization has to be accomplished. Therefore, the amount of Lutensol added to the C-NP dispersion was systematically increased starting from the critical value found for successful stabilization of PAAm core microgels.

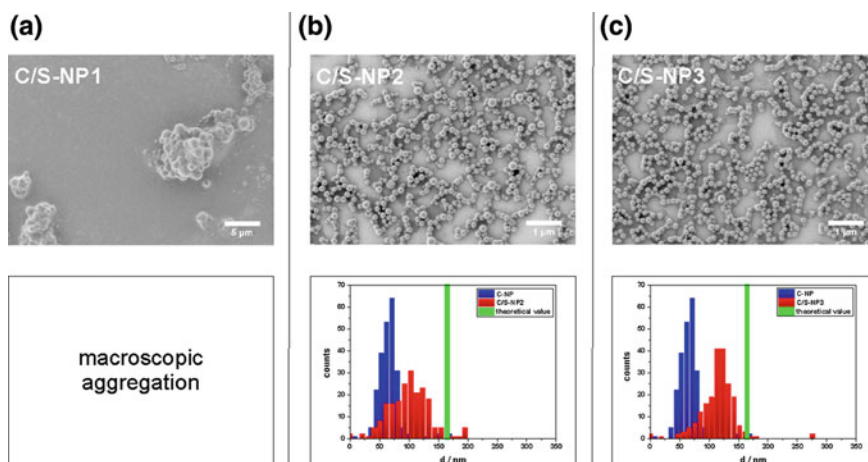
Table 5.12 Synthetic details for the preparation of PAAm/PMMA core/shell nanoparticles by seeded precipitation polymerization

Sample	Seed particles		Monomer		Surfactant		
	Type	c_{seed} Np/L	Type	c_{MMA} w.r.t. m_{seed} eq.-wt.	Type	c_{surf} w.r.t. m_{seed} wt.-%	c_{surf} w.r.t. $m_{\text{seed}} + \text{MMA}$ wt.-%
C/S-NP1	PAAm-HG	$4.3 \cdot 10^{15}$	MMA	10	Lutensol	16.7	2.8
C/S-NP2	PAAm-HG	$4.3 \cdot 10^{15}$	MMA	10	Lutensol	33.3	5.6
C/S-NP3	PAAm-HG	$4.3 \cdot 10^{15}$	MMA	10	Lutensol	16.7	11.1

Polymerizations were carried out at 70 °C by initiating with KPS from the continuous phase. Table 5.12 lists the synthetic recipes for the conducted polymerization experiments.

Figure 5.82 depicts representative SEM images of the resulting purified (dialysis) dispersions and the respective particle size distributions (in comparison to the non-swollen C-NP particles from cyclohexane dispersion and the theoretical values) obtained from SEM analysis.

It was found that even though an additional amount of 2.8 % Lutensol (w.r.t. seed particles + MMA) was sufficient to ensure the colloidal stability of the seed particles, it did not result in a stable dispersion of core/shell particles. In this case macroscopic aggregation occurred (Fig. 5.82a). Upon increasing the amount of surfactant to 5.6 and 11.1 % the dispersions showed good stability during and after the polymerization. Even though in those two cases (C/S-NP2 and C/S-NP3) the measured particle diameters were smaller than the theoretical values, the respective particle sizes increased, thus indicating the successful formation of PAAm/PMMA

**Fig. 5.82** SEM investigations on PAAm/PMMA core/shell nanoparticles. Representative images and size distributions obtained thereof: **a** C/S-NP1, **b** C/S-NP2 and **c** C/S-NP3

core/shell nanoparticles (see Fig. 5.82a and b). Since the measured particle sizes of C/S-NP2 and C/S-NP3 did not vary significantly, it is assumed that the final particles size is not influenced by the amount of surfactant and that a Lutensol content of 5.6 % is sufficient to ensure good colloidal stability of the core/shell nanoparticles.

Regarding the core/shell particles sizes, the theoretical values were calculated by assuming full conversion of MMA. Therefore, the observed discrepancies between the measured particles sizes and the theoretical ones is assumed to stem from incomplete conversion of the monomer in combination with the formation of oligomers still soluble in the solvent mixture. Both—free monomers and oligomers—do not add up to the shell formation. Further investigations of the proposed core/shell structure by TEM were hindered by the low T_g of the PMMA shell. Although sputtering of carbon films on either C/S-NP2 or C/S-NP3 particles enabled to visualize the particles (data not shown), a core/shell structure could not be detected.

Conclusion

In summary, model studies described in this chapter were intended to investigate the method of seeded precipitation polymerization as a potential pathway for stimuli-responsive core/shell nanoparticles containing a stimuli-responsive shell. For this purpose, PAAm microgel cores were synthesized and successfully dispersed in a mixture of MeOH/water/MMA by the utilization of Lutensol AT-50. Seeded precipitation polymerizations initiated by KPS from the continuous phase were found to yield stable dispersions for Lutensol contents higher than 5 wt.-% with respect to the mass of seed particles. The increase in particle sizes of the final dispersions (observed by SEM) is assumed to be assigned to the successful core/shell structure formation. In this case, the observed non-swollen state of the seed particles in the MeOH/water/MAA mixture is further proposed to result in a defined boundary between the PMMA shell and the PAAm core. Nevertheless, successful preparation of core/shell nanoparticles crucially depends on various important parameters such as the polarity of: (a) the solvent, (b) the monomer and (c) the respective shell forming polymer. Transferring this concept to stimuli-responsive analogues is assumed to require the specific adjustment of these parameters to the different materials.

5.5.2 PAAm/PU Core/Shell Nanoparticles by Free Radical Polymerization of AAm in Preformed Nanocapsules

Polycondensation reactions on the interface of droplets in inverse miniemulsions represent a well established approach to the formation of polyurethane or polyurea nanocapsules [103]. Hereby, the incorporation of water soluble compounds can easily be achieved by dissolving the desired substance in the dispersed phase prior to emulsification [112]. Based on this concept, the work described in this chapter

deals with the formation of core/shell nanoparticles consisting of a polyurea shell and a crosslinked polyacrylamide hydrogel core. Investigations on the synthetic route to these materials serve as preliminary studies for transferring this method to the preparation of stimuli-responsive analogues.

In contrast to the approach described in the previous chapter which was based on building up a microgel core and the subsequent formation of a polymeric shell around it, the preparation method proposed here represents an orthogonal pathway. In the first step, nanocapsules are prepared by the polycondensation reaction of a bifunctional isocyanate with a diamine ethylenediamine on the interface of droplets in an inverse miniemulsion. Here, the dispersed phase consists of an aqueous solution containing the diamine as monomer for the polyurea (PU) creation together with a radically polymerizable hydrophilic monomer, a crosslinker and a water soluble azo initiator for the formation of a hydrogel network subsequent to capsule formation. The continuous phase consists of a solution of the non-ionic surfactant Lubrizol U in cyclohexane. After miniemulsification, the diisocyanate is added to the continuous phase at room temperature in order to build the polyurea shell upon reaction with the diamine on the droplets surface. Since the isocyanato groups are characterized by a much faster reaction with the amine groups of EDA than with water present in the droplets, polymeric shells can successfully be prepared. In a second step, the capsule dispersion is heated to initiate the free radical copolymerization of the vinyl monomer with the bifunctional crosslinker to build up a hydrogel (HG) network in the capsule, thus yielding HG/PU core/shell particles. Figure 5.83 schematically illustrates the proposed synthetic pathway.

Synthesis and characterization of PAAm/PU core/shell nanoparticles.

Based on the synthetic concept described above, PAAm/PU core/shell

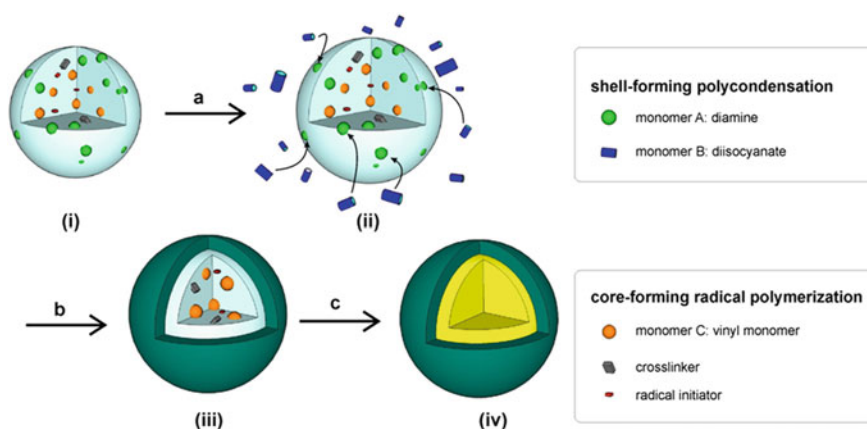
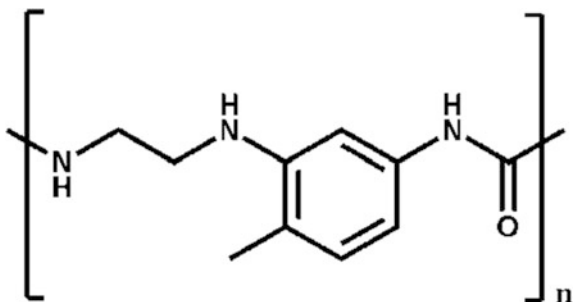


Fig. 5.83 Schematic representation of the described synthetic pathway to core/shell nanoparticles by: **a, b** shell formation around aqueous droplets (i), (ii) by interfacial polycondensation; **c** free radical polymerization of vinyl monomers in capsules (iii) containing a monomer and crosslinker solution; (iv) resulting hydrogel/polyurethane core/shell nanoparticles

Fig. 5.84 Molecular structure of the shell-forming polyurea



nanoparticles were prepared as follows. In the first step, nanocapsules were formed by the interfacial polycondensation reaction of ethylenediamine (EDA) (present in the droplets) with 2,4-toluenediisocyanate (TDI) (added to the continuous phase). The molecular structure of the resulting shell-forming polymer is depicted in Fig. 5.84.

The prepared capsules contained a liquid core consisting of an aqueous solution of acrylamide (AAM) as hydrophilic monomer, methylene bisacrylamide (MBA) as crosslinker, VA-060 as thermal initiator and NaCl as osmotic pressure agent. The AAM-aq/PU nanocapsules were investigated with respect to their morphology by SEM and TEM. The results are shown in Fig. 5.85a, b.

In the next step, the microgel core was formed by free radical copolymerization of AAM with MBA as crosslinker upon thermal initiation from the capsule interior. The synthesized PAAM-HG/PU core/shell particles were investigated by SEM and TEM in analogy to the AAM-aq/PU capsules containing the liquid core. The results are shown in Fig. 5.85c, d.

Comparing the SEM and TEM images of the AAM-aq/PU capsules and the PAAM-HG/PU core/shell particles it becomes obvious that the morphologies differ considerably. The nanocapsules containing the liquid core are characterized by a collapsed structure. This non-spherical shape is assumed to be a result of the drying process prior to the electron microscopic investigations. The diameter of the polyurea capsule shell is too small to stabilize the spherical shape upon drying. In contrast, the core/shell particles containing the hydrogel core exhibit a more pronounced spherical shape which is assumed to be a result of the stabilization of the structure by the polymeric network in the interior, thus preventing a collapse of the shell. Even though further characterization methods are assumed to give a more detailed insight in the actual structure of this material, these first results indicate a successful core/shell particles formation.

Conclusion

In summary, the preliminary results obtained from the experiments described in this chapter strongly suggest the investigated synthetic approach to be a potential pathway to core/shell nanoparticles containing a hydrogel core. However, more detailed studies are necessary in order to prove the proposed core/shell structure. As an example, calorimetric studies on the free radical polymerization in the

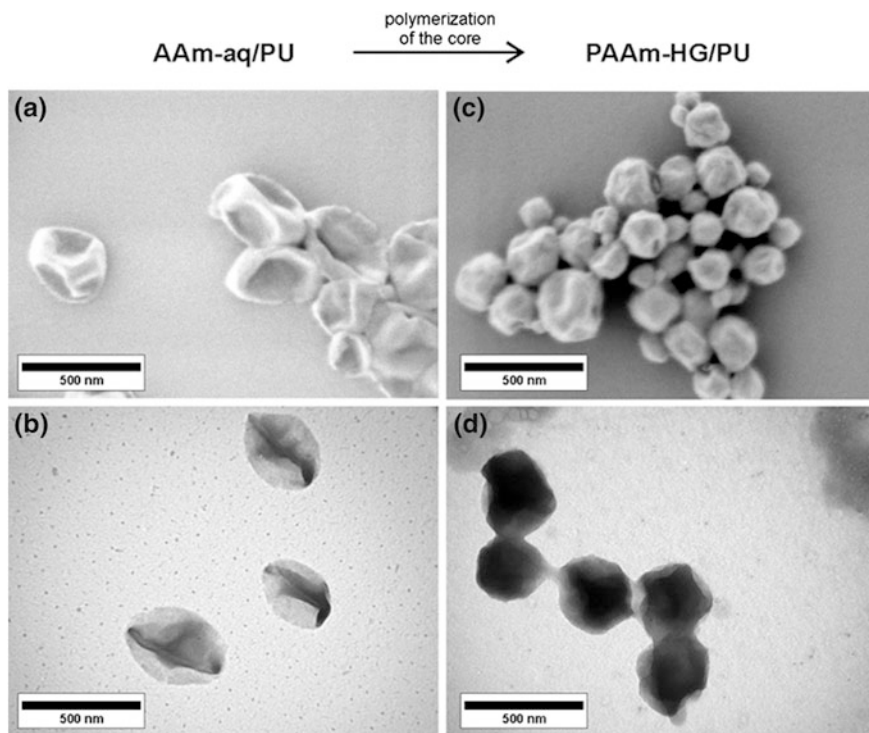


Fig. 5.85 Electron microscopic investigations on the preparation of core/shell nanoparticles: **a** SEM image of AAm-aq/PU; **b** TEM image of AAm-aq/PU; **c** SEM image of PAAm-HG/PU and **d** TEM of PAAm-HG/PU

capsules are assumed to demonstrate the successful hydrogel core formation. The versatility in monomer choice for core preparation is limited to vinyl monomers without hydroxyl- or amine groups because of their side reactions with TDI.

5.5.2.1 Preparation of a Light-Sensitive Polyurethane as Potential Material for Photo-Cleavable Nanocapsules

In the previous chapter the successful formation of PAAm/PU core/shell particles was demonstrated by building up a hydrogel network in preformed polyurea nanocapsules. As mentioned before, transferring this general approach to the preparation of stimuli-responsive analogues is of high interest for release applications from the resulting materials. Here, the respective polymeric shell should serve as an initial diffusion barrier for compounds embedded in the hydrogel core. Appli-ance of a specific stimulus should render the former hard shell permeable for the substances to be released. Among other approaches, this can be achieved by a degradation of the shell-forming polymer. The work described in this chapter deals

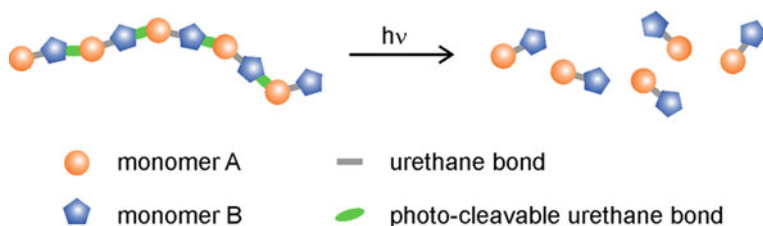


Fig. 5.86 Schematic illustration of the concept of a photo-degradable polyurethane

with the preparation of a photo-degradable polyurethane by a polycondensation reaction. As the polymer contains light-cleavable groups in the polymer backbone, irradiation results in its degradation to the respective monomeric/oligomeric units. The proposed new material is assumed to be transferable to the formation of core/shell particles containing a light-responsive shell in a fashion similar to plain PU shells described in Sect. 5.5.2. Figure 5.86 schematically illustrates the described concept of the photo-sensitive polymer.

Firstly, the formation of a new polyurethane containing light-cleavable *o*-nitrobenzyl groups in the polymeric backbone is investigated. Secondly, the polymer degradation upon irradiation in solution is examined.

Synthesis and characterization of a photo-degradable polyurethane (PD-PU). The synthesis of the photo-degradable polyurethane exploits the polycondensation reaction of the previously synthesized dialcohol 2-NPDM molecule (see Sect. 5.1.1.1) as chromophore with TDI. Figure 5.87 depicts the synthetic pathway.

The polymerization was performed under anhydrous conditions in DMF at 100 °C. Afterwards the polymer was precipitated twice from methanol, dried and characterized by NMR spectroscopy and GPC. Figure 5.88 depicts the ¹H-NMR spectrum of the polymer in DMSO.

The ¹H-NMR spectrum of the PD-PU polymer strongly indicates the successful polymerization since the peak integral ratio of the protons assigned to the 2-NPDM core and the TDI core is equal to one. This indicates the identical incorporation of these two moieties in the backbone. Furthermore, GPC measurements of the polymer in THF yielded a molecular weight of $M_w = 5,200$ g/mol with respect to a polystyrene standard. The relatively low molecular weight is assumed to be a result of the inherent sensitivity of the degree of polymerization of step-wise polymerizations to the stoichiometry and the conversion of the reaction. It is assumed that the

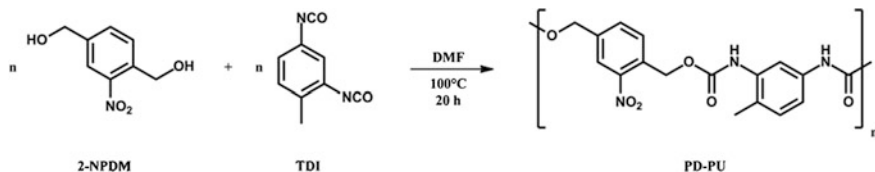


Fig. 5.87 Synthetic pathway to PD-PU

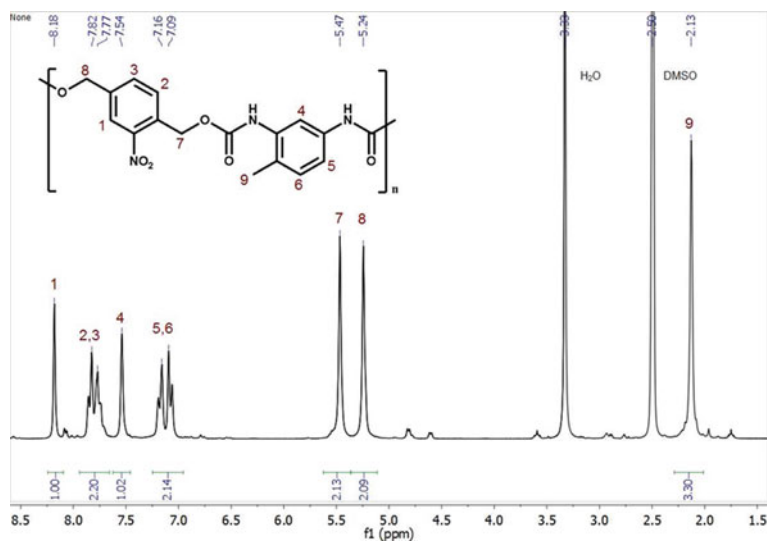


Fig. 5.88 ¹H-NMR spectrum of PD-PU in DMSO-d₆

latter parameter can be increased by catalyzing the polycondensation reaction with dibutyltin dilaurate (DBTDL) in further experiments. Nevertheless, the determined molecular weight from this first experiment demonstrates a successful polymerization with a degree of polymerization of around 15.

Photolytic degradation experiments of PD-PU. Having demonstrated the successful preparation of a photo-degradable polyurethane, the proposed photolytic degradation of the polymer backbone upon the irradiation with UV light was investigated next. For this purpose, a solution of the polymer in THF was irradiated for 3 h with UV light of the wavelengths of $\lambda = 315\text{--}390$ nm. The resulting solution was investigated with regard to the molecular weight of the proposed fragments by GPC. Figure 5.89 depicts the elution curve of the irradiated sample in comparison to the non-irradiated polymer as well as the proposed light-induced cleavage reaction.

By comparing the GPC elution curves of the initial polymer to the irradiated sample, it becomes obvious that the molecular weight decreased dramatically upon irradiation. The molecular weight of the irradiated sample was determined to $M_w = 370$ g/mol from the respective elution curve in comparison to a polystyrene standard. The observed value is remarkably close to the molecular weight of the depicted degradation product in Fig. 5.89a ($M = 313$ g/mol). Since the discrepancy can be explained by the utilization of GPC as a relative measuring method, a successful degradation of the polymer into small “monomeric” fragments is assumed.

Conclusion and outlook

In summary, a new photo-degradable polyurethane PD-PU containing light-cleavable *o*-nitrobenzyl groups in the backbone was successfully synthesized by

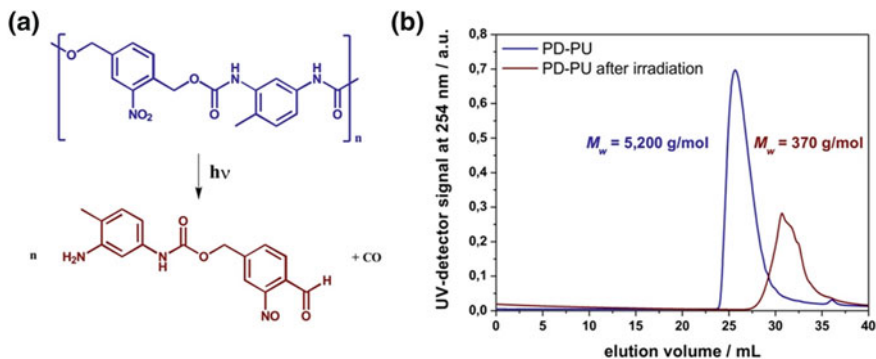


Fig. 5.89 Photolytic degradation of PD-PU: **a** proposed photoreaction of PD-PU; **b** GPC elution curves of the initial PD-PU polymer in comparison to the irradiated sample

polycondensation polymerization in solution. Irradiation experiments of the material with UV light resulted in the successful degradation of the polymeric backbone, yielding low molecular weight fragments. This behavior is assumed to be of high interest for the preparation of either light-cleavable polyurethane nanocapsules or the formation of core/shell nanoparticles which contain a photo-sensitive PD-PU shell. In order to realize these potential materials, the polycondensation reaction of the 2-NPDM chromophore with TDI on the surface of droplets in inverse miniemulsion has to be studied. To this extend, replacing the solvent for the dispersed phase by an organic solvent (e.g. DMSO) immiscible with the continuous phase (cyclohexane) is assumed to enable the described synthetic approach.

5.6 Surface Functionalization of Microgels with Photo-Reactive Chromophores

As mentioned before, microgels represent a highly interesting class of materials since they combine the characteristics of macroscopic hydrogels (e.g., structural integrity in combination with fluid-like transport characteristics) with those of colloidal dispersions (e.g., colloidal stability, facile synthesis and control over particle size). Additional functionalities can be introduced to the microgels by modification of the particles surface with functional groups. As an example, the introduction of e.g., targeting vectors for drug delivery applications is an important field. Moreover, functionalization with reactive moieties to trigger the particles interaction with different compounds or with each other is another interesting research area. Here, the attachment of photo-reactive chromophores represents a versatile approach to realize this concept. Especially, the utilization of [2 + 2] and [4 + 4] forward and backward photo-cycloadditions is assumed to give rise to

reversible particle–particle or particle-compound interactions which can be controlled by light as external trigger.

In order to realize the described concept by the modification of the surface of hydrogel nanoparticles, several limitations have to be taken into account: (a) The hydrogel material has to contain reactive groups which are present on the surface of the microgel and enable a functionalization reaction. In the case of hydrogels, especially hydroxyl-, carboxyl- or amine groups fulfill this criterion since they are hydrophilic which enables their facile incorporation in the microgels. In addition, these moieties enable the desired swelling of the network. (b) Modification reactions with the mentioned functional groups are mainly based on esterifications, amide-, urethane- or urea formations. (c) An efficient reaction based on these mechanisms is severely limited by side reactions in water as continuous phase. (d) Specific functionalization of the microgel's surface in water is hindered by the swollen state of the gel networks since diffusion of reagents into the particles results in a modification of the interior as well.

Based on these considerations, the work described in this chapter deals with the development of a synthetic protocol for the facile and effective surface modification of microgels with photo-reactive chromophores. To this extend, the functionalization of PHEMA and p(HEMA-*co*-MAA) microgels with cinnamoyl groups was examined. The respective materials were designed as nanometric building blocks for the preparation of self-healing hydrogel thin films.

5.6.1 Surface Modification of PHEMA and p(HEMA-*co*-MAA) Microgels with Cinnamoyl Groups

Concerning the introduction of photo-reactive moieties on microgel surfaces, the utilization of several functional groups is imaginable. In the context of reversible bond formation upon irradiation, the photo-dimerization reactions of anthracene and cinnamate derivatives are well established approaches [5, 113, 114]. Incorporation of these into hydrophilic polymers or dendrimers was recently shown to enable the formation of hydrogels upon irradiation induced crosslinking [115]. Such light-sensitive materials exhibit highly interesting self-healable properties [6, 115–117]. Transferring this concept to microgels containing cinnamoyl groups on the surface is assumed to give rise to the light-induced formation of macroscopic hydrogels by interparticular crosslinking upon photo-dimerization. Primarily, the successful functionalization of microgels with cinnamoyl groups has to be achieved. In previous chapters, PHEMA and p(HEMA-*co*-MAA) microgels were shown to exhibit good swelling properties in either organic or aqueous media, respectively. The observed good gel properties in combination with the high amount of hydroxyl groups available for modification reactions render them ideal candidates for the preparation of photo-reactive gel nanoparticles.

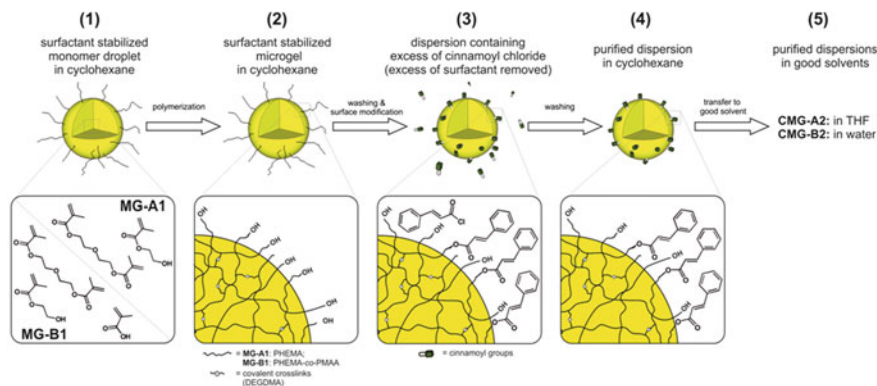


Fig. 5.90 Schematic representation of the synthetic pathway followed to generate cinnamate-containing PHEMA and p(HEMA-co-MAA) nanoparticles by inverse miniemulsion copolymerization (1, 2) followed by surface functionalization with cinnamate groups (3) and their purification (4) and transfer into the respective good solvents (5). Reprinted with permission from [118]. Copyright 2011 WILEY-VCH

As mentioned above, the efficient functionalization of hydrogel nanoparticles only at the surface is a rather complex task. In order to realize this, a synthetic protocol has to be developed which takes the described limitations into account. The approach described in this chapter is based on a modification of non-swollen microgel particles in an organic solvent.

Preparation of PHEMA and p(HEMA-co-MAA) microgels with cinnamoyl groups on the surface. The synthetic pathway to PHEMA and p(HEMA-co-MAA) microgels containing cinnamoyl groups on the surface is schematically illustrated in Fig. 5.90.

In a first step (Fig. 5.90(1, 2)), the unfunctionalized microgels were synthesized by free radical copolymerization of the respective monomers in inverse miniemulsions. PHEMA microgels (MG-A1) were obtained by copolymerization of HEMA with DEGDMA as crosslinker. MAA was used as a comonomer in a second set of polymerizations in order to enhance the microgels stability and swellability in water, thus allowing studies not only in organic solvents but also in aqueous systems. Thus, water swellable p(HEMA-co-MAA) microgels (MG-B1) were formed by crosslinking copolymerization of HEMA with MAA and DEGDMA.

Since the dispersed phase of the miniemulsions consisted in every case of a mixture of the respective monomers without water as additional solvent, the resulting dispersions in cyclohexane contained microgel particles in their non-swollen state. This enabled to specifically functionalize the particles surface with hydrophobic compounds due to a hindered diffusion of the reagents into the particle interior. The modification can be achieved by reacting the hydroxyl groups of PHEMA and p(HEMA-co-MAA) with different functional groups. Esterification reactions are in this context a promising tool but their utilization is limited to certain

synthetic routes. As an example, the DCC activated coupling of free carboxylic acid groups to the HEMA hydroxyl group is enabled by the utilization of cyclohexane as organic solvent for the continuous phase. Nevertheless, in the case of p(HEMA-*co*-MAA) microgels, this method is assumed to result in an intra- or inter-particle coupling of the MAA groups with the HEMA hydroxyl moieties. Therefore, nucleophilic substitution of carboxyl chlorides by the HEMA hydroxyl groups represents a more promising approach. Even though, anhydride formation can occur as side reaction with MAA groups in MG-B1 microgels, these bonds are assumed to be cleaved by transferring the functionalized particles to the aqueous phase.

Based on these considerations, MG-A1 and MG-B1 microgels were allowed to react with an excess amount of cinnamoyl chloride in cyclohexane (Fig. 5.90(3)) Non-reacted cinnamoyl chloride and excess of surfactant from the microgel synthesis were removed by repeated washing of the microgels with cyclohexane (Fig. 5.90(4)). The obtained dispersions of cinnamoyl functionalized PHEMA (CMG-A1) and p(HEMA-*co*-MAA) (CMG-B1) in cyclohexane were freeze dried and the obtained powders were easily redispersed in good solvents for the polymers (THF and water, respectively), thus forming microgels CMG-A2 and CMG-B2 (Fig. 5.90(5)). In the swollen state, particle dispersions of cinnamoyl functionalized PHEMA microgels in THF (CMG-A2) and p(HEMA-*co*-MAA) in water (CMG-B2) were stable without any additional surfactant due to steric

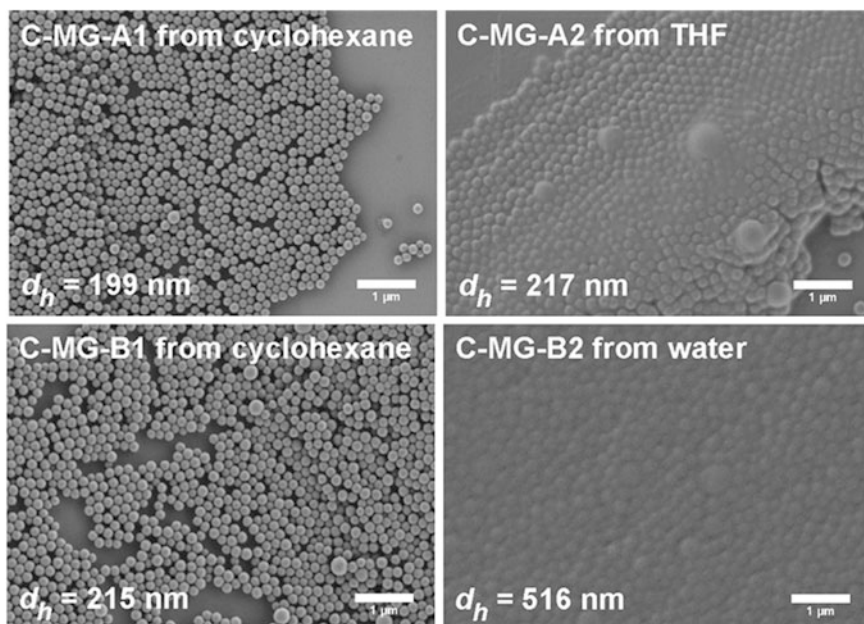


Fig. 5.91 Characterization of the synthesized microgels in different solvents. SEM images of dropcast samples and hydrodynamic diameters of the synthesized microgels obtained from DLS. Reprinted with permission from [87]. Copyright 2011 Wiley Periodicals, Inc

stabilization of the dangling chains at the particle surface. Figure 5.91 shows representative SEM images of the obtained systems and the hydrodynamic diameters of the synthesized microgels obtained from DLS measurements. It is worth noticing that CMG-B1 and CMG-B2 are chemically the same microgels, but CMG-B1 is dispersed in cyclohexane while CMG-B2 is in water. This microgel underwent a remarkable increment in its size when transferred from cyclohexane to water, reflected on their hydrodynamic diameters, from $d_h = 215$ nm in cyclohexane to $d_h = 516$ nm in water. As demonstrated in a previous chapter, the size change experienced by CMG-B1 when forming CMGB2 is caused by the deprotonation of the carboxylic acid groups belonging to the PHEMA-*co*-PMAA during its redispersion in water at pH 12. Thus, electrostatic repulsion of the anionic groups generated at basic pH plus the enhanced solubility in water of the respective carboxylates leads to a high swellability of the microgel increasing in consequence its hydrodynamic diameters.

As demonstrated, the surface-functionalized particles exhibited good colloidal stability in various solvents. In a last experiment, UV-vis measurements on microgel films dropcast from dispersions on quartz slides were conducted in order to demonstrate the successful attachment of the cinnamoyl groups to the particles surfaces. Figure 5.92 depicts the respective spectra measured by Dr. Pablo Froimowicz.

As can be seen from the UV-vis spectra in Fig. 5.92, a well pronounced absorption band at $\lambda_{max} = 280$ nm can be observed for both samples. The absorption band at this wavelength was assigned to the cinnamate moieties, thus demonstrating their successful attachment to the microgels.

Conclusion

In summary, an efficient synthetic route to the specific surface modification of PHEMA and p(HEMA-*co*-MAA) (hydrogel) nanoparticles with cinnamoyl moieties was demonstrated. The method is based on the reaction of the HEMA hydroxyl groups with cinnamoyl chloride in cyclohexane dispersions of the non-

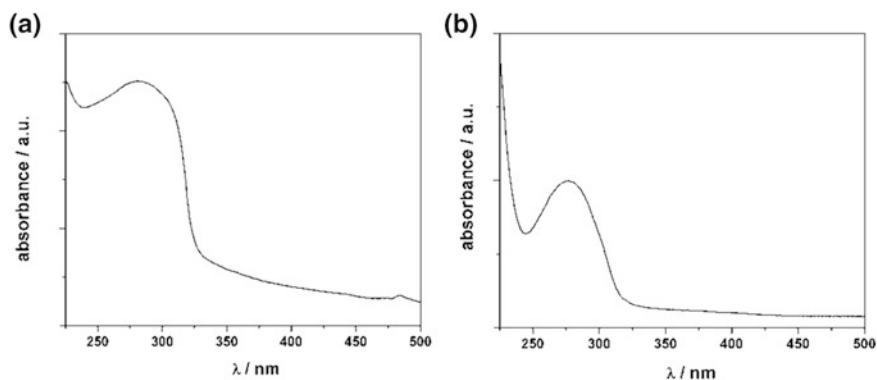


Fig. 5.92 UV-vis spectroscopic investigations on films of C-MG-A2 and C-MG-B2 microgels dropcast on quartz slides from THF and water, respectively. Data obtained from P. Froimowicz. Reprinted with permission from [87]. Copyright 2011 Wiley Periodicals, Inc

swollen microgels. The observed good film formation of these materials from either THF (C-MG-A2) or water (C-MG-B2) is assumed to give rise to the preparation of stable macroscopic hydrogel films upon interparticulate crosslinking reactions by light-induced dimerization of the cinnamates.

5.6.2 Self-Healing Hydrogel Thin Films from Photo-Reactive Microgels

The surface functionalized photo-reactive microgels described in the previous chapter were further investigated by Dr. Pablo Froimowicz with regard to their potential for the preparation of self-healing hydrogel thin films.

In brief, polymeric materials with self-healing capabilities are increasingly attracting attention [119, 120] not only because of the variety of applications in which they may be applied, but also due to the challenging strategies that must be mastered during their design and generation. In this context, it is clear that a combination of concepts and tools from different disciplines would be particularly advantageous for successfully obtaining these polymeric self-healing materials. For example, in most of the polymeric self-healing materials reported in the past years, combinations of fundamentals and techniques from organic chemistry, polymer and materials sciences and/or (nano-)technologies are found, such as: dimerization reactions [121], reversible chemical reactions [122], hydrogen bonding [123], supramolecular interactions [124], crosslinking polymerization [115, 122], (nano-)encapsulation of reactive monomers [125], and resolution [126]. These examples highlight how sophisticated molecular designed materials can be conceived as the result of the synergistic contribution between disciplines. However, most of the reported self-healing polymeric materials are robust structures and only a few hydrogels were shown to be capable to selfrepair. In this context the use of reversible photo-crosslinkable nanoparticles as nano-building blocks for the formulation of nanostructured hydrogel thin films—bearing the capability to self-heal via swelling—represents a very attractive novel approach.

The synthesis of this self-healable film was based on the combination of two desirable properties for such materials, namely: reversible crosslinkable building blocks and capability of rearrangement of polymeric structures by swelling. The previously described nanoparticles were used to form films by casting, followed by interparticulate crosslinking polymerizations via the light-induced forward dimerization reaction of the cinnamate groups incorporated before. The reversibility of this macroscopic network formation was studied by photo-inducing the backward

Results from these investigations are published as “Photo-Reactive Nanoparticles as Nanometric Building Blocks for the Generation of Self-Healing Hydrogel Thin Films” Pablo Froimowicz, Daniel Klinger, Katharina Landfester *Chem. Eur. J.* **2011**, *17*, 12465. Reprinted with permission from [118]. Copyright 2011 WILEY-VCH Verlag GmbH & Co. KGaA, Weinheim.

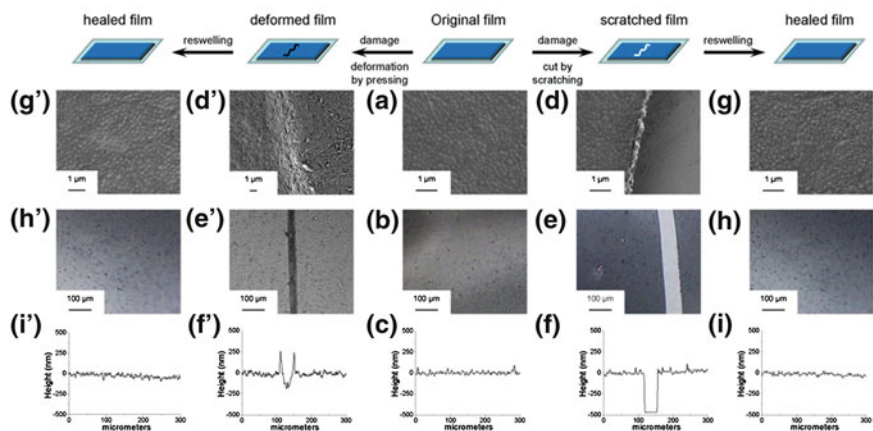


Fig. 5.93 Comparison between an idealized cartoon and the described system showing the films before damage (a–c), after damage via scratching (d–f) and pressing (d'–f'), as well as after self-healing via reswelling (g–I and g'–i') by SEM (a, d, d', g and g'), digital picture of an optical microscope (b, e, e', h and h') and its respective roughness profile (c, f, f', I and i') from a profiler device. Data obtained from P. Froimowicz. Reprinted with permission from [118]. Copyright 2011 WILEY–VCH

dimerization reaction and carrying out several cycles of light-triggered cross-linking and de-crosslinking. The swelling-induced self-healing ability of these films after being artificially being damaged was demonstrated and is shown in Fig. 5.93.

Finally, the possibility to embed additives into this self-healable macroscopic film with different chemical compounds before being photo-chemically cross-linked was evaluated.

References

1. Klinger, D., Nilles, K., Theato, P.: *J. Polym. Sci. Part A Polym. Chem.* **48**(4), 832–844 (2010)
2. Russew, M.-M., Hecht, S.: *Adv. Mater.* **22**(31), 3348–3360 (2010)
3. Seiffert, S., Oppermann, W., Saalwachter, K.: *Polymer* **48**(19), 5599–5611 (2007)
4. Gupta, S., Kuckling, D., Kretschmer, K., Choudhary, V., Adler, H.J.: *J. Polym. Sci. Part A Polym. Chem.* **45**(4), 669–679 (2007)
5. Kuang, G.-C., Ji, Y., Jia, X.-R., Li, Y., Chen, E.-Q., Zhang, Z.-X., Wei, Y.: *Tetrahedron* **65**(17), 3496–3501 (2009)
6. Connal, L.A., Vestberg, R., Hawker, C.J., Qiao, G.G.: *Adv. Funct. Mater.* **18**(20), 3315–3322 (2008)
7. Shi, D.J., Matsusaki, M., Kaneko, T., Akashi, M.: *Macromolecules* **41**(21), 8167–8172 (2008)
8. Jiang, J.Q., Qi, B., Lepage, M., Zhao, Y.: *Macromolecules* **40**(4), 790–792 (2007)
9. Klinger, D., Landfester, K.: *Soft Matter* **7**(4), 1426–1440 (2011)

10. Buhler, S., Lagoja, I., Giegrich, H., Stengele, K.P., Pfeleiderer, W.: *Helv. Chim. Acta* **87**(3), 620–659 (2004)
11. Barzynski, H., Sanger, D.: *Angew. Makromol. Chem.* **93**(FEB), 131–141 (1981)
12. Braun, D., Berger, J.: *Kolloid Z. Z. Polym.* **250**(2), 142–147 (1972)
13. Conforti, P.F., Garrison, B.J.: *Chem. Phys. Lett.* **406**(4–6), 294–299 (2005)
14. Reichmanis, E., Smith, B.C., Gooden, R.: *J. Polym. Sci. Part A Polym. Chem.* **23**(1), 1–8 (1985)
15. Malatest, V., Ingold, K.U.: *Tetrahedron Lett.* **14**(35), 3307–3310 (1973)
16. Rehak, V., Novak, F., Kuncicky, J., Cepcians I.: *Tetrahedron Lett.* **11**(23), 1967 (1970)
17. Kopecek, J.: *J. Polym. Sci. Part A Polym. Chem.* **47**(22), 5929–5946 (2009)
18. Lecner, M.D.: *J. Serb. Chem. Soc.* **70**(3), 361–369 (2005)
19. Al-Manasir, N., Zhu, K.Z., Kjoniksen, A.L., Knudsen, K.D., Karlsson, G., Nystrom, B.: *J. Phys. Chem. B* **113**(32), 11115–11123 (2009)
20. Landfester, K., Musyanovych, A.: *Chem. Des. Responsive Microgels* **234**, 39–63 (2010)
21. Atzet, S., Curtin, S., Trinh, P., Bryant, S., Ratner, B.: *Biomacromolecules* **9**(12), 3370–3377 (2008)
22. Weaver, J.V.M., Bannister, I., Robinson, K.L., Bories-Azeau, X., Armes, S.P., Smallridge, M., McKenna, P.: *Macromolecules* **37**(7), 2395–2403 (2004)
23. Karg, M., Pastoriza-Santos, I., Perez-Juste, J., Hellweg, T., Liz-Marzan, L.M.: *Small* **3**, 1222–1229 (2007)
24. Sorrell, C.D., Carter, M.C.D., Serpe, M.J.: *Adv. Funct. Mater.* **21**(3), 425–433 (2011)
25. Debord, J.D., Lyon, L.A.: *J. Phys. Chem. B* **104**(27), 6327–6331 (2000)
26. Kang, J.-H., Moon, J.H., Lee, S.-K., Park, S.-G., Jang, S.G., Yang, S., Yang, S.-M.: *Adv. Mater.* **20**(16), 3061–3065 (2008)
27. Stuart, M.A.C., Huck, W.T.S., Genzer, J., Muller, M., Ober, C., Stamm, M., Sukhorukov, G.B., Szleifer, I., Tsukruk, V.V., Urban, M., Winnik, F., Zauscher, S., Luzinov, I., Minko, S.: *Nat. Mater.* **9**(2), 101–113 (2010)
28. Jeong, B., Gutowska, A.: *Trends Biotechnol.* **20**(7), 305–311 (2002)
29. Kawaguchi, H., Fujimoto, K.: *Bioseparation* **7**(4–5), 253–258 (1998)
30. Etrych, T., Jelinkova, M., Rihova, B., Ulbrich, K.: *J. Controlled Release* **73**(1), 89–102 (2001)
31. Vicent, M.J., Duncan, R.: *Trends Biotechnol.* **24**(1), 39–47 (2006)
32. Langer, R.: *Nature* **392**(6679), 5–10 (1998)
33. Urich, K.E., Cannizzaro, S.M., Langer, R.S., Shakesheff, K.M.: *Chem. Rev.* **99**(11), 3181–3198 (1999)
34. Kataoka, K., Harada, A., Nagasaki, Y.: *Adv. Drug Deliv. Rev.* **47**(1), 113–131 (2001)
35. Hamidi, M., Azadi, A., Rafiei, P.: *Adv. Drug Deliv. Rev.* **60**(15), 1638–1649 (2008)
36. Das, M., Zhang, H., Kumacheva, E.: *Annu. Rev. Mater. Res.* **36**, 117–142 (2006)
37. Oh, J.K., Drumright, R., Siegwart, D.J., Matyjaszewski, K.: *Prog. Polym. Sci.* **33**(4), 448–477 (2008)
38. Klinger, D., Landfester, K.: *Macromolecules* **44**(24), 9758–9772 (2011)
39. Eichenbaum, G.M., Kiser, P.F., Shah, D., Simon, S.A., Needham, D.: *Macromolecules* **32**(26), 8996–9006 (1999)
40. Eichenbaum, G.M., Kiser, P.F., Dobrynin, A.V., Simon, S.A., Needham, D.: *Macromolecules* **32**(15), 4867–4878 (1999)
41. Nayak, S., Lyon, L.A.: *Angew. Chem. Int. Ed.* **44**(47), 7686–7708 (2005)
42. Franssen, O., Stenekes, R.J.H., Hennink, W.E.: *J. Controlled Release* **59**(2), 219–228 (1999)
43. Schachschal, S., Adler, H.-J., Pich, A., Wetzels, S., Matura, A., van Pee, K.-H.: *Colloid Polym. Sci.* **289**(5–6), 693–698 (2011)
44. Klinger, D., Landfester, K.: *J. Polym. Sci. Part A Polym. Chem.* **50**(6), 1062–1075 (2012)
45. Deka, S.R., Quarta, A., Di Corato, R., Falqui, A., Manna, L., Cingolani, R., Pellegrino, T.: *Langmuir* **26**(12), 10315–10324 (2010)
46. Zhang, Y., Zhu, W., Wang, B.B., Ding, J.D.: *J. Controlled Release* **105**(3), 260–268 (2005)

47. Pich, A., Karak, A., Lu, Y., Ghosh, A.K., Adler, H.J.P.: *Macromol. Rapid Commun.* **27**(5), 344–350 (2006)
48. Murthy, N., Thng, Y.X., Schuck, S., Xu, M.C., Frechet, J.M.J.: *J. Am. Chem. Soc.* **124**(42), 12398–12399 (2002)
49. Sankaranarayanan, J., Mahmoud, E.A., Kim, G., Morachis, J.M., Almutairi, A.: *ACS Nano* **4**(10), 5930–5936 (2010)
50. Dou, H., Jiang, M.: *Polym. Int.* **56**, 1206–1212 (2007)
51. Das, M., Mardiyani, S., Chan, W.C.W., Kumacheva, E.: *Adv. Mater.* **18**(1), 80–83 (2006)
52. Wells, L.A., Sheardown, H.: *Eur. J. Pharm. Biopharm.* **65**(3), 329–335 (2007)
53. Lorenz, M.R., Holzapfel, V., Musyanovych, A., Nothelfer, K., Walther, P., Frank, H., Landfester, K., Schrezenmeier, H., Mailänder, V.: *Biomaterials* **27**, 2820–2828 (2006)
54. Fischer, R., Waizenegger, T., Kohler, K., Brock, R.: *Biochim. Biophys. Acta Gene Struct. Expr.* **1664**, 365–374 (2002)
55. Jensen, K.D., Nori, A., Tijerina, M., Kopeckova, P., Kopecek, J.: *J. Controlled Release* **87**, 89–105 (2003)
56. Hillaireau, H., Couvreur, P.: *Cell. Mol. Life Sci.* **66**, 2873–2896 (2009)
57. Connor, S.D., Schmid, S.L.: *Nature* **422**(6), 37–44 (2003)
58. Haag, R., Kratz, F.: *Angew. Chem. Int. Ed.* **45**, 1198–1215 (2006)
59. Marcucci, F., Lefoulon, F.: *Drug Discov. Today Targets* **9**, 219 (2004)
60. Nayak, S., Lee, H., Chmielewski, J., Lyon, L.A.: *J. Am. Chem. Soc.* **126**, 10258 (2004)
61. Saunders, B.R., Laajam, N., Daly, E., Teow, S., Hu, X., Stepto, R.: *Adv. Colloid Interface Sci.* **147–148**, 251–262 (2009)
62. Standley, S.M., Kwon, Y.J., Murthy, N., Kunisawa, J., Shastri, N., Guillaudeu, S.J., Lau, L., Frechet, J.M.J.: *Bioconj. Chem.* **15**(6), 1281–1288 (2004)
63. Babin, J., Pelletier, M., Lepage, M., Allard, J.F., Morris, D., Zhao, Y.: *Angew. Chem. Int. Ed.* **48**(18), 3329–3332 (2009)
64. Kloxin, A.M., Kasko, A.M., Salinas, C.N., Anseth, K.S.: *Science* **324**(5923), 59–63 (2009)
65. del Campo, A., Boos, D., Spiess, H.W., Jonas, U.: *Angew. Chem. Int. Ed.* **44**(30), 4707–4712 (2005)
66. Kawaguchi, S., Yekta, A., Winnik, M.A.: *J. Colloid Interface Sci.* **176**(2), 362–369 (1995)
67. Candau, F., Zekhnini, Z., Heatley, F., Franta, E.: *Colloid Polym. Sci.* **264**(8), 676–682 (1986)
68. Franssen, O., van Ooijen, R.D., de Boer, D., Maes, R.A.A., Herron, J.N., Hennink, W.E.: *Macromolecules* **30**(24), 7408–7413 (1997)
69. Franssen, O., van Ooijen, R.D., de Boer, D., Maes, R.A.A., Hennink, W.E.: *Macromolecules* **32**(9), 2896–2902 (1999)
70. Abdurrahmanoglu, S., Firat, Y.: *J. Appl. Polym. Sci.* **106**, 3565–3570 (2007)
71. Franssen, O., Vos, O.P., Hennink, W.E.: *J. Controlled Release* **44**, 237–245 (1997)
72. Franssen, O., Vandervennet, L., Roders, P., Hennink, W.E.: *J. Controlled Release* **60**(2–3), 211–221 (1999)
73. Landfester, K., Willert, M., Antonietti, M.: *Macromolecules* **33**(7), 2370–2376 (2000)
74. Landfester, K.: *Angew. Chem. Int. Ed.* **48**(25), 4488–4507 (2009)
75. Klinger, D., Aschenbrenner, E., Weiss, C.K., Landfester, K.: *Polym. Chem.* **3**(1), 204–216 (2012)
76. Kim, S.H., Chu, C.C.: *J. Biomed. Mater. Res. A* **49**(4), 517–527 (1999)
77. Griset, A.P., Walpole, J., Liu, R., Gaffey, A., Colson, Y.L., Grinstaff, M.W.: *J. Am. Chem. Soc.* **131**(7), 2469–2471 (2009)
78. Agasti, S.S., Chompoosor, A., You, C.-C., Ghosh, P., Kim, C.K., Rotello, V.M.: *J. Am. Chem. Soc.* **131**(16), 5728–5729 (2009)
79. Johnson, J.A., Lu, Y.Y., Burts, A.O., Xia, Y., Durrell, A.C., Tirrell, D.A., Grubbs, R.H.: *Macromolecules* **43**(24), 10326–10335 (2010)
80. Lin, Q., Huang, Q., Li, C., Bao, C., Liu, Z., Li, F., Zhu, L.: *J. Am. Chem. Soc.* **132**(31), 10645–10647 (2010)
81. Saito, H., Hoffman, A.S., Ogawa, H.I.: *J. Bioact. Compat. Polym.* **22**(6), 589–601 (2007)

82. Choi, S.K., Thomas, T., Li, M.-H., Kotlyar, A., Desai, A., Baker Jr, J.R.: *Chem. Commun.* **46**(15), 2632–2634 (2010)
83. Beijnen, J.H., Wiese, G., Underberg, W.J.M.: *Pharm. Weekbl. Sci. Ed.* **7**(3), 109–116 (1985)
84. Kawaguchi, H.: *Prog. Polym. Sci.* **25**(8), 1171–1210 (2000)
85. Tokarev, I., Minko, S.: *Adv. Mater.* **22**(31), 3446–3462 (2010)
86. Fomina, N., McFearin, C., Sermsakdi, M., Edigin, O., Almutairi, A.: *J. Am. Chem. Soc.* **132**(28), 9540–9542 (2010)
87. Klinger, D., Landfester, K.: *Macromol. Rapid Commun.* **32**(24), 1979–1985 (2011)
88. Kim, M., Choi, J.-C., Jung, H.-R., Katz, J.S., Kim, M.-G., Doh, J.: *Langmuir* **26**(14), 12112–12118 (2010)
89. Landfester, K.: *Adv. Mater.* **13**(10), 765–768 (2001)
90. Landfester, K.: *Macromol. Rapid Commun.* **22**(12), 896–936 (2001)
91. Deye, J.F., Berger, T.A., Anderson, A.G.: *Anal. Chem.* **62**(6), 615–622 (1990)
92. Dutta, A.K., Kamada, K., Ohta, K.: *J. Photochem. Photobiol. A Chem.* **93**(1), 57–64 (1996)
93. Lin, C.-C., Metters, A.T.: *Adv. Drug Deliv. Rev.* **58**(12–13), 1379–1408 (2006)
94. Bromberg, L., Temchenko, M., Hatton, T.A.: *Langmuir* **18**(12), 4944–4952 (2002)
95. Nayak, S., Gan, D.J., Serpe, M.J., Lyon, L.A.: *Small* **1**(4), 416–421 (2005)
96. Berndt, I., Pedersen, J.S., Richtering, W.: *Angew. Chem. Int. Ed.* **45**(11), 1737–1741 (2006)
97. Tan, J.P.K., Wang, Q., Tam, K.C.: *J. Controlled Release* **128**(3), 248–254 (2008)
98. Kiser, P.F., Wilson, G., Needham, D.: *Nature* **394**(6692), 459–462 (1998)
99. Sahiner, N., Alb, A.M., Graves, R., Mandal, T., McPherson, G.L., Reed, W.F., John, V.T.: *Polymer* **48**(3), 704–711 (2007)
100. Jones, C.D., Lyon, L.A.: *Macromolecules* **33**(22), 8301–8306 (2000)
101. Gan, D.J., Lyon, L.A.: *J. Am. Chem. Soc.* **123**(31), 7511–7517 (2001)
102. Paiphansiri, U., Tangboriboonrat, P., Landfester, K.: *Macromol. Biosci.* **6**(1), 33–40 (2006)
103. Crespy, D., Stark, M., Hoffmann-Richter, C., Ziener, U., Landfester, K.: *Macromolecules* **40**(9), 3122–3135 (2007)
104. Downey, J.S., Frank, R.S., Li, W.H., Stover, H.D.H.: *Macromolecules* **32**(9), 2838–2844 (1999)
105. Li, K., Stover, H.D.H.: *J. Polym. Sci. Part A Polym. Chem.* **31**(13), 3257–3263 (1993)
106. Li, K., Stover, H.D.H.: *J. Polym. Sci. Part A Polym. Chem.* **31**(10), 2473–2479 (1993)
107. Fitch, R.M.: *J. Elastomers Plast.* **3**, 146–156 (1971)
108. Croucher, M.D., Winnik, M.A.: In: Candau, F., Ottewill, R.H. (eds.) *Scientific Methods for the Study of Polymer Colloids and Their Applications*, pp. 35–72. Kluwer Academic Publishers, Dordrecht (1990)
109. Bai, F., Yang, X.L., Huang, W.Q.: *J. Appl. Polym. Sci.* **100**(3), 1776–1784 (2006)
110. Li, W.H., Stover, H.D.H.: *Macromolecules* **33**(12), 4354–4360 (2000)
111. Jiang, S., Sudol, E.D., Dimonie, V.L., El-Aasser, M.S.: *J. Appl. Polym. Sci.* **108**(6), 4096–4107 (2008)
112. Paiphansiri, U., Dausend, J., Musyanovych, A., Mailaender, V., Landfester, K.: *Macromol. Biosci.* **9**(6), 575–584 (2009)
113. Chen, Y., Geh, J.L.: *Polymer* **37**(20), 4481–4486 (1996)
114. Fu, Q., Cheng, L.L., Zhang, Y., Shi, W.F.: *Polymer* **49**(23), 4981–4988 (2008)
115. Froimowicz, P., Frey, H., Landfester, K.: *Macromol. Rapid Commun.* **32**(5), 468–473 (2011)
116. Zheng, Y.J., Mieie, M., Mello, S.V., Mabrouki, M., Andreopoulos, F.M., Konka, V., Pham, S.M., Leblanc, R.M.: *Macromolecules* **35**(13), 5228–5234 (2002)
117. Zheng, Y.J., Andreopoulos, F.M., Micic, M., Huo, Q., Pham, S.M., Leblanc, R.M.: *Adv. Funct. Mater.* **11**(1), 37–40 (2001)
118. Froimowicz, P., Klinger, D., Landfester, K.: *Chem. Eur. J.* **17**(44), 12465–12475 (2011)
119. Murphy, E.B., Wudl, F.: *Prog. Polym. Sci.* **35**(1–2), 223–251 (2010)
120. Wu, D.Y., Meure, S., Solomon, D.: *Prog. Polym. Sci.* **33**(5), 479–522 (2008)
121. Chung, C.M., Roh, Y.S., Cho, S.Y., Kim, J.G.: *Chem. Mater.* **16**(21), 3982 (2004)

122. Chen, X.X., Dam, M.A., Ono, K., Mal, A., Shen, H.B., Nutt, S.R., Sheran, K., Wudl, F.: *Science* **295**(5560), 1698–1702 (2002)
123. Nair, K.P., Breedveld, V., Weck, M.: *Macromolecules* **44**(9), 3346–3357 (2011)
124. Cordier, P., Tournilhac, F., Soulie-Ziakovic, C., Leibler, L.: *Nature* **451**(7181), 977–980 (2008)
125. White, S.R., Sottos, N.R., Geubelle, P.H., Moore, J.S., Kessler, M.R., Sriram, S.R., Brown, E.N., Viswanathan, S.: *Nature* **409**(6822), 794–797 (2001)
126. South, A.B., Lyon, L.A.: *Angew. Chem. Int. Ed.* **49**(4), 767–771 (2010)

Chapter 6

Conclusion and Outlook

The work presented in this thesis deals with the development of novel photo-sensitive microgels and nanoparticles as potential materials for the loading and light-triggered release/accessibility of functional compounds. The motivation and unifying basis for the different projects is to get a profound understanding of the stimuli-responsive behavior of these materials. This is achieved by combining the design, realization and characterization of specific response mechanisms on a molecular level with detailed investigations on the influence of these features on the overall sensitivity of the nanoscale polymeric gel particles.

In the following, a short summary of the reached achievements as well as outlooks of possible research directions based on the different approaches is given.

6.1 Photo-Sensitive Microgels Based on Light-Cleavable Crosslinkers

Externally controlling the crosslinking density in microgels by light is one approach to photo-triggered release applications. Here the corresponding increase in mesh size results in increased rates of diffusion of functional substances in the network. In this thesis the successful development of two classes of photo-sensitive microgels was demonstrated: (i) polymeric gel nanoparticles swellable and degradable in organic solvents and (ii) hydrogel nanoparticles swellable and degradable in aqueous media. Both types of microgels are based on newly synthesized light-cleavable crosslinkers containing *o*-nitrobenzyl derivatives as the photo-reactive chromophores.

6.1.1 Photo-Degradable Microgels Based on Photo-Cleavable Monomeric Crosslinkers: Light-Induced Swelling and Degradation in Organic Solvents

Two classes of newly synthesized photo-cleavable crosslinking molecules were used to prepare photo-degradable PMMA microgels by copolymerization in direct miniemulsion. The crosslinkers were designed to exhibit significant differences in their photolysis rates depending on the irradiation conditions, therefore enabling the independent and successive degradation of the resulting microgels following either a wavelength-controlled or an irradiation-time controlled approach. This specific performance in organic solvents represents a great potential for the controlled release of two different functional compounds embedded in two types of microgels out of a mixed dispersion thereof. In this context, e.g. the embedding of metallic nanoparticles would give rise to new light-triggered catalytic materials. The high versatility of the newly developed photo-cleavable crosslinkers was demonstrated by the utilization of a hydrophilic monomer (HEMA) as solvent for the crosslinkers and the preparation of hydroxyl functionalized photo-sensitive PHEMA microgels by an inverse miniemulsion process as well. By taking advantage of potential coupling reactions of functional compounds with the hydroxyl groups (e.g. esterifications, ether formations, etc.) a post polymerization functionalization of the network could be envisioned.

6.1.2 Photo-Degradable Hydrogel Nanoparticles Based on Photo-Cleavable Monomeric Crosslinkers: Light-Induced Swelling and Degradation in Aqueous Media

The concept of light-degradable microgels was successfully transferred to water swellable gel nanoparticles. Here, copolymerization of the crosslinkers with HEMA and MAA in an inverse miniemulsion resulted in double stimuli-responsive p(HEMA-co-MAA) microgels which exhibited a pH-dependent swelling and light-induced degradation behavior. Preliminary investigations on non-photo-sensitive p(HEMA-co-MAA) microgels demonstrated the successful loading with myoglobin as a model protein and its subsequent release. It was found that a *post-formation* loading method by electrostatic interactions between protein and gel network in combination with a pH-induced entrapment was very efficient. Cell tests were performed on fluorescent microgels of the same composition and revealed good cellular uptake and negligible cytotoxicity of these materials. The photo-sensitive analogues are assumed to behave similarly. Thus, they represent highly interesting potential carriers for delivery applications.

6.1.3 Photo-Degradable Hydrogel Nanoparticles Based on Photo-Cleavable Polymeric Crosslinkers: Light-Induced Swelling and Degradation in Aqueous Media

In a first attempt, free radical copolymerizations of methacrylated dextrans with acrylamide in inverse miniemulsion were investigated and revealed the adaptability of the functionalized polysaccharides as crosslinkers for the preparation of enzymatically degradable microgels. This concept was further extended to double stimuli-responsive enzymatically- and light-degradable microgels by the utilization of acrylate functionalized dextrans containing a photo-labile linker between the polymerizable vinyl group and the polysaccharide backbone. It was shown that irradiation with UV light enabled either complete particle degradation or the adjustment of a desired specific degree of swelling by tuning the irradiation time accordingly. In addition, a two step degradation profile based on the subsequent appliance of the two orthogonal stimuli was realized. This behavior renders these materials promising candidates for either triggered release or accessibility applications in aqueous media. Especially the water solubility of the light-cleavable crosslinkers is assumed to give rise to a potential in situ embedding of functional water soluble compounds (e.g. proteins) already during microgel formation by free radical (co)polymerization in the aqueous droplets.

6.2 Light-Sensitive Microgel-Doxorubicin Conjugates: Labile Drug Attachment via a Photo-Cleavable Linker

A novel functional monomer consisting of a doxorubicin molecule bound to a radically polymerizable methacrylate group via a photo-labile linker was designed to enable the covalent attachment of the drug molecule to a polymeric network. In contrast to previously described approaches based on network degradation, it is assumed that an effective release only at the targeted site can be induced by the light-induced cleavage of the linker molecule while leaving the microgel structure intact. An efficient synthetic pathway to the described doxorubicin-photo-labile linker-methacrylate monomer was successfully developed. The molecular structure of the compound was designed to exhibit a minor extinction coefficient of the doxorubicin moiety at the wavelength targeted for cleavage. As demonstrated by irradiation time-dependent UV-vis measurements, this enabled the photolytically triggered drug detachment without light-induced changes in the pharmaceutically active molecule. Furthermore, a mild preparation method for p(HEMA-*co*-MAA) microgels was elaborated in order to ensure the potential incorporation of the Dox-PL-MA in situ during nanoparticles formation without damaging the drug molecule.

In future, doxorubicin-microgel conjugates should be investigated with regard to the incorporation efficiency of doxorubicin, the light-triggered release profile of the drug from the network in PBS and its influence on cell viability.

6.3 Photo-Resist Nanoparticles

Hydrophobic nanoparticles consisting of a photo-resist polymer were prepared in a facile way by free radical polymerization of a photo-labile *o*-nitrobenzyl ester of methacrylic acid in miniemulsion. These lattices were designed to be degradable upon a light-induced change of the hydrophobicity of the respective material. Deprotection of the methacrylic acid groups on the polymeric backbone was easily achieved by the photolytic cleavage of the *o*-nitrobenzyl esters. As a result, conversion of the initial hydrophobic polymer into hydrophilic PMAA induced in situ particle dissolution in water. With the aim to investigate the potential of the described particles for release applications, Nile red was encapsulated as a model compound and fluorescent probe. Thus, it enabled to study not only the particle degradation process (via solubilization of in situ generated PMAA during photocleavage of the photo-resist polymer), but also the possibility to perform controlled release experiments. In comparison to the potential release of hydrophilic compounds from photo-sensitive hydrogel nanoparticles, the liberation of hydrophobic substances in aqueous medium dramatically extends the field of potential applications for light-responsive carriers. Moreover, the confinement of a photo-resist material to nanoscale structures gives rise to potential new ways of surface patterning by e.g. colloidal lithography.

6.4 Towards Stimuli-Responsive Core/Shell Nanoparticles Containing a Hydrogel Core

The loading and release efficiency of stimuli-responsive microgels can be enhanced by introducing a degradable/swellable (polymeric) shell around the respective microgel core. Since this shell serves as a diffusion barrier, leakage of embedded compounds can be prevented. In this thesis, two synthetic pathways for the preparation of non-stimuli-responsive core/shell nanoparticles as model compounds were investigated.

First, the seeded precipitation polymerization of PMMA around preformed PAAm hydrogel nanoparticles was found to yield PAAm/PMMA core/shell nanoparticles. Examinations on the synthetic parameters revealed a dependency of the successful formation of these materials on the type and amount of surfactant necessary to stabilize both the seed microgels and the core/shell particles. Transferring this concept to stimuli-responsive analogues containing a sensitive shell and core is assumed to give rise to a highly interesting class of carrier systems for delivery applications.

Second, PAAm/PU core/shell nanoparticles were prepared by the microgel formation in preformed PU nanocapsules. Here, the PU shell was formed by interfacial polycondensation on the surface of droplets containing monomers and crosslinkers for the subsequent microgel formation by free radical

copolymerization. It is of special interest to render the shell permeable for potentially embedded functional substances upon the appliance of a specific stimulus. Therefore, a photo-degradable polyurethane as potential material for a light-responsive shell was prepared and cleavage of the polymer main chain was successfully demonstrated upon irradiation in solution. Thus, the formation of core/shell particles containing a light-responsive shell in a fashion similar to plain PU shells represents an attractive field for further examinations.

6.5 Surface Modification of Microgels with Photo-Reactive Chromophores

A synthetic protocol for the facile and effective surface functionalization of PHEMA and p(HEMA-*co*-MAA) microgels with cinnamoyl groups was developed. The attachment of photo-reactive moieties on the microgels surfaces gives rise to trigger the (reversible) particles interaction with different compounds or with each other by light-induced [2+2] cycloaddition reactions. The adaptability of this concept was demonstrated by using the respective materials as nanometric building blocks for the formation of self-healing hydrogel thin films by Dr. P. Froimowicz.

As a concluding remark it can be stated, that the photo-responsive microgels and nanoparticles developed in this thesis exhibit great potential for loading and release applications. Especially the detailed investigations on controlling the stimuli-responsive behavior on a molecular level are of high importance to be able to adjust the properties of these materials for specific applications. The acquired insights in the underlying mechanisms of response represent a profound basis for further research in this area. In future, it is of interest to investigate the loading efficiency of these carrier systems with functional compounds such as enzymes or catalytically active metal nanoparticles and examine their triggered release or catalytic activity.

Chapter 7

Experimental Part

7.1 Materials

All chemicals were commercially available, purchased from sigma Aldrich and used without further purification unless otherwise stated. Methyl methacrylate (MMA), 2-hydroxyethyl methacrylate (HEMA) diethyleneglycol dimethacrylate (DEGDMA) and divinyl benzene (DVB) were purified over basic aluminium oxide to remove contained inhibitor. Methacrylic acid (MAA), triethylamine and 2,4-toluenediisocyanate (TDI) were distilled under reduced pressure prior to use. Acrylamide was obtained from Fluka Chemicals. Doxorubicin Hydrochloride was obtained from AppliChem. Initiators (2,2'-azobis(2-methyl-butyrionitrile) (V-59); 2,2'-azobis(4-methoxy-2,4-dimethylvaleronitrile) (V-70); 2,2'-azobis(N,N'-dimethyleneiso-butylamide) dihydro-chloride (VA-044)) were obtained from Wako Chemicals. Lubrizol U (poly(isobutylene-succinimide pentamine)) was kindly provided by Lubrizol, France. Poly(ethylene-*co*-butylene)-*block*-poly(ethylene-glycol) [P(E/B)-*b*-PEO, KLE] [$M_n(\text{P(E/B)}) = 5,800 \text{ g/mol}$; $M_n(\text{PEO}) = 6,200 \text{ g/mol}$] was prepared by anionic polymerization by Melanie Droege. Lutensol AT-50 was kindly provided by BASF.

7.2 Instrumentation

^1H - (300 MHz) and ^{13}C -NMR (75 MHz) spectra were measured using a Bruker spectrometer. UV-vis measurements were performed using a Perkin Elmer Lambda 25 UV/VIS spectrometer. A NICOMP zetasizer measuring at a fixed scattering angle of 90° was used to determine particle size distributions by dynamic light scattering (DLS). The measurements were carried out at 25°C on diluted dispersions in the respective solvents. Irradiations were either carried out by using a 365 nm emitting UV-LED with a maximum power of 150 W or an OSRAM HBO 100 W/2 mercury short arc lamp, either combined with a UG-11 and a W-320 filter resulting in an output of wavelengths of $\lambda = 315\text{--}390 \text{ nm}$ or

used without any filters resulting in a broadband spectrum of emitted light. HPLC measurements were conducted using an Agilent quaternary gradient pump (series 1100) combined with an Agilent photodiode array detector (DAD series 1200). A Gemini 1530 (Carl Zeiss AG, Oberkochen, Germany) with an InLens detector was used to take scanning electron micrographs (SEM). The samples were prepared by drop-casting of diluted dispersions on a silicon wafer. Fluorescence spectroscopy was performed on a Tecan plate reader using a Hellman 96 well quartz plate. Each measurement was performed in triplicate.

7.3 Synthesis of Light-Cleavable Monomeric Crosslinkers

(2-Nitro-1,4-phenylene)dimethanol (2NPDM). The procedure of Piggott and Karuso [1] was followed. Briefly, 5 equivalents of a 1 M borane-THF complex solution in THF were added under nitrogen to a stirred ice-cooled solution of 1 equivalent of 2-nitroterephthalic acid in anhydrous THF. After complete addition, the reaction mixture was allowed to warm to room temperature for 1 h and then stirred over night at 40 °C. Destruction of the excess borane by dropwise addition of water was followed by removal of the organic solvent under reduced pressure. The resulting aqueous phase was extracted three times with ethyl acetate, the organic layers were combined, dried with anhydrous magnesium sulfate and the solvent was removed under reduced pressure. Recrystallization of the obtained yellow solid from chloroform yielded (2-nitro-1,4-phenylene)dimethanol as yellowish needles. Yield 90 %.

mp 91–93 °C. Elemental analysis calc. for $C_8H_9NO_4$: C, 52.46; H, 4.95; N, 7.65; found: C, 52.40; H, 5.09; N, 7.69. 1H NMR (DMSO- d_6): δ = 8.05 (s, 1H), 7.81 (d, 1H, J = 8.0 Hz), 7.68 (d, 1H, J = 8.0 Hz), 4.93 (s, 2H), 4.69 (s, 1H). ^{13}C NMR (DMSO- d_6): δ = 146.70, 142.86, 136.41, 131.35, 128.24, 121.66, 61.52, 59.77. MS (FD) m/z 183.7 (M^+)

2,2'-(2-nitro-1,4-phenylene)bis(methylene)bis(oxy)bis(oxomethylene)bis(oxy)bis-(ethane-2,1-diyl)bis(2-methylacrylate) (CL-1A). A solution of 2-hydroxyethyl methacrylate (HEMA) (1.86 g, 14.3 mmol) in anhydrous THF (5 mL) was added dropwise to a solution of carbonyldiimidazol (CDI) (2.39 g, 14.3 mmol) in anhydrous THF (20 mL). After stirring the reaction mixture over night at room temperature, a solution of 2NPDM (1.31 g, 7.15 mmol) in anhydrous THF (20 mL) together with a 1.75 mol/L sodium ethanolate suspension (0.2 mL, 0.35 mmol) was added to the activated HEMA (2). Additional stirring for 5 d at room temperature was followed by filtration and reduction of the filtrate to dryness under reduced pressure. The residue was purified by column chromatography over silica using $CHCl_3/MeOH$ (20:1) as eluent and yielded CL-1A (1.84 g, 3.72 mmol) as a slightly yellow colored oil. Yield 52 %.

Elemental analysis calc. for $C_{22}H_{25}NO_{12}$: C, 53.33; H, 5.09; N, 2.83; found: C, 53.53; H, 5.07; N, 2.81. 1H NMR ($CDCl_3$): δ = 8.17 (s, 1H), 7.68 (s, 1H), 7.67 (s, 1H), 6.12 (d, 1H, J = 5.2 Hz), 5.59 (m, 4H), 5.23 (s, 2H), 4.41 (m, 8H) ppm 1.93

(d, 6H, $J = 3.6$ Hz). ^{13}C NMR (CDCl_3): $\delta = 167.05, 154.60, 147.19, 136.79, 135.79, 133.27, 131.96, 128.99, 126.27, 124.60, 67.77, 66.12, 65.82, 62.17, 18.24$. MS (FD) m/z 493.9 (M^+)

2,2'-(2-nitro-1,4-phenylene)bis(methylene)bis(oxy)bis(oxomethylene)bis(azane-diyl)-bis(ethane-2,1-diyl) bis(2-methylacrylate) (CL-2A). 2NPDM (1.00 g, 5.5 mmol) was dissolved in anhydrous THF (10 mL) and added dropwise to a solution of 2-isocyanatoethyl methacrylate (1.71 g, 11.0 mmol) in anhydrous THF (15 mL) under nitrogen. The reaction mixture was heated to 65 °C and stirred for 24 h at this temperature. FT-IR measurements showed complete disappearance of the corresponding isocyanato absorption band at 2260 cm^{-1} , thus indicating complete conversion of the latter. The solvent was evaporated and the residue was purified by column chromatography over silica using $\text{CHCl}_3/\text{MeOH}$ (10:1) as eluent yielding 72 % of CL-2A (1.95 g, 4.0 mmol) as a slightly yellow colored oil which slowly solidified at 5 °C.

Elemental analysis calc. for $\text{C}_{22}\text{H}_{27}\text{N}_3\text{O}_{10}$: C, 53.55; H, 5.51; N, 8.52; found: C, 53.75; H, 5.77; N, 8.47. ^1H NMR (CDCl_3): $\delta = 8.06$ (s, 1H), 7.58 (s, 1H), 7.56 (s, 1H), 6.11 (m, 2H), 5.58 (m, 2H), 5.49 (s, 2H), 5.18 (m, 4H), 4.24 (t, 4H, $J = 5.4$ Hz), 3.51 (q, 4H, $J = 5.5$ Hz), 1.93 (s, 6H). ^{13}C NMR (CDCl_3): $\delta = 167.30, 155.80, 147.47, 137.94, 135.91, 132.83, 132.67, 129.16, 126.16, 124.14, 65.00, 63.55, 63.28, 40.44, 18.29$. MS (FD) m/z 494.6 (M^+)

Bis(2-(methacryloyloxy)ethyl) -(2-nitro-1,4-phenylene)bis(methylene) di-succinate (CL-3A). Mono-2-(methacryloyloxy)ethyl succinate (2.53 g, 11.0 mmol) was dissolved in anhydrous benzene and oxalylchloride (2.79 g, 2 mmol) was added under nitrogen at room temperature. The reaction mixture was slowly heated to 85 °C and refluxed for 3 h. After cooling to room temperature, benzene and excess oxalylchloride were removed under reduced pressure. The obtained acyl chloride (**3**) was dissolved in anhydrous THF (35 mL) and a solution of 2NPDM (1.00 g, 5.5 mmol) and triethylamine (1.21 g, 12.0 mmol) in THF (15 mL) was added dropwise. After stirring the mixture over night at room temperature, precipitated solids were removed by filtration and the solution was reduced to dryness. The residue was dissolved in DCM (100 mL), washed three times with water, dried with MgSO_4 and evaporated. The resulting red oil was purified by column chromatography over silica using $\text{CHCl}_3/\text{MeOH}$ (40:1) as eluent and afforded 40 % of pure CL-3A (1.34 g, 2.2 mmol).

Elemental analysis calc. for $\text{C}_{28}\text{H}_{33}\text{NO}_{14}$: C, 55.35; H, 5.47; N, 2.31; found: C, 55.24; H, 5.54; N, 2.38. ^1H NMR (CDCl_3): $\delta = 8.02$ (s, 1H), 7.56 (s, 1H), 7.55 (s, 1H), 6.05 (m, 2H), 5.52 (m, 2H), 5.46 (s, 2H), 5.13 (s, 2H), 4.28 (m, 8H), 2.65 (m, 8H), 1.87 (s, 1H). ^{13}C NMR (CDCl_3): $\delta = 171.80, 167.06, 147.49, 137.34, 135.89, 132.94, 131.84, 129.32, 126.07, 124.31, 64.67, 63.02, 62.49, 62.26, 28.85, 18.23$. MS (FD) m/z 606.8 (M^+)

4-(4-(1-Hydroxyethyl)-2-methoxy-5-nitrophenoxy)butanol (HEMNPB). The product was prepared based on the synthetic protocols by Holmes. [2, 3]

Methyl 4-(4-Acetyl-2-methoxyphenoxy)butanoate (5). Acetovanillone (**4**) (41.00 g, 246.7 mmol) was suspended together with 1.1 equivalents of methyl 4-bromobutyrate (49.63 g, 274.1 mmol) and 1.5 equivalents of potassium

carbonate (51.1 g, 370.0 mmol) in anhydrous dimethyl formamide (200 mL) and stirred under argon for 16 h. Afterwards, the reaction mixture was diluted with an excess amount of water to dissolve all inorganic salts and then extracted with ethyl acetate. Removal of the organic solvent after drying with MgSO_4 yielded the keto-ester product (**5**) in quantitative crude yield (99 %, 65.25 g, 245.0 mmol).

Elemental analysis calc. for $\text{C}_{14}\text{H}_{18}\text{O}_5$: C, 63.15; H, 6.81; found: C, 62.89; H, 6.43. ^1H NMR (CDCl_3): $\delta = 7.53$ (m, 2H), 6.88 (d, 1H, $J = 8.2$ Hz), 4.13 (t, 2H, $J = 6.3$ Hz), 3.90 (s, 2H), 3.68 (s, 2H), 2.53 (t, 2H, $J = 7.3$ Hz), 2.18 (m, 2H). ^{13}C NMR (CDCl_3): $\delta = 196.90, 173.56, 152.74, 149.42, 130.67, 123.30, 111.43, 110.64, 67.88, 56.11, 51.77, 30.44, 26.30, 24.41$. MS (FD) m/z 265.9 (M^+)

Methyl 4-(4-Acetyl-2-methoxy-5-nitrophenoxy)butanoate (6). Subsequent nitration was achieved by drop wise adding a solution of the keto-ester (**5**) (10.0 g, 37.6 mmol) in acetic anhydride (30 mL) to a mixture of acetic anhydride (40 mL) and nitric acid (70 %, 200 mL) at 0 °C. After stirring for 3 h, the mixture was precipitated in 500 mL of ice water and kept in the refrigerator for 2 days. The precipitated product was filtered, repeatedly washed with ice water and the obtained solid recrystallized from MeOH/ H_2O yielding 53 % (6.20 g, 19.9 mmol) of the nitrated product.

Elemental analysis calc. for $\text{C}_{14}\text{H}_{17}\text{NO}_7$: C, 54.02; H, 5.50; N, 4.50; found: C, 53.89; H, 5.70; N, 4.41. ^1H NMR (CDCl_3): $\delta = 7.60$ (s, 1H), 6.74 (s, 1H), 4.15 (t, 2H, $J = 6.2$ Hz), 3.95 (s, 1H), 3.70 (s, 1H), 2.56 (t, 2H, $J = 7.2$ Hz), 2.53 (s, 3H), 2.26–2.13 (m, 2H). ^{13}C NMR (CDCl_3): $\delta = 200.15, 173.36, 154.46, 149.01, 138.54, 133.02, 108.95, 108.21, 68.59, 56.73, 51.88, 30.50, 30.40, 24.32$. MS (FD) m/z 311.0 (M^+)

4-(4-(1-Hydroxyethyl)-2-methoxy-5-nitrophenoxy)butanoic acid (8). In the next step, the reduction of the keto group was conducted by dissolving **6** (6.5 g, 20.9 mmol) in 100 mL MeOH/THF (1/2 v/v) and adding sodium borohydride (948 mg, 25.1 mmol). After stirring for 1 h at room temperature, sodium borohydride (237 mg, 6.3 mmol) was added and the reaction mixture was stirred over night at room temperature. This procedure was directly followed by inducing the ester cleavage by addition of 50 mL of NaOH (1 N) in 25 mL of water and stirring the mixture at room temperature for 7 h. The organic solvents were removed under reduced pressure and the resulting water phase was slowly acidified with diluted hydrochloric acid. The crude product was obtained by extracting the water phase with ethyl acetate and evaporation of the dried organic layers. Recrystallization from ethyl acetate/hexane afforded the photo-labile molecule (**8**) in 86 % yield as a pale yellow solid.

Elemental analysis calc. for $\text{C}_{13}\text{H}_{17}\text{NO}_7$: C, 52.17; H, 5.73; N, 4.68; found: C, 52.10; H, 5.88; N, 4.69. ^1H NMR (CDCl_3): $\delta = 7.41$ (s, 1H), 7.24 (s, 1H), 5.37 (q, 1H, $J = 6.2$ Hz), 3.97 (t, 2H, $J = 6.4$ Hz), 3.82 (s, 3H), 2.37 (t, 2H, $J = 7.2$ Hz), 2.00 (m, 2H), 1.35 (d, 3H, $J = 6.2$ Hz). ^{13}C NMR (CDCl_3): $\delta = 174.64, 153.77, 146.29, 138.85, 138.06, 108.70, 108.620, 67.98, 64.68, 55.96, 29.92, 24.58, 23.92$. MS (FD) m/z 299.2 (M^+)

4-[4-(1-Hydroxyethyl)-2-methoxy-5-nitrophenoxy]butanol (HEMNPB) (9). 1.5 g of **8** (5.0 mmol) were dissolved in 25 mL of anhydrous THF and 1 M

borane-THF complex solution in THF (12.5 mL, 12.5 mmol) were added dropwise at 0 °C. The reaction mixture was allowed to warm to room temperature while stirring for 1 h and was then stirred at 40 °C over night. Afterwards, the solution was cooled to 0 °C and 40 mL of ice water were added to destroy excess borane. The organic solvent was removed under reduced pressure and remaining aqueous phase was extracted with ethyl acetate. The combined organic layers were dried over MgSO₄, filtered and the solvent was removed under reduced pressure. The obtained crude product was recrystallized from chloroform affording pure **9** in 79 % yield (1.127 g, 3.95 mmol).

mp 165-169 °C. Elemental analysis calc. for C₁₃H₁₉NO₆: C, 54.73; H, 6.71; N, 4.91; found: C, 54.73; H, 7.01; N, 4.79. ¹H NMR (CDCl₃): δ = 7.55 (s, 1H), 7.29 (s, 1H), 5.55 (q, 1H, *J* = 6.3 Hz), 4.10 (t, 2H, *J* = 6.1 Hz), 3.97 (s, 3H), 3.73 (t, 2H, *J* = 6.2 Hz), 1.98 (m, 2H), 1.77 (m, 2H), 1.55 (d, 3H, *J* = 6.3 Hz). ¹³C NMR (CDCl₃): δ = 153.67, 146.38, 138.87, 137.94, 108.62, 108.30, 68.91, 64.65, 61.40, 55.96, 28.89, 25.23, 24.60. MS (FD) *m/z* 285.0 (M⁺)

2-((1-(4-(4-(2-(methacryloyloxy)ethylcarbamoyloxy)butoxy)-5-methoxy-2-nitro-phen-yl)ethoxy)carbonylamino)ethyl methacrylate (CL-4B). 2-Isocyanatoethyl methacrylate (1.14 g, 7.4 mmol) was dissolved in anhydrous THF (5 mL) and added to a solution of HEMNPB (**9**) (1.00 g, 3.5 mmol) and dibutyltin dilaurate (0.11 g, 0.18 mmol) in anhydrous THF (25 mL) under nitrogen. After the mixture was heated to 65 °C and stirred for 48 h at this temperature, FT-IR measurements showed complete disappearance of the corresponding isocyanato absorption band at 2260 cm⁻¹. This being an indicator for complete conversion of the isocyanate, the solvent was then removed under reduced pressure and the residue was purified by column chromatography over silica using CHCl₃/MeOH (10:1) as eluent. The obtained slightly yellow colored oil slowly solidified in the refrigerator and was found to consist of pure CL-4B (1.32 g, 2.2 mmol, 63 %).

Elemental analysis: calc. for C₂₇H₃₇N₃O₁₂: C, 54.45; H, 6.26; N, 7.06, found C, 54.73; H, 6.59; N, 6.70. ¹H NMR (CDCl₃): δ = 7.56 (s, 1H), 6.98 (s, 1H), 6.37 (q, 1H, *J* = 6.3 Hz), 6.10 (d, 2H, *J* = 7.7 Hz), 5.59 (m, 2H), 5.06 (s, 1H), 4.96 (t, 1H), 4.13 (m, 8H), 3.93 (s, 1H), 3.48 (m, 4H), 1.93 (d, 6H, *J* = 4.6 Hz), 1.81 (m, 4H), 1.81 (m, 1H), 1.59 (d, 3H, *J* = 6.3 Hz). ¹³C NMR (CDCl₃): δ = 167.29, 156.47, 155.20, 153.97, 147.20, 139.69, 135.96, 133.81, 126.05, 108.92, 69.10, 68.85, 64.48, 63.70, 63.65, 56.30, 40.18, 25.62, 25.46, 22.17, 18.27. MS (FD) *m/z* 595.5 (M⁺)

4-(4-(1-(Methacryloyloxy)ethyl)-2-methoxy-5-nitrophenoxy)butanoic acid (10). To an ice-cooled suspension of **8** (1.750 g, 5.85 mmol) and triethylamine (1.775 g, 17.54 mmol) in 70 mL of anhydrous DCM, methacryloyl chloride (1.746 g, 14.62 mmol) was added dropwise at 0 °C under argon atmosphere. The reaction mixture was allowed to warm to room temperature while stirring over night and the resulting solution was washed with Na₂CO₃ (5 %), HCl (1 %), and water. The organic solvent was evaporated, the residue was dissolved in acetone/water and stirred over night, insoluble components were removed by filtration and the mixture was extracted with DCM. After washing the resulting solution with HCl (1 %) and water, the organic phase was dried over MgSO₄ and the solvent

was removed. Purification by column chromatography over silica using MeOH/CHCl₃ (1:5 v/v) as eluent yielded pure **10** in 43 % yield.

Elemental analysis: calc. for C₁₇H₂₁NO₈: C, 55.58; H, 5.76; N, 3.81, found C, 55.41; H, 5.84; N, 3.96. ¹H NMR (CDCl₃): δ = 7.59 (s, 1H), 7.02 (s, 1H), 6.52 (q, 1H), 6.17 (s, 1H), 5.61 (s, 1H), 4.12 (t, 2H), 3.92 (s, 3H), 2.61 (t, 2H), 2.19 (qnt, 2H), 1.95 (s, 3H), 1.66 (d, 3H). ¹³C NMR (CDCl₃): δ = 178.21, 166.08, 154.01, 147.12, 139.76, 136.35, 133.58, 125.73, 109.10, 108.11, 68.76, 68.04, 56.20, 30.21, 23.99, 22.04, 18.32. MS (FD) *m/z* 367.1 (M⁺)

1,1'-(4,4'-(4,4'-(Ethane-1,2-diylbis(azanediyl))bis(4-oxobutane-4,1-diyl))bis(oxy)bis(5-methoxy-2-nitro-4,1-phenylene))bis(ethane-1,1-diyl)bis(2-methylacrylate) (CL-5B). A solution of **10** (0.847 g, 2.30 mmol), DMAP (0.054 g, 0.44 mmol) and ethylene diamine (0.065 g, 1.10 mmol) in 40 mL of anhydrous DCM was cooled to 0 °C and stirred at this temperature for 30 min. DCC (0.520 g, 2.52 mmol) was dissolved in 10 mL of anhydrous DCM and added to the reaction mixture which was allowed to warm to room temperature while stirring over night. Filtration to remove the produced urea was followed by washing the organic solution with saturated NH₄Cl, saturated Na₂CO₃, and brine. The organic phase was dried over MgSO₄ and the solvent was evaporated under reduced pressure. The resulting residue was purified by column chromatography using silica and MeOH/CHCl₃ as eluent yielding pure CL-5B as a pale yellow solid (0.422 g, 0.56 mmol) (51 %).

Elemental analysis: calc. for C₃₆H₄₆N₄O₁₄: C, 56.99; H, 6.11; N, 7.38; found C, 57.13; H, 6.02; N, 7.49. ¹H NMR (CDCl₃): δ = 7.58 (s, 2H), 7.01 (s, 2H), 6.50 (q, 2H), 6.46 (s, 2H), 6.17 (s, 2H), 5.61 (s, 2H), 4.09 (t, 4H), 3.92 (s, 6H), 3.38 (dd, 4H), 2.40 (t, 4H), 2.16 (qnt, 4H), 1.95 (s, 6H), 1.65 (d, 6H). ¹³C NMR (CDCl₃): δ = 173.44, 166.23, 154.02, 147.23, 139.96, 136.46, 133.68, 125.89, 109.21, 108.24, 68.87, 68.70, 56.39, 40.38, 32.90, 24.88, 22.14, 18.43. MS (FD) *m/z* 759.6 (M + 1⁺), 1518.1 (2 M⁺)

7.4 Synthesis of Enzymatically Degradable Macromolecular Cross-Linkers

Synthesis of dextran methacrylates. *All Experiments were conducted by Eugen Aschenbrenner following the procedure described below.* Dextran was functionalized using a modification of the protocol presented by Kim et al. [4]. In brief, the polysaccharide was dissolved in a 10 wt% LiCl solution of DMF at 90 °C. After cooling the reaction mixture to 60 °C, an equimolar amount of triethylamine (with respect to the anhydride) was added, followed by dropwise addition of a defined amount of methacrylic anhydride. The reaction was allowed to proceed for 2 h and the stopped by cooling to room temperature and precipitating in 2-propanol. The precipitate was separated by centrifugation (Sigma 3K30, 5 min @ 10,000 min⁻¹), dissolved in water, precipitated in 2-propanol and centrifuged

Table 7.1 Synthetic details and results for the preparation of Dex-MA crosslinkers with various degrees of substitution

Sample	Dextran $M_w/g/mol$	MA/Dex-OH ^a	DS	Yield %
Dex-MA1	40,000	0.05	0.12	90
Dex-MA2	40,000	0.10	0.17	82
Dex-MA3	40,000	0.15	0.33	89
Dex-MA4	6,000	0.05	0.09	45
Dex-MA5	6,000	0.10	0.19	39
Dex-MA6	6,000	0.15	0.29	31
Dex-MA7	40,000	0.03	0.05	78

^a Molar ratio of methacrylic anhydride/hydroxyl groups of dextran

again. Residual water soluble reactants were removed by dialysis (regenerated cellulose MWCO 3.5 k) against water 2 days. Subsequently, the product was dried in vacuum and analyzed by ¹H-NMR spectroscopy in D₂O. Exact amounts of chemicals are listed in Table 7.1.

The DS was evaluated from ¹H NMR spectra by calculating the ratio of the peak areas of the olefinic peak at 6.2 ppm relative to the anomeric proton of dextran assigned to the peak at 4.9 ppm by using the formula below.

$$DS(Dex - MA) = \frac{A[\text{olefinic} - H @ 6.2 \text{ ppm}]}{A[\text{anomeric} - H @ 4.9 \text{ ppm}]}$$

7.5 Synthesis of Enzymatically and Light-Degradable Macromolecular Crosslinkers

4-(4-(1-(acryloyloxy)ethyl)-2-methoxy-5-nitrophenoxy)butanoic acid (AEMN PBA) (11). 4-(4-(1-Hydroxyethyl)-2-methoxy-5-nitrophenoxy)butanoic acid (**8**) (1.000 g, 3.34 mmol) was dissolved under argon in anhydrous dichloromethane (40 mL). Triethylamine (1.014 g, 10.00 mmol) was added and the solution was cooled to 0 °C. Acryloyl chloride (0.756 g, 8.35 mmol) was dissolved in 10 mL of anhydrous dichloromethane and added dropwise to the reaction vessel. The mixture was stirred over night and allowed to warm up to room temperature. Afterwards, the solution was washed in every case three times with sodium carbonate solution, diluted hydrochloric acid and deionized water. The organic solvent was evaporated under reduced pressure and the resulting solid was stirred in acetone/water over night. Insoluble contents were removed by filtration and the remaining phase was extracted three times with dichloromethane. The combined organic layers were washed with diluted hydrochloric acid and deionized water, dried over MgSO₄ and the solvent was removed. The remaining yellow solid was purified by column chromatography over silica using CHCl₃/MeOH 10:1 v/v as eluent and pure AEMNPBA (**11**) (0.771 g, 2.18 mmol) was obtained in 65 % yield as yellow solid.

Elemental analysis: calc. for C₁₆H₁₉NO₈: C, 54.39; H, 5.42; N, 3.96; found C, 54.27; H, 5.46; N, 3.84. ¹H NMR (CDCl₃): δ = 7.59 (s, 1H), 7.00 (s, 1H), 6.53 (q, 1H, *J* = 6.4 Hz), 6.43 (dd, 1H, *J* = 1.5 Hz, *J* = 17.3 Hz), 6.15 (dd, 1H, *J* = 10.4 Hz, *J* = 17.3 Hz), 5.87 (dd, 1H, *J* = 1.5 Hz, *J* = 10.4 Hz), 4.12 (t, 2H, *J* = 6.2 Hz), 3.92 (s, 3H), 2.61 (t, 2H, *J* = 7.1 Hz), 2.18 (m, 2H), 1.65 (d, 1H, *J* = 6.4 Hz). ¹³C NMR (CDCl₃): δ = 178.44, 164.93, 154.04, 147.15, 139.79, 133.34, 131.39, 128.23, 109.10, 108.14, 68.63, 68.04, 56.28, 30.22, 23.97, 22.01. MS (FD) *m/z* 353.2 (M⁺)

Dextran-Photo-Labile Linker-Acrylate (Dex-PL-A). In the first step, oxalyl chloride (0.333 g, 2.62 mmol) in 5 mL of anhydrous dichloromethane was added dropwise to an ice cooled solution of AEMNPBA (0.771 g, 2.18 mmol) in 30 mL of anhydrous dichloromethane under argon. Few drops of DMF were added and the mixture was stirred at room temperature for 2.5 h. The solvent was removed under reduced pressure and the flask was vented with argon. The resulting oil of **12** was dissolved in 5 mL of anhydrous DMF and added dropwise to a solution of dextran (6,000 g/mol, 1.596 g, 0.226 mmol, 9.044 mmol glucopyranosyl groups), LiCl (4.0 g) and NEt₃ (0.572 g, 3.39 mmol) in 50 mL of anhydrous DMF. The reaction mixture was stirred at room temperature over night and then heated to 60 °C for 1 h. After cooling the solution to room temperature, the modified dextran was obtained by precipitation in isopropanol. The crude product was dissolved in water, precipitated again in isopropanol. This purification procedure was repeated for a total of 2 times and the functionalized dextran was obtained in 58 % yield as slightly yellow colored powder from freeze drying of the aqueous solution. The degree of substitution (*DS*) was obtained from ¹H NMR spectroscopy by calculating the peak area ratio of the 6 (olefinic, aromatic and tertiary benzylic) protons assigned to the multiplets from 7.70–5.60 ppm relative to the anomeric protons of dextran assigned to the multiplet at 5.25–4.75 ppm by using the formula below.

$$DS(Dex - PL - A) = \frac{A[6H(PL - A)@7.70 - 5.60ppm]/6}{A[1H(anomeric)@5.25 - 4.75ppm]}$$

A *DS* of 0.17 was determined meaning that in a dextran chain of 34 glucopyranosyl groups every 6th group is functionalized with the photo-labile linker acrylate.

7.6 Synthesis of Doxorubicin-Methacrylate Containing a Photo-Labile Linker

Synthesis of doxorubicin-photo-labile-linker-methacrylate (Dox-PL-MA). This chapter only contains the synthetic details for the successful synthetic route B as described in the results and discussion section.

4-(4-Acetyl-2-methoxy-5-nitrophenoxy)butanoic acid (13). Methyl 4-(4-acetyl-2-methoxy-5-nitrophenoxy)butanoate (**6**) (5.0 g, 16.0 mmol) was dissolved in a mixture of THF (80 mL) and MeOH (40 mL). 40 mL of 1 N NaOH and 20 mL of water were added and the reaction mixture was stirred at room temperature for 16 h. The organic solvents were removed under reduced pressure and the residue was carefully acidified with diluted hydrochloric acid (6 N). The obtained yellow colored suspension was extracted 4 times with ethyl acetate, the organic layers were combined, dried with MgSO_4 and the solvent was evaporated. The remaining solid was recrystallized from ethyl acetate/hexane affording pure **13** (3.591 g, 12.1 mmol) in 76 % yield.

Elemental analysis: calc. for $\text{C}_{13}\text{H}_{15}\text{NO}_7$: C, 52.53; H, 5.09; N, 4.71; found C, 52.51; H, 5.24; N, 4.83. ^1H NMR (CDCl_3): $\delta = 7.57$ (s, 1H), 6.69 (s, 1H), 4.11 (t, 2H, $J = 6.4$ Hz), 3.89 (s, 3H), 2.46 (t, 2H, $J = 7.1$ Hz), 2.42 (s, 4H), 2.11 (m, 2H). ^{13}C NMR (CDCl_3): $\delta = 200.01, 174.88, 154.25, 148.87, 138.26, 132.60, 108.67, 108.02, 68.45, 56.55, 30.30, 30.03, 24.03$. MS (FD) m/z 297.2 (M^+)

tert-Butyl(2-(4-(4-acetyl-2-methoxy-5-nitrophenoxy)butanamido)ethyl)carbamate (14). 4-(4-Acetyl-2-methoxy-5-nitrophenoxy)butanoic acid (**13**) (2.380 g, 8.01 mmol) were dissolved in a mixture of DCM (100 mL) and DMF (10 mL) under anhydrous conditions. DMAP (0.196 g, 1.60 mmol) were dissolved in 5 mL of DMF and added to the formerly prepared solution. The mixture was cooled to 0 °C and a solution of N-BOC-EDA (1.283 g, 8.01 mmol) in 5 mL of DMF was added. After stirring the reaction mixture for 30 min, DCC (1.982 g, 9.61 mmol) was dissolved in 5 mL of DCM and added to the reaction vessel. The mixture was allowed to warm to room temperature while stirring over night. After additional stirring for 24 h, the mixture was filtered and the organic solvents were evaporated. The residue was dissolved in ethyl acetate (150 mL) and washed with saturated NH_4Cl , saturated Na_2CO_3 and brine. The combined organic layers were dried with MgSO_4 and the solvent was removed under reduced pressure. Purification was achieved by column chromatography over silica using chloroform/methanol (7.5/1) as eluent and afforded pure **14** (2.961 g, 6.74 mmol). Yield: 84 %.

Elemental analysis: calc. for $\text{C}_{20}\text{H}_{29}\text{N}_3\text{O}_8$: C, 54.66; H, 6.65; N, 9.56; found C, 54.39; H, 6.58; N, 9.67. ^1H NMR (CDCl_3): $\delta = 7.61$ (s, 1H), 6.74 (s, 1H), 6.34 (s, 1H), 4.91 (s, 1H), 4.15 (t, 2H, $J = 6.2$ Hz), 3.95 (s, 3H), 3.32 (m, 4H), 2.49 (s, 3H), 2.41 (t, 2H, $J = 7.2$ Hz), 2.20 (m, 2H), 1.42 (s, 9H). ^{13}C NMR (CDCl_3): $\delta = 200.20, 172.63, 157.14, 154.36, 149.01, 138.57, 132.93, 108.92, 108.24, 79.89, 68.89, 56.73, 41.00, 34.07, 32.61, 30.50, 28.45, 24.79$. MS (FD) m/z 439.5 (M^+)

tert-Butyl(2-(4-(4-(1-hydroxyethyl)-2-methoxy-5-nitrophenoxy)butanamido)ethyl)carbamate (15). To a solution of **14** (1.407 g, 3.22 mmol) in a mixture of THF (7 mL) and methanol (43 mL) was added sodium borohydride (61 mg, 1.61 mmol) in small portions. After stirring the reaction mixture over night at room temperature, 5 mL of water were added to destroy excess NaBH_4 . The solvents were removed under reduced pressure and the residue was purified by column chromatography using chloroform/methanol (7.5/1) as eluent. Pure **15** (1.162 g, 2.63 mmol) was obtained as slightly yellow colored solid in 82 % yield.

Elemental analysis: calc. for $C_{20}H_{31}N_3O_8$: C, 54.41; H, 7.08; N, 9.52; found C, 54.31; H, 7.01; N, 9.37. 1H NMR ($CDCl_3$): δ = 7.54 (s, 1H), 7.31 (s, 1H), 6.39 (s, 1H), 5.53 (qd, 1H, J = 6.2, 3.6 Hz), 4.96 (s, 1H), 4.08 (t, 2H, J = 6.1 Hz), 3.27 (m, 4H), 2.80 (s, 1H), 2.40 (t, 2H, J = 7.1 Hz), 2.16 (m, 2H), 1.81 (s, 1H), 1.53 (d, 3H, J = 6.2 Hz), 1.41 (s, 9H). ^{13}C NMR ($CDCl_3$): δ = 172.90, 157.04, 156.17, 154.16, 147.01, 139.72, 137.40, 109.32, 108.98, 79.91, 68.70, 65.79, 56.50, 40.75, 40.34, 32.84, 28.46, 24.94, 24.46. MS (FD) m/z 442.8 ($M + 1^+$)

2-(((2-(4-(4-(1-Hydroxyethyl)-2-methoxy-5-nitrophenoxy)butanamido)ethyl)-carb-amoyl)oxy)ethyl methacrylate (20). Synthesis of **20** was performed in three steps as described below.

Deprotection of the N-BOC protected amino group of 15 to form 19. To a solution of **15** (750 mg, 1.70 mmol) in 35 mL of $CHCl_3$ was added TFA (17 mL) and the solution was stirred for 10 min. The solvent and excess TFA were removed under reduced pressure and quantitative formation of **19** was demonstrated by TLC.

Activation of HEMA with p-nitrophenyl chloroformate. HEMA (1.290 g, 9.9 mmol) and triethylamine (1.200 g, 11.9 mmol) were dissolved in 20 mL of anhydrous THF and cooled to 0 °C. *p*-Nitrophenyl chloroformate (2.000 g, 9.9 mmol) was dissolved in 5 mL of THF and added to the reaction mixture. The resulting solution was stirred for 5 h at 0 °C and was subsequently allowed to warm to room temperature while stirring for 16 h. The mixture was filtrated in order to remove the precipitated triethylamine hydrochloride and the solvent was removed under reduced pressure. Pure 2-(((4-nitrophenoxy)carbonyl)oxy)ethyl methacrylate was obtained by precipitation from cold methanol (-20 °C) as white solid.

1H NMR ($CDCl_3$): δ = 8.29 (d, 2H, J = 9.2 Hz), 7.39 (d, 2H, J = 9.2 Hz), 6.17 (s, 1H), 5.63 (s, 1H), 4.51 (m, 4H), 1.97 (s, 3H). ^{13}C NMR ($CDCl_3$): δ = 167.17, 155.55, 152.56, 145.65, 135.88, 126.58, 125.49, 121.91, 67.03, 62.01, 18.40.

Synthesis of photo-labile-linker-methacrylate (20). The deprotected amine of **19** (579 mg, 1.70 mmol) and triethylamine (710 mg, 7.0 mmol) were dissolved in anhydrous DMF and the activated *p*-nitrophenyl carbonate of HEMA (500 mg, 1.70 mmol) was added as solid under argon atmosphere. The resulting solution was stirred for 48 h at room temperature. Afterwards, the solvent and excess Net_3 were removed under reduced pressure and the residue was dissolved in ethyl acetate and washed extensively with saturated $NaHCO_3$. The organic layer was dried with $MgSO_4$ and the solvent was evaporated. The obtained solid was purified by column chromatography using chloroform/methanol (7.5/1) as eluent. The photo-labile-linker methacrylate (**20**) was obtained as slightly yellow colored solid in 78 % yield (0.660 g, 1.33 mmol).

Elemental analysis: calc. for $C_{22}H_{31}N_3O_{10}$: C, 53.11; H, 6.28; N, 8.45; found C, 53.18; H, 6.19; N, 8.42. 1H NMR ($CDCl_3$): δ = 7.55 (s, 1H), 7.31 (s, 1H), 6.35 (s, 1H), 6.11 (s, 1H), 5.58 (s, 1H), 5.54 (m, 1H), 5.18 (s, 1H), 4.28 (m, 4H), 4.10 (t, 2H, J = 6.1 Hz), 3.97 (s, 3H), 3.33 (m, 4H), 2.42 (t, 2H, J = 7.1 Hz), 2.18 (m, 2H), 1.93 (s, 3H), 1.54 (d, 3H, J = 6.3 Hz). ^{13}C NMR ($CDCl_3$): δ = 173.04,

167.44, 156.93, 154.15, 147.02, 139.80, 137.38, 136.09, 126.26, 109.38, 109.01, 68.75, 65.82, 63.05, 62.88, 56.52, 41.15, 40.09, 32.86, 24.91, 24.44, 18.40. MS (FD) m/z 496.9 (M^+).

Activation of 20 as *p*-nitrophenyl carbonate (21). A solution of **20** (0.150 g, 301.5 μmol) and triethylamine (50.2 μL , 361.8 μmol) in 10 mL of anhydrous THF (10 mL) was cooled to 0 °C. *p*-Nitrophenyl chloroformate was dissolved in 10 mL of THF and added to the reaction mixture. The solution was allowed to warm to room temperature while stirring over night. Afterwards, the mixture was stirred for additional 2 h at 40 °C and then cooled to 0 °C. The precipitated ethylamine hydrochloride was removed by filtration and the solvent was removed under reduced pressure. Column chromatography over silica using ethyl acetate as eluent afforded pure **21** in 55 % yield (110 mg, 166.0 μmol).

Elemental analysis: calc. for $\text{C}_{29}\text{H}_{34}\text{N}_4\text{O}_{14}$: C, 52.57; H, 5.17; N, 8.46; found C, 52.67; H, 5.32; N, 8.66. ^1H NMR (CDCl_3): δ = 8.25 (d, 2H, J = 9.2 Hz), 7.61 (s, 1H), 7.34 (d, 2H, J = 9.2 Hz), 7.11 (s, 1H), 6.53 (q, 1H, J = 6.4 Hz), 6.30 (s, 1H), 6.12 (s, 1H), 5.59 (s, 1H), 5.13 (s, 1H), 4.31 (m, 4H), 4.13 (t, 2H, J = 6.1 Hz), 4.00 (s, 3H), 3.36 (m, 4H), 2.42 (t, 2H, J = 7.1 Hz), 2.20 (m, 2H), 1.93 (s, 3H), 1.77 (d, 3H, J = 6.4 Hz). ^{13}C NMR (CDCl_3): δ = 172.83, 167.40, 155.47, 154.28, 151.55, 147.88, 145.61, 140.12, 136.13, 131.49, 126.21, 125.46, 121.79, 109.26, 108.19, 73.91, 68.80, 63.13, 62.87, 56.68, 41.18, 40.25, 32.76, 24.85, 22.16, 18.43. MS (FD) m/z 662.0 (M^+).

Doxorubicin-photo-labile-linker-methacrylate (Dox-PL-MA). Doxorubicin hydro-chloride (50.0 mg, 86.2 μmol) was dissolved in anhydrous DMF and triethylamin (36 μL , 258.6 μmol) was added to the solution. The activated photo-labile-linker-methacrylate (**21**) was added as solid and the reaction mixture was stirred at room temperature for 36 h. The solvent was removed under reduced pressure and the remaining brick red solid was purified by repeated column chromatography over silica using chloroform/methanol mixtures of various compositions (7.5/1–22.5/1) as eluent. The pure Dox-PL-MA (41 mg, 49.1 μmol) was obtained as red solid in 57 % yield.

^1H NMR ($\text{CDCl}_3/\text{MeOD}$ 3/1): δ = 7.95 (d, 1H, J = 7.7 Hz), 7.72 (t, 1H, J = 8 Hz), 7.44 (m, 1H), 7.35 (d, 1H, J = 8.4 Hz), 6.92 (m, 1H), 6.25 (m, 1H), 6.04 (s, 1H), 5.52 (s, 1H), 5.23 (s, 1H), 4.77–4.63 (m, 3H), 4.35–4.15 (m, 5H), 4.00 (m, 5H), 3.90–3.80 (m, 4H), 3.50–3.40 (m, 1H), 3.33–2.91 (m, 7H), 2.34–2.29 (m, 3H), 2.08–2.01 (m, 3H), 1.86 (s, 3H), 1.76–1.58 (m, 1H), 1.52–1.49 (m, 3H), 1.21–1.10 (m, 3H). ^{13}C NMR ($\text{CDCl}_3/\text{MeOD}$ 3/1) δ = 214.27, 187.17, 186.70, 173.67, 167.47, 160.99, 157.09, 155.47, 155.41, 154.84, 153.89, 146.94, 139.51, 135.86, 135.56, 135.42, 134.06, 133.16, 126.14, 120.71, 119.75, 118.52, 111.57, 111.19, 108.94, 108.21, 100.51, 97.88, 76.55, 71.58, 68.79, 68.45, 67.34, 65.91, 65.10, 62.80, 62.72, 61.37, 56.56, 56.21, 46.84, 40.39, 39.42, 35.82, 33.41, 32.50, 24.84, 22.04, 18.04, 16.49. MS (ESI) m/z 1,089.37 ($M + \text{Na}^+$) 68.8 %BPI

7.7 Synthesis of a Light-Sensitive Monomer for the Preparation of Polymeric Photo-Resist Nanoparticles

4,5-Dimethoxy-2-nitrobenzyl methacrylate (DMNB-MA). A solution of 4,5-dimethoxy-2-nitrobenzylalcohol (5.000 g, 23.45 mmol) and triethylamin (2.610 g, 25.80 mmol) in 60 mL of anhydrous dichloromethane (DCM) was cooled down to 0 °C under argon. Methacryloyl chloride (2.697 g, 25.80 mmol) was dissolved in 15 mL of anhydrous DCM and added dropwise under stirring. The reaction mixture was allowed to warm to room temperature over night and was then washed 3 times each with aqueous Na₂CO₃ (5 % w/v) and deionized water. The organic phase was dried over MgSO₄ and the solvent was removed under reduced pressure. The resulting solid was recrystallized from ethanol yielding pure DMNB-MA as yellow colored solid in 86 % yield.

Elemental analysis: calc. for C₁₃H₁₅NO₆: C, 55.51; H, 5.38; N, 4.98; found C, 55.37; H, 5.29; N, 5.16. ¹H NMR (CDCl₃): δ = 7.72 (s, 1H), 7.03 (s, 1H), 6.20 (s, 1H), 5.65 (m, 1H), 5.59 (s, 2H), 3.96 (d, 6H), 2.00 (s, 3H). ¹³C NMR (CDCl₃): δ = 166.76, 153.63, 148.35, 140.12, 136.14, 127.46, 126.35, 110.32, 108.41, 63.50, 56.56, 56.44, 18.48. MS (FD) *m/z* 281.0 (M⁺)

7.8 Synthesis of a Photo-Degradable Polyurethane by Polycondensation

Photo-degradable polyurethane (PD-PU). To a solution of 2NPDM (300 mg, 16.38 mmol) in 10 mL of anhydrous DMF was added a solution of freshly distilled 2,4-toluenediisocyanate (TDI) (285.26 mg, 16.38 mmol) under argon atmosphere. The reaction vessel was sealed and the solution was stirred at 100 °C for 20 h. Afterwards, the reaction was quenched by the addition of 2 mL of water and the mixture was cooled to room temperature. The photo-degradable polymer was obtained by precipitation from ice cold methanol. Purification was achieved by centrifugation, dissolving the polymer in THF and repeated precipitation from methanol. After this procedure was conducted in total 3 times, drying of the solid in vacuum afforded PD-PU (368 mg) in 63 % yield.

¹H NMR (DMSO-*d*₆): δ = 8.18 (s, 1H), 7.80 (m, 2H), 7.54 (s, 1H), 7.13 (m, 2H), 5.47 (s, 2H), 5.24 (s, 2H), 2.13 (s, 3H). GPC (THF, polystyrene standard): *M_w* = 5,200 g/mol; PDI = 2.01.

7.9 Photo-Degradation Studies of Light-Cleavable Molecules in Solution

7.9.1 Photo-Degradation Studies in Solution via ^1H NMR and Mass Spectroscopy

The respective compounds were dissolved in THF with a concentration of $3.0 \cdot 10^{-3}$ mol/L. Irradiations were performed in a quartz cuvette for 10 h using a mercury short arc lamp combined with the described filters and an intensity of $I = 17$ mW/cm² for the wavelengths of $\lambda = 315\text{--}390$ nm. The reaction mixture was divided into two fractions and both were evaporated to dryness under reduced pressure. One fraction was investigated by ^1H -NMR spectroscopy, the other fraction was investigated by field desorption mass spectrometry.

7.9.2 Photo-Degradation Studies by UV-vis Measurements

A quartz cuvette containing a solution ($c = 4.5 \cdot 10^{-4}$ mol/L) of the respective compound in THF was placed under a UV lamp ($\lambda = 315\text{--}390$ nm, $I = 17$ mW/cm²) and the samples were irradiated for fixed time intervals. UV-vis measurements were performed subsequently.

7.9.3 Kinetic HPLC Measurements

Solutions in THF were prepared and irradiated analogously to those used for the ^1H -NMR spectroscopic measurements. Samples were taken at fixed time intervals and directly measured by HPLC using a solvent gradient of THF/water from 40/60 to 30/70. Photolytic conversion was determined by the decrease of the peak area of the starting compound.

7.10 Synthesis of Microgels and Polymeric Nanoparticles

7.10.1 General Synthetic Protocol for the Formation of Microgels and Non-Crosslinked Polymeric Nanoparticles by Free Radical (Co)Polymerization in (Inverse) Miniemulsion

Crosslinked microgels and non-crosslinked polymeric nanoparticles were synthesized by free radical polymerization in (inverse) miniemulsion. The dispersed phase was prepared by mixing the respective monomers, the osmotic pressure agent, the respective crosslinker and a potential solvent. For initiations from the dispersed phase, the initiator was added to the solution. Afterwards, the mixture was added to the continuous phase consisting of a solution of the respective surfactant in the specific solvent. The (inverse) miniemulsion was formed by first stirring the mixture at 1,750 rpm for 1.5 h and then homogenizing the obtained preemulsion by ultrasonication for 2 min at 90 % intensity (Branson sonifier W450 Digital, 0.5" tip) at 0 °C. For initiation from the continuous phase the respective initiator was added then to the (inverse) miniemulsion. Polymerizations were carried out over night in an oil bath set at the specific polymerization temperature. Deviations from this general procedure are listed in the following chapters.

7.10.2 Micro-/Nanogels

7.10.2.1 General Purification Procedure

After the polymerization, any coagulates were removed by filtration and the resulting dispersions were centrifuged to collect the particles. The supernatant was removed and replaced by the solvent forming the continuous phase. Redispersion was carried out using a vortex. In order to remove excess surfactant, the dispersions were further washed three times following the procedure described above. Finally, the dispersions of the particles in the specific solvent were examined with regard to the particle size distributions by means of dynamic light scattering (DLS) and scanning electron microscopy (SEM). Freeze drying of the purified dispersions removed unreacted monomer and yielded the (crosslinked) particles as powders.

7.10.2.2 General Swelling Procedure: Purification, Determination of the Sol/Gel Content and the Degree of Swelling

For swelling experiments of the microgels, the freeze dried particles were swollen in a good solvent for the network-forming polymer at room temperature. Three additional washing steps by centrifugation and redispersion in the respective solvent were performed to remove the sol content which consists of all the non-reacted monomers, the soluble oligomers, polymers and non-crosslinked particles. For every type of microgel the supernatants of the washing steps were combined and evaporated yielding the sol content. The particle dispersions were also evaporated and represented the gel content. By gravimetical analysis, the sol/gel content was determined and gives a description of the crosslinking efficiency.

Finally, the dried particles were redispersed in a good solvent for the network-forming polymer over night at room temperature. Particle size distributions were determined by DLS and the degree of swelling was determined as the volume ratio between the particles in their non-swollen state (purified dispersion after synthesis) and the swollen microgels (transferred to a good solvent for the network-forming polymer).

7.10.2.3 PMMA Microgels

This chapter contains the synthetic details for the preparation of PMMA microgels by miniemulsion polymerization as described in [Sect. 5.1.1.1](#). The dispersed phase was prepared by mixing MMA (1.00 g, 10.00 mmol), hexadecane (41 mg, 0.18 mmol), 2,2'-azobis(2-methyl-butyronitrile) (V-59) (20 mg, 0.10 mmol) and 2.5 mol-% of the respective crosslinker. The continuous phase consisted of a solution of the nonionic surfactant Lutensol AT-50 (66 mg) in 10 mL of water. Synthetic details are listed in [Table 7.2](#) in [Sect. 5.1.1.1](#). Polymerizations were carried out at 70 °C. Purification was achieved by washing the dispersions three times with demineralized water (centrifugation at 14,000 rpm for 25 min; redispersion by vortex). Finally, the dispersions were centrifuged at 5,000 rpm for 5 min and the supernatant was collected and centrifuged again for 5 min at the same speed. The supernatant of this procedure represents the final dispersion of the MGs in water. Freeze drying of the so purified dispersions yielded the crosslinked PMMA gel particles as white powders. The freeze dried particles were swollen for 3 days at 0.5 % (w/v) in THF at room temperature. Three additional washing steps were performed to remove the sol content (centrifugation at 14,000 rpm for 60 min; redispersion in THF). Finally, the dried particles were redispersed either in THF or chloroform by swelling at a concentration of 0.5 % (w/v) over night at room temperature.

Table 7.2 Nominal compositions of the dispersed phase of different p(HEMA-*co*-MAA) microgels

Sample	Monomer		Crosslinker		Solvent/osmotic pressure agent	
	Type	<i>m/g</i>	Type	<i>m/mg</i>	Type	<i>m/g</i>
MG-A + (MG-A1)	HEMA	1.500	DEGDMA	70.0	H ₂ O	70.0
	–	–				
MG-B	HEMA	1.425	DEGDMA	70.0	H ₂ O	70.0
	MAA	0.0075				
MG-C	HEMA	1.350	DEGDMA	70.0	H ₂ O	70.0
	MAA	0.150				
MG-D + (MG-B1)	HEMA	1.275	DEGDMA	70.0	H ₂ O	70.0
	MAA	0.225				
FL-MG	HEMA	0.6375	DEGDMA	37.5	H ₂ O	70.0
	MAA	0.1614				
	Bodipy-1	0.0070				
HG-MG-0-I	HEMA	1.275	–	–	H ₂ O	70.0
	MAA	0.225				
HG-MG-4B-I	HEMA	1.275	CL-4B	185.0	H ₂ O	70.0
	MAA	0.225				
HG-MG-0-II	HEMA	1.275	–	–	H ₂ O	70.0
	MAA	0.225			DMSO	375.0
HG-MG-4B-II	HEMA	1.275	CL-4B	185.0	H ₂ O	70.0
	MAA	0.225			DMSO	375.0
HG-MG-5B-II	HEMA	1.275	CL-5B	235.0	H ₂ O	70.0
	MAA	0.225			DMSO	375.0
M-MG-0	HEMA	0.6375	DEGDMA	37.5	H ₂ O	150
	K-MA	0.1614			PBS	150

7.10.2.4 PHEMA Microgels

PHEMA microgels were prepared by free radical copolymerization of HEMA and various crosslinkers in inverse miniemulsion. The dispersed phase was prepared by mixing HEMA (1.5 g, 11.5 mmol), water (70 mg, 3.9 mmol) and 2.5 mol-% of the respective crosslinker. The continuous phase consisted of a solution of the amphiphilic block copolymer P(E/B)-*b*-PEG (75 mg) as nonionic surfactant in 12.5 g of cyclohexane. Sample nomenclature in dependency on the used crosslinkers is listed in Figure 33 in Sect. 5.1.1.2. Initiation was carried out from the continuous phase by adding V-59 (50 mg, 0.3 mmol) as thermal initiator to the formed inverse miniemulsion and polymerizations were carried out at 70 °C. Purification was achieved by washing the dispersions three times with cyclohexane (centrifugation at 10,000 rpm for 30 min; redispersion by vortex). Freeze-drying of the so purified dispersions removed unreacted monomer and yielded the crosslinked PHEMA gel particles as white powders. The freeze-dried particles were swollen over night at 5 % (w/v) in chloroform/methanol (1/1 v/v) at room temperature.

7.10.2.5 p(HEMA-*co*-MAA) Microgels

Crosslinked p(HEMA-*co*-MAA) microgels and non-crosslinked reference particles were synthesized by free radical copolymerization in inverse miniemulsion. Different microgels with various compositions of the dispersed phase were synthesized. Table 7.2 lists the synthetic details. In all cases, the continuous phase consisted of a solution of the amphiphilic block copolymer P(E/B)-*b*-PEG (75 mg) as nonionic surfactant in 12.5 g of cyclohexane. After miniemulsification, V-59 (50 mg, 0.3 mmol) as thermal initiator was added and polymerizations were then carried out over night in an oil bath set at 70 °C.

After the polymerization, purification was carried out by washing the particles four times with cyclohexane (centrifugation at 10,000 rpm for 30 min; redispersion by vortex). Freeze-drying removed unreacted monomer and yielded the crosslinked p(HEMA-*co*-MAA) gel particles as white to slightly yellow colored powders. The freeze-dried particles were swollen over night at 5 % (w/v) in water adjusted to pH 12 at room temperature. Three additional washing steps by centrifugation at 17,500 rpm for 90 min at 15 °C and redispersion in deionized water were performed to remove the sol content. The purified particles were freeze-dried and redispersed in the respective aqueous media by simple swelling at room temperature for 6 h at the desired concentration.

pH-Dependent Swelling Experiments of p(HEMA-*co*-MAA) Microgels

The pH values of microgel dispersions in water (0.05 % w/v) were varied from pH 4 to pH 12 by adding aqueous NaOH solution (0.05 N), and hydrodynamic diameters of the particles were measured by DLS for every pH value.

Determination of the Incorporation Efficiency of Light-Cleavable Crosslinkers

UV-vis measurements of microgel dispersions in DMSO were conducted to determine the amount of incorporated crosslinking molecules. For quantification, spectra of the swollen photo-degradable microgels (0.2 % w/v) were compared to calibration curves of solutions of the respective crosslinkers in dispersions of non-photo-degradable p(HEMA-*co*-MAA) microgels (0.2 % w/v). The relative quantity of incorporated crosslinker was determined with respect to HEMA and MAA amounts before polymerization as mol-% of theory.

Determination of the Amount of Ionizable Maa Groups

Potentiometric titration experiments were conducted. The pH values of the different aqueous microgel dispersions (0.5 % w/v) were adjusted to about pH 4 by adding diluted hydrochloric acid (0.05 N). The resulting mixture was allowed to equilibrate for 1 h and was then titrated to around pH 10 by adding NaOH (0.05 N). After every base addition step, the dispersions were allowed to equilibrate for 15 min under stirring and ultrasonicated for 2 min. Subsequently the pH was measured.

7.10.2.6 Microgels Based on Polyacrylamide Crosslinked with Functionalized Dextrans

Dispersed phases were prepared by dissolving acrylamide (AAm) and either dextran methacrylate (Dex-MA) or dextran-photo-labile-linker-acrylate (Dex-PL-A) in an aqueous 0.5 M NaCl solution. While the total ratio of (AAm+funct.Dex)/solvent was kept constant with 1/1 w/v, the ratio of functionalized dextran to acrylamide was varied. For initiation from the aqueous phase, the respective initiators (VA-044, KPS) were added to the dispersed phase. The solution was added under stirring to the continuous phase consisting of a solution of the non-ionic surfactant Lubrizol U (100 mg) in 10 g of cyclohexane. For initiation with oil soluble initiators from the continuous phase, either V-59 or V-70 was added to the inverse miniemulsion after homogenizing. The polymerizations were carried out over night in an oil bath set at a fixed temperature. For initiation with KPS, TEMED was added to the homogenized miniemulsion and the polymerization was carried out at room temperature over night. For compositions of the dispersed phases and polymerization temperatures see Sect. 5.2.1 for p(AAm-co-Dex-MA) and Sect. 5.2.2 for p(AAm-co-Dex-PL-A) microgels.

After the polymerizations, filtered dispersions were washed 5 times with cyclohexane (centrifuged at 5,000 rpm for 30 min and redispersed by vortex). Freeze drying yielded the crosslinked gel particles as white powders. Transfer of the nanogels to the aqueous phase was achieved by simply swelling the dried powders over night in water at 0.5 % (w/v) at room temperature. Two additional washing steps by centrifugation at 14,000 rpm for 90 min and redispersion in deionized water were performed. The purified particles were again freeze dried and redispersed in the respective medium by swelling at room temperature for 6 h at the desired concentration.

7.10.2.7 PAAm Microgels as Seed Particles

PAAm C-NP were prepared and purified analogously to p(AAm-co-Dex-MA) microgels but varied in the composition of the dispersed phase. The latter consisted of acrylamide (1.000 g, 14.0 mmol) and methylene bisacrylamide (MBA) (50 mg, 0.32 mmol) dissolved in 1 mL of an aqueous NaCl solution (0.5 N).

7.10.3 *Photo-Resist Nanoparticles and Polystyrene Reference Nanoparticles*

Light degradable PDMNB-MA photo resin nanoparticles (PR-NP) as well as polystyrene reference lattices (PS-NP) were prepared by free radical miniemulsion polymerization. The dispersed phase was prepared by dissolving the monomer

(0.100 g), hexadecane (0.040 g) and 2,2'-Azobis(2-methylbutyronitrile) (V-59) as initiator (0.010 g) in CHCl_3 (0.900 mL). For Nile red containing particles the respective amount of dye was first dissolved in chloroform and the resulting solution was used to form the dispersed phase. The mixture was then added to the continuous phase consisting in every case of a solution of the anionic surfactant sodium dodecylsulfate (SDS) (0.012 g, 0.3 % w/v) in 4 mL of water. The mini-emulsion was formed by first stirring the mixture at 1,750 rpm for 1 h at room temperature and then homogenizing the obtained preemulsion by pulsed ultrasonication (15 s pulse, 30 s pause, in total 10 min) at 70 % intensity (Branson sonifier W450 Digital, 0.125" tip) at 0 °C. Polymerizations were carried out overnight at 70 °C. The used amounts of dye for the different reactions are shown in Sect. 5.4. After polymerization, the dispersions were stirred in an open reaction vessel at 70 °C for additional 8 h to remove chloroform. The total volume was kept constant by adding deionized water. Coagulates were removed by filtration and the resulting dispersions were extensively dialyzed against deionized water for 10 days. Solid contents were determined by gravimetric analysis.

7.10.3.1 Determination of the Encapsulation Efficiency of Nile Red

Dialyzed dye-containing particles were freeze dried and subsequently dissolved in a good solvent for both the dye and the respective polymers (0.016 % w/v), namely: DMSO for PR-NP and 1,4-dioxane for PS-NP. Encapsulation efficiency (*EE*) was determined by fluorescence using calibration curves of Nile red in the respective solvents containing equal solid contents of dissolved plain particles.

7.11 Loading of p(HEMA-co-MAA) Microgels with Myoglobin and Subsequent Release Experiments

To 18 mL of a stock solution of myoglobin ($c = 1 \text{ mg/mL}$) in water with a pH adjusted to pH 6.75 were added 2 mL of a dispersion of MG-D p(HEMA-co-MAA) microgels in water ($c = 1 \text{ mg/mL}$). The pH of the mixture was adjusted to pH 6.75 by the addition of diluted NaOH and HCl. After equilibration at room temperature overnight, the pH was adjusted to pH 4.5 by the addition of diluted HCl and the particles were collected by centrifugation (10,000 rpm; 30 min). The supernatant (20 mL) was examined by UV-vis spectroscopy. The pellet of the centrifugation was redispersed in 20 mL of water adjusted to pH 4.5 using a vortex. The loaded microgels were washed two more times following the described procedure and the supernatants of every washing step were investigated by

UV–vis spectroscopy. Subsequently to the last centrifugation step, the microgels were redispersed in PBS with pH 7.4 (20 mL). A sample (200 μ L) was taken and investigated by UV–vis spectroscopy. The dispersion of the loaded microgels in PBS was shaken at 37 °C and samples were taken after predetermined time intervals. The release of myoglobin into the surrounding medium was investigated by removing the microgels from each sample by centrifugation and comparing the UV–vis spectra of the supernatants to a calibration curve of myoglobin in PBS.

7.12 Degradation Experiments of Microgels

7.12.1 Photo-Degradation

Samples of 0.125 % (w/v) in the respective organic solvent, phosphate buffer solution (PBS) or water adjusted to the desired pH were placed in a quartz cuvette and irradiated with the respective UV light source. At predetermined times, samples were collected and turbidity measurements were conducted by using a NICOMP Zetasizer. The volume of the irradiated sample was retained by returning the withdrawn samples to the cuvette after every measurement. The turbidity was obtained by calculating the ratio of the scattering intensity at 90° of the irradiated samples relative to the one of the non-irradiated samples. For irradiation experiments of p(AAm-*co*-Dex-PL-A) microgels, turbidity was measured in transmission by using a He–Ne Laser emitting at $\lambda = 633$ nm. Irradiation was carried out on a 90° angle relative to the Laser beam by using a UV-LED emitting at $\lambda = 365$ nm with an intensity of $I = 30$ mW/cm². Transmitted light intensity of the Laser was measured by a photo diode combined with a GG-385 edge filter to block scattered UV light.

7.12.2 Enzymatic Degradation

Dispersions of purified nanogels in water (0.0625 % w/v) were placed in a quartz cuvette and the sample temperature was adjusted to 37 °C using a brass heating mantle combined with a cryostat. Enzymatic degradation of either p(AAm-*co*-Dex-MA) or p(AAm-*co*-Dex-PL-A) microgels was examined by adding 10 μ L of dextranase solution (47 wt %) to 3 mL of a dispersion of the respective purified gel particles in water. Particle degradation was monitored by turbidity measurements in transmission as described above.

7.13 Degradation Experiments of Photo-Resist Particles

Dispersions of nanoparticles with 0.01 % (w/v) in deionized water adjusted to the desired pH were placed in a quartz cuvette and irradiated under stirring with UV light at room temperature. Samples were taken at distinct irradiation times and analyzed by turbidity measurements, UV-vis and fluorescence spectroscopy as well as SEM.

7.14 Synthesis of Core/Shell Nanoparticles

7.14.1 Seeded Precipitation Polymerization

7.14.1.1 PAAm/PMMA Core/Shell Nanoparticles

An aqueous dispersion (1.5 mL) of C-NP PAAm seed particles (2.0 % w/v) was diluted with 16.5 mL of demineralized water and 12 mL of methanol. To the resulting dispersion with a microgel concentration of $4.3 \cdot 10^{15}$ N_p/L in 30 mL of MeOH/water (40/60 v/v) was added Lutensol AT-50 in various amounts. MMA (150 mg, 10 eqv.-wt. with respect to C-NP) was added and the dispersion was stirred at room temperature for 30 min while purging with argon. The seeded precipitation polymerization was initiated by adding KPS (15 mg) to the reaction mixture and heating to 70 °C. After stirring for 20 h at 70 °C the resulting dispersion was cooled to room temperature and extensively dialyzed against demineralized water for 10 days. Exact amounts of Lutensol AT-50 are listed in Table 12 in Sect. 5.5.1

7.14.2 Free Radical Polymerization in Polyurea Nanocapsules

7.14.2.1 PAAm/PU Core/Shell Nanoparticles

PAAm/PU core/shell nanoparticles were prepared by free radical copolymerization of acrylamide with MBA in polyurea nanocapsules formed previously by interfacial polycondensation in inverse miniemulsion. The dispersed phase of the inverse miniemulsion consisted of a solution of acrylamide (712.5 mg, 10.0 mmol), MBA (37.5 g, 0.243 mmol), VA-060 (15.0 mg, 0.036 mmol) and ethylene diamine (39.0 mg, 0.651 mmol) in an aqueous NaCl solution (750 μL, 0.5 M). The mixture was then added under vigorous stirring to the continuous phase consisting of a solution of the non-ionic surfactant Lubrizol U (50 mg) in cyclohexane (10 g). Miniemulsification was achieved by homogenizing the

preemulsion by ultrasonication for 2 min at 90 % intensity (Branson sonifier W450 Digital, 0.5" tip) at 0 °C. Shell formation was achieved by the drop wise addition of TDI (170.0 mg, 0.976 mmol) dissolved in cyclohexane (4 g) to the inverse miniemulsion under stirring. After 6 h, a sample of 2 mL was collected containing the AAm-aq./PU nanocapsules with a liquid core. The remaining dispersion was heated to 70 °C and stirred for additional 12 h to achieve the free radical copolymerization of acrylamide with MBA in the capsule core. After polymerization, the dispersion was filtered and washed three times with cyclohexane (centrifugation: 6,000 rpm, 20 min; redispersion: vortex). The purified dispersion (12 mL) was added to 12 mL of a solution of SDS (72 mg, 0.25 mmol) in water and ultrasonicated for 20 s. The dispersion was stirred in an open reaction vessel for 5 days in order to evaporate the cyclohexane. This procedure afforded PAAm-HG/PU core/shell nanoparticles dispersed in water.

7.15 Surface Functionalization of Microgels

In order to functionalize the microgels with cinnamoyl moieties, 5 mL of the PHEMA MG-A1 and p(HEMA-*co*-MAA) MG-B1 dispersions in cyclohexane were stirred at room temperature and a solution of excess cinnamoyl chloride (143 mg, 0.86 mmol) in 2.5 mL cyclohexane was added. After stirring the dispersions over night, unreacted cinnamoyl chloride was removed by collecting the particles by centrifugation (6,000 rpm; 45 min) and redispersion in cyclohexane. Two additional washing steps following the procedure described above, were carried out for further purification. Finally, the obtained dispersions of the cinnamoyl functionalized PHEMA particles C-MG-A1 and the cinnamoyl functionalized p(HEMA-*co*-MAA) microgels C-MG-B1 were transferred to a good solvent for the network-forming polymer by swelling the freeze dried PHEMA particles for 1 day with 0.5 % (w/v) in THF at room temperature and the p(HEMA-*co*-MAA) hydrogel particles for 1 day with 0.5 % (w/v) in water with 0.1 N sodium hydroxide set to pH 12. In this case, the pH was adjusted afterwards to neutral (pH 7) by titration of the dispersion with 0.01 N hydrochloric acid. Two additional washing steps by centrifugation at 6,000 rpm for 25 min and redispersion in Milli-Q water were performed to remove the sol content.

References

1. Piggott, A.M., Karuso, P.: *Tetrahedron Lett.* **46**(47), 8241–8244 (2005)
2. Holmes, C.P.: *J. Org. Chem.* **62**(8), 2370–2380 (1997)
3. Holmes, C.P., Jones, D.G.: *J. Org. Chem.* **60**(8), 2318–2319 (1995)
4. Kim, S.H., Chu, C.C.: *J. Biomed. Mater. Res. A* **49**(4), 517–527 (1999)

Curriculum Vitae and Publications

Curriculum Vitae

Name: Daniel Klinger
Date of birth: 29.11.1981
Place of birth: Mainz

Education

- 09/1993–03/2001 **Gymnasium Nieder-Olm** (high school), **Nieder-Olm, Germany**
Abitur (A-levels)
- 04/2002–01/2008 **Johannes Gutenberg Universität Mainz, Mainz, Germany**
Academic studies
Degree: diploma-chemist
- 08/2005–03/2006 **Seoul National University, Seoul, Republic of Korea**
Visiting student in the group of Prof. J.-Y. Chang
Topic: *Controlled Radical Polymerization of Blocked Isocyanate Monomers*
- 06/2007–02/2008 **Johannes Gutenberg University Mainz, Mainz, Germany**
Diploma thesis in the group of Dr. P. Théato
Topic: *Synthesis and Characterization of Novel Photo-Switchable Amphiphilic Block Copolymers*
- 08/2008–09/2011 **Max-Planck-Institute for Polymer Research, Mainz, Germany**
PhD student in the group of Prof. Katharina Landfester

List of Publications

- 01** **D. Klinger**, J.-Y. Chang, P. Théato
Poly(4-vinylbenzoyl azide): A New Isocyanato Group Generating Polymer
Macromol. Rapid Comm. **2007**, *28*, 718
- 02** K. Nilles, **D. Klinger**, P. Théato
Reactive Derivates of 4-Vinylbenzoic Acid: Building Blocks for Defined
Functional Polymeric Architectures
Polymer Preprints **2007**, *48*, 1009
- 03** **D. Klinger**, K. Nilles, P. Théato
Polymeric 1-Iminopyridinium Ylides as New Photo-Switchable Polymers
J. Polym. Sci.: Part A **2010**, *48* (4), 832
- 04** P. Théato and **D. Klinger**
Synthesis of Photo-Reactive Block Copolymers Based on
1-Iminopyridinium Ylides
Aust. J. Chem. **2010**, *63*, 1164
- 05** **D. Klinger** and K. Landfester
Photo-Sensitive PMMA Microgels: Light-Triggered Swelling and Degradation
Soft Matter **2011**, *7* (4), 1426
- 06** P. Froimowicz, **D. Klinger**, K. Landfester
Photo-Reactive Nanoparticles as Nanometric Building Blocks for the Generation
of Self-Healing Hydrogel Thin-Films
Chem. Eur. J. **2011**, *17*, 12465
- 07** **D. Klinger** and K. Landfester
Polymeric Photo-Resist Nanoparticles: Light-Induced Degradation
of Hydrophobic Polymer in Aqueous Dispersion
Macromol. Rapid Comm **2011**, *32* (24), 1979
- 08** **D. Klinger** and K. Landfester
Dual Stimuli-Responsive Poly(2-hydroxyethyl methacrylate-*co*-meth-acrylic
acid) Microgels Based on Photo-Cleavable Crosslinkers:
pH-Dependent Swelling and Light-Triggered Degradation
Macromolecules **2011**, *44* (24), 9758
- 09** **D. Klinger**, E. M. Aschenbrenner, C. K. Weiss, K. Landfester
Enzymatically Degradable Nanogels by Inverse Miniemulsion Copolymerization
of Acrylamide with Dextran-Methacrylates as Crosslinkers
Polym. Chem. **2012**, *3*, 204
- 10** **D. Klinger** and K. Landfester
Enzymatic- and Light-Degradable Hybrid Nanogels: Crosslinking of
Polyacrylamide with Functionalized Dextrans Containing Photo-Cleavable
Linkers
J. Polym. Sci.: Part A **2012**, *50* (6), 1062
- 11** **D. Klinger** and K. Landfester
Stimuli-Responsive Microgels for the Loading and Release of Functional
Compounds: Fundamental Concepts and Applications
Polymer **2012**, *53*, 5209